REFERENCE ONLY

UNIVERSITY OF LONDON THESIS

Degree PhD Year 2005 Name of Author AHMED, I.

Phosphate Based Glasses and Glass-Fibres for Tissue Engineering

Thesis submitted by

Ifthkar Ahmed

For the degree of
DOCTOR OF PHILOSOPHY

Eastman Dental Institute
Division of Biomaterials and Tissue Engineering
University College London
256 Gray's Inn Road
London
WC1X 8LD

-2005-

ProQuest LLC
789 East Eisenhower Parkway
P.O. Box 1346
Ann Arbor, MI 48106-1346

Dedicated to

my Grandparents, my Mum, my Sisters and my Brother

Acknowledgements:

First and foremost, I would like to thank my supervisor, and Head of Division, Professor Jonathan Knowles. Without his invaluable advice and guidance, I would not have been able to complete my research project. I would also like to thank my second supervisor, Dr. Mark Lewis for his helpful assistance during my PhD. In addition I would also like to thank Dr. Showan Nazhat for his time, advice and guidance, especially with regards to writing papers.

I would like to acknowledge the MRC Muscle Cell Biology group (Hammersmith Hospital), for conducting the biocompatibility studies on the glass fibres produced. Thanks go to Charlotte Collins for conducting the experiments, and her supervisors Professor Irwen Olsen and Dr. Jenny Morgan.

I am very grateful to Dr. Geoff Hawkes (Queen Mary University of London), for conducting the NMR analysis, and to Tiziana for her assistance in analysing the data. Thanks also go to Dr. Robert Hill (Imperial College, London) for his advice and assistance in calculating the Network Connectivity of the glasses investigated.

I would also like to thank the staff at Dionex (U.K.) for the helpful technical advice provided.

Thanks also go to the Biomaterials staff (Graham Palmer, George Georgiou, Anne Young and Nicky Mordan) for their invaluable assistance and advice, and to my research colleagues, Sam Ho, Roopa Prabhakar and Anita Patel, for putting up with me for the past three years. I am especially indebted to Sam and Anita, for their patience and support in completing my PhD thesis.

Many thanks go to the Lord Downing Fund, and the Engineering and Physical Sciences Research Council (EPSRC) for providing the funding for this project.

Finally, I would like to take this opportunity to thank my Grandmother, my Mum, my Sisters, my Brother, my Cousins and my Uncles for watching over me, and encouraging me to complete the PhD, and also for putting up with me over the last three years (especially my sisters).

Abstract:

The aims of the project were to produce and characterise phosphate-based glasses and glass-fibres, which were to be utilised as cell delivery vehicles. Initially the project aim was to attach muscle cells to the fibres in order to formulate alternative therapies for diseases such as Muscular Dystrophy. However, as the project progressed other cell types were also evaluated for the biocompatibility of the glass-fibres produced.

Using a custom built fibre-rig (UCL) glass fibres were produced from compositions based on the ternary P_2O_5-CaO-Na_2O glass system. These glasses were composed of ionic components that already exist in the body and thus minimal inflammatory responses were expected. This glass system had been investigated within the department, where the P_2O_5 content was fixed at 45 mol%, with the CaO and Na_2O mol% making up the remainder. Initial studies revealed that fibres could not be produced from these compositions, and this was attributed to the structure of the glasses. By increasing the phosphate content to 50 and 55 mol% P_2O_5, glass fibres were successfully produced. Thus it was ascertained that a minimum of 50 mol% P_2O_5 was required for fibre production. Further analysis revealed that these ternary compositions proved to be too soluble for cell attachment.

A quaternary component, boric oxide (B_2O_3), was added in order to reduce the degradation rates obtained. This was added due to the fact that B_2O_3 is a well known glass former. Further analysis revealed that B_2O_3 did reduce the

degradation rates, however, these compositions also proved to be too soluble for cell attachment and proliferation to occur.

A further quaternary component, iron oxide (Fe_2O_3), was investigated. This was because iron is a naturally occurring ion within the body; therefore, no inflammatory responses were expected. Fe_2O_3 was incorporated at 1 – 5 mol% substituted for Na_2O. It was seen that there was an order of magnitude difference with the degradation rates ranging from 1 – 5 mol% Fe_2O_3. Furthermore, it was seen that compositions containing 4 – 5 mol% Fe_2O_3 were sufficient for successful cell attachment and differentiation of muscle precursor cells.

A further series of glasses were also investigated, incorporating silicon as the quaternary component. Silica was chosen due to the large volume of literature focusing on silica based glasses, with the well known Bioglass®. Silicon was incorporated at 1- 5 mol%, and it was seen that silicon totally disrupted the glass network.

Table of Contents:

List of Tables:

Chapter 2 Materials and Methods:

Chapter 3 The Ternary P_2O_5-CaO-Na_2O Glass System:

Chapter 4 The Quaternary P_2O_5-CaO-Na_2O-B_2O_3 Glass System:

Chapter 5 The Quaternary P_2O_5-CaO-Na_2O-Fe_2O_3 Glass System:

Chapter 6 The Quaternary P_2O_5-CaO-Na_2O-SiO_2 Glass System:

List of Figures:

Chapter 1 Literature Review:

Chapter 2 Materials and Methods:

Chapter 3 The Ternary P_2O_5-CaO-Na_2O Glass System:

Chapter 6 The Quaternary P_2O_5-CaO-Na_2O-SiO_2 Glass System:

CHAPTER 1

Literature Review

1.0 The History of Glass:

1.1 Introduction:

The earliest known synthetic glasses were created in Asia Minor several millennia ago. Some isolated examples were said to be as early as 7000 BC, but it was clear that by the year 2500 BC there were many sources, probably first in Mesopotamia and then in Egypt. About 2000 years ago, the blowing of glass articles with a pipe was invented. This advance in technology was followed by a rapid increase in the use of glassware. The first glassmakers were motivated to create decorative objects, using sintered bodies of silica and desert soda (sodium oxide) with appropriate colorants such as copper, manganese, and iron salts. There seemed to be no demonstrated interest in transparency at this time. Glassblowing spread quickly through the Roman Empire, and soon glass bowls and drinking vessels were in use throughout society, in both ordinary households and among the ruling classes. The desire for clear and transparent vessels came with this remarkable growth of blown glass production. The earlier and sometimes parallel development of ceramic and metallurgical processes undoubtedly influenced and aided the growth of early glass technology. Improvements in furnaces and raw materials used were all applicable to glassmaking (1).

Although sand and alkali were known from the earliest days of glass to be necessary ingredients, the role of lime (calcium oxide) was not apparent until

much later. It was only in the 17th, 18th and 19th centuries that the increase in chemical durability brought about by the addition of lime to alkali silicate glasses became understood.

Most of the current commercial glasses are soda-lime-silica glasses. It is significant that the compositions of these glasses have changed little over the centuries, ranging from 65% to 75% silica, with alkali ranging from 10% to 20%, and lime making up the balance (1).

1.2 History of Glass Structure Studies:

During the early phases of glass studies (1) it was realised that the formation of glass was mainly a kinetic phenomenon, and that the kinetic processes involved were controlled by the detailed structure of the materials concerned. In 1926 Goldschmidt (2) indicated that SiO_2, GeO_2, B_2O_3, P_2O_5, As_2O_3, As_2S_3, Sb_2O_3 as well as BeF_2, were all able to form glass by themselves. In other words, they were all 'glass formers'.

The first detailed descriptions of the expected 'crystal' structures and the reasons that such structures formed glasses were proposed by Zachariasen (3), Hagg (4), and Goldschmidt (2). They were crystallographers / chemists who, since the discovery of X-rays, had studied crystal structures and approached the problem of glass structure and formation from the results obtained starting with these studies. Arguably, Zachariasen's rules constituted the most famous work in glass science

to date. His rules described what he considered to be the necessary conditions for glass formation:

- An oxygen is linked to not more than two central atoms;
- The number of oxygen atoms surrounding a central atom must be small;
- Oxygen polyhedra share corners – not edges or faces – with each other;
- At least three corners in each oxygen polyhedra must be shared;

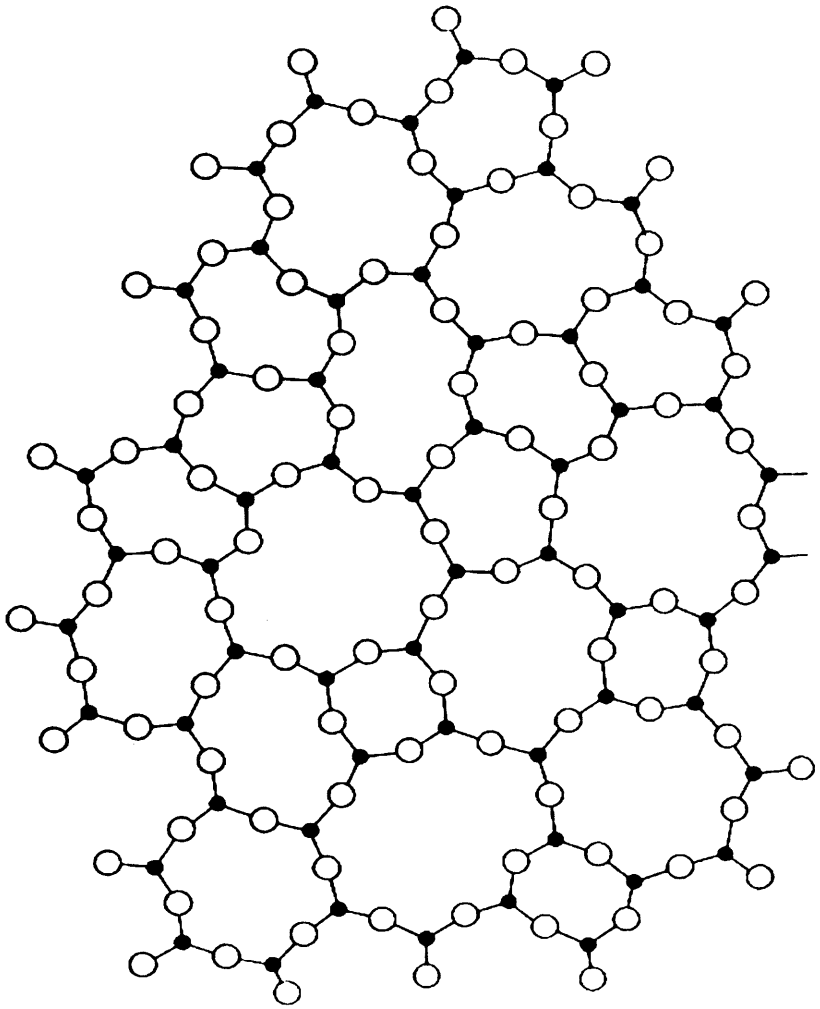

Figure 1.1: Zachariasen's model of an oxide glass in two dimensions (3).

Zachariasen summarised his 1932 paper (3) by stating that the atomic arrangement suggested was in complete agreement with the characteristic properties of glasses. He stated that the atoms in glass were linked together by forces essentially the same as in crystals. Over large temperature ranges the atoms were oscillating about definite equilibrium positions, and as in crystals, extended three dimensional networks were formed, but the principal difference between a crystal network and a glass network was the presence of symmetry and periodicity in the crystal network, and its absence in the glass network.

In general, the four rules stated above would have to be satisfied for glass formation to occur. However, over the years the validity of these rules has been debated, and many workers have argued for and against Zachariasen's "Continuous Random Network Theory".

A further theory of glass structure and formation was presented a year later by Warren and co-workers, who re-examined the scattering of X-rays by SiO_2 glass (5). Their interpretations of the experimental results were consistent with the model proposed by Zachariasen. It was Warren who used the term "Random Network", to describe structures that were consistent with Zachariasen's model. In one of his papers Warren stated that, 'via the method of Fourier analysis of the X-ray diffraction patterns, fairly definite and unique pictures have been obtained of the atomic arrangements in vitreous B_2O_3 and SiO_2. The results are in complete agreement with Zachariasen's predictions concerning the structures of the oxide glasses' (6).

On the other hand, Hagg (4) objected to Zachariasen's describing of glass formation tendencies from the view point of crystal structures, rather than from the view point of liquid structure, since glass was after all formed by the cooling of a liquid (5). Also, according to Zachariasen's theory, any metal or non-metal oxide should form a glass. However, the non-existence of a glassy form of TiO_2 or Al_2O_3 could not be explained using this theory. Hagg (4) who focused on the glass forming process from the point of view of the cooling process, believed that glasses consisted of chains or two-dimensional nets (sheets), and this was the main difference to Zachariasen's interpretation. Using this theory he was able to explain why species like SiO_2 formed glass and TiO_2 did not. Only materials which had one or two-dimensional, unlimited cross-linked units in the corresponding crystals would be able to form a glass. For example, SiO_2 exists in crystalline form as chain and ring silicates, which have unlimited cross-linking. However, TiO_2 'only' exists in the form of three defined crystal modifications, where oxygen atoms co-ordinate Ti in an octahedral form. There are no long chains or ring structures known (7).

While each of these schemes satisfactorily identified glass-forming oxides, none of them satisfactorily defined 'glass-forming ability'. This was based, in part, on the fact that they did not factor Zachariasen's fourth rule into their classification (5). To date no precise structural model exists which covers all the various glass types.

1.3 History of Phosphate-based Glass:

It was discovered very early that phosphorous pentoxide was a glass former. What made it different from the other classic glass formers was that although it formed a tetrahedral three-dimensional network, due to phosphorous being pentavalent; one of the four oxygens was double bonded, i.e. not coupled to the network, thus limiting its network connectivity. Although a silica like structure was possible, as in aluminium phosphate, normal alkali and alkaline-earth glasses tended to have chainlike structures due to the pentavalency of the phosphorous ion (1).

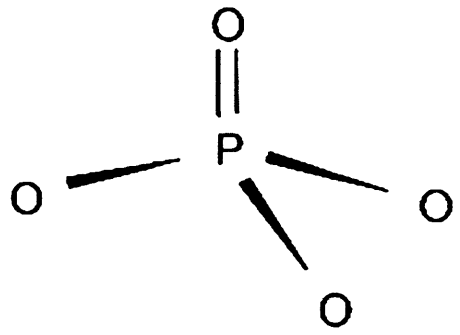

Figure 1.2a: PO_4^{3-} phosphate ion.

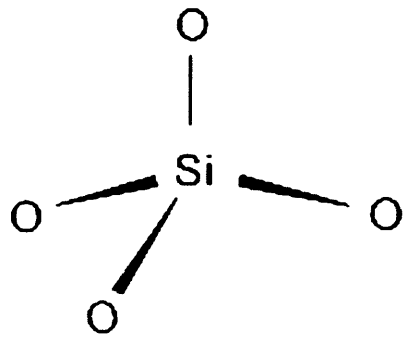

Figure 1.2b: SiO_4^{4-} monosilicate ion.

In 1871 Professor G.G. Stokes (8), presented a report to the 'British Association for the Advancement of Science', on the preparation and optical properties of various glass compositions prepared by the Late Mr. Harcourt, over a forty year period. It was stated that due to the problem of working with silicates, mainly due to the difficulty of synthesis and the pasty character of the fused glasses, Mr. Harcourt's experiments were conducted with phosphates, combined in many cases with fluorides, and sometimes with borates, tungstates, molybdates and or titanates. The glasses formed, also involved the elements potassium, sodium, lithium, barium, strontium, calcium, magnesium and many others. The main enquiry regarding these glasses was to find a glass which would achromatize (deprive the sample of colour) each other so as to exhibit no secondary spectrum.

In 1941, Kreidl and Weyl (9) discussed the history of phosphate-based glasses, and it appears that phosphates were used by many of the early investigators. They state that phosphorous pentoxide, which was first used to improve the colour of heavy flint glasses, was later recognised as a valuable constituent of optical glasses, with its excellent ultraviolet transmission, and low softening points. They also stated that glasses with a high content of P_2O_5 have poor chemical resistivity, and that this was largely overcome by the addition of alumina. The low melting and processing temperatures along with the low viscosity of the phosphate glasses also made them very useful as solder glasses.

Another very useful and important use for phosphate glasses emerged in 1988. Silicate glasses were usually preferred for laser glasses because of their

thermomechanical properties. However, phosphates were found to have superior laser characteristics, such as line widths, and laser cross section etc. as well as a low non-linear refractive index and fundamentally zero dependence of optical path length on temperature. One other and perhaps their most interesting property was their ability to dissolve ionic platinum, thus creating phosphate-based glasses which were free of inclusions. This was a very necessary quality for a high-power laser glass. Often it was desirable to have a glass with a very low softening point as well as a high thermal expansion coefficient, and phosphate glasses had been developed for such purposes. The high expansion coefficient with the associated low T_g was quite reasonable, because it was expected that by increasing the amount of flux, and thus, decreasing the melting or glass temperature (i.e. decreasing the bond strength in the solid), the thermal expansion coefficient would also increase for the same reason. However, and unfortunately in most cases, the usual additional consequence of this reduced bond strength was a decrease in chemical durability, which correlated with an increase in solubility (degradation) or corrosion rate (10).

Interestingly, Tick (11) discovered a fairly wide range of glass compositions in the lead tin fluorophosphate system. Some of the compositions within this group, developed for ophthalmic applications, showed a valuable combination of properties, such as low melting temperature (T_m), low glass temperature (i.e low glass transition temperature, T_g), and high thermal expansion coefficient (TEC), whilst retaining respectable chemical durability. The durability was strongly dependant on the amount of lead and tin within the glasses, but not strongly on

the amount of fluorine. Even very small changes of the lead content had a very strong impact on the durability. Even more surprising was that these glasses could be melted at approximately 400 °C, with a T_g approximately 100 °C, and yet still have chemical durability's comparable to that of soda-lime-silica glasses. The chemistry of the system was complex, and part of the behaviour of these glasses was attributed to phase separation. Tick stated that the durability was most sensitive to the lead content of the glasses and suggested that phase separation, probably arising from liquid –liquid immiscibility, occurred where the continuity of the more soluble phase would control the rate at which the network dissolved.

Brow *et al* (12) using x-ray photoelectron spectroscopy (XPS), examined the structure of the glasses made by Tick. They concluded that distorted Sn (O, F) polyhedra which were present in analogous crystalline compounds were also present in the Sn fluorophosphates glasses, and that these polyhedra probably had the greatest effect on glass properties. The low coordination number of Sn could lead to chain or layer structures, which could explain the low T_g, whereas the formation of F – P sites, seemed to have the greatest effect on the glass aqueous durability.

1.4 Structural Studies on Phosphate-based glasses by Van Wazer:

In 1950, a series of papers were published by John R. Van Wazer on the structure and properties of the condensed phosphates. The first of these was published by Van Wazer and Holst (13). This paper addressed general considerations about phosphoric acids, and acids corresponding to many condensed phosphates were prepared. Van Wazer and Holst stated that studies of orthophosphates, pyrophosphates, aluminium tetrametaphosphate, sodium trimetaphosphate, and the alpha and delta forms of phosphorous pentoxide had been completed. In all cases the structures were shown to be built up of interlinked PO_4^{3-} groups composed of four oxygen atoms situated at the corners of a tetrahedron in the centre of which was the phosphorous atom. The concept of phosphorous surrounded tetrahedrally by four oxygens was in accord with quantum theory and the combining of atomic dimensions. In condensed phosphates, the PO_4^{3-} tetrahedra were joined together by the sharing of oxygen atoms. Due to bond angle measurements, no more than two and probably only one oxygen atom could be shared between any two tetrahedra (See Figures below, redrawn from Van Wazer and Holst [13]).

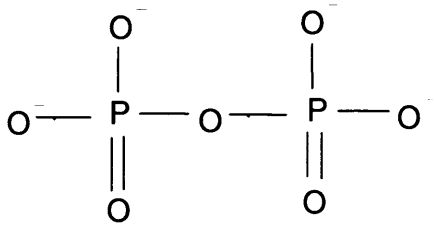

Single connection:

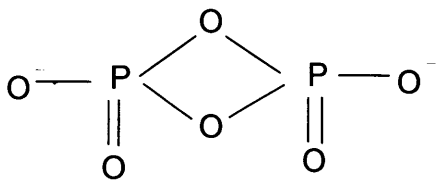

Double connection:

Figure 1.3a: Singly connected PO_4^{3-} group. Figure 1.3b: Double connection.

Due to the sharing of two oxygens between a pair of tetrahedra entailing the formation of a four membered ring, and hence a pronounced distortion of the bond angles, the single connection of Figure 3a was to be preferred.

The second of these papers by Van Wazer was regarding the theory of the molecular structure of sodium phosphate glasses (14). The author mainly focused on the binary Na_2O - P_2O_5 (sodium oxide and phosphorous pentoxide) system. Van Wazer wrote that according to recent views (he was quoting Zachariasen's work), the silicate and phosphate glasses consisted of a network of interlinked SiO_4^{2-} or PO_4^{3-} tetrahedra, in the interstices of which were interspersed cations, such as sodium. It had previously been demonstrated that in any environment in which reactions involving the degradation of condensed phosphates can occur, molecular arrangements where three of the oxygens of a PO_4^{3-} tetrahedron are shared with other tetrahedra will be exceedingly unstable, with respect to those in which one or two oxygens are shared. And since rearrangement and interchange of tetrahedra undoubtedly took place in sodium phosphate melts, there would be no PO_4^{3-} groups sharing three oxygens in the melt, as long as there was one sodium for each phosphorous. Therefore, the sodium phosphate glasses could be split into two groups (14). Van Wazer referred to these as Case 1, for which the Na_2O / P_2O_5 mole ratio was equal to or greater then unity, and case 2 for the range between pure P_2O_5 and $Na_2O.P_2O_5$.

Case 1: there are no branching points and hence the PO_4^{3-} groups must be interlinked into chains or rings.

Case 2: there are no terminal groups and branching is found, with the fraction of the total number of PO_4^{3-} groups at which branching occurs equal to $(P_2O_5\text{-}Na_2O) / P_2O_5$.

The third paper from this series was on solubility fractionation and other solubility studies. Van Wazer (15) stated that according to expectations, the polyphosphate mixtures corresponding to Case 1 of the theory were found to dissolve at a rate that was relatively independent of average molecular size until the average became very large. Then the rate determining step in the dissolution process consisted of untangling and freeing of the chains. According to theoretical predictions, a minimum was found in the rate of dissolution near the $Na_2O.2P_2O_5$ composition. In addition to this it was found that precipitates consisting of mixtures of crystalline pyro- and tripoly- phosphates were formed immediately upon the dissolution of glasses near the $5Na_2O.3P_2O_5$ composition. Methods used in the solubility fractionation of organic polymers were applied to the separation of fractions from sodium phosphate glasses lying in the range between the meta- and pyro- phosphate compositions. The fractions were analysed by pH titrations to find the ratio of the equivalent of total phosphorous to end-group phosphorous. The curves plotted from results obtained agreed satisfactorily with the chain length distributions found in Van Wazer's previous paper (14).

Van Wazer's fourth paper in this series, was regarding complex ion formation in polyphosphate solutions (16). Due to the fact that the common cations, except those of the alkali metals, ammonia and the amines, readily formed precipitates

with most of the phosphates, the range of concentrations were quite restricted and many of the standard methods of studying complexes could not be applied. Therefore, Van Wazer was limited to two experimental methods based on polarographic and electrometric pH techniques. Considering the structure of chains of the interlinked PO_4^{3-} tetrahedra, Van Wazer stated that a chelate ring might be completed between any two adjacent PO_4^{3-} tetrahedra. He went on to advance the hypothesis by stating that the strong complexing ability of the linear polyphosphates was due to the formation of these chelate rings (See figure 4 below, redrawn from Van Wazer [16]).

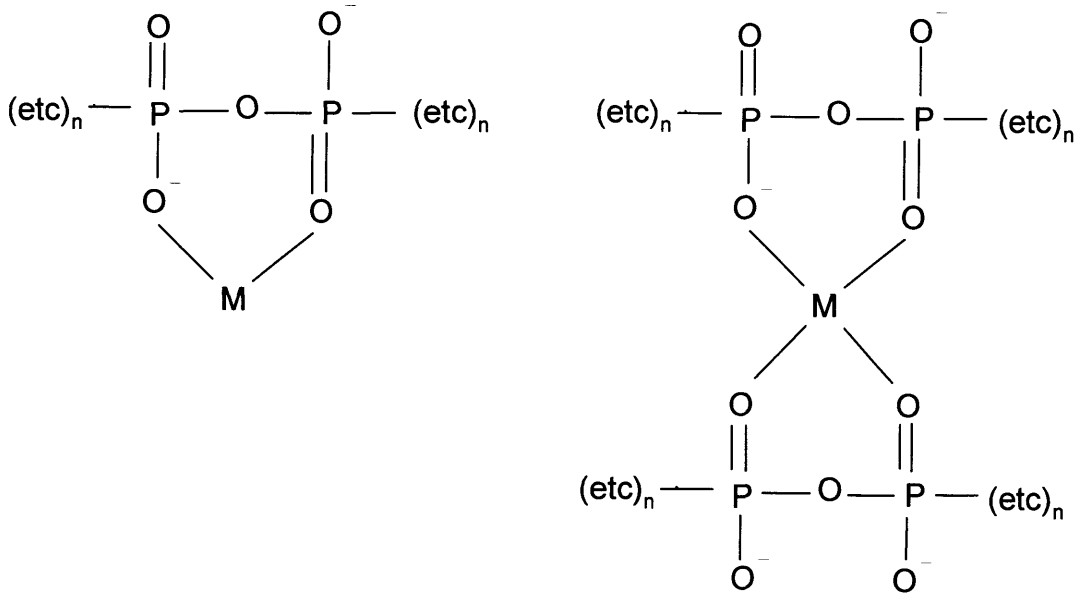

Figure 1.4: Formation of chelate rings between PO_4^{3-} tetrahedra (16).

1.5 Other Phosphate Related Structural Studies:

In 1956 Griffith (17) working in the Inorganic Chemicals Division, Monsanto, wrote a paper entitled 'New Sodium Phosphates'. Orthophosphoric acid was reacted with monosodium orthophosphate at elevated temperatures to form melts of acid metaphosphates. When seeded these melts yielded a new variety of crystalline phosphates which have the general formula $M_xH_y(PO_3)_{x+y}$, where M = metal ion. The following new compounds were prepared: $Na_2H_2(PO_3)_4$, $Na_2H(PO_3)_3$, $[Na_3H(PO_3)_4]_n$, $Na_2(NH_4)_2(PO_3)_4$, $CaNa_2(PO_3)_4$, and $Ka_2Na_2(PO_3)_4$, and for some, their properties were studied. Figure 1.5 shows the phase diagram of the Na_2O – H_2O – P_2O_5 system, and the various phase transformations that occurred (See Figure 1.5, redrawn from Griffith [17]).

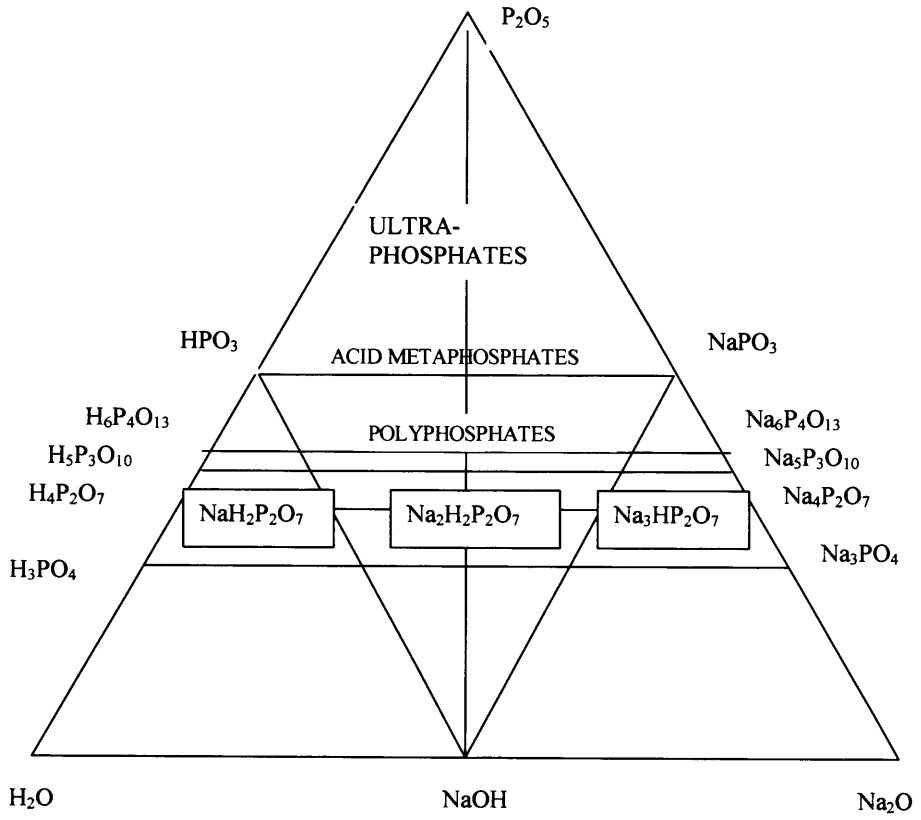

Figure 1.5: Phase Diagram of the Na_2O – H_2O – P_2O_5 system (17).

In the early 1960's Helen Ondik *et al* (18) published a paper on the monoclinic form of sodium tetrametaphosphate tetrahydrate. The structure was investigated using x-ray diffraction, and the crystals of the monoclinic form were said to be needle like in habit, and elongated along the c – axis. The unit cell dimensions were also given. Ondik (19) later published another paper on the structure of sodium tetrametaphosphate tetrahydrate, this time however, it was the triclinic form of the crystal that was investigated.

Starting in the 1970's a group of researchers working at the Laboratoire de Cristallographie, based in the Centre National de la Recherche Sciientifique (CNRS), in Grenoble (France), conducted a number of studies on the elucidation of the structures of alkali and alkali earth phosphates. The two main researchers that contributed to this research were M.T. Averbuch-Pouchot, and A. Durif. Previous to this, nearly all of the literature obtained focused mainly on binary phosphate glasses (i.e. various combinations of sodium oxide and phosphorous pentoxide). However, Averbuch-Pouchot and Durif concerned themselves with mainly ternary phosphate-based glasses, based on oxides of calcium, sodium and phosphorous. The structures under investigation were as diverse as $CaNa_4(PO_3)_6$ and $CaNa(PO_3)_3$ (20). $CaNa(PO_3)_3.3H_2O$ (21), and tetrapotassium tetrametaphosphate tetrahydrate ($K_4P_4O_{12}.\ 2H_2O$) (22). In the mid 1980's they wrote two review papers, entitled 'Contribution to the Crystal Chemistry of Tetrametaphosphates (I) and (II)'. These papers later also became chapters in 2 books by Durif and Averbuch-Pouchot entitled "Crystal Chemistry of Condensed Phosphates" (23) and "Topics in Phosphate Chemistry" (24).

Also during the 1990's both Durif and Averbuch-Pouchot have continued to publish their research on the crystal chemistry of phosphates and phosphate based compounds (25;26). There were also researchers in other laboratories, working on the determination of the crystal structures of phosphate compounds, both binary and ternary (27-31).

1.6 Phosphate Glass-Fibre Studies:

One of the earliest studies conducted on glass-fibres was done by Murgatroyd (91). There was considerable debate at that time regarding the orientation of the weaker bonds within the glass upon melting, and the aligning of them along the axis of the fibre. Otto and Preston (92) then published a paper entitled 'Evidence Against Oriented Structure in Glass Fibres'. They stated that the determination of fibre strength yielded approximately the same results, whether made by tensile or torsion tests under stresses applied longitudinally or at 45° to the length. Therefore, there could not be any orientation in any one direction. Brannan (93) wrote a paper entitled 'Further Evidence Against the Orientation of Structure in Glass Fibres'. He stated that the elastic properties of fine glass filaments of high strength lent no support to the view that the bonds were preferentially oriented. In particular, Poisson's ratio had a normal value very similar to that of the bulk glass, and that heat treatment of these fibres did not change Poisson's ratio.

However, Goldstein and Davies in 1955 (86) wrote that the concept of glass as a polymer of silicon, phosphorous, or other glass forming atoms connected by oxygen atoms suggested that fibres with oriented linear chains may be prepared.

Under drawing conditions indicated by the theory of viscoelastic properties of high polymers, fibres of sodium metaphosphate glass were prepared. The X-ray diffraction patterns obtained were similar to those of organic fibres with oriented chain molecules. Under analogous treatment, sodium metasilicate failed to give such effects. Milberg and Daly (94) also investigated the structure of sodium metaphosphate glass fibres, using cylindrical distribution functions obtained from the x-ray scattering pattern. The results indicated that the sodium metaphosphate fibres were made up of long chains of PO_4 tetrahedra, and that the axes of these chains had a strong preference for lying along the fibre axis direction.

Bruckner and Stockhurst (134) demonstrated how structure-sensitive properties of glass fibres were dependent on the variety of drawing parameters during fibre production, and how the structure of fibres was dependent on these parameters as opposed to the bulk glasses, and with fibres of different prehistories. The properties were also said to indicate significant anisotropies and orientation effects in the fibre structures.

A calcium sodium metaphosphate ($CaNa(PO_3)_3$ fibre was developed at Monsanto by Edward Griffith in 1978 (133). This fibre was said to exhibit an effective aspect ratio, and that it could also be used with a wide range of coupling agents, which increased its tensile strength and flexural modulus. The potential applications envisaged for this fibre were in reinforcing thermoplastics, thermosets and elastomers.

Kurkjian (135) investigated the properties of phosphate glasses. In particular the strengths of fibres drawn from three metaphosphate glasses. Karabulut *et al* (136) investigated the mechanical and structural properties of sodium, iron,

aluminium, phosphate and zinc, iron, aluminium, phosphate glasses and glass fibres. The fibres were exposed to air for ten days, and it was found that the tensile strength of all fibres decreased from 15% to 35%. Mossbauer and IR spectroscopy indicated that the structure of the bulk glass and corresponding fibres were similar for the compositions studied.

Choueka *et al* (124) investigated the effects of annealing temperatures on calcium phosphate fibres, designed for the reinforcement of bioabsorbable fracture fixation devices. The composition of these fibres also contained sodium, zinc and a 4.5% iron oxide content. It was found that annealing these fibres at higher temperatures reduced their degradation, and that upon degradation these fibres were still able to maintain their structural integrity.

Lin *et al* (138) investigated ternary calcium-iron phosphate glasses and glass-fibres with varying iron oxide content ranging from 5 to 22 wt%. The fibres drawn from the glass containing 22 wt% iron oxide, exhibited the highest tensile strength (over 1000 MPa). A cortical bone plug method was used to assess the biocompatibility of these glasses with hard and soft tissues. The tissues surrounding the samples showed no inflammation at 9 weeks.

1.7 Thermal Analysis on Phosphate Glasses:

To obtain thermal parameters, the two main pieces of equipment used are the Differential Scanning Calorimetry (DSC) and Differential Thermal Analysis (DTA). The DSC is a rapid quantitative and accurate way to determine the glass transition (T_g) temperature of the material in question (see section 2.3). However, its use can be rather limited due to limits imposed by maximum temperature usage.

The DTA however, is a more useful method of obtaining thermal parameters, as the temperature ranges used on the DTA can extend to 1000 °C and beyond. Along with obtaining T_g values, the T_c (crystallisation temperature) and T_m (melting temperature) of the materials under investigation can also be obtained.

The T_g temperature is a property of the bulk material, and is defined as the point at which a material changes from a glassy (solid) state to a rubbery state. The melting point occurs when the thermal vibration becomes so great that the bonds are broken and the atoms become mobile.

Crystallisation however, first requires the formation of a measurable number of nuclei, and then the occurrence of a measurable crystal growth rate. Crystal structures are regular three dimensional patterns of atoms in space. The regularity with which these atoms are packed into solids arises from geometrical conditions which are imposed by directional bonding and close packing (138). A

nucleus is a precursor to a crystal, and it also has an assemblage of atoms, but it does not have recognisable growth habit planes. Thus nucleation occurs because the atoms are constantly vibrating and moving around as a result of the thermal energy in the system. Once a critical sized nucleus has formed, crystal growth may occur by advancement of deposited atomic layers. The growth would clearly depend on how rapidly atoms could diffuse from liquid regions to the interface (139).

Hudgens and Martin (32) investigated a series of anhydrous lithium phosphate glasses, the glass transition temperatures of which were investigated using DSC (differential scanning calorimetry). They stated that the original 3D structure of vP_2O_5 degraded with the addition of alkali. This breakdown then allowed rearrangement to a 1-D chain structure at the metaphosphate composition where long chains or rings were formed. They noted that the T_g of the metaphosphate composition was only 50°C less than the T_g of vP_2O_5. They therefore proposed that the entanglement of the long chains caused an increase in T_g as the metaphosphate composition was approached. In addition they proposed that the T_g was also dependant on the nature and type of the cation. If the alkali was replaced by an alkaline earth of the same radius but double the charge, then the cation could cross-link two phosphate chains and the T_g would increase substantially.

Suzuya *et al* (33) also investigated the structure of vP_2O_5 and alkali phosphate glasses. T_g analysis conducted showed a decrease up to 10 mol% Na_2O, which

they state may have corresponded to the depolymerisation of the 3-D network structure. The T_g then reached a minimum at ≈ 20 mol% Na_2O and thereafter increased, which reflected the 3-D network restructuring associated with extended-range order.

Uo *et al* (34) looked at various compositions based on the ternary P_2O_5 – CaO – Na_2O system. A DTA system was used to investigate the thermal parameters in the glasses. They stated that the T_g and (T_c) temperatures decreased with increasing P_2O_5 content, and as CaO was progressively substituted for Na_2O.

Shih *et al* (35) investigated the thermal and corrosion behaviour of P_2O_5 – Na_2O – CuO glasses. It was found that the glass formation region was within the $P_2O_5 \geq 40$, $CuO \leq 50$ and $Na_2O \leq 60$ mol% ranges. It was found that substitution of CuO for Na_2O increased the T_g, the softening temperature, as well as the hardness and chemical durability, and decreased the thermal expansion coefficient.

Thermal analysis in the form of DSC or DTA is used routinely in the characterisation process for glasses. Data obtained pertaining to T_g studies is useful, as the T_g is a measure of the bulk glass, as opposed to specific properties. Also, with DTA analysis, information related to the crystallisation of the glass, and the melting temperature can also be obtained. The latter of which is crucial, as the melting temperature is required in order to pull glass-fibres.

1.8 Degradation Studies on Phosphate-Based Glasses:

During the 1950s other researchers were also looking into the structure of phosphates and phosphate-based glasses. Bell *et al* (36) published a paper on the preparation of sodium tetrametaphosphate, and also drew the structure of a P_4O_{10} molecule. Strauss and Treitler (37) published a paper on the chain branching in glassy polyphosphates. The occurrence of an initial decrease of both viscosity and pH in freshly prepared aqueous solutions of glassy sodium polyphosphates was investigated with samples whose Na / P ratios ranged from 0.968 to 1.055. They stated that this effect was due to the hydrolysis of weak bonds in the polymer molecules, which they confirmed by showing that the first order rate constants of both the reduced viscosity and pH decreased.

It was known that both the cyclic tetrametaphosphate and linear tetraphosphate polymer hydrolysed to form orthophosphate as a final product. However, little was known about their rates or reaction equations. The hydrolysis of tetraphosphate was thought to have more than one mode of attack by a water molecule. If only the middle oxygen bridge was attacked, two moles of pyrophosphate were formed initially; if only an end bridge was attacked, one mole of each of the triphosphate and orthophosphate were produced. While a uniform attack on all oxygen bridges would produce tri-, pyro- and orthophosphate in equimolar amounts. Therefore, Crowther and Westman (38) measured the rates of hydrolysis of sodium tetrametaphosphate and tetraphosphate at 65.5°C. They stated that tetrametaphosphate anions hydrolysed to tetraphosphate which in turn hydrolysed

to triphosphate and orthophosphate, and not pyrophosphate. Thus it was the terminal oxygen bridges in the tetraphosphate and not the central bridges that were attacked preferentially. The reactions were said to be of first order and acid catalysed.

Rates of aqueous dissolution were reported for a series of phosphate-based glasses by Bunker *et al* (39), having the composition (50 – X) M_2O, (X) CaO, 50 P_2O_5. Phosphate-based glasses frequently have poor chemical durability in aqueous solutions, for this reason many glass technologists have often avoided using phosphate glasses in applications where their unique physical properties, such as high thermal expansion coefficients, low melting points and optical characteristics, would otherwise make them superior to silicate glasses.

Dissolution reactions involving the consumption of H^+ and OH^- were investigated using pH stat titration techniques, solution analyses using inductively coupled plasma emission, depth profiling of corroded glass surfaces for H^+ and other elements using elastic recoil detection analysis and Rutherford backscattering (39). These analytical results indicated that phosphate glasses dissolved uniformly due to acid- or base-catalysed hydration of the polymeric phosphate network. The rate and nature of the hydration appeared to be controlled by the surface pH and / or charge which developed at the glass / solution interface. Bunker *et al* went on to say that in order to understand the wide range of chemical durability's and to develop phosphate-based glasses with optimum durability and physical properties for given applications and environmental conditions, it was necessary to understand how the hydrogen containing species, specifically H_2O,

OH^- and H^+ (or H_3O^+), reacted at the glass / solution interface. In order to determine the dissolution mechanisms it was important to outline the types of reactions that can occur between water and glass, these included acid / base reactions, hydrolysis reactions, and hydration reactions.

Studies conducted on short chain polymers indicated that that there were three types of acid / base sites on polymeric phosphates (see Figure1.6, redrawn from Bunker et al [89]);

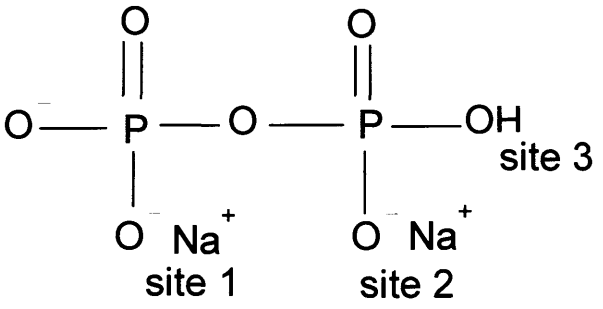

Figure 1.6: Acid base sites on polymeric phosphates (89).

These sites are depicted as they appear in the bulk glass. Sites 1 and 2 can be protonated in solution at appropriate pH values. Van Wazer had demonstrated that sites which lie along the chain, such as site 1, had a pKa (dissociation constant) which lay between pH1 and pH2 (13). These 'middle' groups were thus in the anionic form when the solution pH was above pH2 and were associated with cations such as Na^+ and Ca^{2+}. The chain terminating groups, sites 2 and 3, were said to be weak diprotic acids. Van Wazer's results indicated that the pKa values for these groups were sensitive to the presence of ions in solution such as

Na^+ and Ca^{2+}. The acid / base reactions discussed above were able to aid glass dissolution by disrupting the ionic interactions between chains. These reactions controlled the pH at the glass surface and the acid or base consumption observed in the pH stat titrations (39).

The second type of reaction to consider was the hydrolysis reaction. This reaction resulted in the cleavage of P–O–P bonds, which could lead to the ultimate destruction of the polymeric phosphate network to produce orthophosphate (PO_4^{3}). See Figure 1.7 below, redrawn from Bunker et al (89).

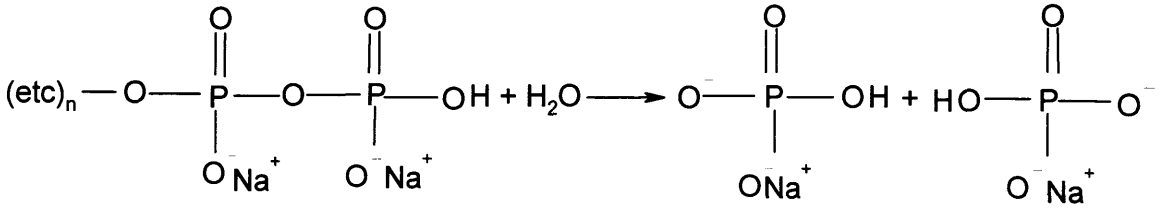

Figure 1.7: Hydrolysis of the linear phosphates (89).

The hydrolysis of the linear polymeric phosphates was said to exhibit clear pH dependence. In acidic solutions this pH dependence was similar to that seen for the phosphate glass dissolution rates. Hydrolysis was also said to be accelerated in acids with a fractional dependence on $[H^+]$. Bunker *et al* also stated that hydrolysis did not appear to be accelerated in basic solutions, and that the rate determining step for the dissolution of these phosphate glasses, was probably not the hydrolysis of the long polymeric chains in the phosphate network.

The third type of reaction that could possibly occur was the hydration reaction. This dissolution mechanism involved the hydration of intact entire phosphate chains. In acidic solutions above pH 3, each terminal phosphate group was predicted to react to consume one proton as the glass dissolved. Middle groups having a pKa below 2 were not protonated. Therefore, two protons would be consumed for each chain which dissolved from the glass. The pH stat results obtained by Bunker *et al* showed that one proton was consumed for every twenty or so phosphorous atoms that went into solution. This meant that the number average chain length of dissolving chains was around 40. The fact that the number average chain length found in solution was the same as that calculated for the bulk glass, suggested that the dissolution mechanism involved hydration of intact entire chains, rather than cleavage of P – O bonds by hydrolysis reactions.

The above paper by Bunker *et al* (89) has become one of the most commonly cited papers, with regards to dissolution in phosphate glasses. It outlined the possible reactions that could occur during the dissolution process, and also cited dissolution rates obtained from the compositions investigated, which were ideal for comparison sake.

1.9 Solid State Nuclear Magnetic Resonance Spectroscopy on Phosphate Glasses:

In 1991 Martin (40) wrote a review on the structure of phosphate glasses. He stated that in normal, low pressure conditions, it appeared that phosphorous retained a four-fold coordination throughout the full composition range from pure P_2O_5 to the fully alkali oxide saturated orthophosphate compound M_3PO_4. The fact that phosphorous retained a fixed coordination greatly simplified the possible structural units that could be built from individual phosphorous centres. Structural simplicity, similar to the phosphates, existed in the binary silicate system and a **Q** site model was proposed to describe the structures of these glasses. Here, each added alkali formed one non-bridging oxygen about a silicon atom. As more and more alkali was added, stoichiometry required more non-bridging oxygens to form around each silicon. A similar approach first appeared to have been applied to the phosphates by Van Wazer. The structural groups are listed below in Figure 1.8 (redrawn from Martin (40).

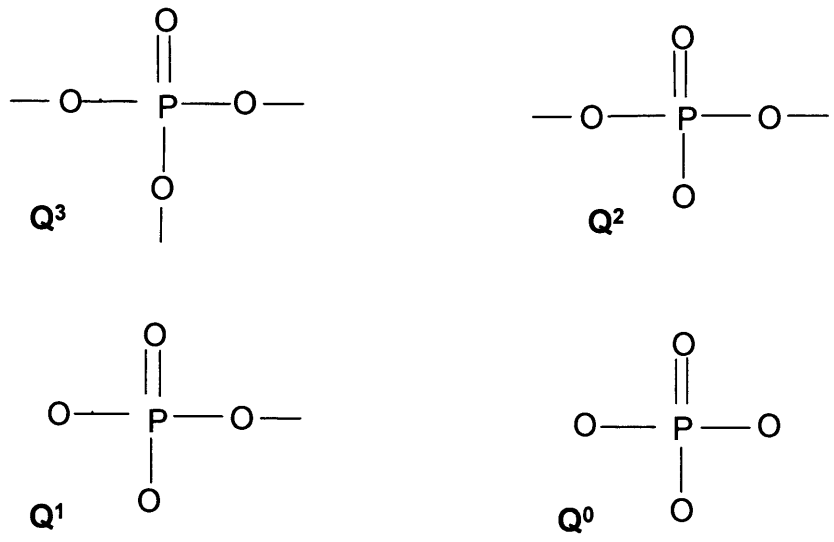

Figure 1.8: **Q** site nomenclature of the phosphate species present in glass (40).

In the **Q** site model of phosphate glasses these different groups participate in the structure to an extent dependant upon composition. As alkali oxide is added to P_2O_5, the phosphate structural groups pass from Q^3 to Q^2 to Q^1 to Q^0 as M_2O / P_2O_5 = R, passes from R = 0 to 1 to 2 and finally 3. In this model, the problem of determining the structure of phosphate glasses becomes one of determining the composition dependence of the individual **Q** – species. Van Wazer used a mathematical approach based upon the hypothesis that the fractions of different groups were controlled by the magnitude of the equilibrium constants describing the reaction of M_2O with each **Q**-species, except of course the fully saturated Q^3 species. These reactions are shown in Figure 1.9.

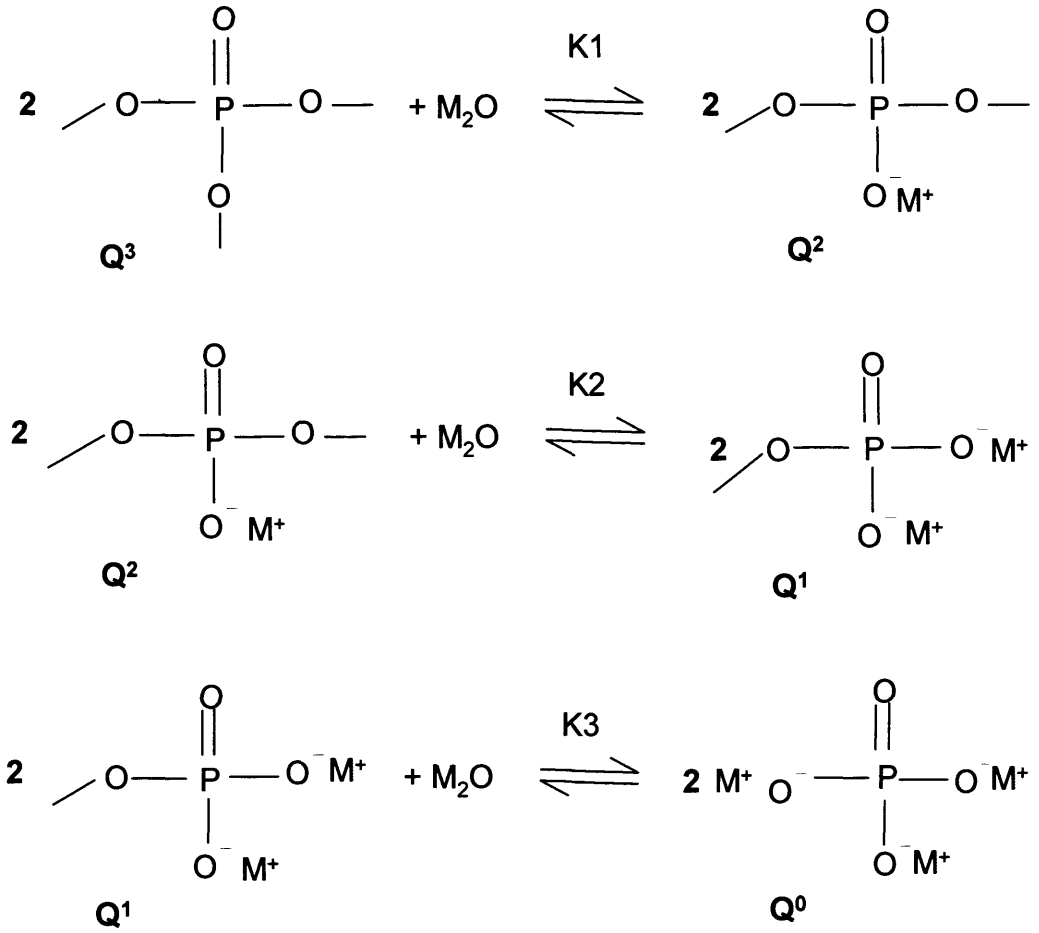

Figure 1.9: Structural changes by adding alkali oxides to P_2O_5 with **Q** – nomenclature (40).

In 1990 Brow *et al* (41) investigated the short range structure of sodium phosphate glasses using MAS-NMR. They stated that MAS-NMR was rapidly becoming an important spectroscopic technique for characterising the structures of solid inorganic materials. A series of $x(Na_2O + H_2O)$. $(1-x)$ P_2O_5 glasses were prepared and characterised by ^{31}P and ^{23}Na MAS-NMR spectroscopy. The spectra obtained revealed the presence of Q^2 and Q^3 tetrahedral sites in glasses where $x < 0.5$, and Q^2 and Q^1 tetrahedral sites were detected in glasses where $x > 0.5$. Quantitative measurements of the respective NMR site populations were in

excellent agreement with Van Wazer's predictions for the structures of ionic phosphates and illustrated the depolymerising effects of residual H_2O on the glass structure.

Hartmann *et al* (42) investigated glasses and glass ceramics in the P_2O_5-CaO-Na_2O-(Al_2O_3) and P_2O_5-CaO-Na_2O-MgO-(Al_2O_3) system. They stated that acidic phosphate glasses with > 50 mol% P_2O_5 consisted of a three dimensional network formed by Q^3 and Q^2 groups, which were unstable to moisture. Phosphate glasses containing nearly 50 mol% of modifying oxides consisted of long chains or rings formed by Q^2 groups with structures similar to organic polymers. Invert phosphate glasses formed exclusively by Q^1 and Q^0 groups were said to be similar to the mineral component of human bone (Hydroxyapatite, $Ca_{10}(PO_4)_6(OH)_2$ i.e. Q^0 groups). Their investigation concluded that the glasses of the system P_2O_5 – CaO - Na_2O possessed only Q^2 and Q^1 groups. The fraction of Q^1 groups increased in proportion to the content of the network modifying oxides, while the fraction of the Q^2 groups decreased. They concluded by stating that the glasses they investigated consisted of short phosphate chains (or rings) along with diphosphate (Q^1) groups.

In 1995 Kirkpatrick and Brow (43) presented a review of the NMR data for phosphate and phosphate containing glasses. They stated that it was useful to think of the structures of phosphate glasses in terms of the polymerisation of the phosphate tetrahedra, because for most compositions the P – O bonds are by far the strongest. The structures of alkali phosphate glasses, for instance, can be

thought of as polymeric units of strongly bonded phosphate tetrahedra held together by weaker O – M – O bonds (where M = alkali cation). The relatively strong P – O – P bonds linking the tetrahedra within the polymers and the consequently relatively weak M – O bonds holding the polymers or isolated tetrahedra together accounted for example, the relatively large thermal expansion coefficients of these materials. ^{31}P NMR data, in conjunction with ^{27}A, ^{29}Si, ^{11}B, ^{7}Li and ^{23}Na data where appropriate, proved very powerful in providing direct evidence about the local structural environments present in these materials.

In 1997 Abrahams *et al* (44) conducted a combined solid state NMR and X-ray powder diffraction (XRPD) study on a series of phosphate-based glasses and glass ceramics, based on the general formula $(P_2O_5)_{0.45}$ $(CaO)_{0.2}$ + $(Na_2O)_{0.35 - x}$, where x = 0.0 – 0.12. They concluded by stating that the ceramics all had Q^1 phosphorous species mainly present as pyrophosphate. For the sodium rich sample (x = O) the principal component was most likely $Na_2CaP_2O_7$, for compositions with x = 0.08, there was a mixture of $Na_2CaP_2O_7$ and α-CaP_2O_7. In the sodium depleted samples (x = 0.12) there was a mixture of the α and β-forms of CaP_2O_7, with the latter dominating.

Another study conducted in 1997 by Abrahams *et al* (45) also focused on combining XRPD and MAS ^{23}Na, ^{27}Al, and ^{31}P NMR spectroscopy to investigate phosphate speciation in a series of glasses and glass ceramics of the general formula $(P_2O_5)_{0.45}$ $(CaO)_{0.24}$ $(Na_2O)_{0.31 - x}(Al_2O_3)_x$, where x = 0.0 – 0.05. The principle phosphate species were shown to be various $P_2O_7^{4-}$ containing phases

(Q^1), and cyclic trimetaphosphates bridged by Ca i.e. $Na_4Ca(PO_3)_6$. See Figure 1.10 (redrawn from Abrahams *et al* (45).

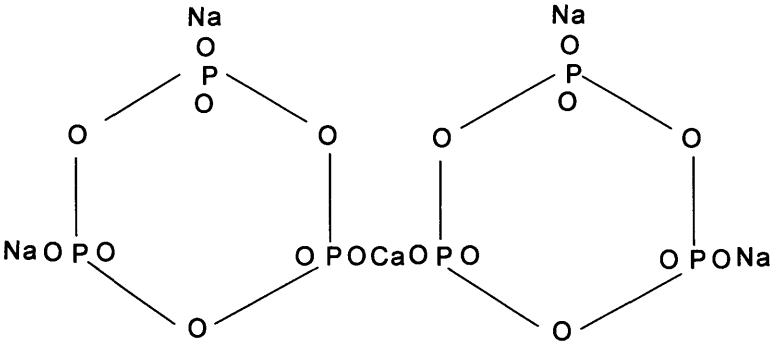

Figure 1.10: Suggested Structure for $Na_4Ca(PO_3)_6$ (45).

The crystal structure of the major phase present ($Na_4Ca(PO_3)_6$, is unknown; however, it had been suggested that the structure was a calcium-bridged trimetaphosphate. Higher concentrations of Al_2O_3 resulted in glass ceramics which were phosphate depolymerised (Q^2 – Q^1) with respect to the parent glasses. At lower levels of Al_2O_3 the aluminium was said to be present in octahedral coordination, while at higher levels it was said to be present in the form of tetrahedrally coordinated aluminium. The predominance of Q^2 units was indicative of cyclic or long-chain phosphates.

By now it was becoming commonplace to use a variety of techniques to verify structures in phosphate glasses. In 1996 Hoppe (46) wrote a paper on a structural model for phosphate glasses. He projected that in addition to the common depolymerisation process, further structural principles were in effect. It was proposed that all of the terminal oxygen atoms, including those doubly bonded within the PO_4^{3-} branching groups, tended to coordinate a network

modifier cation. He went on to say that in the first range this would lead on to an effect which could be called a re-polymerisation based on modifier oxide additions. The coordination of a modifier ion, was the source for the re-polymerisation effect with all of the PO_4^{3-} units finally being four-connected to either P (phosphate) or Me (metal) atoms, with the Me atoms dominantly linked by Me – O – P bridges. Hoppe *et al* (47) also investigated the mixed alkali – alkaline earth effect in Ba and Na metaphosphate glasses, using X-ray diffraction methods. The results obtained suggested a behaviour which was not different from that expected for a random occupation of the Ba^{2+} and Na^{+} ions on the cationic sites. Therefore, it was concluded that the formation of dissimilar pairs of modifier cations was not a large factor in the presence of the mixed samples.

NMR is routinely used for the accurate determination of nuclear moments. The main application of NMR is as a technique for chemical analysis and structure determination. It depends on the fact that the electrons in a molecule shield the nucleus to some extent from the field, causing different atoms to absorb at slightly different frequencies. Such effects are known as chemical shifts. This technique gives detailed information about the surrounding environment around the nucleus under investigation. Only magnetically active nuclei such as isotopes of H, C, N, F and P, which have a nuclear spin different from zero, can be observed using this technique

1.10 Other Techniques used in the Study of Phosphate-Based Glasses:

X-Ray diffraction (XRD) was still the most popular choice of analysis for phosphate-based glasses. Kranold *et al* (48) in 1998 published a paper on the intermediate range order of metaphosphate glasses, studied using X-ray diffraction. Metaphosphate glasses containing the metal ions Me = Li, Na, K, Ag, Mg, Ca, Co, Zn, Sr, Cd, Ba, Pb, Al, and La were all investigated.

In 2000 Brow (49) published a review on the structure of simple phosphates, and discussed phosphate glasses from the vitreous P_2O_5, metaphosphate, pyrophosphate to orthophosphate compositions. The techniques discussed included NMR, Raman spectroscopy, X-ray photoelectron spectroscopy (XPS), high performance liquid chromatography (HPLC) and Neutron Diffraction studies.

1.10.1 Raman and Infra-red Spectroscopy:

Pemberton and Latifzadeh (50) performed Raman spectroscopy on a series of calcium phosphate glasses, in which the CaO content varied from that of the metaphosphate stoichiometry in which the mole ratio of CaO to P_2O_5 was 1.00, to a stoichiometry of which the mole ratio was 1.49. Investigation of the vibrational behaviour showed a depolymerisation of the phosphate chains observed in the vibrational spectra, which was indicated by shifts in the $_{vs}$(POP), $_{vs}$(PO_2), and $_{vas}$(PO_2) vibrations (where vs = very strong, and vas = asymmetric stretch). At the largest CaO concentrations, distinct crystalline phases of ά- and γ- CaP_2O_7 were

seen. Their analysis seemed to suggest that crystallisation occurred from the short chain regions of the glass. Meyer (51) also investigated the structure of binary calcium ultraphosphate glasses by infra-red and Raman spectroscopy.

Hudgens *et al* (52) prepared and examined binary phosphate glasses containing 0 to 50 mol% Li_2O or Na_2O using Raman spectroscopy. Their investigations showed that vitreous P_2O_5 had a band near 1390 cm^{-1} due to the stretching of a terminal P = O bond and another high intensity mode near 640 cm^{-1} due to the symmetric stretch of bridging oxygens. With the addition of alkali oxide to P_2O_5, a new band near 1160 cm^{-1} grew in the Raman spectra, which was due to the stretching modes of a non-bridging oxygen on a Q^2 tetrahedron. With increasing alkali content this band increased in relative amplitude, but did not shift in frequency. This was consistent with the simple depolymerisation of the Q^3 phosphate network. From 20 – 50 mol% alkali oxide the $(P{=}O)_{sym}$ band frequency decreased by approximately 130 cm^{-1}. This shift was said to be due to the delocalisation of π-bonding on Q^3 tetrahedra, from the P = O terminal oxygen bond to the bridging P – O – P oxygen bonds.

Shih *et al* (53) using Fourier Transform Infrared (FTIR) spectroscopy investigated the short range structure of ternary sodium-copper-phosphate [40-70(P_2O_5) – 0 – 60(Na_2O) – (0-50)CuO] glasses. In the ultraphosphate and metaphosphate glasses, the P – O – Cu bonds were formed replacing P – O – Na^+ bonds while keeping the same fraction of P – O – P bonds, as Na_2O was replaced by CuO. Whereas, in the polyphosphate glasses, the formation of P – O – Cu would

replace both P – O – P and P – O – Na^+ bonds. Their results showed the formation of P – O – Cu bonds in these glasses and an increase in cross-link density. Chemical durability and T_g of the glasses also increased.

Peitl *et al* (54) investigated glass ceramics in the P_2O_5 – Na_2O – CaO – SiO_2 system, and FTIR was used to determine the rate of hydroxy carbonate apatite (HCA) formation. From the ion solution measurements conducted it was possible to identify five reaction stages, which lead to HCA formation that correlated with changes in FTIR spectra.

FTIR and Raman spectroscopy are based on absorption and scattering of electromagnetic radiation at different wavenumbers, due to resonance vibrations of different chemical groups of a molecule. The two techniques are thus used to confirm the presence of various structural groups.

1.10.2 XPS Studies on Phosphate-Based Glasses:

Photoelectrons, which have been ejected by the x-ray bombardment of the specimen, could be analysed by the correlation of the expended x-ray radiation and their kinetic energy (E_k). This correlation was given by:

$hv = E_k + E_b$

Where E_b = binding energy, hv = energy of X-ray radiation and E_k = kinetic energy of ejected photoelectrons.

This equation showed that the kinetic energy (E_k) of the emitted electron was dependant on the energy of the incident photon (hv) and its binding energy (E_b). The measured kinetic energy and therefore binding energy would give information about the atom and its orbital state, which was a characteristic for the material. Commonly, photons were used in the soft x-ray region; however, according to different chemical environments, a difference in binding energy for the inner shell electrons can be detected and used for structural investigations. For example, by comparing integrated areas under the peaks, it was possible to estimate the stoichiometry (7).

According to Brow *et al* (49), there has been some controversy about the different oxygen species in phosphate glasses, particularly as it related to the relevance of distinguishing 'double bonded' oxygens from 'non bridging oxygens. For example, a Q^2 tetrahedron is often represented as possessing one P = O and one $P - O^- - R^+$ terminal oxygen bond, with the implication being that the double bond is shorter due to the localisation of the fifth valence electron from P^{5+}. This

description was supported by an earlier XPS study in which the O1s spectra from various phosphate glasses were decomposed into three components representing distinct P = O, P – O^- - R^+ and P – O – P species. However, subsequent diffraction studies of metaphosphate glasses challenge this assumption, revealing instead that the two double bonds (P = O) on a Q^2 tetrahedron are indistinguishable. Given these results, the correct way to decompose the O1s spectra from simple phosphate glasses seemed to be a two-peak fit.

Shih *et al* (53) investigated the ternary sodium-copper-phosphate glasses using FTIR and XPS studies, and found that the XPS studies were in agreement with their FTIR spectroscopy data, mentioned earlier (section 1.81).

1.10.3 Neutron Diffraction Studies on Phosphate-Based Glasses:

In Quantum Physics, neutrons are particles that occur as building blocks of atomic nuclei. In reactors, neutrons can be set free when nuclei decay (fission, radioactivity). All quantum particles can exhibit wave phenomena, similar to what is typically associated with light or sound. Diffraction is one of those phenomena; it occurs when a wave encounters an obstacle whose size is comparable with the wave length of the incident light. If the wave length of a quantum particle is short enough, atoms or their nuclei can serve as diffraction obstacles. When neutrons from a reactor are slowed down and selected, their wave length lies near one Angstrom, the typical separation between atoms in a solid material.

A neutron diffraction measurement requires a neutron source (e.g. a reactor), a target (the material to be studied) and a detector. Other components may also be needed to select the desired neutron wavelength. Neutron diffraction then reveals structural details of the target material, which are measured by recording the way in which neutrons are deflected. Neutrons can also change their speed during the scattering experiment; this is used to study the types of vibrations that can occur in the solid. An important difference between neutron and X-ray diffraction is that neutrons are sensitive to magnetic forces in the material.

Suzuya *et al* (33) investigated the structure of vitreous P_2O_5 and alkali phosphate glasses using neutron scattering. Results for v-P_2O_5, Na ultraphosphate glasses of composition $(Na_2O)_x\ (P_2O_5)_{100\ -\ x}$ (x = 10, 20), and alkali metaphosphate glasses, $MePO_3$ (where Me = Li, Na, K, Rb and Cs) were presented. Intermediate-range order in v-P_2O_5, which was characterized by two neutron diffraction peaks at Q = 1.30 and 2.12 Å - 1, could be substantially represented by a Random Packing Structural Units (RPSU) model based on parallel oriented P_4O_{10} molecular units. The RPSU model uses structural units or molecules distributed according to the random packing of hard spheres with either uncorrelated (random) or identical (parallel) orientations. The addition of an alkali metal modifier (Na), affects the intermediate range structure due to the depolymerisation of the PO_4^{3-} network and reconstruction of the network associated with extended-range order.

Hoppe *et al* (55;56) used neutron diffraction studies to investigate the variation in P – O bonding in phosphate glasses. Two different lengths of P – O bonds in the

PO_4^{3-} units of phosphate glasses were found. The two lengths were related to bonds of the phosphorous atom with the terminal and bridging oxygen atoms. These lengths changed as a function of the P_2O_5 content and of the species of the modifier cation.

Walter *et al* (57) investigated the short and intermediate range order of invert glasses of the system $CaO\text{-}Na_2O\text{-}MgO\text{-}P_2O_5$, using a combination of X-ray, MAS-NMR and neutron diffraction studies. A depolymerisation effect of the phosphate chains was seen with decreasing P_2O_5 content from 39.4 to 28.7 mol%. With progressive depolymerisation the structure of the glasses became more compact, which was indicated by the shortening of the distances between the MeO (Me = metal ion) polyhedra and between the decreasingly long PO_4^{3-} chains, which correlated with an increase in the packing density. These changes induced as a consequence, an increase in the glass transition temperature (T_g), and the chemical durability.

1.10.4 High Performance Liquid Chromatography Studies on Phosphate based Glasses:

Sales *et al* (58) investigated the distributions of phosphate-anion chains and rings in a variety of zinc-phosphate based glasses, using HPLC. The phosphate-anion distributions in simple binary zinc phosphate glasses were compared to those found in multi-cation alkali-zinc phosphate glasses. It was found and suggested that the multi-cation zinc phosphate glasses were chemically durable, and could be tailored to exhibit transition temperatures sufficiently low for co-processing with

a variety of plastics to form novel organic – inorganic composite materials. The ease of glass formation was attributed to the ability of a large number of different metal cations to frustrate crystallisation. All of the HPLC data obtained was consistent with Zn acting as a simple modifier in these glasses. Sales *et al* (59) also wrote a review about chromatographic studies on the structures of amorphous phosphates. The experimental details of the HPLC technique were presented, along with the strengths and limitations of the technique. The information obtained using HPLC was compared with other techniques such as NMR and XPS.

High-performance liquid chromatography (HPLC) is a form of liquid chromatography used to separate compounds that are dissolved in solution. It is a sensitive technique for separating or analysing mixtures, in which the sample is forced through the chromatography column under pressure.

1.11 Biocompatibility Studies on Phosphate-Based Glasses:

In 1985 Drake and Allen (60) wrote about the use of controlled-release glass (CRG) for the controlled delivery of bioactive materials. Approximately 15 trace elements were considered to be essential for the survival of animal life. Copper and cobalt were two that had been associated with deficiency diseases. Deficiency of either of these elements could cause economic losses from clinical disease and reduced efficiency of production in live stock farming. In many areas of the world, supplementation must be provided to avoid these losses. Copper

can be supplied to animals by either the parenteral or oral route; however, parenteral treatments were only effective for a short term period. A continuous supply of cobalt must be provided orally to maintain the vitamin B_{12} synthesis in the rumen. Metallic cobalt bullets had been used in both sheep and cattle to counteract deficiency states. They were effective in sheep, but in cattle their efficacy was limited, and it had also been reported that the rate of release of cobalt declined rapidly within weeks of administration. In an attempt to provide a regular, long term supply of trace elements, a series of CRGs were formulated. Cu-CRG was administered as a bolus to a variety of experimental and domestic animals, and it was confirmed that it provided a sustained supply of copper to the gastrointestinal tract for up to 3 months. Similarly, Co-CRG provided a sustained release of cobalt for up to 5 months.

Uo *et al* (34) investigated the properties and cytotoxicity on various compositions based on the $Na_2O - CaO - P_2O_5$ formula. Cytotoxicity tests were conducted with human cells. The cells were cultured in medium (α-MEM) containing 10% foetal bovine-serum. They stated that the cytotoxicity decreased with increasing CaO content and with decreasing P_2O_5 content. It was suggested that this was due to the change in pH and ionic strength of the medium, due to the dissolution of the glasses. In acidic compositions which contained more than half P_2O_5, the pH of the media became acidic due to the dissolution of the glasses. This was stated to be the main cause of the cytotoxicity of these samples. In contrast glasses containing 50 mol% P_2O_5, which were said to be neutral, did not affect the pH of the media, but did affect the ion concentration of the media.

Franks *et al* (61) and Salih *et al* (62) investigated the development of soluble glasses for biomedical use. In their studies, glasses were developed for biomedical applications containing P_2O_5 as a network former, and CaO and Na_2O as modifiers. These glasses were considered to be of potential clinical value in orthopaedic and dental surgery; however, the biological response to these materials was not well understood. To determine the effects of these glasses two human osteoblast cell lines, MG63 and HOS (TE85), were incubated *in vitro* in the presence of increasing concentrations of extracts of the glasses. The effects of the extracts on cell growth were measured using an MTT assay, and an ELISA assay was used to measure the expression of bone sialoprotein (BSP), osteonectin (ON), and fibronectin (FN) antigens which play a fundamental part in the integrity and function of hard connective tissue. The results showed that the proliferation of the cells was adversely affected by the more soluble glasses, which also down-regulated the expression of the bone-associated proteins. In contrast, the extract of the glass with the lowest dissolution rate, which contained elevated levels of Ca^{2+}, was found to enhance bone cell growth and antigen expression. Franks *et al* (63) also investigated the thermal parameters and crystallisation of the above mentioned glass systems. In a further study conducted by Franks *et al* (64) the quaternary component magnesium oxide (MgO) was added to the above ternary glass system, and cell proliferation along with the solubility was investigated. The MTT assay conducted suggested that the growth of MG63 cells in the presence of four different glass extracts remained largely unaffected, and after five days in culture, apparently increased cell proliferation in some cases, particularly for the glasses containing 7 or more mol%

Mg. Knowles *et al* (65) further investigated the solubility and ion release in a similar glass system; however, they incorporated the quaternary component potassium oxide (K_2O) in their glass system. A review was also written by Knowles (66) which discussed the potential clinical applications currently under investigation with phosphate based glasses.

Kesisoglou *et al* (67) looked at the effects of various phosphate-based glasses on T – lymphocytes *in vitro*. Host responses to implanted materials can lead to the production of inflammatory mediators and thus induce potentially adverse reactions, including the activation of T-lymphocytes. Extracts of phosphate-based glasses modified via the addition of Ca, Co, Zn and Fe oxides were found to cause only very low levels of activation of human peripheral blood T-lymphocytes over a period of 6 days, as measured by changes in DNA synthesis.

Gough *et al* (68) investigated the synthesis and degradation, along with the *in vitro* cell responses of sodium phosphate glasses for craniofacial bone repair. The biocompatibility studies were conducted using a macrophage cell line and primary human osteoblasts. These studies suggested minimal macrophage activation, and high osteoblast biocompatibility. A further study conducted by Gough *et al* (69) investigated the characteristics of human craniofacial osteoblasts cultured on sodium phosphate, and sodium - calcium phosphate glasses. The characteristics investigated were attachment, proliferation, alkaline phosphatase activity, collagen- type 1 production and mineralization. It was seen that osteoblasts were able to attach, spread and proliferate in a manner comparable

with the positive control. Formation of a collagen-rich mineralized matrix was also seen.

Ahmed *et al* (70;71) investigated ternary phosphate glasses and glass-fibres based on the Na_2O – CaO – P_2O_5 glass system. These glasses had a varying phosphate content of 45 to 50 to 55 mol%, and the CaO content was kept constant at 30, 35 and 40 mol%. It was concluded that the glasses and glass-fibres were too soluble for cell attachment. Ahmed *et al* (72) then incorporated the quaternary component iron oxide (Fe_2O_3) into the above glass system (from between 1 – 5 mol% of Fe_2O_3) and it was seen from the biocompatibility studies conducted that iron phosphate glass fibres containing 4 -5 mol% Fe_2O_3, were sufficient for cell attachment and differentiation. The biocompatibility studies were conducted using a muscle precursor cell line derived from the H-"Kb-tsA58 immortomouse. It was seen that myotubes formed along the axis of the fibres (which was indicative of differentiation). The biocompatibility of these compositions was attributed to the enhanced chemical durability of the glass fibres.

Bitar *et al* (73) investigated the effects of seeding human oral osteoblasts, oral fibroblasts and hand flexor tendon fibroblasts on phosphate-based glasses. The data indicated that glasses containing higher calcium content supported the attachment, growth and maintenance of differentiation of the human osteoblasts and fibroblasts.

1.12 Aims and Objectives:

The compositions initially to be investigated are based on the ternary P_2O_5-CaO-Na_2O glass system. The phosphate content will initially be varied from between 45 to 55 mol%, along with the calcium oxide content (from between 30, 35 and 40 mol%). Some of these glass systems have previously been investigated within the department and elsewhere (7) and there have already been a number of research papers concerning various compositions within this glass system (34, 39, 40, 44-45, 61-78). However, glass-fibres have not been produced and/or characterised from any of these of these compositions.

The quaternary compositions proposed to be investigated, have not previously been produced, investigated or characterised. Neither have glass-fibres been produced from these compositions. Therefore, this was also a novel aspect of the studies conducted. The first quaternary component to be used will be boric oxide (B_2O_3). Boric oxide being known as a classic glass former was one reason for its use. It was also known to be relevant to some biological species. The second quaternary component to be used was Iron oxide. Iron oxide is known to reduce the degradation rates in glasses; however, it is not a classic glass former. Also, due to the fact that iron is naturally found in the body, these compositions were also expected to be biocompatible. The third quaternary component to be used is silicon dioxide. Silicon dioxide is also a well known classic glass former, and there have been numerous publications regarding the use of silica in glass, especially with regards to Larry Hench's Bioglass®.

Aims:

To create a range of soluble phosphate-based glass and glass-fibres which could potentially be used as cell delivery vehicles and/or Tissue Engineering scaffolds.

Objectives:

1. To produce glass-fibres of different diameter size from the glasses investigated, using a custom built fibre-rig.
2. To characterise the phosphate based glasses and glass-fibres produced using thermal, x-ray powder diffraction (XRPD) and nuclear magnetic resonance (NMR) analyses. Thermal analysis would be most beneficial in obtaining the melting temperatures of the glasses, in order to pull fibres from the compositions investigated. XRPD and NMR would help to understand the structural arrangements within the glass. With further knowledge, it may also be also be possible to correlate the NMR and XRPD data with predictions of the structure of the glasses.
3. To obtain the solubility of these glasses and glass-fibres in terms of weight loss and pH changes.
4. To modify the solubility of the glasses and glass-fibres by incorporating oxides of boron, iron, and silica. These are all known to have a strong effect on the glass network.
5. To determine the rates of ion release and to identify the ionic species in the degradation products using ion chromatography.

CHAPTER 2

Materials and Methods

2.0 Materials and Methods:

2.1 General:

Four glass systems were prepared and investigated. The first system was based on a ternary phosphate, calcium (lime) and sodium (soda) P_2O_5 – CaO – Na_2O glass system. Nine glass compositions were investigated within this system, where the phosphate content was fixed at 45, 50 and 55 mol% (P_2O_5), and the CaO was varied at 30, 35 and 40 mol% for each phosphate content investigated. The balance was Na_2O. (See Table 2.1)

Table 2.1: Glass codes including oxide composition in mol%, along with melting and annealing temperatures for glass system 1.

Glass Codes	P_2O_5 (mol%)	CaO (mol%)	Na_2O (mol%)	Melt Temp / time (deg C / hr)	Temp annealed
$P_{45}Ca_{30}Na_{25}$	45	30	25	1000 / 1	350
$P_{45}Ca_{35}Na_{20}$	45	35	20	1000 / 1	350
$P_{45}Ca_{40}Na_{15}$	45	40	15	1050 / 1	350
$P_{50}Ca_{30}Na_{20}$	50	30	20	1000 / 1	350
$P_{50}Ca_{35}Na_{15}$	50	35	15	1000 / 1	350
$P_{50}Ca_{40}Na_{10}$	50	40	10	1050 / 1	350
$P_{55}Ca_{30}Na_{15}$	55	30	15	1000 / 1	350
$P_{55}Ca_{35}Na_{10}$	55	35	10	1000 / 1	350
$P_{55}Ca_{40}Na_5$	55	40	5	1050 / 1	350

An attempt was made to produce glass fibres from each of the glass compositions in Table 2.1, along with the compositions of each of the following three glass systems.

The second system investigated was based on the quaternary phosphate, calcium, sodium and boron (P_2O_5 – CaO – Na_2O – B_2O_3) glass system. Fifteen glass compositions were investigated within this system. In this study the phosphate content was kept constant at 50 mol% and the calcium content was again varied at 30, 35 and 40 mol%. Boron was substituted in place of sodium, from between 1 – 5 mol%. See Table 2.2.

Table 2.2: Glass codes including oxide composition in mol%, and melting and annealing temperatures for glass system 2.

Glass Codes	P_2O_5 (mol%)	CaO (mol%)	Na_2O (mol%)	B_2O_3 (mol%)	Melt Temp / time (deg C / hr)	Temp annealed
$P_{50}Ca_{30}Na_{19}B_1$	50	30	19	1	1000 / 1	350
$P_{50}Ca_{35}Na_{14}B_1$	50	35	14	1	1000 / 1	350
$P_{50}Ca_{40}Na_9B_1$	50	40	9	1	1050 / 1	350
$P_{50}Ca_{30}Na_{18}B_2$	50	30	18	2	1000 / 1	350
$P_{50}Ca_{35}Na_{13}B_2$	50	35	13	2	1000 / 1	350
$P_{50}Ca_{40}Na_8B_2$	50	40	8	2	1050 / 1	350
$P_{50}Ca_{30}Na_{17}B_3$	50	30	17	3	1000 / 1	350
$P_{50}Ca_{35}Na_{12}B_3$	50	35	12	3	1000 / 1	350
$P_{50}Ca_{40}Na_7B_3$	50	40	7	3	1050 / 1	350
$P_{50}Ca_{30}Na_{16}B_4$	50	30	16	4	1000 / 1	350
$P_{50}Ca_{35}Na_{11}B_4$	50	35	11	4	1000 / 1	350
$P_{50}Ca_{40}Na_6B_4$	50	40	6	4	1050 / 1	350
$P_{50}Ca_{30}Na_{15}B_5$	50	30	15	5	1000 / 1	350
$P_{50}Ca_{35}Na_{10}B_5$	50	35	10	5	1000 / 1	350
$P_{50}Ca_{40}Na_5B_5$	50	40	5	5	1050 / 1	350

The third glass system investigated was based on the quaternary phosphate, calcium, sodium and Iron (P_2O_5 – CaO – Na_2O – Fe_2O_3) glass system. Fifteen glass compositions were investigated within this system. Again the phosphate was fixed at 50 mol%, with the calcium oxide content varied at 30, 35 and 40 mol%. The Fe_2O_3 was added in place of the sodium oxide content, from between 1 – 5 mol%. See Table 2.3.

Table 2.3: Glass codes including oxide composition in mol%, and melting and annealing temperatures for glass system 3.

Glass Codes	P_2O_5 (mol%)	CaO (mol%)	Na_2O (mol%)	Fe_2O_3 (mol%)	Melt Temp / time (deg C / hr)	Temp annealed
$P_{50}Ca_{30}Na_{19}Fe_1$	50	30	19	1	1000 / 1	370
$P_{50}Ca_{35}Na_{14}Fe_1$	50	35	14	1	1000 / 1	370
$P_{50}Ca_{40}Na_9Fe_1$	50	40	9	1	1050 / 1	370
$P_{50}Ca_{30}Na_{18}Fe_2$	50	30	18	2	1000 / 1	370
$P_{50}Ca_{35}Na_{13}Fe_2$	50	35	13	2	1000 / 1	370
$P_{50}Ca_{40}Na_8Fe_2$	50	40	8	2	1050 / 1	370
$P_{50}Ca_{30}Na_{17}Fe_3$	50	30	17	3	1000 / 1	370
$P_{50}Ca_{35}Na_{12}Fe_3$	50	35	12	3	1000 / 1	370
$P_{50}Ca_{40}Na_7Fe_3$	50	40	7	3	1050 / 1	370
$P_{50}Ca_{30}Na_{16}Fe_4$	50	30	16	4	1000 / 1	370
$P_{50}Ca_{35}Na_{11}Fe_4$	50	35	11	4	1000 / 1	370
$P_{50}Ca_{40}Na_6Fe_4$	50	40	6	4	1050 / 1	370
$P_{50}Ca_{30}Na_{15}Fe_5$	50	30	15	5	1000 / 1	370
$P_{50}Ca_{35}Na_{10}Fe_5$	50	35	10	5	1000 / 1	370
$P_{50}Ca_{40}Na_5Fe_5$	50	40	5	5	1050 / 1	370

The fourth glass system investigated was based on the quaternary phosphate, calcium, sodium and silica (P_2O_5 – CaO – Na_2O – SiO_2) glass system. Again 15 glass compositions were investigated within this system. This glass system also contained a fixed phosphate content of 50 mol% (P_2O_5). The calcium oxide was again varied at 30, 35 and 40 mol%. The silicon (SiO_2) content was substituted for sodium oxide (Na_2O) from between 1 – 5 mol%. See Table 2.4.

Table 2.4: Glass codes along with oxide composition in mol%, and melting and annealing temperatures, for glass system 4.

Glass Codes	P_2O_5 (mol%)	CaO (mol%)	Na_2O (mol%)	SiO_2 (mol%)	Melt Temp / time (deg C / hr)	Temp annealed
$P_{50}Ca_{30}Na_{19}Si_1$	50	30	19	1	1000 / 1	370
$P_{50}Ca_{35}Na_{14}Si_1$	50	35	14	1	1000 / 1	370
$P_{50}Ca_{40}Na_9Si_1$	50	40	9	1	1050 / 1	370
$P_{50}Ca_{30}Na_{18}Si_2$	50	30	18	2	1000 / 1	370
$P_{50}Ca_{35}Na_{13}Si_2$	50	35	13	2	1000 / 1	370
$P_{50}Ca_{40}Na_8Si_2$	50	40	8	2	1050 / 1	370
$P_{50}Ca_{30}Na_{17}Si_3$	50	30	17	3	1000 / 1	370
$P_{50}Ca_{35}Na_{12}Si_3$	50	35	12	3	1000 / 1	370
$P_{50}Ca_{40}Na_7Si_3$	50	40	7	3	1050 / 1	370
$P_{50}Ca_{30}Na_{16}Si_4$	50	30	16	4	1000 / 1	370
$P_{50}Ca_{35}Na_{11}Si_4$	50	35	11	4	1000 / 1	370
$P_{50}Ca_{40}Na_6Si_4$	50	40	6	4	1050 / 1	370
$P_{50}Ca_{30}Na_{15}Si_5$	50	30	15	5	1000 / 1	370
$P_{50}Ca_{35}Na_{10}Si_5$	50	35	10	5	1000 / 1	370
$P_{50}Ca_{40}Na_5Si_5$	50	40	5	5	1050 / 1	370

The compositional limits of the ternary system were drawn up based on previous experience, within this department, of that particular glass system (74-78). This ternary glass system was fixed at 45 mol% P_2O_5, and the CaO content ranged from 8 – 40 mol%, with sodium oxide making up the remainder. As stated previously, the main goal of the research undertaken was to produce glass fibres from the glass compositions investigated. Due to unsuccessful attempts at producing glass fibres from the fixed 45 mol% P_2O_5 compositions, the phosphate content was then increased to 50 mol%. This glass system proved to be successful in terms of glass fibre production. Again the CaO content was varied in order to obtain different degradation rates within each of the systems investigated.

A further glass system containing 55 mol% P_2O_5 was evaluated in order to investigate glass-fibre production. This system also proved to be successful in terms of glass fibre production. Three compositions within this system, with varying CaO content were also investigated.

A minimum requirement of 50 mol% P_2O_5 was determined for glass fibre production. This was therefore set for all other compositions investigated in order to maintain the greatest flexibility available in terms of composition design and ion incorporation.

2.2 Glass Making Methodology:

Studies had been conducted previously in order to determine the optimal precursors for adequate glass production (74). Difficulties were encountered with the use of P_2O_5. This chemical is very hygroscopic and very volatile at elevated temperatures, which could lead to problems such as water absorption and loss of P_2O_5 during melting. Both of these effects can ultimately affect the final glass composition.

The chemicals NaH_2PO_4 and $CaHPO_4$ had been previously tested as precursors in an attempt to limit the use of P_2O_5. Using these precursors it was possible to make glasses with up to 16 mol% CaO. Over this limit crystallisation was said to readily occur (74). This was probably due to the presence of water in the glass, which is known to readily nucleate crystallisation in glasses.

It was found that using $CaCO_3$ to deliver CaO in combination with fresh, dry P_2O_5 and NaH_2PO_4 gave optimal results. With these chemicals a wide range of P_2O_5 – CaO – Na_2O glasses could be made. To avoid excessive loss of P_2O_5, appropriate amounts of NaH_2PO_4 and $CaCO_3$ were weighed out first and mixed together. The appropriate amount of P_2O_5 was then weighed out and added to the previous mixture. All three compounds were then thoroughly mixed together and placed into a platinum crucible, which was then placed into a furnace. During the melting process H_2O and CO_2 were evolved, which helped the molten mass to

flux. All the glass compositions made were produced in this way. In the quaternary compositions, B_2O_3, Fe_2O_3 and SiO_2 were also used as precursors.

2.2.1. Chemical Equations and Composition Calculations:

The chemical reactions and glass compositions were calculated as follows:

Calculations for composition with glass code $P_{50}Ca_{30}Na_{20}$ (i.e 50 mol% P_2O_5, 30 mol% CaO and 20 mol% Na_2O).

Using NaH_2PO_4;

$$2\ NaH_2PO_4 \longrightarrow Na_2O + P_2O_5 + 2\ H_2O.$$

RMM = 240 g mol^{-1} 62 g mol^{-1} 142 g mol^{-1} 36 g mol^{-1}

Therefore, mole fraction of oxides resulting from breakdown of 2 NaH_2PO_4:

62 / 240 = 0.258 (for Na_2O)

142 / 240 = 0.592 (for P_2O_5)

36 / 240 = 0.15 (for H_2O)

Mole% was calculated as such: for 20 mol% Na_2O

$$\frac{0.20 \times 62}{0.258} = 48.06\text{g of } NaH_2PO_4 \text{ to be used (for a 20mol\% } Na_2O \text{. glass composition).}$$

However, using 48.06g of NaH_2PO_4 would also yield:

48.06 x 0.592 = 28.45g of P_2O_5.

Total amount of P_2O_5 required is (50 mol%):

0.50 x 142 = 71g of P_2O_5 required.

Therefore, 71 – 28.45 = 42.55g of P_2O_5 would have to be added (as the last compound to the mixture, due to its hygroscopic nature).

The addition of CaO was done through the following procedure:

Using $CaCO_3$;

$CaCO_3 \longrightarrow CaO + CO_2$

RMM = 100 $gmol^{-1}$ 56 g mol^{-1} 44 g mol^{-1}

Therefore, the mole fraction of the oxide from breakdown of $CaCO_3$;

56 / 100 = 0.56 (for CaO)

44 / 100 = 0.44 (for CO_2)

Mole% calculated for a 30 mol% CaO composition was;

$\frac{0.30 \times 56}{0.56}$ = 30g of $CaCO_3$. Is to be used for a 30 mol% composition.

(Due to $CaCO_3$ having a RMM of 100, whatever mol% of CaO was required, resulted in exactly the same weight (in grams) of $CaCO_3$ to be used).

2.2.2 Chemical Equations and Calculations for Quaternary Compounds Used:

B_2O_3 (Boric oxide).

Reaction: B_2O_3 ⟶ B_2O_3

RMM = 69.62 g mol^{-1} 69.62 g mol^{-1}

Mole fraction = 69.62 / 69.62 = 1.

Example 1, for a 5 mol% B_2O_3 composition;

$\frac{0.05 \times 69.62}{1}$ = 3.481g of B_2O_3 to be added to the mixture.

All of the quaternary compounds used were substituted in place of sodium oxide.

Fe_2O_3 (Ferric oxide).

Reaction: Fe_2O_3 ⟶ Fe_2O_3

RMM = 159.7 g mol^{-1}, again the mol fraction would also = 1,

Therefore, for a 3 mol% Fe_2O_3 addition,

$\frac{0.03 \times 159.7}{1}$ = 4.791g of Fe_2O_3 to be added.

SiO_2 (Silicon dioxide):

Reaction: SiO_2 ⟶ SiO_2

RMM = 60.08 g mol^{-1}, and mol fraction will = 1,

Therefore, for a 1 mol% SiO_2 addition,

$\frac{0.01 \times 60.08}{1}$ = 0.6008g of SiO_2 to be added.

2.3 Differential Thermal Analysis:

2.3.1 Glass Formation Process:

In order to understand the parameters measured by the differential thermal analyser (DTA), the process of glass formation will be discussed. A glass is an amorphous solid without long-range order that undergoes a glass transition. Glass formation usually takes place via the cooling of the molten mass rapidly past the crystallisation point, with solidification at the glass transition temperature (T_g). For the successful formation of a glass, the crystallisation temperature (T_c) range must be passed quickly. Figure 2.1 illustrates this process.

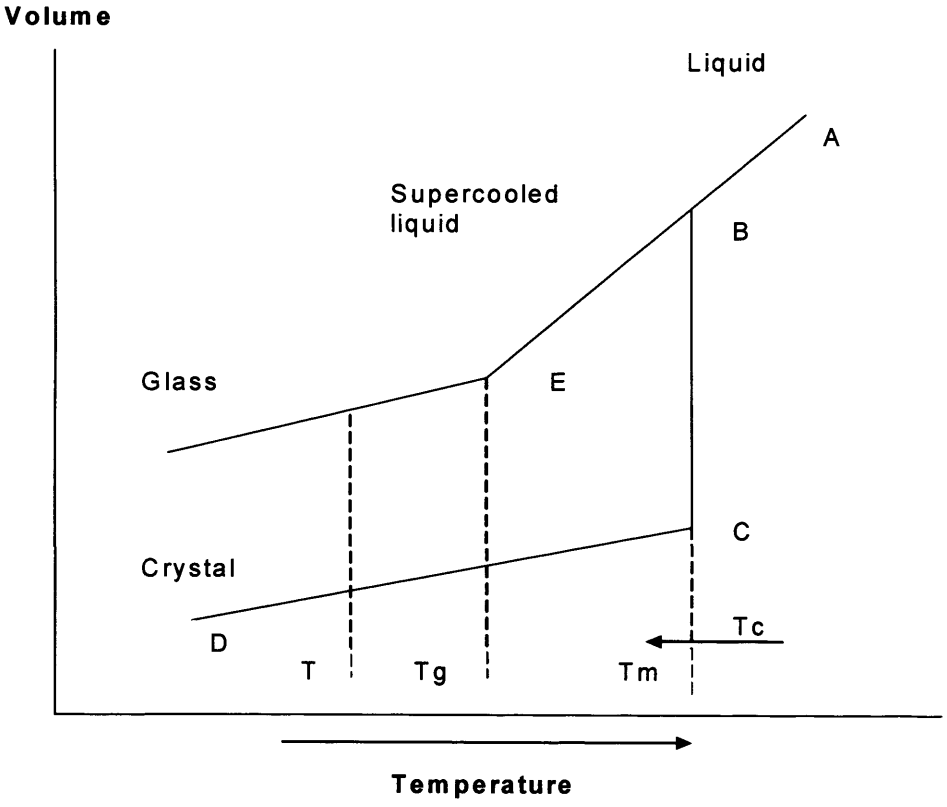

Figure 2.1: Glass formation process.

Considering the molten liquid mass (state A), a continuous decrease in temperature would decrease the volume along line AB. However, if the decrease in temperature was carried out slowly enough, crystallisation at the melting point T_m would occur and a crystalline product would form along line CD. Conversely, if the temperature was reduced fast enough, the crystallisation process would not occur at T_m, and the volume change would follow along line BE until it reached room temperature, which would then result in formation of a glass (74). Therefore glasses can also be considered to be supercooled liquids as they possess many properties which are characteristic of the liquid state.

2.3.2 The Glass Transition Temperature:

Phosphate based glasses possess unique properties, amongst them being large thermal expansion coefficients, low optical dispersion and low glass transition temperatures (T_g). The glass transition is a temperature range where the rate of structural relaxation is slow enough to be detected. The T_g is defined as the temperature at which a polymeric, amorphous material is converted from the glassy state to the elastic plastic (rubbery) state (79). It is characterised by changes in the temperature-dependence of properties during heating or cooling. In a glass, the atoms are frozen into fixed positions. Temperature-dependent properties change because the amplitude of vibration of the atoms around that position is influenced by temperature. As the temperature is lowered towards the glass transition, the mobility of the atoms decreases and time is required for

relaxation of the material to the equilibrium state. T_g is heating rate dependant with higher heating rates giving rise to higher T_g values.

2.3.3 Differential Thermal Analysis:

Differential thermal analysis (DTA) is a technique which can detect exothermic and endothermic phase changes. During a run, the temperature of a sample is continuously monitored with a thermocouple against an inert material as a reference sample. The temperature as a function of time is linear until an exothermic or endothermic event happens. The sample and reference are placed side by side in a heating block, which are connected to thermocouples.

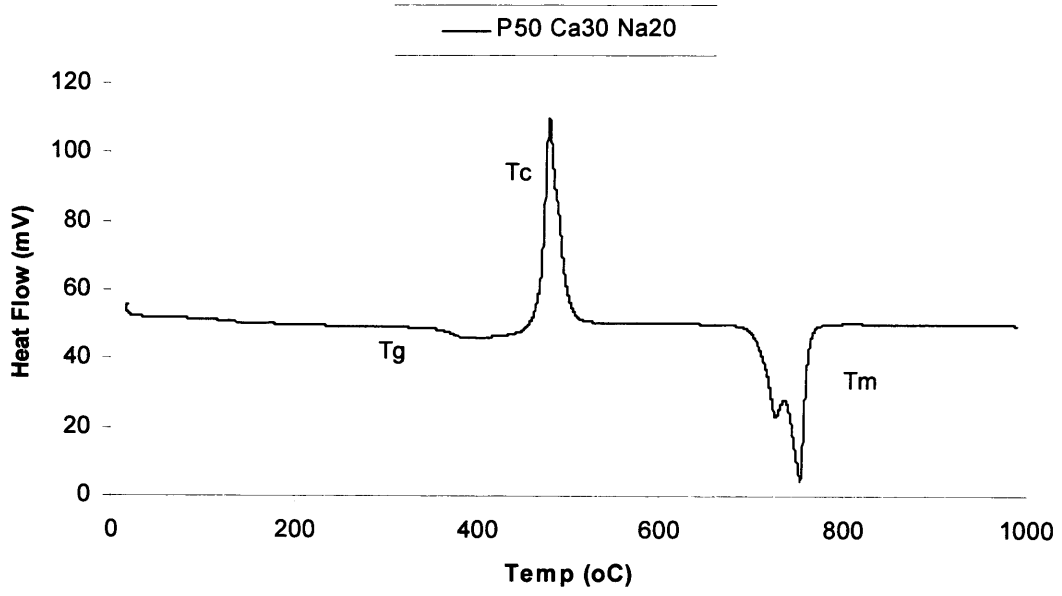

Figure 2.2: Typical DTA trace with two temperature events seen for the T_m (melting temperature).

When sample and reference are at the same temperature, then the net output is zero. A thermal event in the sample will result in a temperature difference ΔT, which is detected by the net voltage of the thermocouples. A third thermocouple is used to monitor the temperature of the heating block and the results are presented in ΔT against temperature. The temperature of the peak is taken as the onset of the derivation from the baseline T_1 or as the peak temperature T_2. See figure 2.2 above. Thermal analysis has an important use in glass making. Not only can it be used to determine important parameters such as the melting point (T_m) of the glass, and the glass transition temperature (T_g), it can also be used to try and understand the phenomenon of glass phase separation (74).

2.3.4 The Method for DTA Analysis:

Bulk glass pieces and glass fibre samples of the varying compositions investigated were ground to a powdery form for 20 minutes using a vibratory agate mill (Fritsch, Germany). The three main thermal parameters measured using DTA were, T_g the glass transition temperature, T_c the crystallisation temperature and T_m the melting temperature.

The analysis was conducted on a Setaram differential thermal analyser (DTA), using an inert nitrogen atmosphere and a heating rate of 20°C min^{-1} up to a maximum temperature of 1000°C. The data was baseline corrected by carrying out a blank run and subtracting this from the plot obtained.

2.4 XRD Analysis:

X-ray diffraction is one of the most powerful techniques for determining the structures of solids and the molecules they contain. It can be used not only to determine the separations of layers of atoms but also to determine the locations of the atoms.

To understand the principles involved, we first need to know that waves may interfere with each other. If two waves of electromagnetic radiation were in the same region of space, and if the peaks of one wave coincided with the other, they would add together to give a stronger wave. This strengthening is known as 'constructive interference'. When the combined wave is detected photographically or electronically, the spot obtained would be brighter, than the spot from the individual wave. However, when the peaks of one wave coincide with the troughs of the other, they partially cancel each other out. This cancellation is called 'destructive interference'. No spot at all is detected when the peaks and troughs match exactly and cancellation is complete.

In contrast diffraction is the interference between the waves, caused by an object in their path. The resulting pattern of bright spots against a dark background is called a 'diffraction pattern'. A crystal can cause diffraction in a beam of x-rays, and a bright spot of constructive interference is obtained, when the crystal is held at a certain angle to the beam. X-rays are used, because only their wavelengths

are short enough to measure distances comparable to the separations of atoms in crystals (80).

2.4.1 The Method Used for XRD Analysis:

Glass disks of the various compositions investigated were annealed at their respective crystallisation temperatures (obtained from DTA analysis) to investigate the phases that crystallised from the glass. The data was collected on a Philips PW1780 powder diffractometer in flat plate geometry, using Ni filtered Cu K_α radiation. Data was collected from 10° to 100° 2θ with a step size of 0.02° and a count time of 12 seconds. The phases were identified using the Crystallographica Search-Match software (Oxford Cryosystems, Oxford, UK) and the International Centre for Diffraction Data (ICDD) database (volumes 1 – 45).

2.5 NMR Analysis:

2.5.1 Solid State NMR Spectroscopy:

Nuclear magnetic resonance (NMR) spectroscopy is another powerful method for structural analysis of inorganic and organic compounds, especially of disordered materials such as glasses. This technique gives detailed information about the surrounding environment around the nucleus under investigation. Only magnetically active nuclei such as isotopes of H, C, N, F and P, which have a nuclear spin different from zero, can be observed using this technique.

2.6 Glass Preparation:

2.6.1 Standard Glass Preparation:

The glass compositions were prepared using NaH_2PO_4, $CaCO_3$ and P_2O_5 (BDH, UK) as starting materials. The precursors were weighed out on an analytical balance (Precisa, England), and then placed into a 200ml volume Pt/10%Rh crucible type 71040 (Johnson Matthey, Royston, U.K.). The crucible was then placed into a furnace at between 1000 and 1050°C dependant on the final glass composition for 1 hour (see Tables 2.1 – 2.4 above).

The glass was then poured into a graphite mould, which had been preheated to between 350°C and 370°C in a second furnace (Dicor, York Division. U.K.) dependant on the composition (see Tables 2.1 – 2.4). The mould was then returned to the furnace in order to anneal the glass, thereby removing any residual stresses within the glass. After an hour the furnace was switched off and allowed to slowly cool to room temperature.

2.6.2 Glass Cutting and Storage:

The glass rods obtained from the mould, were then cut into 2mm thick disks of 15mm diameter using a Testbourne diamond saw. The optimal cutting liquid was found to be methanol (BDH, UK.). After cutting, the discs were thoroughly dried with cotton tissue.

Any remaining glass rods were stored in sample tubes (Sterilin, U.K.). This storage method was found to be sufficient to overcome the problem of moisture absorption from the atmosphere, which can occur with phosphate based glasses.

2.6.3 Density Measurements:

Density measurements were conducted using Archimedes principle on an analytical balance (Mettler Toledo, U.K.) with a density kit. The density kit was assembled onto the balance and then dry and wet measurements were taken.

Due to the highly soluble nature of some of the glass compositions investigated, ethanol was used as the liquid for the measurements. The formula used to obtain the density was:

$$\rho = \frac{M_d}{M_d - M_w} \times T$$

Where ρ = density, M_d = mass of dry sample, M_w = mass of sample submerged in ethanol liquid, and T = temperature of liquid used.

2.7 pH Measurements:

The glass combination pH electrode was calibrated using pH calibration standards (Colourkey Buffer Solutions. BDH, UK). pH measurements were conducted in the solution (deionised water) which contained the discs, after they had been transferred to a fresh solution. These measurements were conducted at every time point for the duration of the study, using a Jenway 3045 Ion Analyser with an attached glass combination pH electrode (BDH, UK). The pH of the deionised water was adjusted to neutral (7 ± 0.2) before being dispensed at every time point.

2.7.1 Purified Water:

All the dissolution studies were conducted using high purity water. This was obtained from a PURELAB UHQ-PS (Elga Labwater, UK), which further purified the water obtained from an existing water purification system, to a purity level of 18.2 $M.\Omega.cm^{-1}$ resistivity.

2.8 Glass Fibre Preparation:

2.8.1 Standard Glass Fibre Production:

Glass fibres were produced using a fibre drawing method, from a custom built Fibre-rig (Eastman Dental Institute, UCL) (see Figure 2.3).

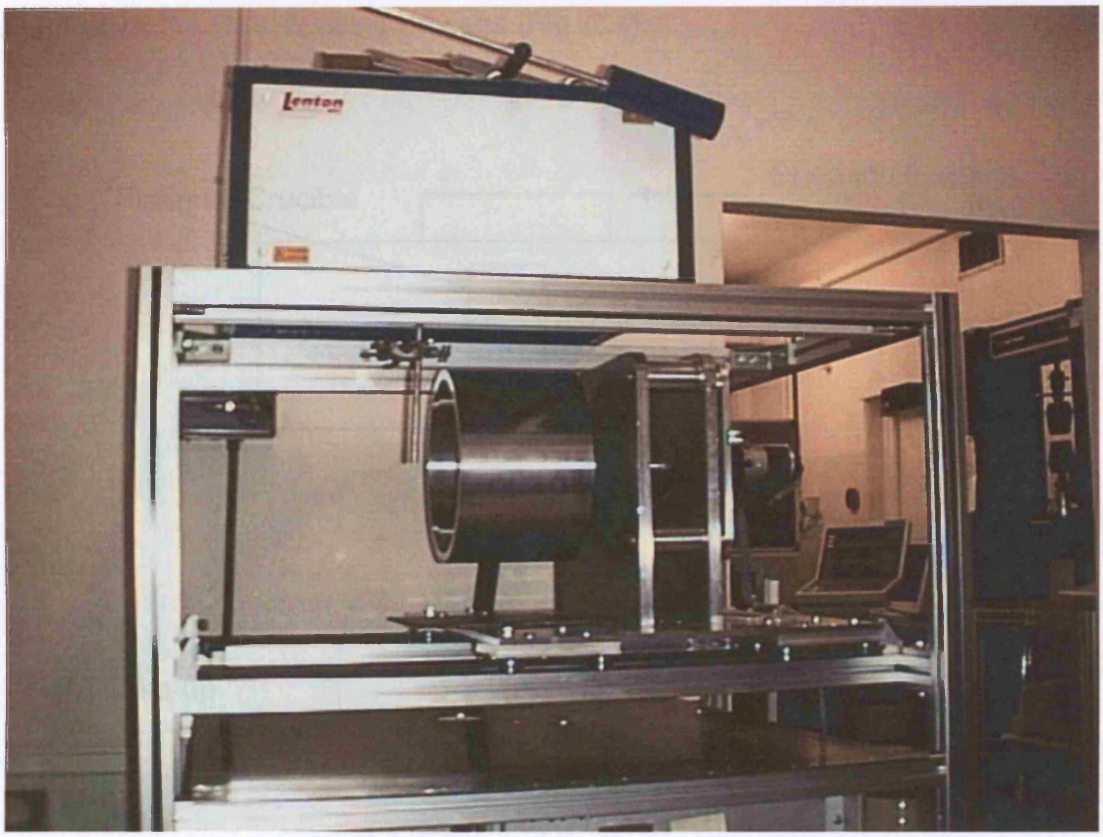

Figure 2.3: A custom built fibre-rig (Eastman Dental Institute, UCL).

The fibre-rig consisted of a top loading furnace (Lenton Furnaces) with a Pt/10%Rh crucible (Johnson Matthey, UK) and a bushing tip approximately 15mm long with an approximate 1mm hole. Glass compositions were placed into the crucible and left for an hour to melt and to homogenise, whilst the bushing was plugged. The temperature of the furnace was then lowered to achieve a viscosity suitable for fiberisation of the glass. These temperatures varied from between 950 – 1150°C depending on the glass composition. Please see below for a diagram of the fibre-drawing process (Fig. 2.4).

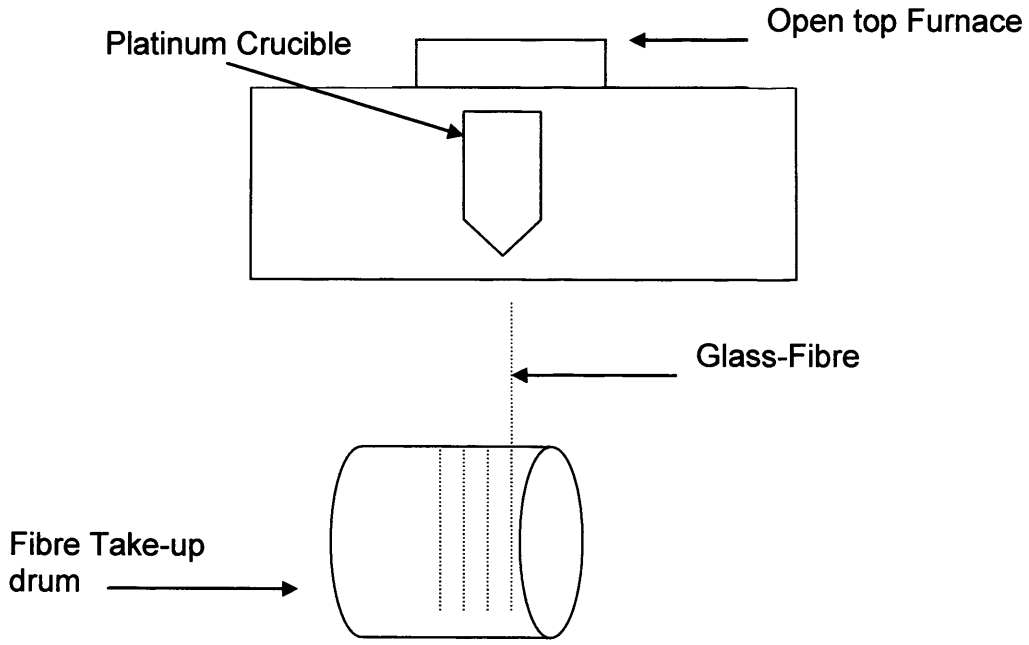

Figure 2.4: Diagram of Fibre-drawing process.

Different fibre diameters were obtained from the compositions investigated, by pulling the glass fibres at different revolutions per minute (RPM) which were directly equivalent to metres per minute, as the circumference of the drum was exactly one metre. The speeds used were 400, 800, 1200 and 1600 RPM.

2.8.2 Glass Fibre Diameter Measurements:

To measure the diameter of the fibres obtained, a small bundle of parallel aligned fibres from each fibre diameter of each composition investigated were placed into a PTFE mould and embedded in resin (Struers, UK). The samples in resin were left to polymerise for a day and then extracted from the mould.The samples were then cut and polished and examined under a microscope, which was attached to a CoolSnap Digital Image Analysis system (ISS Group Ltd, Manchester, U.K.). Image Pro Plus software was used to measure the diameter of the fibres in microns. The microscope was calibrated using a standard microscope calibration slide. The mean values and errors presented were calculated and averaged from measurements taken from 50 fibre diameters. The pictures were taken at x10 magnification. Figures 2.4 and 2.5 below represent examples of the images obtained.

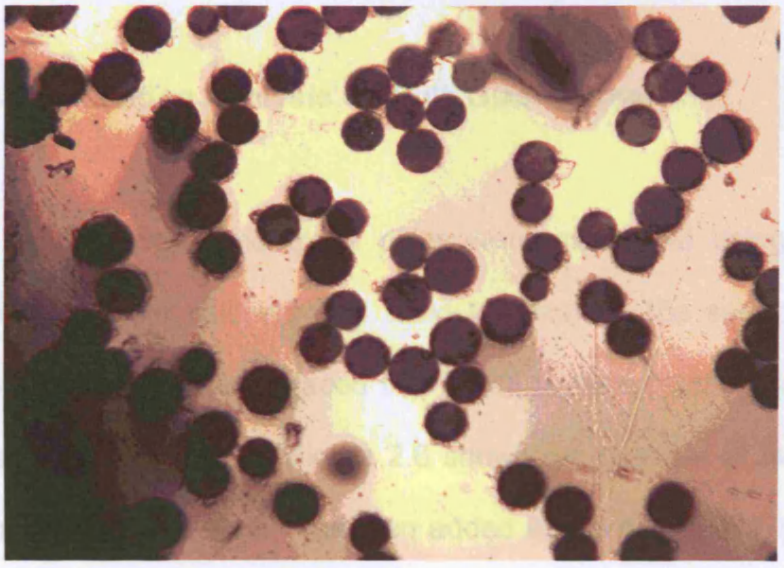

Figure 2.5: Example of fibres embedded in resin (400RPM, from composition $P_{50}C_{35}N_{15}$, taken on light microscope at x10 magnification).

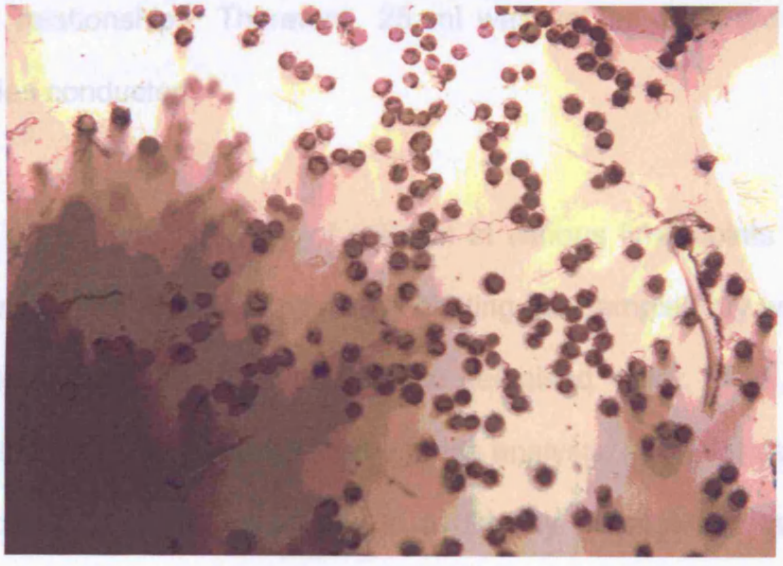

Figure 2.6: Example of fibres embedded in resin (1200RPM, from composition $P_{50}C_{35}N_{15}$ taken on a light microscope at x10 magnification).

2.9 Degradation Studies:

2.9.1 Degradation Analysis on Bulk Glass Samples:

The dimensions of the glass discs were measured using a pair of Mitutoyo Digimatic vernier callipers and used to calculate the surface area.. The discs were then weighed and placed into 75 ml volume plastic containers, which were sealed with plastic lids. Figure 2.6 shows an example of the glass discs made. 25 ml of deionised water was then added to the containers, prior to placing them into an incubator at 37°C ± 1°C. The test protocol used was based around protocols drawn up for toxicity testing of biomaterials from the British Standards Institute (BSI, ISO 10993). The standards did not specify any volume to surface area relationship. Therefore, 25 ml was set as standard for the degradation studies conducted.

The discs were taken out of solution at various time points (daily intervals), and excess moisture was removed by blotting the samples dry with tissue. The discs were weighed, and then placed into deionised water. The sample solution was stored in order to undertake pH and ion analysis, at a later stage. Another reason for changing the solution was to avoid any precipitation build-up on the discs, which was experienced whilst conducting the same test in a static environment.

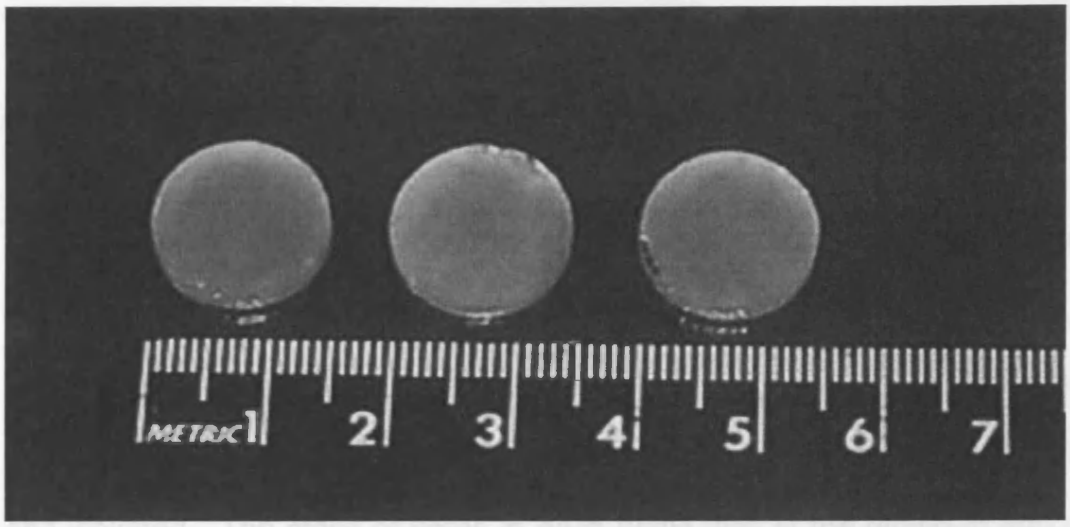

Figure 2.7: Discs prior to placing them into containers.

As degradation is affected by surface area, the data was presented as weight loss per unit area. To obtain the rate of weight loss, the initial weight (M_0) of each sample was measured as well as the weight loss at time *t* (M_t) to give a weight loss per unit area thus:

$$\text{Weight loss} = \frac{(M_0 - M_t)}{A}$$

where A is the surface area (mm^2).

The measurements were carried out in triplicate. The data was plotted as weight loss per unit area against time. The slope of this graph gave a dissolution rate in terms of $mg.mm^{-2}.h^{-1}$, which was determined by fitting a straight line through the data and also passing through the origin.

2.9.2 Degradation Analysis on Glass-Fibre Samples:

The glass-fibre dissolution rate was measured using a weight loss method. This method was an effective way of ranking the glass-fibre compositions, in terms of the dissolution rates obtained.

A small batch of fibres approximately 30 mm long were placed into a glass bottle and weighed. The mass of fibres in each bottle was in the region of 400 – 500 mg. This was kept constant for all the glass-fibre degradation analyses conducted. The bottles were filled with deionised water (adjusted to pH 7), and then placed into an incubator at 37°C ± 1°C. After a certain period of time (dependant on composition), the water was removed and the glass bottles dried overnight at 60°C, and then reweighed. The weight loss was expressed in ($mg.g^{-1}$). The slope of the plots obtained gave a rate value in terms of $mg.g^{-1}.hr^{-1}$.

2.10 Ion Release Measurements:

2.10.1 Introduction to Ion Chromatography:

An ion chromatography analyser typically consists of a liquid eluent, a high-pressure pump, a sample injector, a separator column, a chemical suppressor, and a measurement cell.

Prior to running samples, the ion analyser was calibrated using standard solutions. These solutions can contain a known amount of a single ion under investigation, or a combination of several ions to be detected in a single run. By comparing the data obtained from a sample to that obtained from the standard, sample ions could be identified and quantitated. A computer running the chromatography software automatically converted each peak in the chromatograms to a sample concentration and produced a tabulated printout of the results.

The IC analysis consists of four stages (see Figure 2.7).

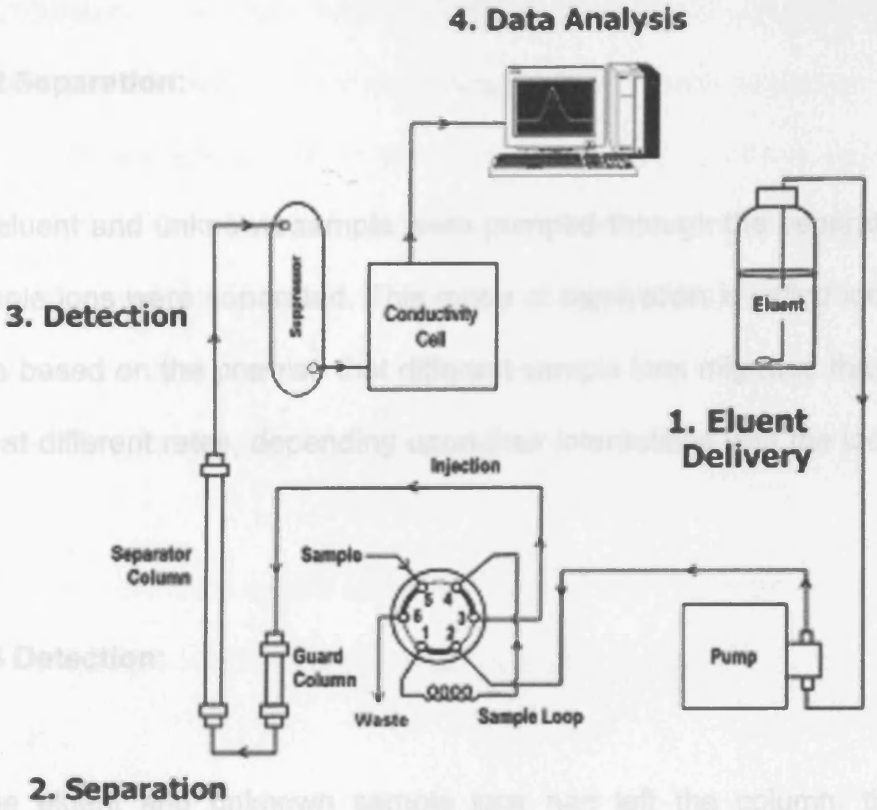

Figure 2.8: Ion analysis process.

2.10.1.1 Eluent Delivery:

The eluent is a liquid that helps to separate the sample ions, and carries the sample through the ion chromatography system. The ICS – 1000 is an isocratic delivery system. This meant that the eluent composition and concentration remained constant throughout the run. The unknown sample liquid was injected into the eluent stream either manually or automatically, via an automated sampler.

The pump then forced the eluent and sample through a separator column, which was a chemically-inert tube packed with a polymeric resin.

2.10.1.2 Separation:

As the eluent and unknown sample were pumped through the separator column, the sample ions were separated. This mode of separation is called ion exchange and was based on the premise that different sample ions migrated through the IC column at different rates, depending upon their interactions with the ion exchange sites.

2.10.1.3 Detection:

After the eluent and unknown sample ions had left the column, they flowed through a suppressor that selectively enhanced detection of the unknown sample ions while suppressing the conductivity of the eluent. The measurement cell monitored and measured a property of the unknown sample ions as they emerged from the suppressor and produced a signal based on a chemical or physical property of the analyte.

2.10.1.4 Data Analysis:

The measurement cell transmitted a voltage signal to a computer running the chromatography software. The chromatography software analysed the data by comparing the sample peaks in the chromatogram to those produced from a standard solution. The software also identified the ions based on retention time, and quantified each analyte by integrating the peak area or peak height. The results were displayed as a chromatogram, with the concentrations of ionic analytes automatically determined and tabulated.

The above mentioned process was the basis of how IC analysis worked. The individual methods used in more detail are stated in section 2.11.

2.11 Ion release in general:

Whilst conducting the bulk glass degradation studies, ion release profiles were also investigated using a Dionex ICS – 1000, and a Dionex ICS – 2500 Ion Chromatography system. Ion release studies had been attempted in the past, using ion selective electrodes. However, the reproducibility of results using electrodes was unsatisfactory due to the short shelf life span of the electrodes.

The ICS-1000 with attached autosampler was used for the routine analysis of sodium (Na^{+}) and (Ca^{2+}) ions. The ICS – 2500 was used for the routine analysis of transition metals, and the PO_4^{3-}, $P_2O_7^{4-}$, $P_3O_9^{3-}$ and $P_3O_{10}^{5-}$ phosphate anions. As stated earlier, only these four phosphate standards were available commercially. The structures of the four phosphate ions investigated are shown in Figures 2.8a – 2.8d.

Figures 2.9a – 2.9d: Structures of Anions Investigated:

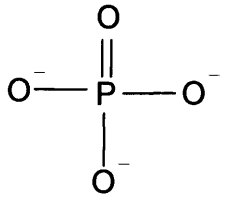

(a)

PO_4^{3-}
[Orthophosphate]

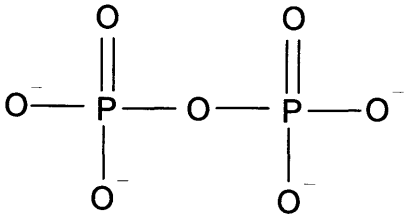

(b)

$P_2O_7^{4-}$
[Pyrophosphate]

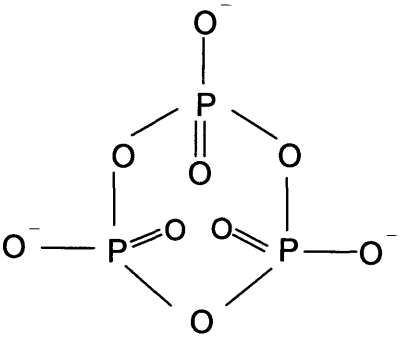

(c)

$P_3O_9^{3-}$
[Cyclic Trimetaphosphate]

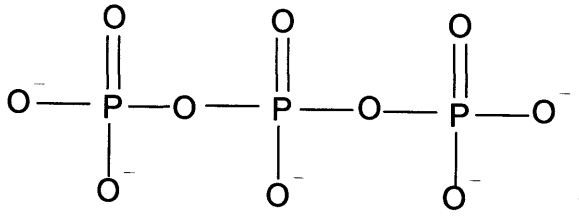

(d)

$P_3O_{10}^{5-}$
[Tripolyphosphate].

2.12 Cation Analysis:

For cation release measurements, an ICS-1000 ion chromatography system (Dionex, UK) was used (see Figure 2.9).

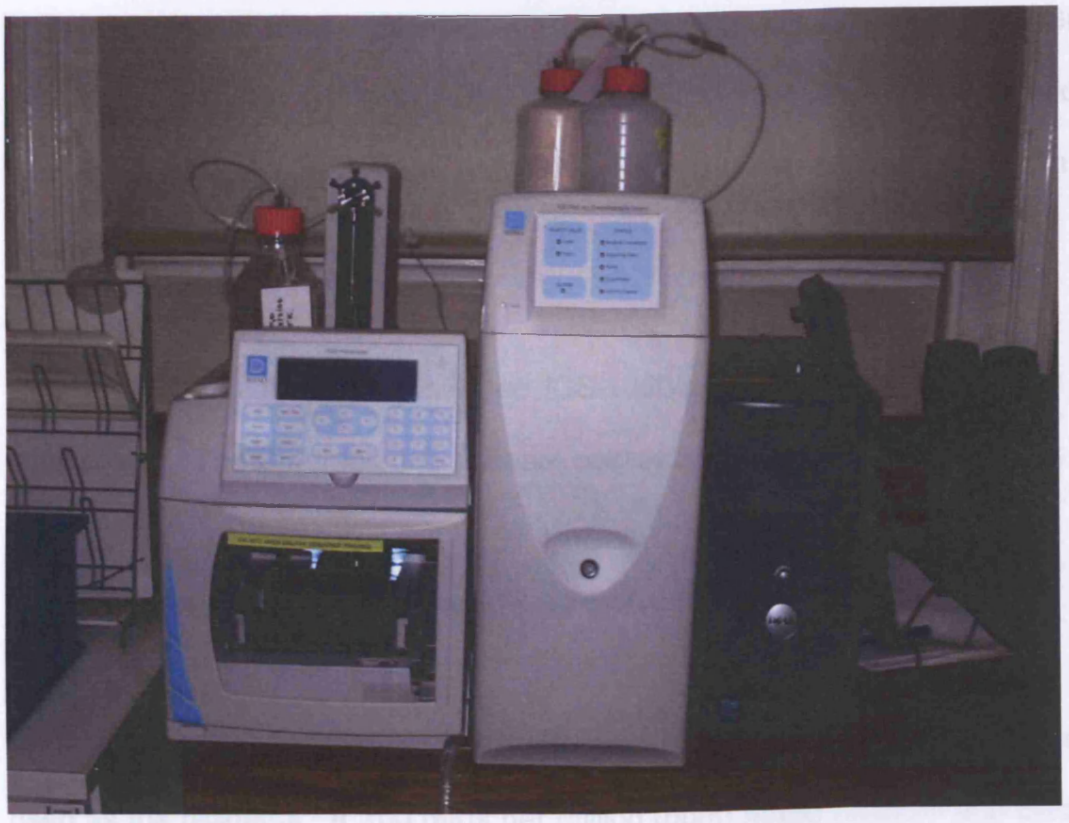

Figure 2.10: The ICS-1000 ion chromatography system.

A 20mM Methanesulfonic acid (MSA, BDH, UK) solution was used as the eluent. The ICS-1000 is an integrated and preconfigured system that performs isocratic IC separations using suppressed conductivity detection.

In this method, cations were eluted using a 4 x 250 mm IonPac® CS12A separator column. All results were calculated against a 4 – point calibration curve using the

predefined calibration routine. The unknown samples were injected onto the system using the AS50 Autosampler (Dionex, U.K.). During the initial analysis, heavy peak shifting was experienced with regards to the calcium ion peak. It was ascertained that this was due to the binding of the phosphate species in solution to the column. This was rectified via injecting the test solution through 'OnGuard II A' cartridges (Dionex, U.K.), prior to running the samples. These cartridges contained an anion exchange resin that bound to the anions present in the solution.

Coupled with AutoSuppression®, the ICS-1000 provided high performance with ease of use. The Chromeleon® software package was used for data analysis.

2.12.1 Cation Reagents and Standard Solution Preparation:

Sodium Chloride (Sigma) and Calcium Chloride ($CaCl_2.2H_2O$) (BDH, UK) were used as the reagents. A 100 parts per million (ppm) mixed (sodium and calcium) stock solution was prepared, from which serially diluted 50, 25, 10 and 1 ppm standard solutions were prepared.

2.12.2 Cation Standard Solution Calculations:

The concentrations for each of the standards prepared were calculated in parts per million.

Equation 1: Calculation for sodium ion analysis.

Reagent used was NaCl (sodium chloride).

RMM of NaCl = 58.44 g mol^{-1}.

RMM of Na^+ = 22.99 g mol^{-1},

$\frac{58.44}{22.99}$ = 2.542g

Therefore; 2.542 g of NaCl in 1 litre of water gave a stock solution of 1000 ppm for Na^+ ions. Consequently, 25.42 mg of NaCl in 100 ml volumetric flask, gave a stock solution of 100 ppm Na^+ ions.

Equation 2: Calculation for Calcium.

Reagent used was $CaCl_2.2H_2O$ (sodium chloride).

RMM of $CaCl_2.2H_2O$ = 147.02 g mol^{-1}.

RMM of Ca^{2+} = 40.08 g mol^{-1},

$\frac{147.02}{40.08}$ = 3.668 g

Therefore; 3.668 g of $CaCl_2.2H_2O$ in 1 litre of water gave a stock solution of 1000 ppm of Ca^{2+} ions. Consequently, 36.68 mg of $CaCl_2.2H_2O$ in 100 ml volumetric flask, gave a stock solution of 100 ppm Ca^{2+} ions.

2.13 Anion Release Analysis:

For anion release measurements, an ICS - 2500 ion chromatography system (Dionex, UK) was used (see Figure 2.10).

Figure 2.11: The ICS - 2500 ion chromatography system.

As stated the discs were placed into fresh solutions on a daily basis. The solution was then analysed for cation and anion release. The phosphate anion measurements were conducted on a Dionex ICS-2500 ion chromatography system (Dionex, UK), consisting of a gradient pump with a 25-µl sample loop.

As stated a mixed solution was prepared by adding 25.42 mg of NaCl with 36.68 mg of $CaCl_2.2H_2O$ into a 100 ml volumetric flask which was serially diluted down to 1, 10, 25 and 50 ppm. These were then used as calibration standard solutions.

However, in order to more accurately determine the calibration concentration, the actual amount of the reagents used was taken, and the specific ion concentration was back calculated, rather than trying to weigh specific amounts (See equation 3).

Equation 3: Accurate determination for Calcium.

As can be seen from Equation 2, 36.68 mg of $CaCl_2.2H_2O$ is required for a 100ppm solution. However, during weighing if 37.5mg was used as the initial amount, then the concentration in ppm could be back calculated as follows:

36.68mg = 100 ppm. (However, 37.5 mg have been used as initial amount).

Then $\frac{100}{36.68}$ = 2.73 ppm.

Therefore, 1 mg of $CaCl_2.2H_2O$ = 2.73 ppm.

So, 37.5 x 2.73 = 102.375 ppm.

Therefore, the starting concentration in a 100 ml volumetric flask would be 102.375 ppm, which would then be serially diluted down.

In this method, polyphosphates were eluted using a 4 x 250 mm IonPac® AS16 anion-exchange column packed with anion exchange resin. A Dionex ASRS® (Anion Self-Regenerating Suppressor) was used at 242 mA.

The Dionex EG50 eluent generator equipped with a KOH (potassium hydroxide) cartridge was used in conjunction with the ASRS®. The EG50 eluent generator system electrolytically produced high-purity KOH eluents using deionised water as the carrier stream to the point of use. The use of the EG50 hydroxide eluent generator lead to negligible baseline shifts during the hydroxide gradients, along with greater retention time reproducibility. The sample run time was set at 30 minutes. The gradient program started from 30mM KOH, and after 2 minutes increased from 30 to 60 mM KOH over 10 minutes, and then stayed at 60mM KOH for up to 25 minutes. After which the KOH eluent was reduced to 30 mM for 5 minutes. The unknown samples were injected onto the system using an AS50 Autosampler (Dionex, U.K.). The Chromeleon® software package was used for data analysis.

2.13.1 Anion Reagents and Standard Solution Preparation:

Sodium phosphate tribasic (Na_3PO_4), trisodium trimetaphosphate ($Na_3P_3O_9$), pentasodium tripolyphosphate ($Na_5P_3O_{10}$), were obtained from Sigma-Aldrich (UK). Tetra-sodium pyrophosphate ($Na_4P_2O_7$) was obtained from BDH, UK. A 100ppm working solution containing all of the above 4 reagents was prepared, from which serially diluted 50, 25, 10 and 1 ppm standard solutions were prepared. Higher phosphate group containing reagents (i.e. P_4 or above) were not commercially available.

2.13.2 Anion Standard Solution Calculations:

The concentrations for each of the standards prepared were calculated in parts per million.

Equation 1: Calculation for the PO_4^{3-} anion.

Reagent used was Na_3PO_4 (sodium phosphate).

RMM of Na_3PO_4 = 163.9 g mol^{-1}.

RMM of PO_4 = 95 g mol^{-1},

$$\frac{163.9}{95.0} = 1.73 \text{ g}$$

Therefore; 1.73g of Na_3PO_4 in 1 litre of water gave a stock solution of 1000 ppm of PO_4^{3-} ions. Consequently, 17.3 mg of Na_3PO_4 in 100 ml volumetric flask, gave a stock solution of 100 ppm PO_4^{3-} ions.

Equation 2: Calculation for the $P_2O_7^{4-}$ anion.

Reagent used was $Na_4P_2O_7.10H_2O$ (tetrasodium pyrophosphate).

RMM of $Na_4P_2O_7.10H_2O$ = 446.06 g mol^{-1}.

RMM of P_2O_7 = 174 g mol^{-1},

$\frac{446.06}{174.0}$ = 2.56 g

Therefore; 2.56g of $Na_4P_2O_7.10H_2O$ in 1 litre of water gave a stock solution of 1000 ppm of $P_2O_7^{4-}$ ions. Consequently, 25.6 mg of $Na_4P_2O_7.10H_2O$ in 100 ml volumetric flask, gave a stock solution of 100 ppm $P_2O_7^{4-}$ ions.

Equation 3: Calculation for the $P_3O_9^{3-}$ anion.

Reagent used was $Na_3P_3O_9$ (trisodium trimetaphosphate).

RMM of $Na_3P_3O_9$ = 305.9 g mol^{-1}.

RMM of P_3O_9 = 237 g mol^{-1},

$\frac{305.9}{237}$ = 1.29 g

Therefore; 1.29 g of $Na_3P_3O_9$ in 1 litre of water gave a stock solution of 1000 ppm of $P_3O_9^{3-}$ ions. Consequently, 12.9 mg of $Na_3P_3O_9$ in 100 ml volumetric flask, gave a stock solution of 100 ppm $P_3O_9^{3-}$ ions.

Equation 4: Calculation for the $P_3O_{10}^{5-}$ anion.

Reagent used was $Na_5P_3O_{10}$ (sodium tripolyphosphate).

RMM of $Na_5P_3O_{10}$ = 367.9 g mol^{-1}.

RMM of P_3O_{10} = 253 g mol^{-1},

$\frac{367.9}{253}$ = 1.45 g

Therefore; 1.45 g of $Na_5P_3O_{10}$ in 1 litre of water gave a stock solution of 1000 ppm of $P_3O_{10}^{5-}$ ions. Consequently 14.5 mg of $Na_3P_3O_9$ in 100 ml volumetric flask, gave a stock solution of 100 ppm $P_3O_{10}^{5-}$ ions.

As stated in section 2.11.2, the concentrations of each of the above standards were calculated accurately by back calculating the initial amounts.

2.14 Analysis of Fe^{2+} and Fe^{3+} using Ion Chromatography:

The analysis of iron ions was also conducted on the Dionex ICS-2500 ion chromatography system (Dionex, UK). An IonPac® CS5A column with attached CG5A guard column was used for the determination of iron (Fe^{2+} and Fe^{3+} ions).

The MetPac PDCA eluent used, was obtained as a ready to dilute concentrate, available from Dionex (UK). The MetPac PDCA eluent used pyridine-2, 6-dicarboxylic acid as a strong complexing agent. Most complexing agents separated metal complexes via anion exchange, thus the resulting metal complex would have a negative charge. The metals were then detected by measuring the absorbance at 530nm of the complex formed with the postcolumn PAR reagent diluent.

The MetPac PAR Postcolumn Reagent Diluent (Dionex, U.K.) used 4-(2-pyridylazo) resorcinol (PAR) to form a light-absorbing complex, and was added through a mixing tee, which was pressurised using a separate pneumatic PC10 unit (Dionex, U.K.). The sample run time was set for 10 minutes.

Prior to running the samples, the ICS-2500 was calibrated using iron (II) chloride and iron (III) chloride (Sigma Aldrich, U.K.) as the reagents. A mixed (Fe^{2+} and Fe^{3+}) 100ppm stock solution was made, from which 1, 10, 25 and 50ppm standard solutions were prepared.

CHAPTER 3

The Ternary P_2O_5 – CaO – Na_2O Glass System

3.0 The Ternary P_2O_5 – CaO – Na_2O Glass System:

3.1 Ternary Compositions Investigated:

The ternary compositions investigated are tabulated in Table 3.1 below, including the glass codes used and compositions analysed. Note that the glass codes used represent the mol% of each oxide. The procedures and starting materials used have all been listed in section 2.1.

Table 3.1: Glass codes along with oxide composition in mol%.

Glass Codes	P_2O_5 (mol%)	CaO (mol%)	Na_2O (mol%)
$P_{45}Ca_{30}Na_{25}$	45	30	25
$P_{45}Ca_{35}Na_{20}$	45	35	20
$P_{45}Ca_{40}Na_{15}$	45	40	15
$P_{50}Ca_{30}Na_{20}$	50	30	20
$P_{50}Ca_{35}Na_{15}$	50	35	15
$P_{50}Ca_{40}Na_{10}$	50	40	10
$P_{55}Ca_{30}Ca_{15}$	55	30	15
$P_{55}Ca_{35}Na_{10}$	55	35	10
$P_{55}Ca_{40}Na_5$	55	40	5

3.2 Differential Thermal Analysis:

The DTA traces obtained exhibited clear glass transition (T_g) and crystallisation temperature (T_c) peaks, with some compositions exhibiting two T_c peaks and two melting temperature (T_m) peaks. Figure 3.1 shows the DTA traces obtained from the fixed 45 mol% P_2O_5 compositions.

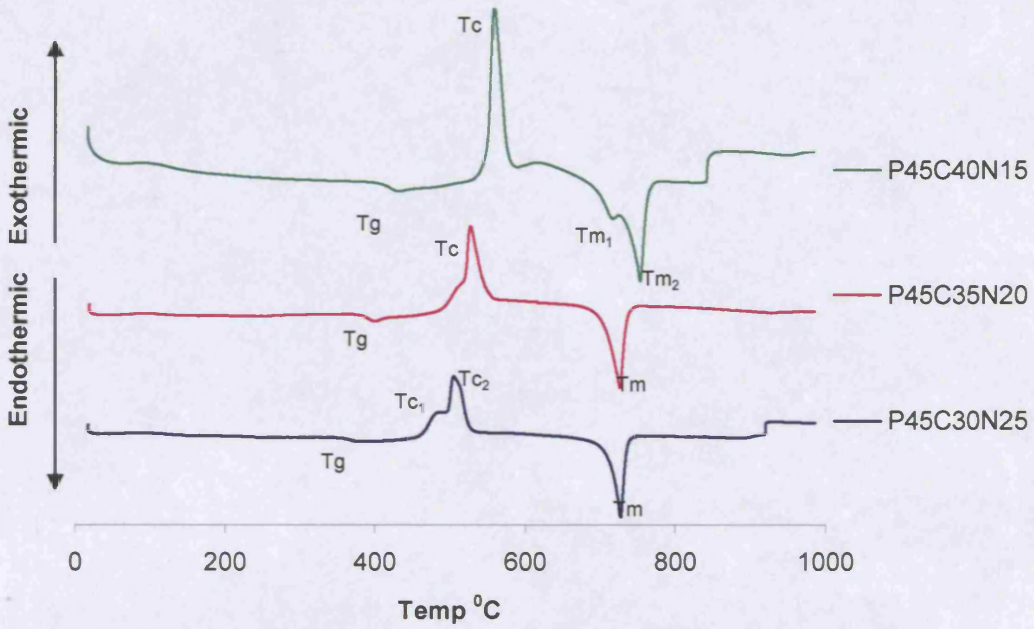

Figure 3.1: DTA traces obtained from the fixed 45 mol% P_2O_5 compositions investigated.

An increase in T_g temperatures was seen with increasing CaO mol% as expected. The occurrence of two T_c peaks (seen for glass code $P_{45}Ca_{30}Na_{25}$ above) was indicative of the existence of two crystalline phases present within that particular

composition. However, for some compositions two T_m peaks were observed, as seen for glass code $P_{45}Ca_{40}Na_{15}$ at 727°C and 761°C respectively.

Two T_m peaks were also observed for glass code $P_{50}Ca_{30}Na_{20}$ at 731°C and 760°C (See Figure 3.2). The melting temperatures of this glass composition were similar to the T_m peaks observed for glass code $P_{45}Ca_{40}Na_{15}$ indicating the presence of similar phases. As previously stated, glass-fibres were only obtained from the fixed 50 and 55 mol% P_2O_5 compositions. As the drawing of glass-fibres involved re-melting of the bulk glass, a viscosity suitable for fibre production needed to be achieved. Thermal analysis was therefore conducted on the glass fibres in order to investigate any thermal differences observed within the compositions.

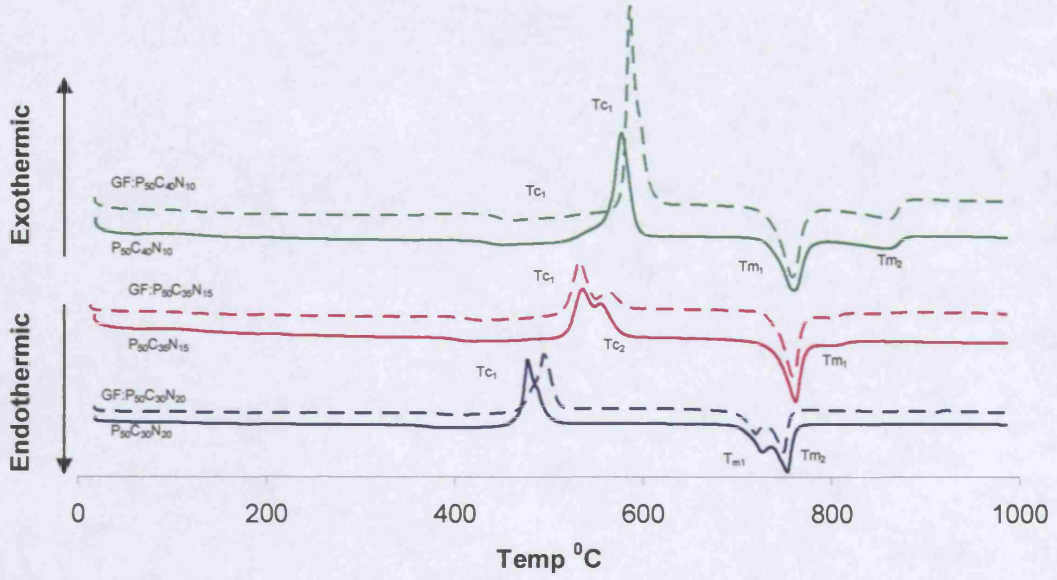

Figure 3.2: DTA traces of bulk glass (solid line) and glass-fibre (broken line) compositions of fixed 50 mol% P_2O_5.

Two T_m peaks for $P_{50}Ca_{40}Na_{10}$ were observed at 769 °C and 870 °C, as compared to 731°C and 760°C seen for glass code $P_{50}Ca_{30}Na_{20}$. Both compositions exhibited single T_c peaks suggesting a single crystalline phase; however the observation of two T_m peaks seen at different temperatures suggested that different phases were present in the compositions. With regards to the glass-fibre traces observed (seen in broken lines) a shift in T_c peaks was seen, however the T_m peaks were almost identical to the bulk glass traces obtained.

Two T_m peaks were also seen for glass codes $P_{55}Ca_{30}Na_{15}$ and $P_{55}Ca_{35}Na_{10}$ (See Figure 3.3 below). However, the T_c peaks seen for the bulk glass exhibited very broad patterns, which could have masked any additional T_c peak present. The DTA traces obtained for the glass fibres exhibited much clearer and defined peaks than those observed from the bulk glass. Another interesting observation was that the glass fibre T_c peaks decreased in temperature, in contrast to the overall increase in the T_c values observed for the glass fibres with fixed 50 mol% P_2O_5.

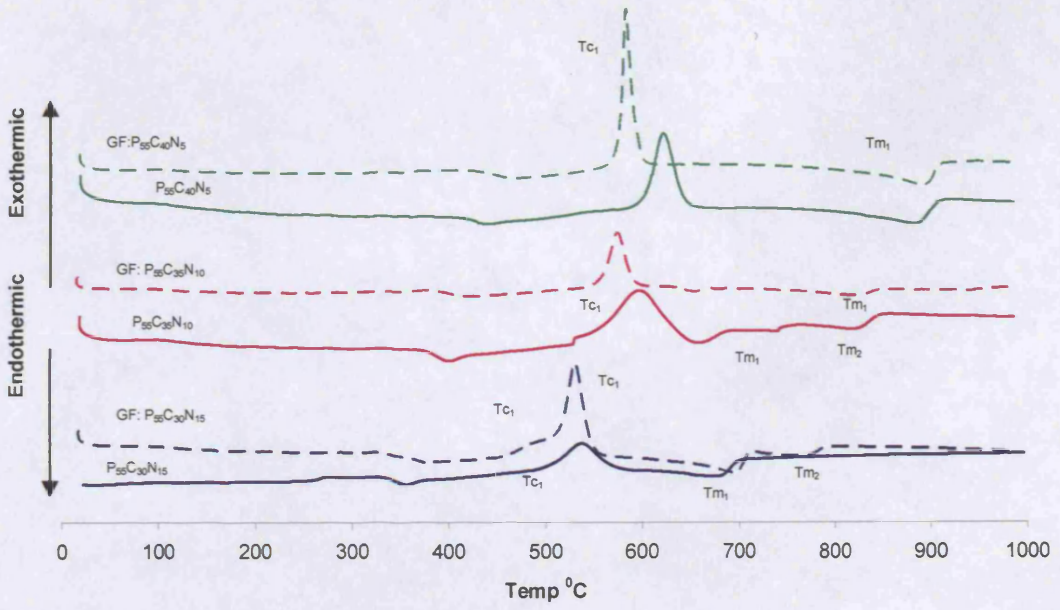

Figure 3.3: DTA traces of bulk glass (solid line) and glass-fibre (broken line) compositions of fixed 55 mol% P_2O_5.

The T_g values obtained showed an increase in temperature with increasing CaO content in the glass systems investigated. An increase in T_g temperature was also observed with increasing P_2O_5 content from 45 to 50 mol%, which then decreased with a further increase in P_2O_5 content to 55 mol%. Figure 3.4 shows the T_g values for the bulk glasses investigated.

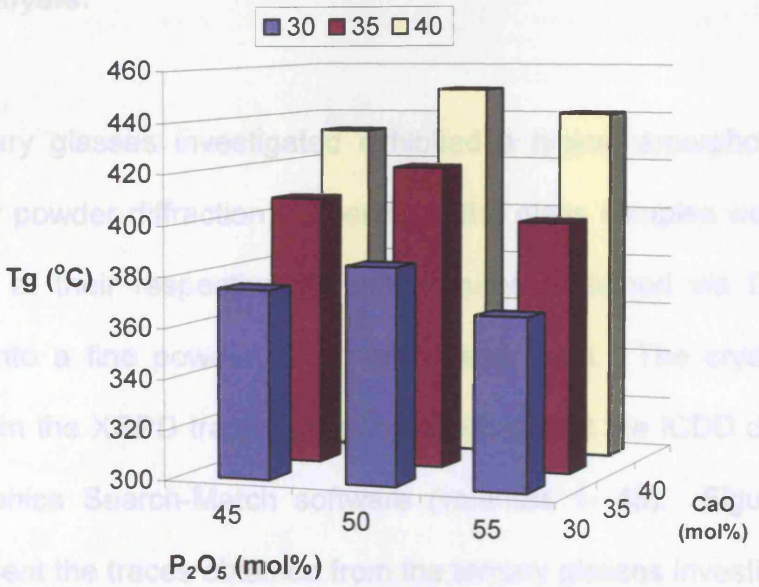

Figure 3.4: 3D graph of T_g values for the ternary compositions investigated.

The T_g values obtained for the bulk glass and glass-fibres are presented in Table 3.2. A slight decrease in T_g values was seen in the glass-fibres (as compared to the bulk glass), with the exception of glass codes $P_{55}Ca_{35}Na_{10}$ and $P_{55}Ca_{40}Na_5$ where an increase in T_g was observed.

Table 3.2: Comparison of bulk glass versus glass-fibre T_g values.

Glass Code	T_g (°C) Bulk Glass	T_g (°C) Glass Fibres
$P_{45}Ca_{30}Na_{25}$	374.88	N / O
$P_{45}Ca_{35}Na_{20}$	407.36	N / O
$P_{45}Ca_{40}Na_{15}$	432.96	N / O
$P_{50}Ca_{30}Na_{20}$	385.79	385.26
$P_{50}Ca_{35}Na_{15}$	420.6	413.27
$P_{50}Ca_{40}Na_{10}$	450.39	446.55
$P_{55}Ca_{30}N_{a15}$	367.77	366.26
$P_{55}Ca_{35}Na_{10}$	399.71	405.51
$P_{55}Ca_{40}Na_5$	440.64	451.95

N/O = not obtained.

3.3 XRD Analysis:

All the ternary glasses investigated exhibited a typical amorphous halo using XRPD (x-ray powder diffraction). Therefore, the glass samples were crystallised for an hour at their respective T_c temperatures (obtained via DTA analysis), ground up into a fine powder, and then re-examined. The crystalline phases observed from the XRPD traces were matched against the ICDD database using Crystallographica Search-Match software (volumes 1- 45). Figures 3.5 – 3.7 below represent the traces obtained from the ternary glasses investigated.

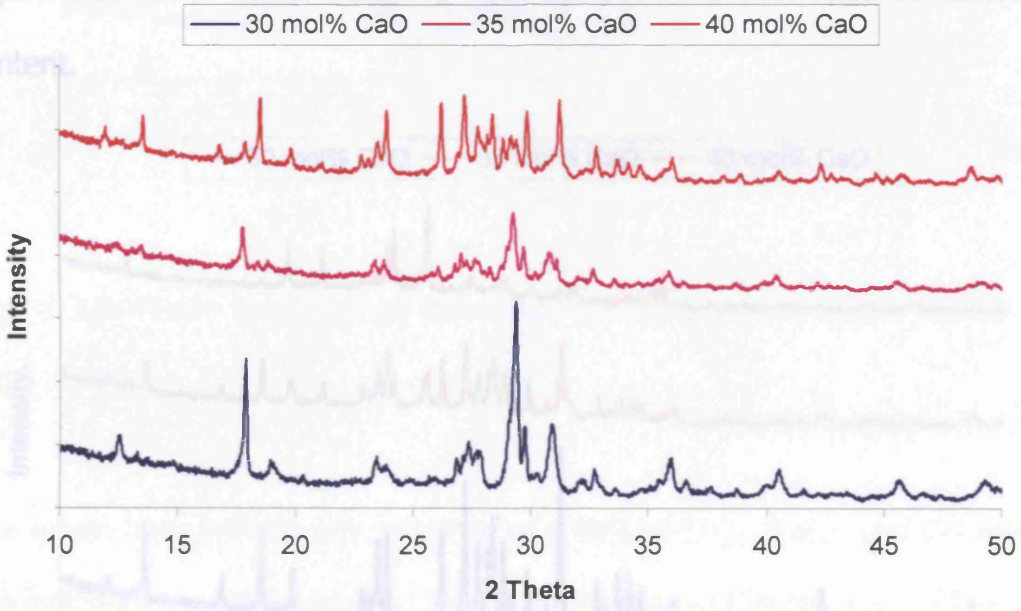

Figure 3.5: XRPD traces obtained from compositions with fixed 45 mol% P_2O_5 content.

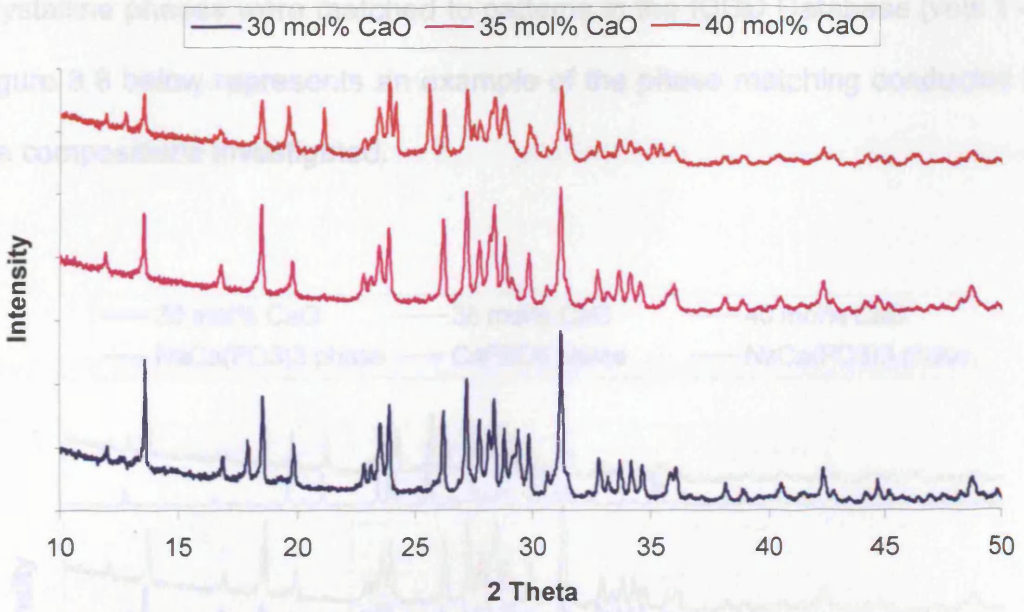

Figure 3.6: XRPD traces obtained from compositions with fixed 50 mol% P_2O_5 content.

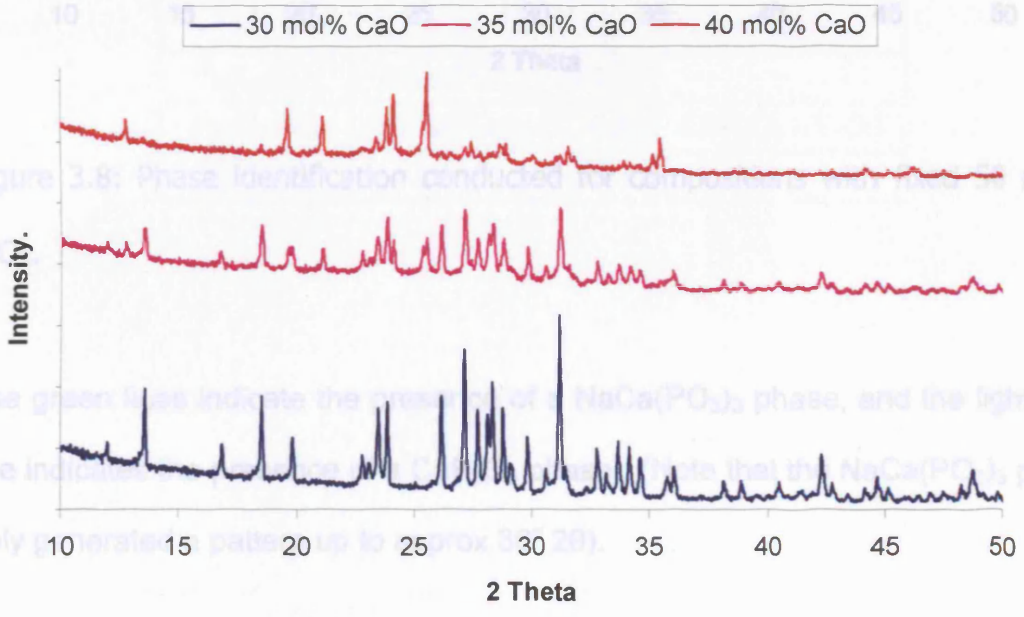

Figure 3.7: XRPD traces obtained from compositions with fixed 55 mol% P_2O_5 content.

Crystalline phases were matched to patterns in the ICDD Database (vols 1 – 45). Figure 3.8 below represents an example of the phase matching conducted for all the compositions investigated.

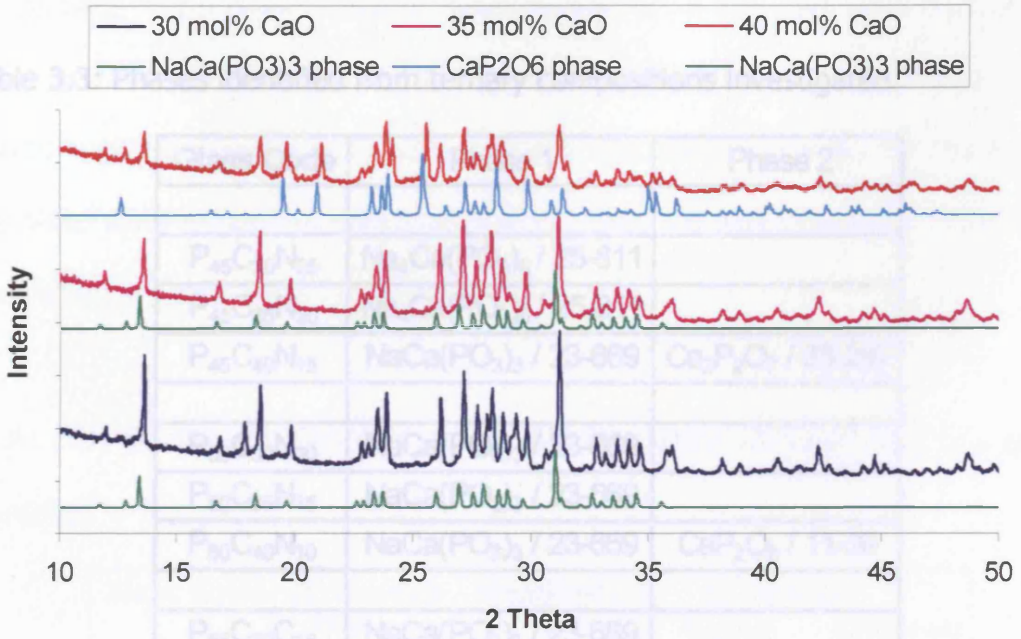

Figure 3.8: Phase identification conducted for compositions with fixed 50 mol% P_2O_5.

The green lines indicate the presence of a $NaCa(PO_3)_3$ phase, and the light blue line indicates the presence of a CaP_2O_6 phase. (Note that the $NaCa(PO_3)_3$ phase only generated a pattern up to approx 36° 2θ).

The phases identified for the ternary compositions investigated are shown in Table 3.3. The phases identified have been tabulated with their respective ICDD card number, to which each specific phase was assigned within the database.

Table 3.3: Phases identified from ternary compositions investigated.

Glass Code	Phase 1	Phase 2
$P_{45}C_{30}N_{25}$	$Na_4Ca(PO_3)_6$ / 25-811	
$P_{45}C_{35}N_{20}$	$Na_4Ca(PO_3)_6$ / 25-811	
$P_{45}C_{40}N_{15}$	$NaCa(PO_3)_3$ / 23-669	$Ca_2P_2O_7$ / 33-297
$P_{50}C_{30}N_{20}$	$NaCa(PO_3)_3$ / 23-669	
$P_{50}C_{35}N_{15}$	$NaCa(PO_3)_3$ / 23-669	
$P_{50}C_{40}N_{10}$	$NaCa(PO_3)_3$ / 23-669	CaP_2O_6 / 11-39
$P_{55}C_{30}C_{15}$	$NaCa(PO_3)_3$ / 23-669	
$P_{55}C_{35}N_{10}$	$NaCa(PO_3)_3$ / 23-669	CaP_2O_6 / 11-39
$P_{55}C_{40}N_5$	CaP_2O_6 / 11-39	

3.4 NMR Analysis:

NMR analysis was conducted at Queen Mary, University of London (QMUL). The ^{31}P NMR spectra were measured using the Bruker AMX 600, at a frequency of 242.9 MHz. The peak positions were measured in Hz, and were converted to ppm by dividing the values by 242.9. The Q-species were identified using the Win1d – NMR (version 5.1) software, and the ratios obtained for the species identified were measured using the WINFIT dm2000 NMR software. The results are shown in Table 3.4.

Table 3.4: Q^n species identified along with the ratios obtained for each species identified.

Glass Code	Q^n Species Identified / PPM no.s		Q^n Species Ratios Obtained	
	(Q^1)	(Q^2)	(Q^1)	(Q^2)
$P_{45}Ca_{30}Na_{25}$	Q^1 / -6.1	Q^2 / -22.1	21.71	78.29
$P_{45}Ca_{35}Na_{20}$	Q^1 / -6.9	Q^2 / -22.4	20.13	79.87
$P_{45}Ca_{40}Na_{15}$	Q^1 / -7.9	Q^2 / -23.7	17.04	82.96
$P_{50}Ca_{30}Na_{20}$		Q^2 / -23.8	1.80	98.20
$P_{50}Ca_{35}Na_{15}$		Q^2 / -24.5	3.21	96.79
$P_{50}Ca_{40}Na_{10}$		Q^2 / -25.2	1.40	98.60
$P_{55}Ca_{30}Na_{15}$		Q^2 / -25.8	0.31	99.69
$P_{55}Ca_{35}Na_{10}$		Q^2 / -26.7	3.51	96.49
$P_{55}Ca_{40}Na_5$		Q^2 / -27.2	1.83	98.17

The spectra obtained for the compositions with fixed 45 mol% P_2O_5 exhibited two main peaks. Band A (~ -20ppm) and Band B (~ -6ppm) with corresponding spinning side bands were found on both the left and right hand side of the two main peaks.

Band A of lower frequency was assigned to Q^2 phosphates, whilst band B of higher frequency was assigned to Q^1 phosphate species. A fit was applied to the spectra obtained, which gave the Q^n species identified from the glasses investigated, and also gave the ratios of the species identified.

3.5 Degradation Studies:

3.5.1 Bulk Glass Degradation Studies:

All bulk glass measurements were conducted in deionised water. Weight loss results were plotted in $mg.mm^{-2}$ against time, and using the line fit in Excel, a line of best fit was fitted through the origin and with a maximal R^2 value. The slope of the fitted lines gave the degradation/dissolution rate in terms of $mg.mm^{-2}.hr^{-1}$.

Some of the data obtained appeared to exhibit an initial $t^{½}$ kinetic at very early time points, after which the data seen was linear. Also, when fitting a straight line to this data the R^2 values obtained were very close to 1. Therefore a linear plot was used to obtain the rate values, in order to compare the rates obtained from each of the compositions investigated.

In a previous study conducted, measurements were taken from discs in a static environment. It was found that some of the compositions investigated (i.e. higher calcium containing glasses) exhibited a more exponential trend, and lines of best fit could not be accurately applied in those cases. This was initially attributed to precipitation build-up observed over long periods of time from some of the glass compositions investigated.

However, the method of changing the solution at every time point proved to be a more accurate form of analysis as no precipitation was experienced, and relatively straight linear plots were obtained from the graphs plotted. See Figures 3.9 – 3.11 below for dissolution plots obtained from the ternary compositions investigated.

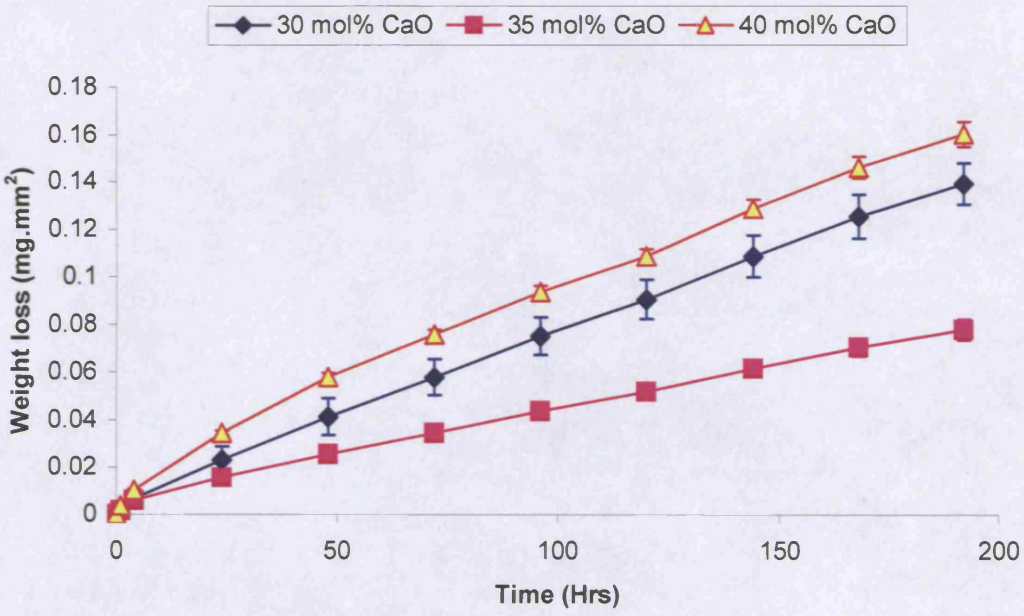

Figure 3.9: Weight loss graph for bulk glass compositions with fixed 45 mol% P_2O_5.

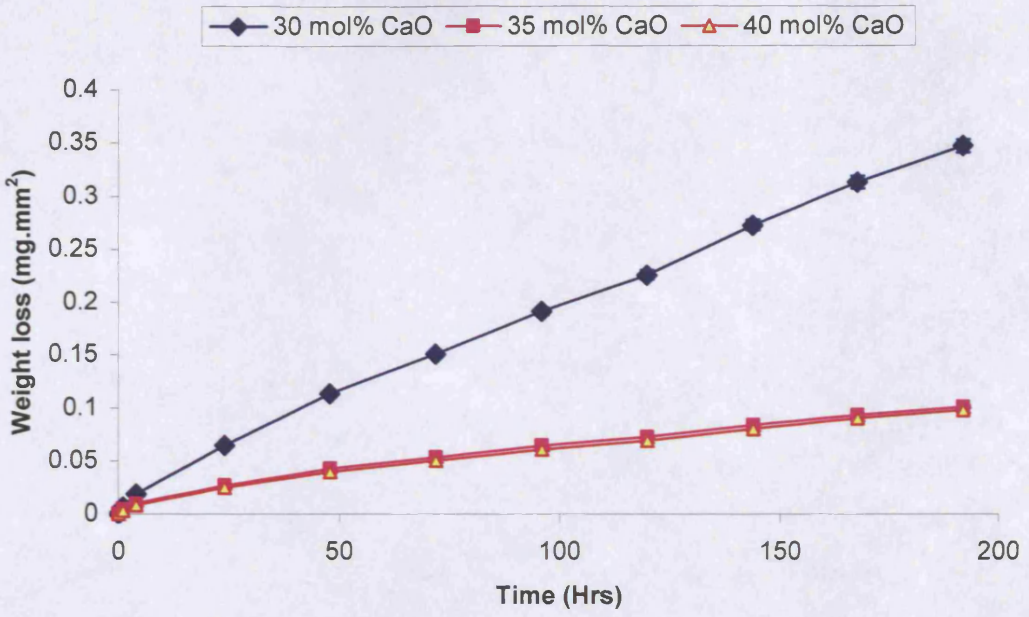

Figure 3.10: Weight loss graph for bulk glass compositions with fixed 50 mol% P_2O_5.

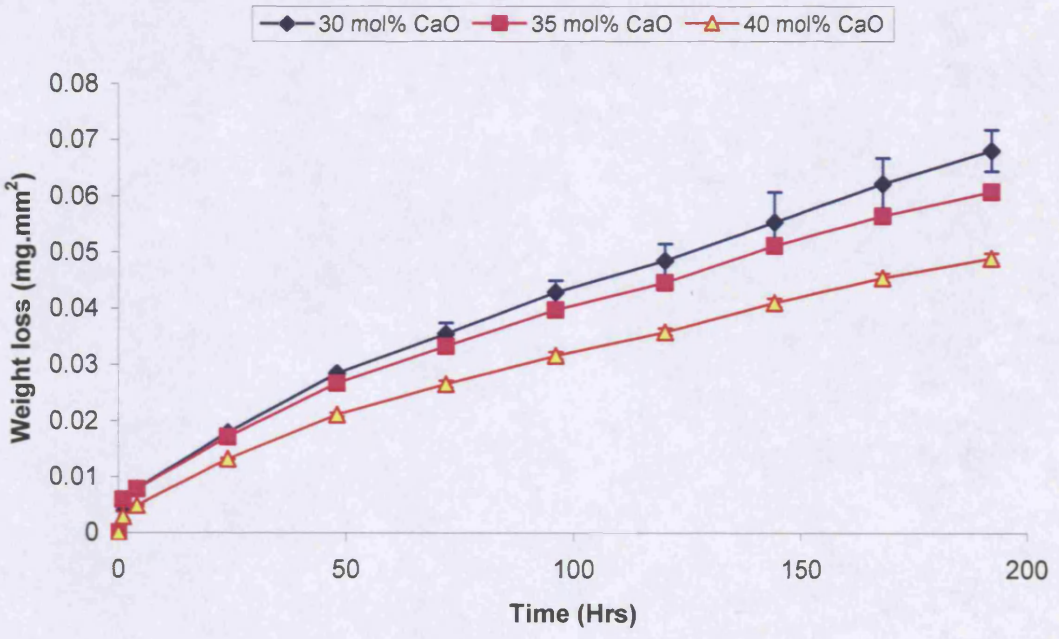

Figure 3.11: Weight loss graph for bulk glass compositions with fixed 55 mol% P_2O_5. (The values obtained from the slopes of the graphs are shown in Table 3.5)

Table 3.5: Bulk glass dissolution rates obtained from the ternary compositions investigated.

Composition (Glass codes)	Dissolution Rates ($mg.mm^{-2}.hr^{-1}$)
$P_{45}Ca_{30}Na_{25}$	0.00075
$P_{45}Ca_{35}Na_{20}$	0.00043
$P_{45}Ca_{40}Na_{15}$	0.00089
$P_{50}Ca_{30}Na_{20}$	0.00189
$P_{50}Ca_{35}Na_{15}$	0.00058
$P_{50}Ca_{40}Na_{10}$	0.00056
$P_{55}Ca_{30}Na_{15}$	0.00039
$P_{55}Ca_{35}Na_{10}$	0.00036
$P_{55}Ca_{40}Na_{5}$	0.00029

As can be seen from the above table, the glass system with fixed 45 mol% P_2O_5 showed an initial decrease in the rate of dissolution with an increase in CaO content. However, with a further (5 mol%) increase in CaO content, the dissolution rate increased and was higher than the 30 mol% CaO composition (glass code $P_{45}Ca_{30}Na_{25}$).

For the glass system with fixed 50 mol% P_2O_5 a decrease in the dissolution rates was observed with increasing CaO content. However, within the system there was a very large decrease in the rates observed, from glass code $P_{50}Ca_{30}Na_{20}$ to glass codes $P_{50}Ca_{35}Na_{15}$ and $P_{50}Ca_{40}Na_{10}$.

With regards to the glass system with fixed 55 mol% P_2O_5, a relatively linear decrease in the dissolution rates was observed with an increase in CaO content.

3.5.2 Glass-Fibre Degradation Studies:

3.5.2.1 Glass-Fibre Diameter Measurements:

Prior to conducting the glass-fibre dissolution studies, glass-fibre diameters were obtained. As stated previously, the fibres were obtained at different RPMs, which pertained to metres per minute, as the circumference of the drum onto which the fibres were pulled was one metre. Figures 3.12 and 3.13 below show the diameters obtained. A decrease in the diameter size was observed with an increase in RPM.

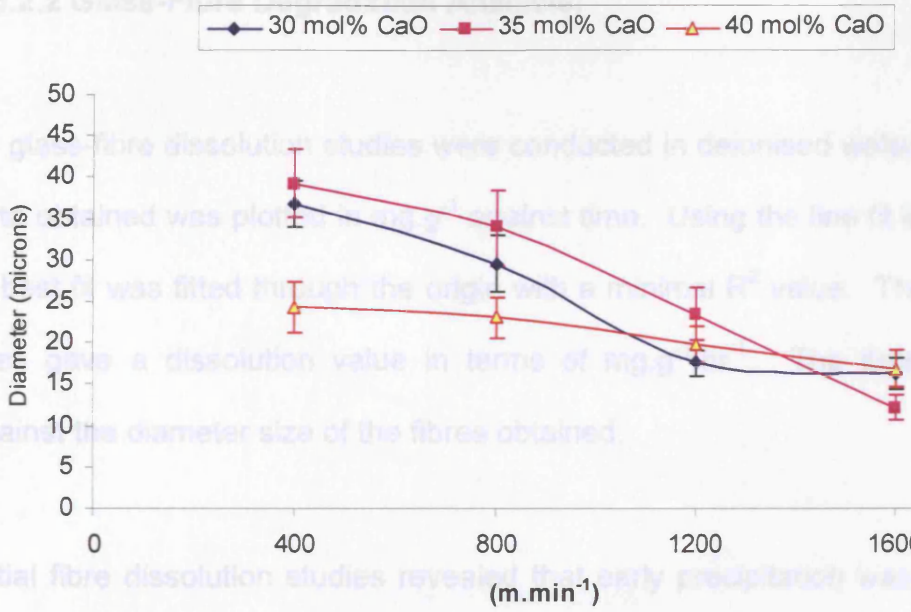

Figure 3.12: Fibre diameters obtained for glasses with fixed 50 mol% P_2O_5.

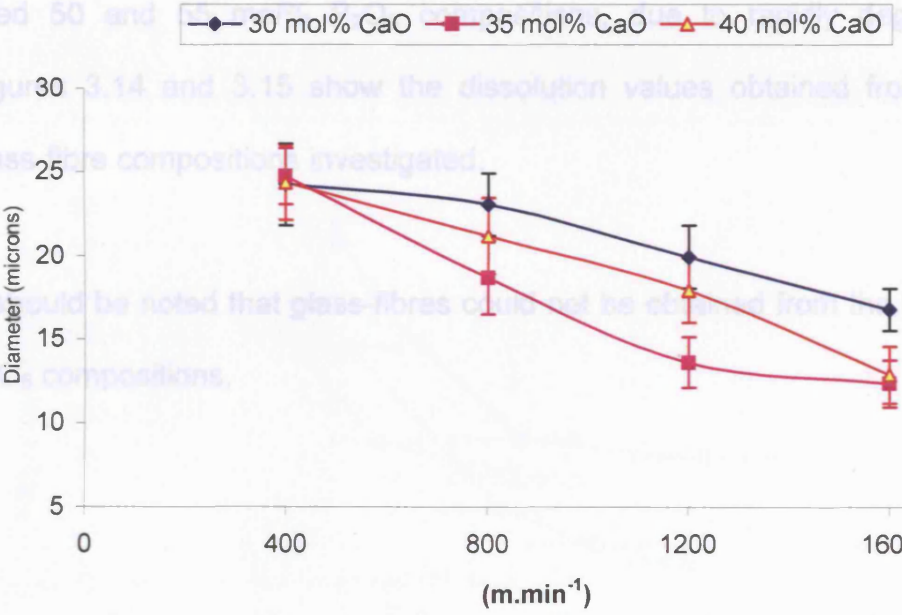

Figure 3.13: Fibre diameters obtained for glasses with fixed 55 mol% P_2O_5.

3.5.2.2 Glass-Fibre Degradation Analysis:

All glass-fibre dissolution studies were conducted in deionised water. Weight loss data obtained was plotted in $mg.g^{-1}$ against time. Using the line fit in Excel, a line of best fit was fitted through the origin with a minimal R^2 value. The slope of the lines gave a dissolution value in terms of $mg.g^{-1}.hr^{-1}$. The data was plotted against the diameter size of the fibres obtained.

Initial fibre dissolution studies revealed that early precipitation was occurring for some of the faster degrading compositions, making it difficult to obtain accurate dissolution rates. Therefore, the dissolution analysis was set for 6 hours for the fixed 50 and 55 mol% P_2O_5 compositions, due to rapidly degrading fibres. Figures 3.14 and 3.15 show the dissolution values obtained from the ternary glass-fibre compositions investigated.

It should be noted that glass-fibres could not be obtained from the fixed 45 mol% P_2O_5 compositions.

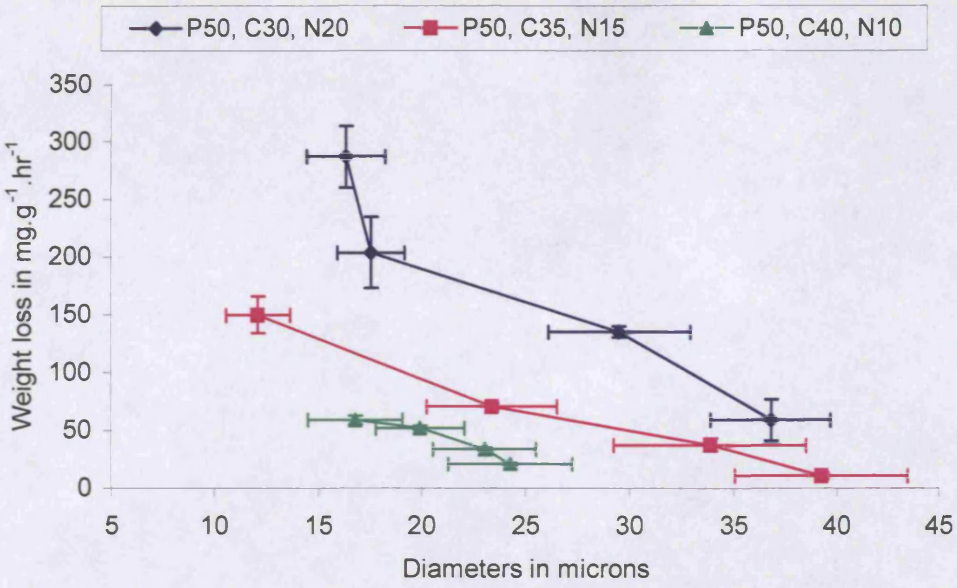

Figure 3.14: Weight loss graph for glass-fibre compositions with fixed 50 mol% P_2O_5.

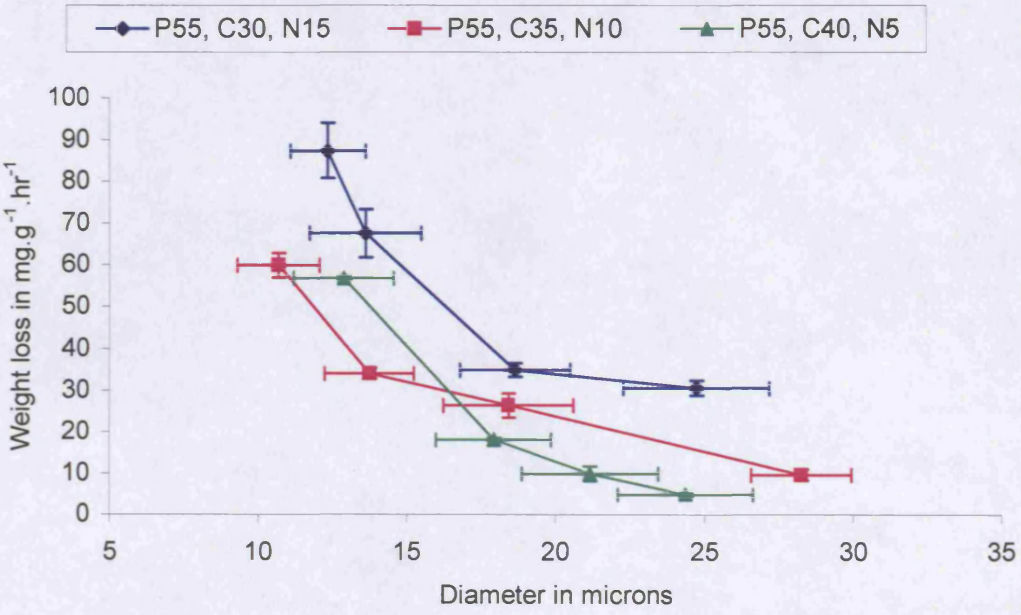

Figure 3.15: Weight loss graph for glass-fibre compositions with fixed 55 mol% P_2O_5.

3.6 pH Measurements:

The pH values of the solutions obtained remained relatively neutral for the duration of the bulk glass degradation study for the fixed 45 mol% P_2O_5 compositions, with the exception of the composition with glass code $P_{45}Ca_{40}Na_{15}$, whose pH value dipped to around pH 6 (see Figure 3.16) . For the compositions with fixed 50 and 55 mol% P_2O_5, the pH values dropped to between pH 3 and pH 4 (see Figures 3.17 and 3.18).

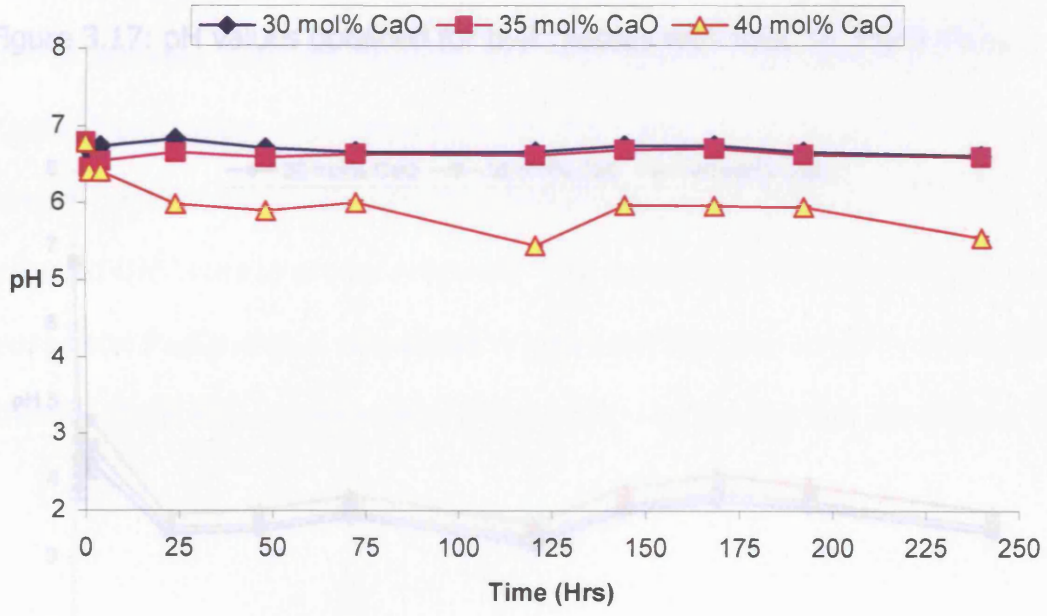

Figure 3.16: pH values obtained for bulk glasses with fixed 45 mol% P_2O_5.

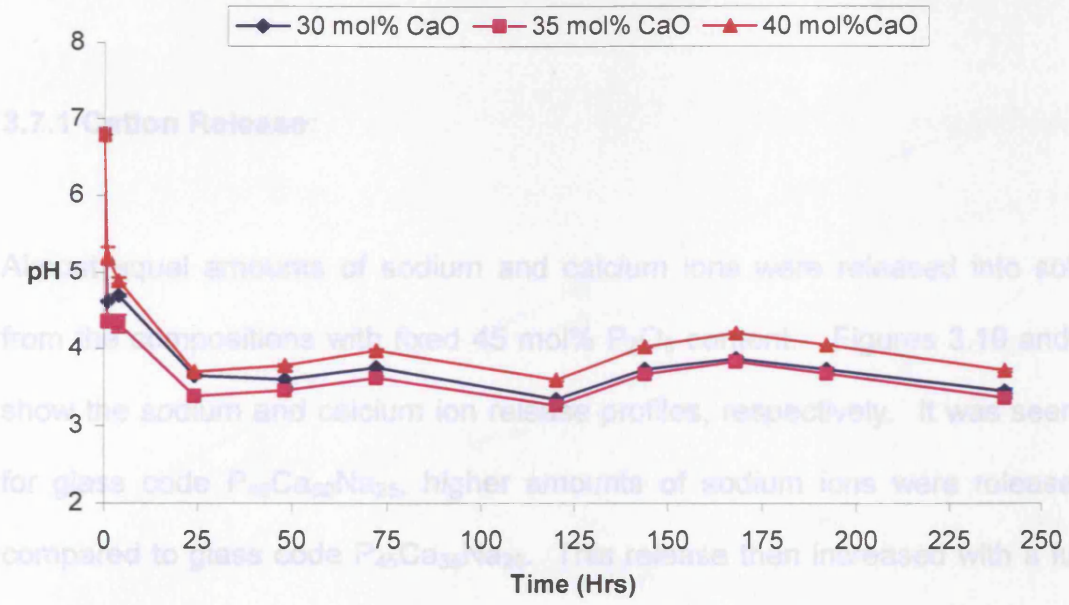

Figure 3.17: pH values obtained for bulk glasses with fixed 50 mol% P_2O_5.

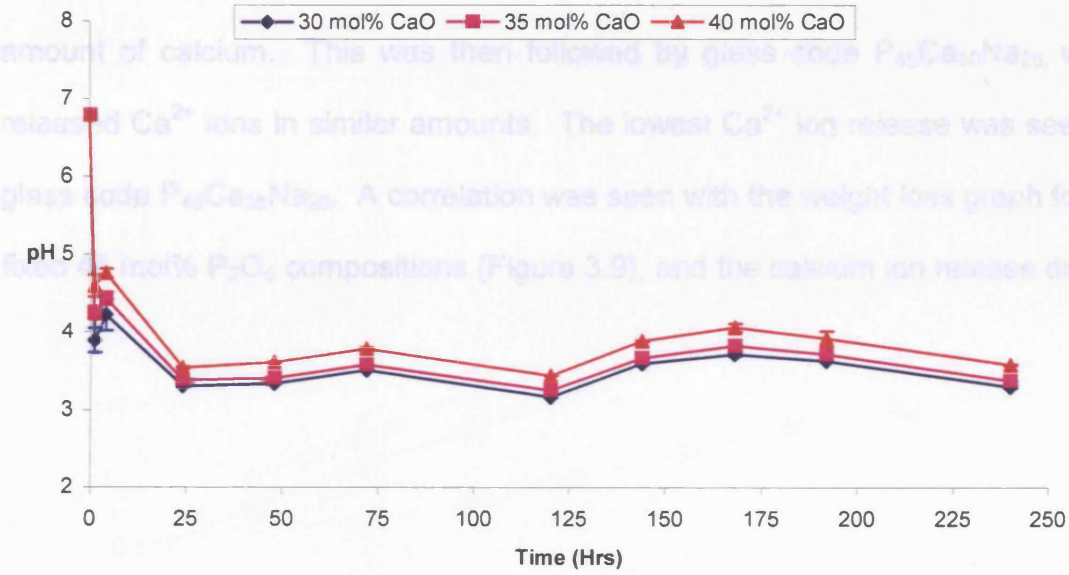

Figure 3.18: pH values obtained for bulk glasses with fixed 55 mol% P_2O_5.

3.7 Ion Release from Glasses with Fixed 45 mol% P_2O_5 Content:

3.7.1 Cation Release:

Almost equal amounts of sodium and calcium ions were released into solution from the compositions with fixed 45 mol% P_2O_5 content. Figures 3.19 and 3.20 show the sodium and calcium ion release profiles, respectively. It was seen that for glass code $P_{45}Ca_{30}Na_{25}$, higher amounts of sodium ions were released as compared to glass code $P_{45}Ca_{35}Na_{20}$. This release then increased with a further increase in CaO content, for glass code $P_{45}Ca_{40}Na_{15}$. The calcium ion release curves showed that the highest Ca^{2+} ion release was seen for glass code $P_{45}Ca_{40}Na_{15,}$ which was expected as this composition contained the highest amount of calcium. This was then followed by glass code $P_{45}Ca_{30}Na_{25,}$ which released Ca^{2+} ions in similar amounts. The lowest Ca^{2+} ion release was seen for glass code $P_{45}Ca_{35}Na_{20}$. A correlation was seen with the weight loss graph for the fixed 45 mol% P_2O_5 compositions (Figure 3.9), and the calcium ion release data.

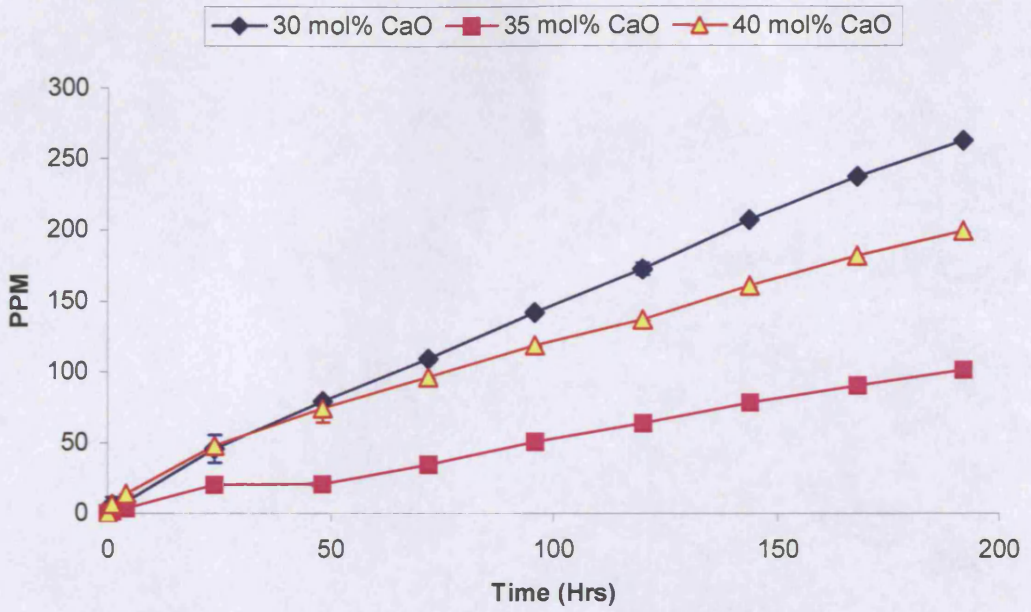

Figure 3.19: Sodium ion release profiles from glasses with fixed 45 mol% P_2O_5 content.

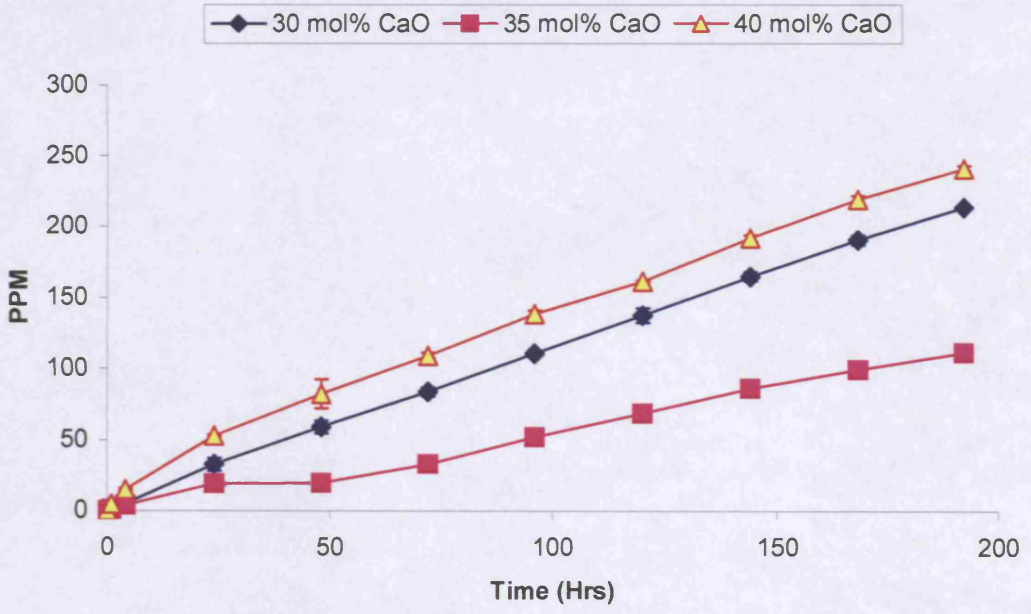

Figure 3.20: Calcium ion release profiles from glasses with fixed 45 mol% P_2O_5 content.

3.7.2 Anion release:

It was seen that the graphs for PO_4^{3-}, $P_2O_7^{4-}$ and $P_3O_{10}^{5}$ anions all exhibited similar plots of release (Figure 3.21, 3.22 and 3.24). The rates of release for these anions all decreased with an increase in CaO content, (or vice versa, decreased with a decrease in Na_2O content). The highest rate of anion release was seen for the cyclic trimetaphosphate $P_3O_9^{3-}$ anion (Figure 3.23). The rate of release for this anion resembled the trends seen from the sodium ion release graph (Figure 3.19).

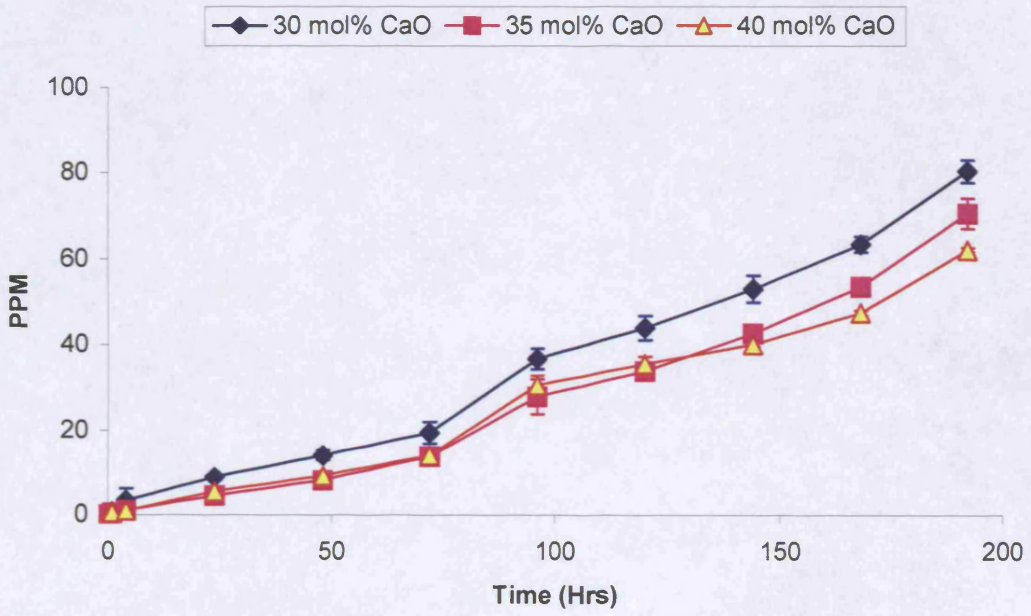

Figure 3.21: Graph showing orthophosphate PO_4^{3-} anion release from glasses with fixed 45 mol% P_2O_5.

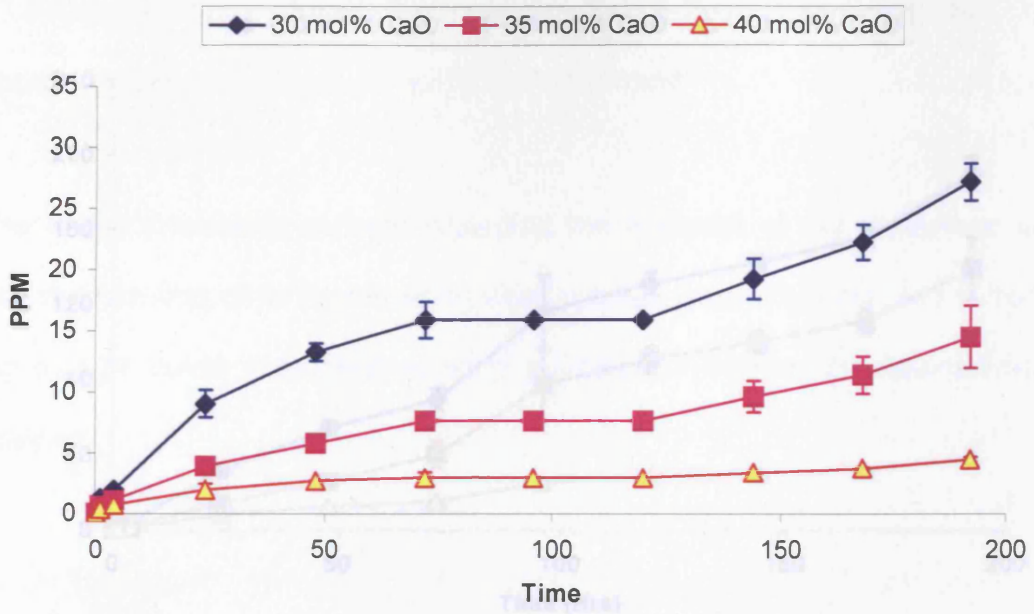

Figure 3.22: Graph showing pyrophosphate $P_2O_7^{4-}$ anion release from glasses with fixed 45 mol% P_2O_5.

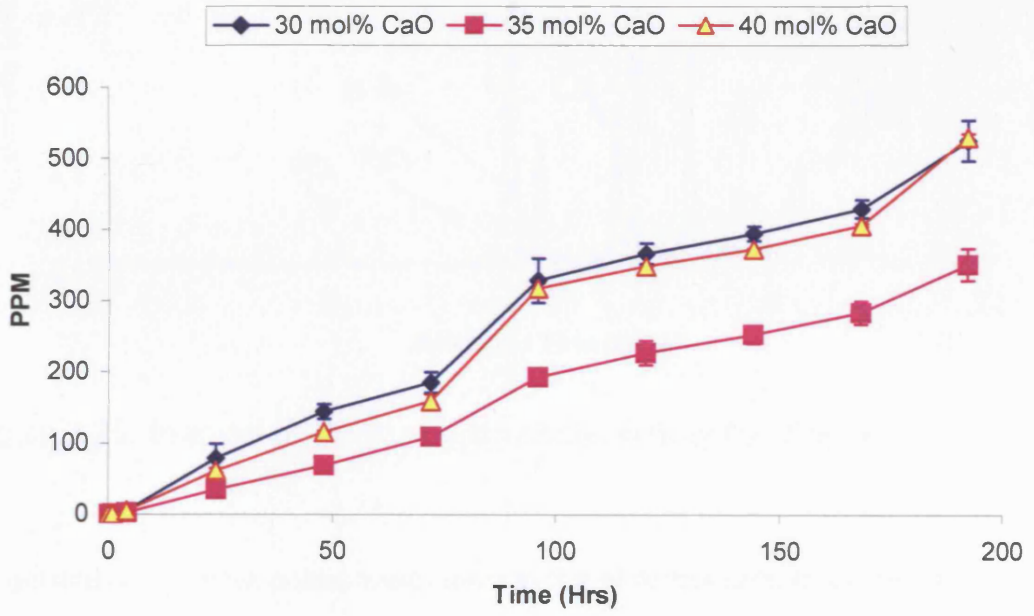

Figure 3.23: Graph showing cyclic trimetaphosphate $P_3O_9^{3-}$ anion release from glasses with fixed 45 mol% P_2O_5.

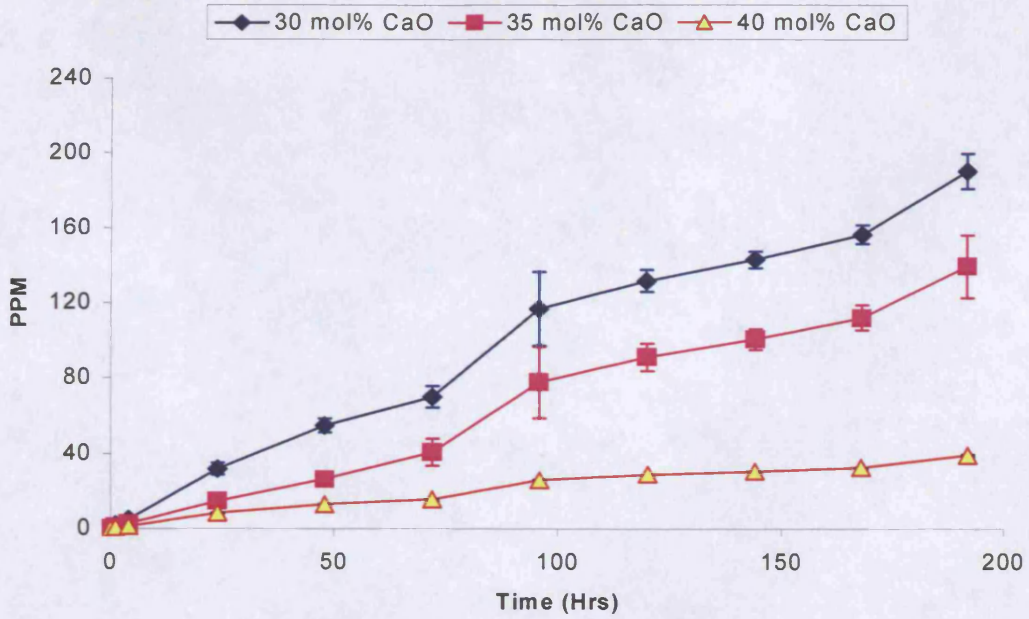

Figure 3.24: Graph showing linear tripolyphosphate $P_3O_{10}^{5-}$ anion release from glasses with fixed 45 mol% P_2O_5.

3.7.3 Quantification of additional peaks using a Response Factor, for Compositions with Fixed 45 mol% P_2O_5 Content:

One of the interesting aspects regarding the analyses of the phosphate anions was the fact that other higher phosphate species were also detected in solution. Figure 3.25 below is representative of a typical chromatogram obtained from IC analysis.

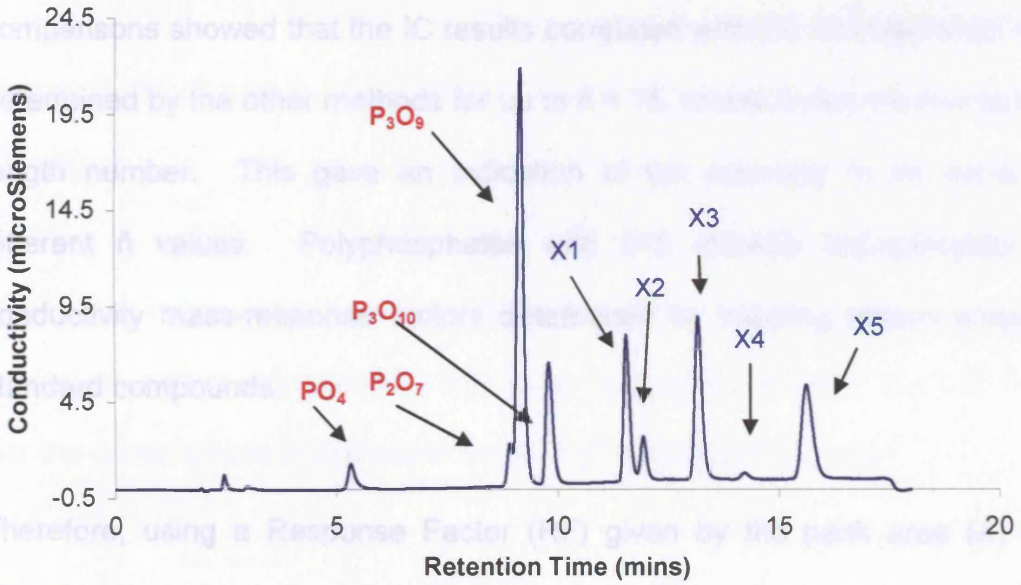

Figure 3.25: Example of chromatogram obtained from the ICS-2500.

In general up to nine peaks were seen in the chromatograms obtained. Since the majority of the peaks eluted before the 30 minute time point, this was set as the sample run time. In turn, this reduced the overall run time to analyse the samples, and minimised the possibility of hydrolytic dissolution of the phosphate species in

solution. The extra peaks observed were labelled as peaks X1 - X5, and an attempt was made to quantify the unidentified longer chain polyphosphates detected in solution.

It had been suggested by Stover *et al* (81) that by using the area under peaks it was possible to semi-quantitatively calculate the additional phosphate peaks seen in the chromatograms obtained. Their study compared the results of the average phosphate chain lengths calculated using peak areas from the IC analysis, with those calculated from ^{31}P NMR and potentiometric pH titrations. The comparisons showed that the IC results correlated with the average chain lengths determined by the other methods for up to $\check{n} = 15$, where $\check{n}$ was the average chain length number. This gave an indication of the accuracy to be expected at different $\check{n}$ values. Polyphosphates with $\check{n}<5$ showed approximately equal conductivity mass-response factors determined by injecting known amounts of standard compounds.

Therefore, using a Response Factor (RF) given by the peak area (A) versus concentration (C), as represented by the gradient obtained from the $P_3O_{10}^{5-}$ calibration (Figure 3.26), it was possible to quantify the additional eluting polyphosphate species.

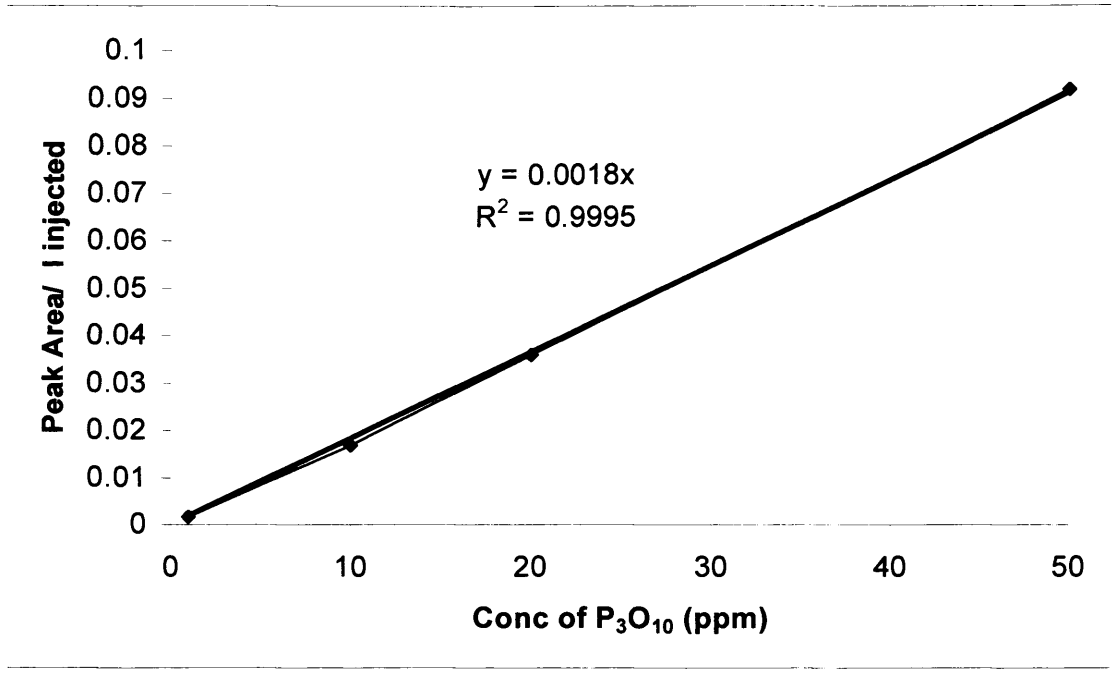

Figure 3.26: Example of Response Factor (RF) obtained from the $P_3O_{10}^{5-}$ calibration.

Similarly, if cyclic metaphosphates were present, these could also be quantified via the RF value obtained from the cyclic trimetaphosphate ($P_3O_9^{3-}$) calibration. For the compositions investigated the $P_3O_{10}^{5-}$ calibration was used.

Using this hypothesis (and the above calculated RF), peaks labelled X1 – X5 were quantified making the assumption that they were linear in structure. Figures 3.27 – 3.31 show the quantification of these additional peaks observed for the fixed 45 mol% P_2O_5 compositions investigated.

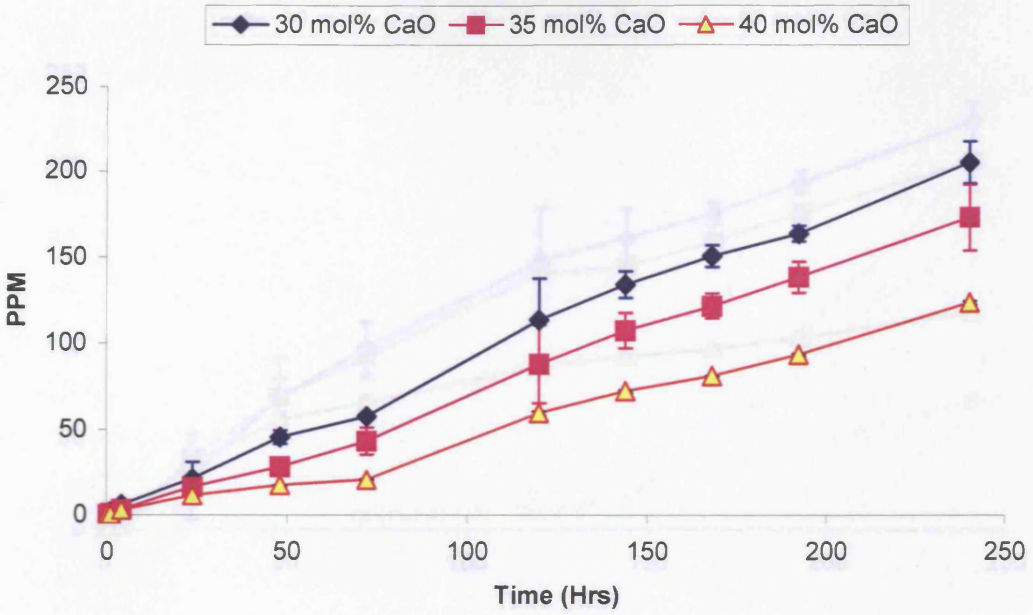

Figure 3.27: Anion release from peak labelled X1.

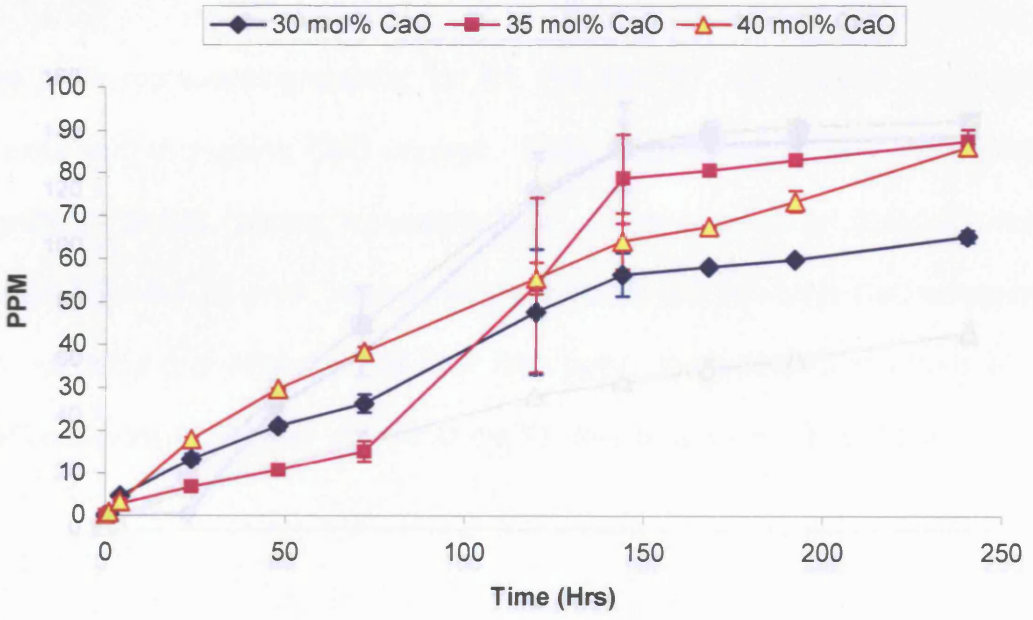

Figure 3.28: Anion release from peak labelled X2.

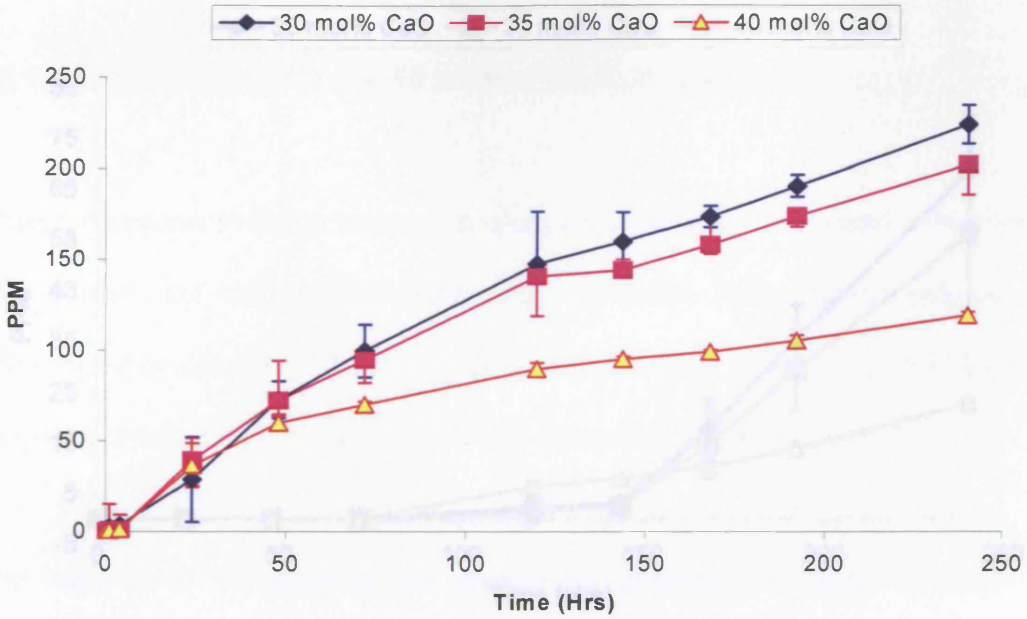

Figure 3.29: Anion release from peak labelled X3.

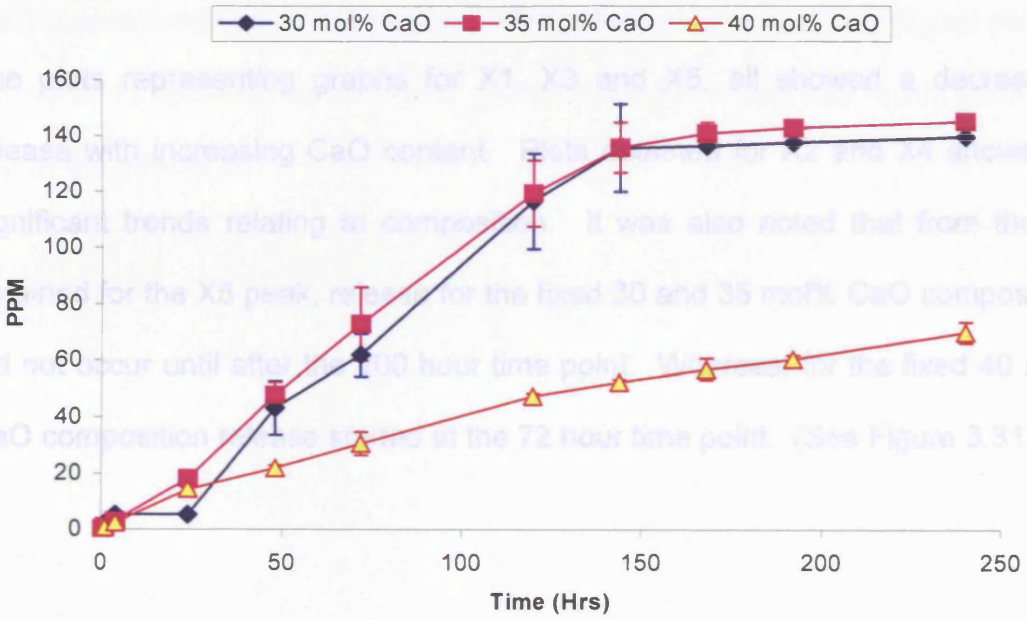

Figure 3.30: Anion release from peak labelled X4.

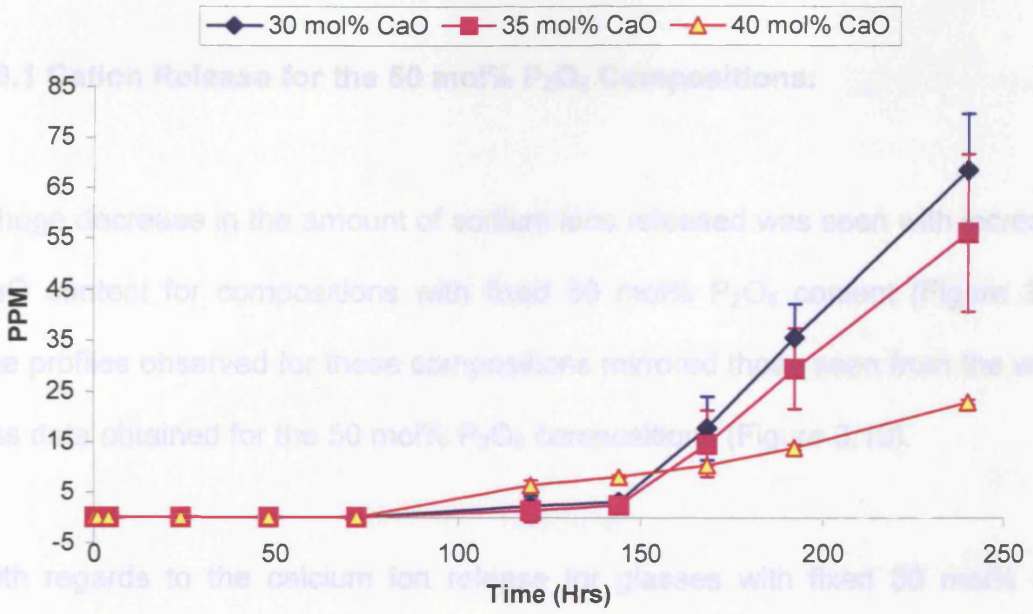

Figure 3.31: Anion release from peak labelled X5.

The plots representing graphs for X1, X3 and X5, all showed a decrease in release with increasing CaO content. Plots obtained for X2 and X4 showed no significant trends relating to composition. It was also noted that from the plot obtained for the X5 peak, release for the fixed 30 and 35 mol% CaO compositions did not occur until after the 100 hour time point. Whereas, for the fixed 40 mol% CaO composition release started at the 72 hour time point. (See Figure 3.31).

3.8 Ion Release from Glasses with Fixed 50 and 55 mol% P_2O_5 Content:

3.8.1 Cation Release for the 50 mol% P_2O_5 Compositions:

A huge decrease in the amount of sodium ions released was seen with increasing CaO content for compositions with fixed 50 mol% P_2O_5 content (Figure 3.32). The profiles observed for these compositions mirrored those seen from the weight loss data obtained for the 50 mol% P_2O_5 compositions (Figure 3.10).

With regards to the calcium ion release for glasses with fixed 50 mol% P_2O_5 (Figure 3.33), a large decrease in the rate of release was seen with an increase in CaO content from 30 to 35 mol%. However, the rate of release seen when the CaO content was further increased to 40 mol% was comparatively higher than the 35 mol% composition at later time points, although it was still much lower than that of the 30 mol%

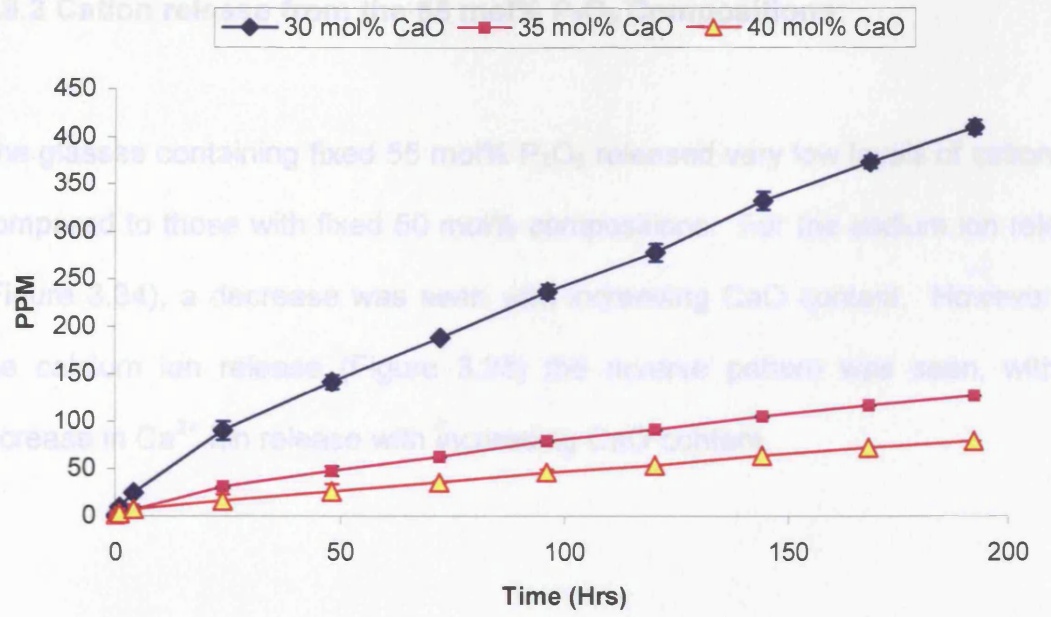

Figure 3.32: Sodium ion release profiles for glasses with fixed 50 mol% P_2O_5.

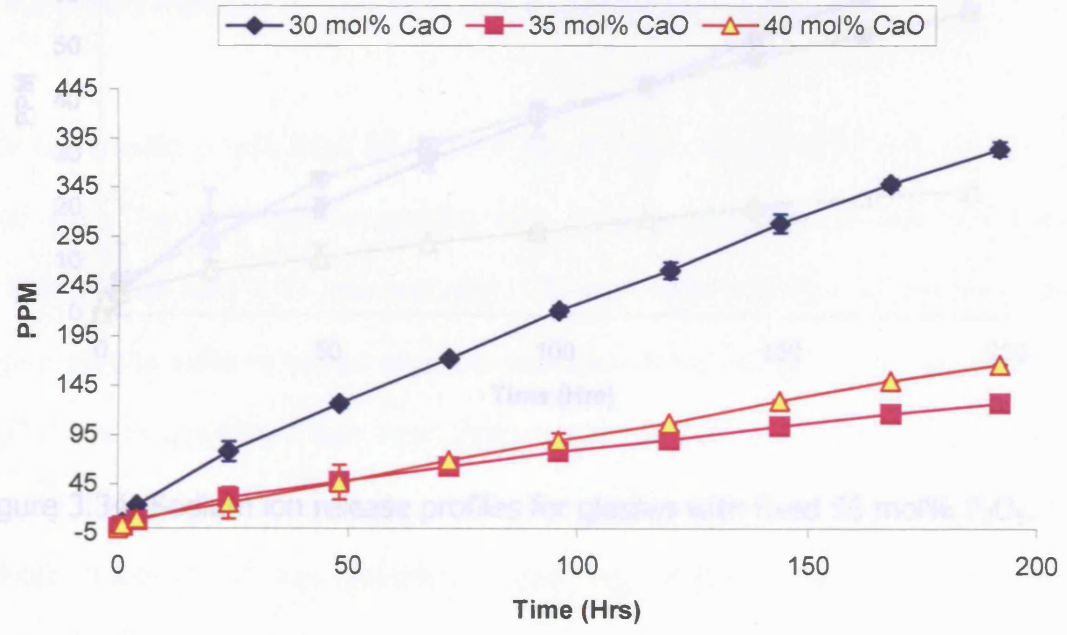

Figure 3.33: Calcium ion release profiles for glasses with fixed 50 mol% P_2O_5.

3.8.2 Cation release from the 55 mol% P_2O_5 Compositions:

The glasses containing fixed 55 mol% P_2O_5 released very low levels of cations as compared to those with fixed 50 mol% compositions. For the sodium ion release (Figure 3.34), a decrease was seen with increasing CaO content. However, for the calcium ion release (Figure 3.35) the reverse pattern was seen, with an increase in Ca^{2+} ion release with increasing CaO content.

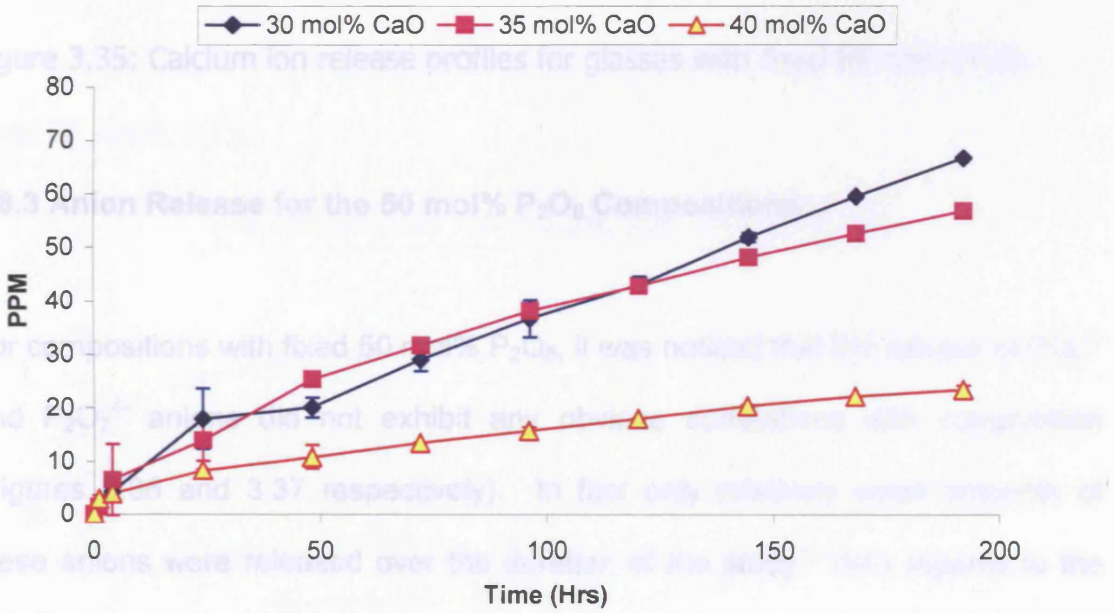

Figure 3.34: Sodium ion release profiles for glasses with fixed 55 mol% P_2O_5.

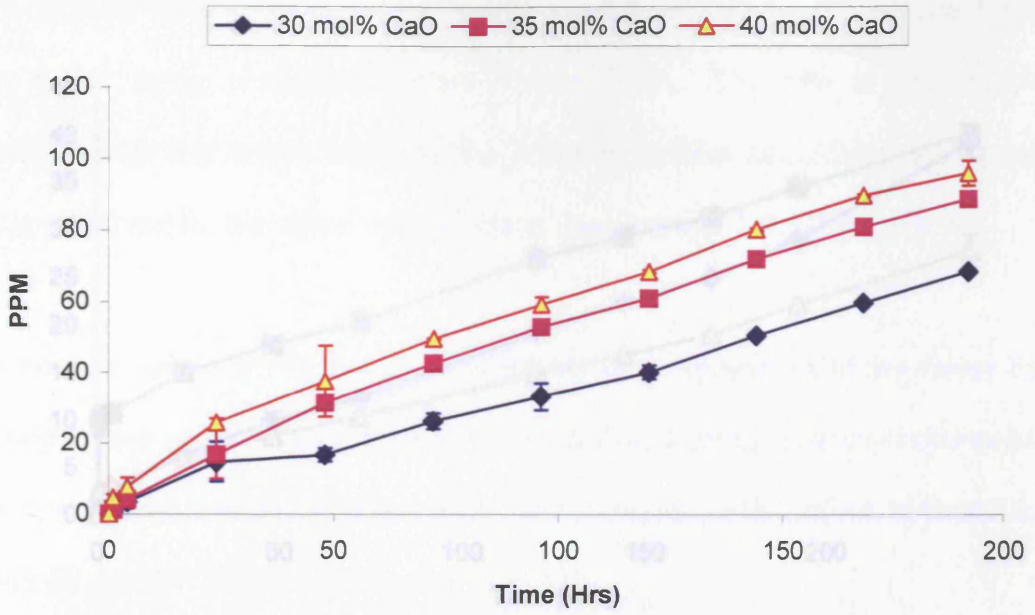

Figure 3.35: Calcium ion release profiles for glasses with fixed 55 mol% P_2O_5.

3.8.3 Anion Release for the 50 mol% P_2O_5 Compositions:

For compositions with fixed 50 mol% P_2O_5, it was noticed that the release of PO_4^{3-} and $P_2O_7^{4-}$ anions did not exhibit any obvious correlations with composition (Figures 3.36 and 3.37 respectively). In fact only relatively small amounts of these anions were released over the duration of the study. With regards to the $P_2O_7^{4-}$ anion analysis, it was seen that an initial amount of this anion was released during the first 24 hours, after which the plots levelled off, indicating that only limited, if any $P_2O_7^{4-}$ was detected. The only exception was the plot for the 30 mol% CaO composition, which increased slightly again after the 150 hour time point.

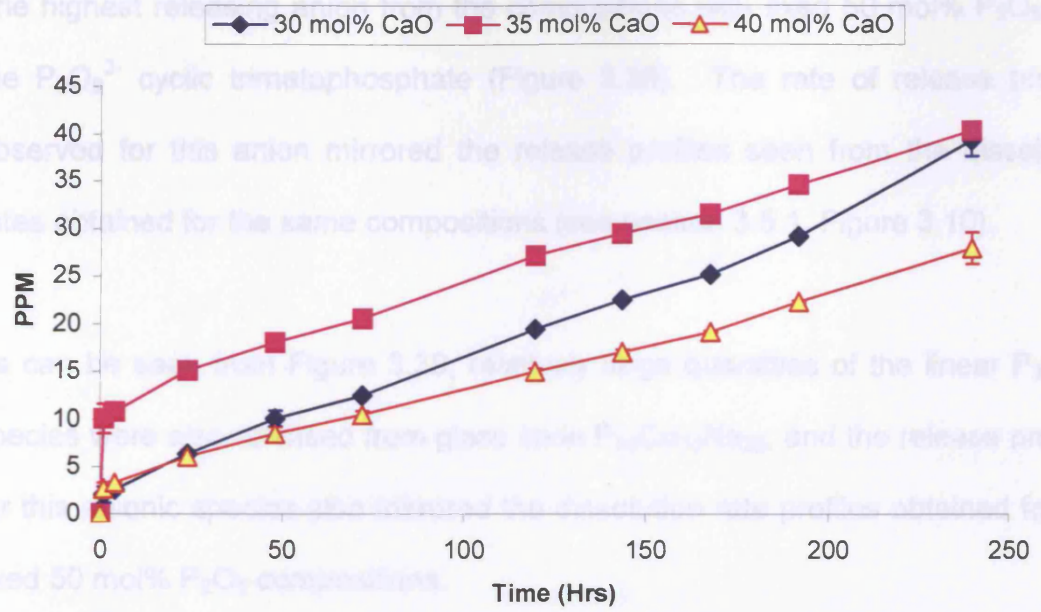

Figure 3.36: Graph showing orthophosphate PO_4^{3-} anion release for glasses with fixed 50 mol% P_2O_5.

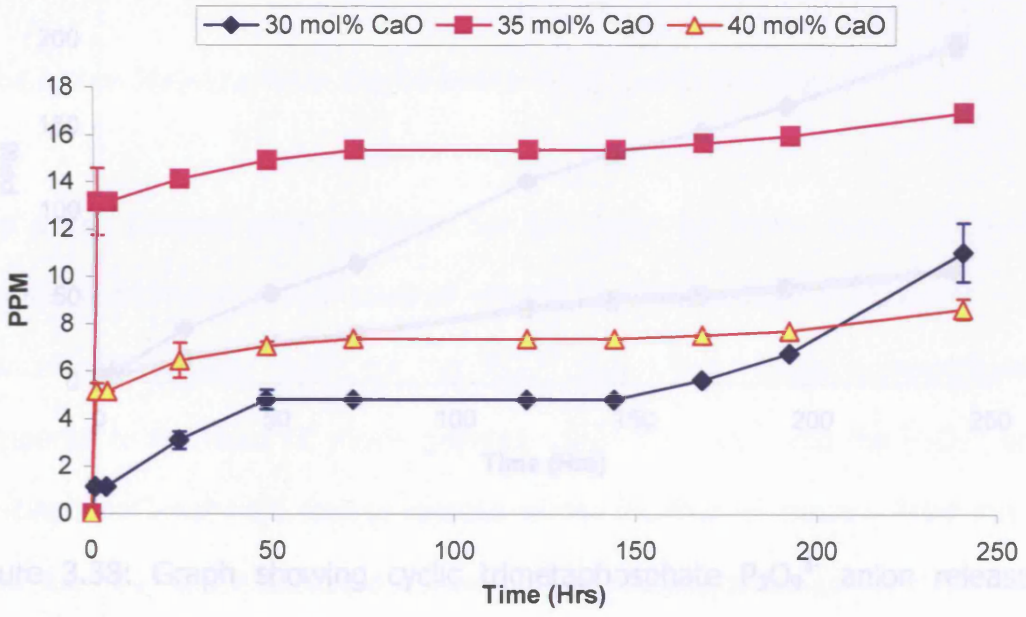

Figure 3.37: Graph showing pyrophosphate $P_2O_7^{4-}$ anion release for glasses with fixed 50 mol% P_2O_5.

The highest releasing anion from the compositions with fixed 50 mol% P_2O_5 was the $P_3O_9^{3-}$ cyclic trimetaphosphate (Figure 3.38). The rate of release profiles observed for this anion mirrored the release profiles seen from the dissolution rates obtained for the same compositions (see section 3.5.1, Figure 3.10).

As can be seen from Figure 3.39, relatively large quantities of the linear $P_3O_{10}^{5-}$ species were also released from glass code $P_{50}Ca_{30}Na_{20}$, and the release profiles for this anionic species also mirrored the dissolution rate profiles obtained for the fixed 50 mol% P_2O_5 compositions.

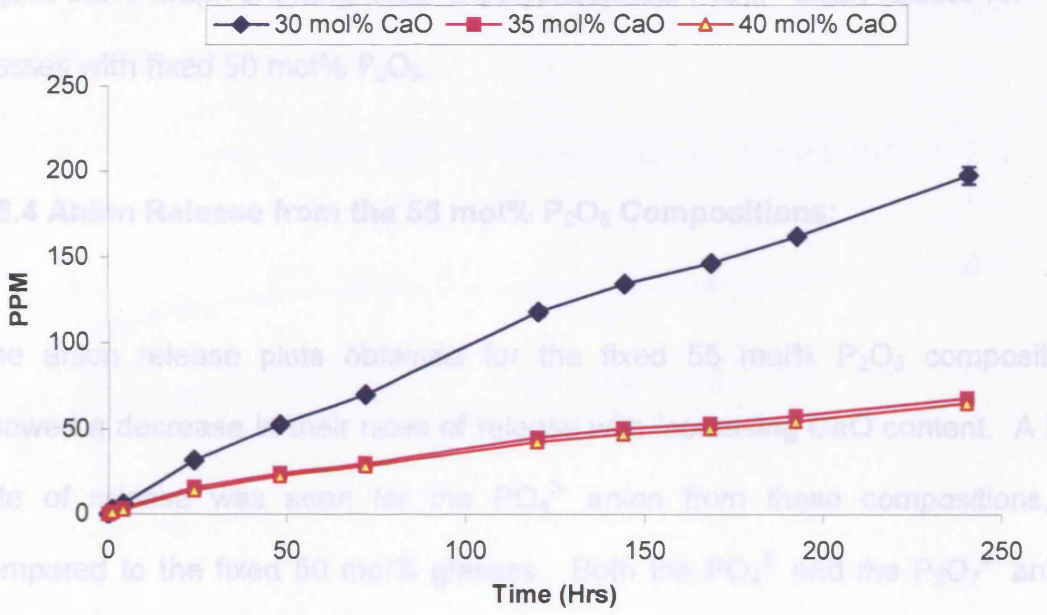

Figure 3.38: Graph showing cyclic trimetaphosphate $P_3O_9^{3-}$ anion release for glasses with fixed 50 mol% P_2O_5.

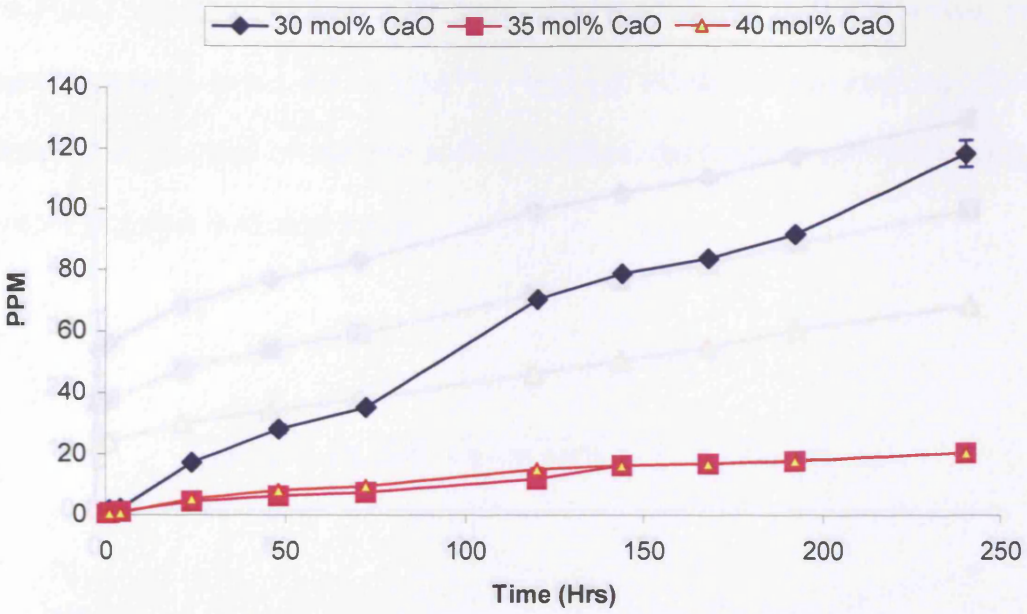

Figure 3.39: Graph showing linear tripolyphosphate $P_3O_{10}^{5-}$ anion release for glasses with fixed 50 mol% P_2O_5.

3.8.4 Anion Release from the 55 mol% P_2O_5 Compositions:

The anion release plots obtained for the fixed 55 mol% P_2O_5 compositions showed a decrease in their rates of release with increasing CaO content. A high rate of release was seen for the PO_4^{3-} anion from these compositions, as compared to the fixed 50 mol% glasses. Both the PO_4^{3-} and the $P_2O_7^{4-}$ anions exhibited an initial high rate of release within the first 24 hours. After this time point the PO_4^{3-} anion exhibited a linear rate of release, whereas the $P_2O_7^{4-}$ curves levelled off (Figures 3.40 and 3.41).

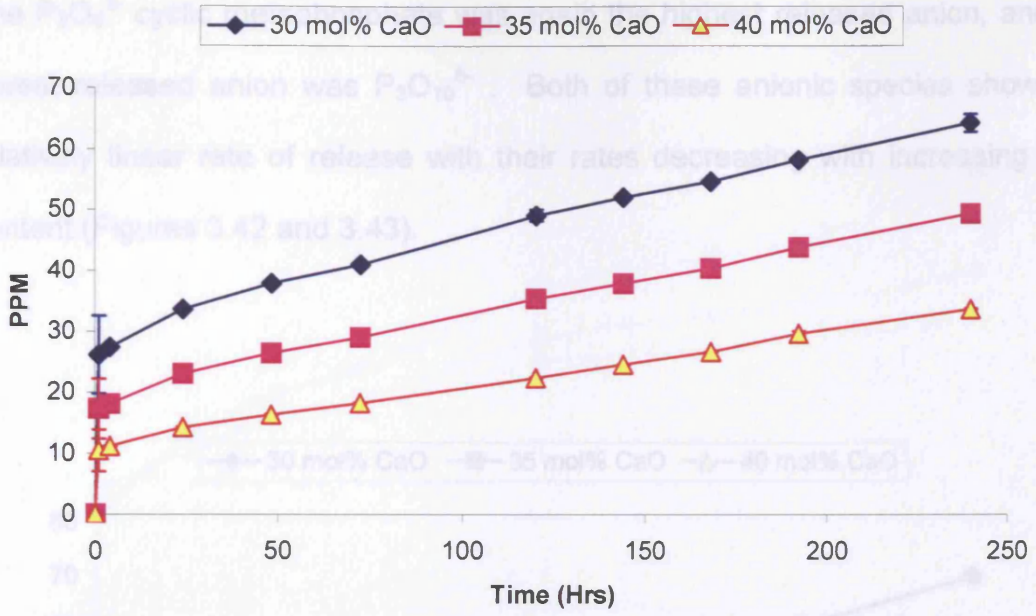

Figure 3.40: Graph showing orthophosphate PO_4^{3-} anion release for glasses with fixed 55 mol% P_2O_5.

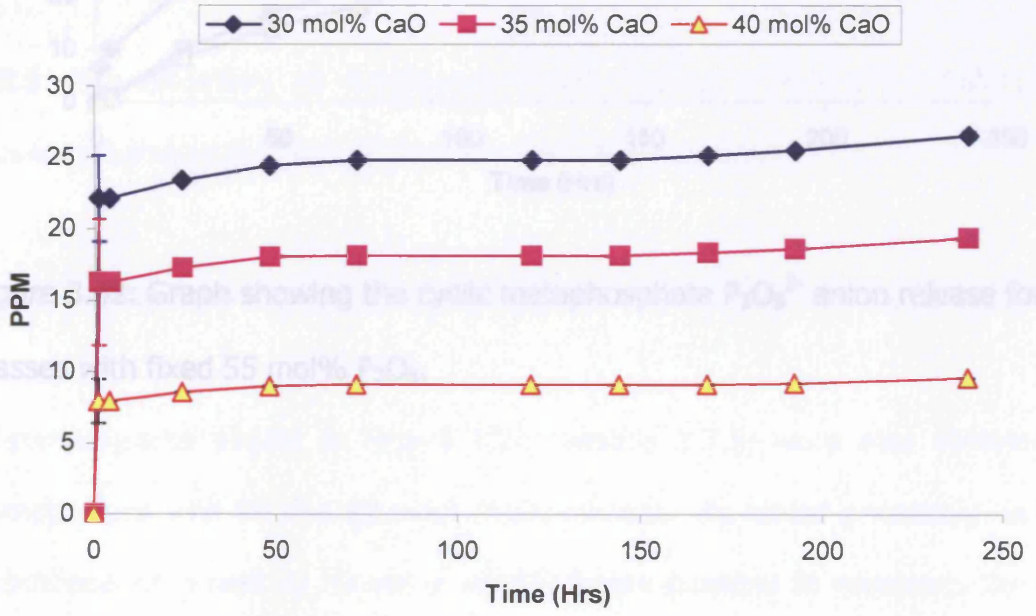

Figure 3.41: Graph showing pyrophosphate $P_2O_7^{4-}$ anion release for glasses with fixed 55 mol% P_2O_5.

The $P_3O_9^{3-}$ cyclic metaphosphate was again the highest released anion, and the lowest released anion was $P_3O_{10}^{5-}$. Both of these anionic species showed a relatively linear rate of release with their rates decreasing with increasing CaO content (Figures 3.42 and 3.43).

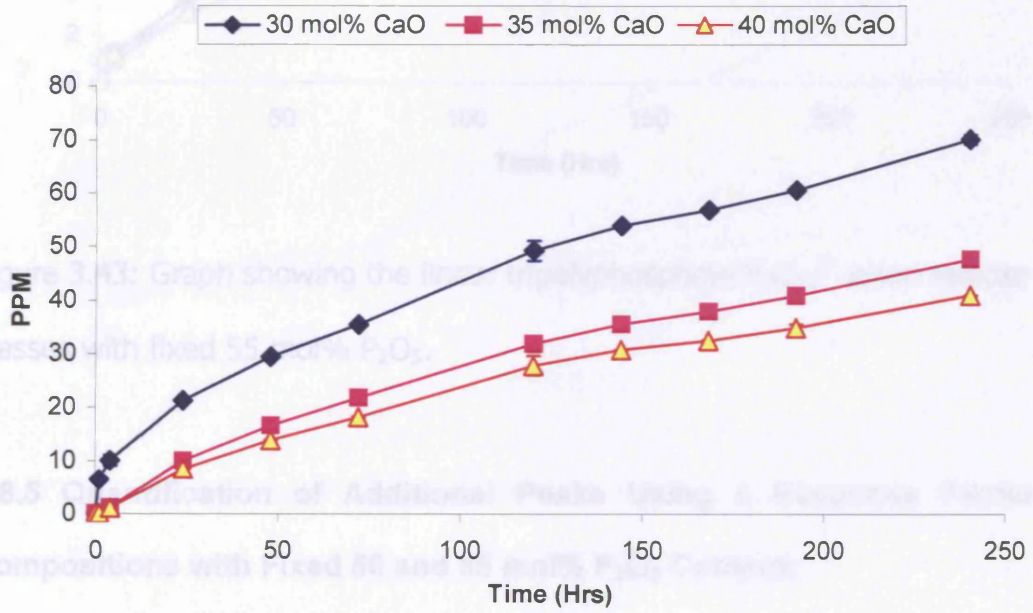

Figure 3.42: Graph showing the cyclic metaphosphate $P_3O_9^{3-}$ anion release for glasses with fixed 55 mol% P_2O_5.

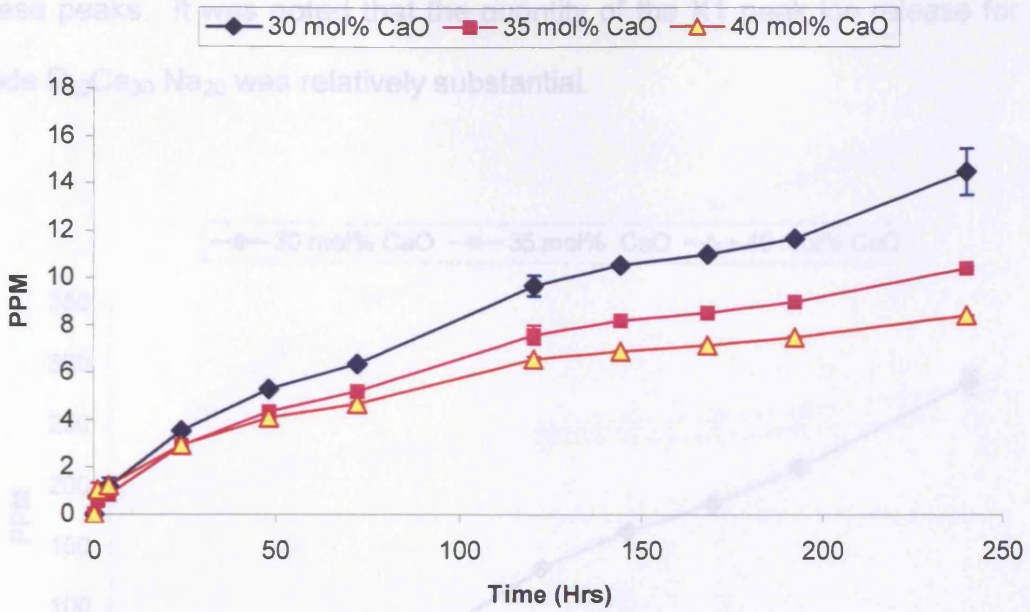

Figure 3.43: Graph showing the linear tripolyphosphate $P_3O_{10}^{5-}$ anion release from glasses with fixed 55 mol% P_2O_5.

3.8.5 Quantification of Additional Peaks Using a Response Factor, for Compositions with Fixed 50 and 55 mol% P_2O_5 Content:

3. 8.5.1 Response Factor Quantification for Glasses with 50 mol% P_2O_5:

Chromatograms similar to Figure 3.25 (section 3.7.3) were also obtained for compositions with 50 and 55 mol% P_2O_5 content. As stated previously, using a hypothesis proposed by Stover *et al* (81) it was possible to quantitate the extra polyphosphate peaks, labelled X1 – X5, observed in the IC chromatograms obtained. Figures 3.44 – 3.48 show the amount of anion release obtained from

these peaks. It was noted that the quantity of the X1 peak ion release for glass code $P_{50}Ca_{30}$ Na_{20} was relatively substantial.

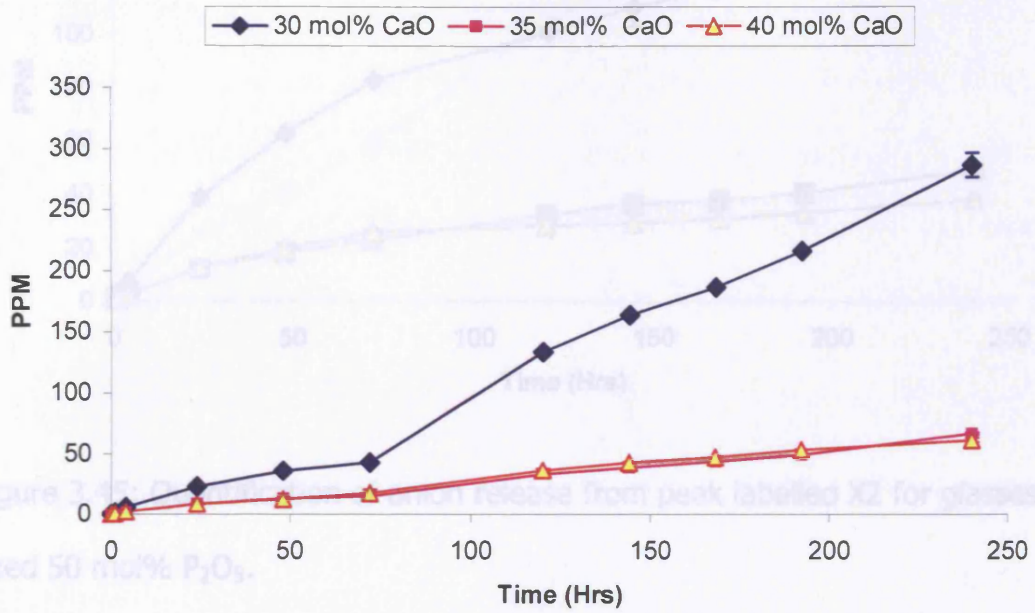

Figure 3.44: Quantification of anion release from peak labelled X1 for glasses with fixed 50 mol% P_2O_5.

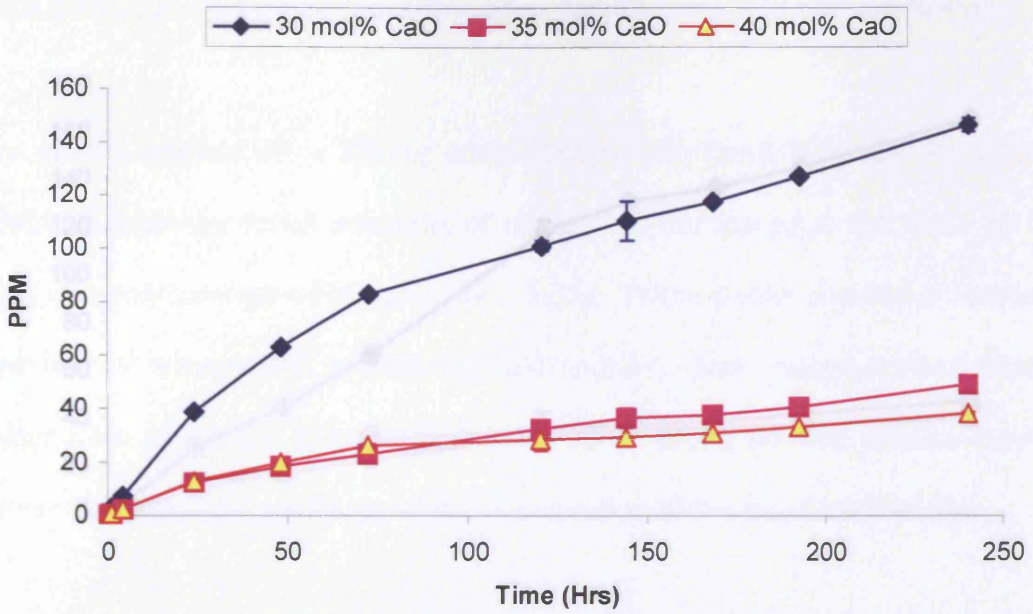

Figure 3.45: Quantification of anion release from peak labelled X2 for glasses with fixed 50 mol% P_2O_5.

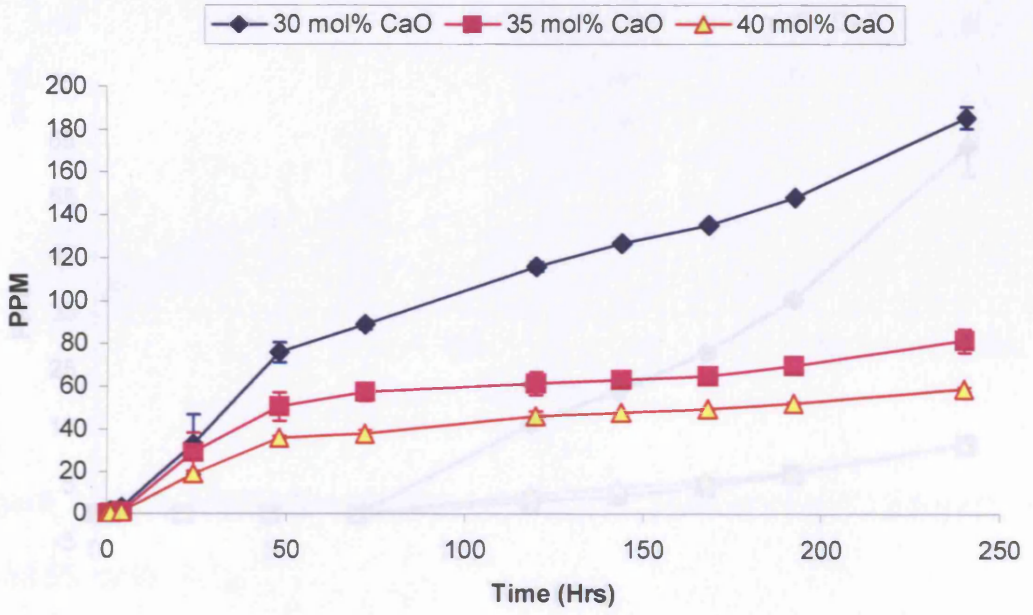

Figure 3.46: Quantification of anion release from peak labelled X3 for glasses with fixed 50 mol% P_2O_5.

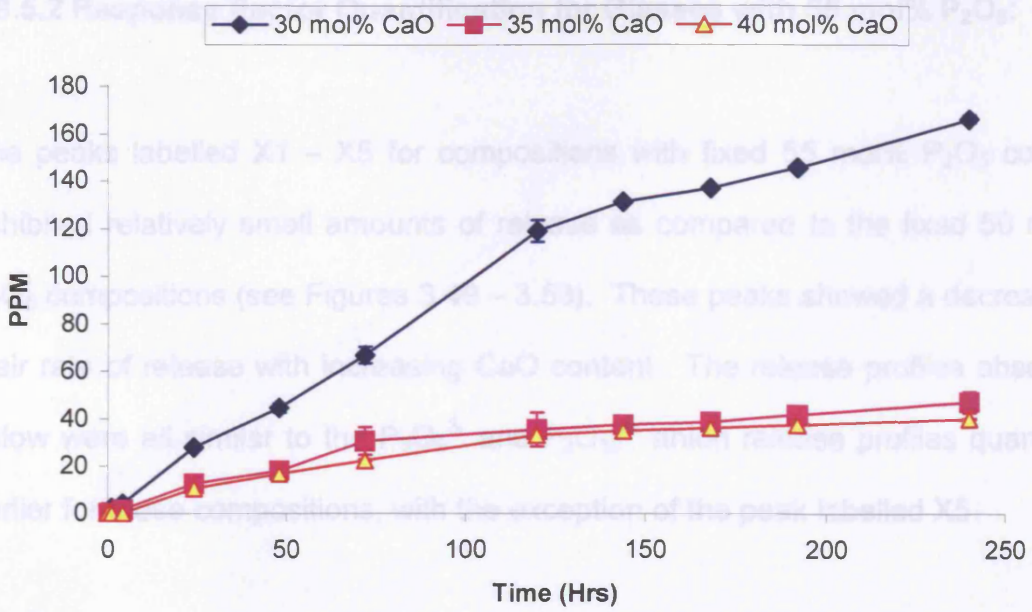

Figure 3.47: Quantification of anion release from peak labelled X4 for glasses with fixed 50 mol% P_2O_5.

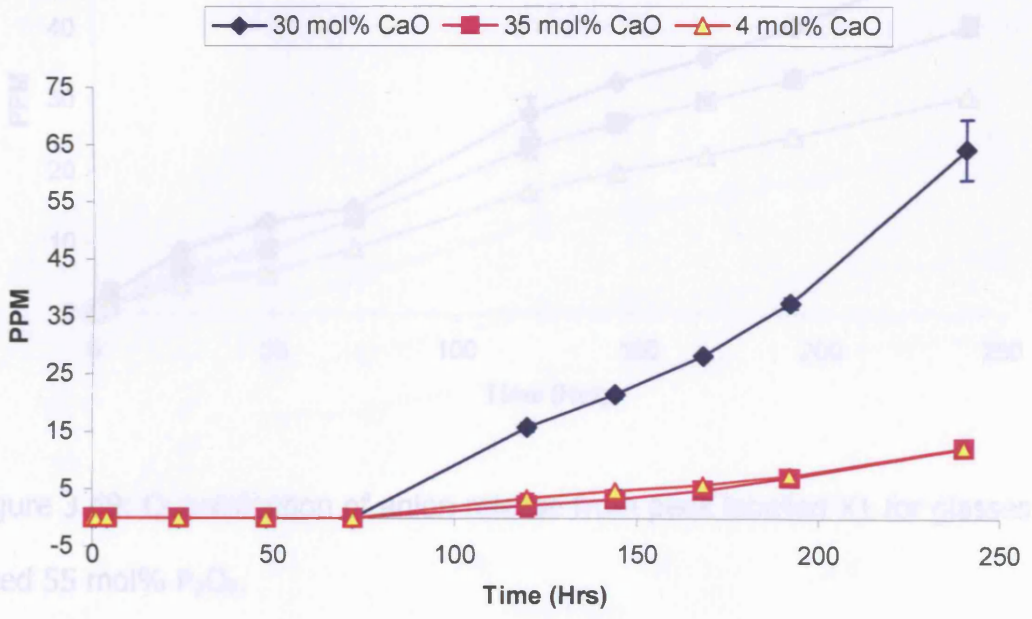

Figure 3.48: Quantification of anion release from peak labelled X5 for glasses with fixed 50 mol% P_2O_5.

3.8.5.2 Response Factor Quantification for Glasses with 55 mol% P_2O_5:

The peaks labelled X1 – X5 for compositions with fixed 55 mol% P_2O_5 content exhibited relatively small amounts of release as compared to the fixed 50 mol% P_2O_5 compositions (see Figures 3.49 – 3.53). These peaks showed a decrease in their rate of release with increasing CaO content. The release profiles observed below were all similar to the $P_3O_9^{3-}$ and $P_3O_{10}^{5-}$ anion release profiles quantified earlier for these compositions, with the exception of the peak labelled X5.

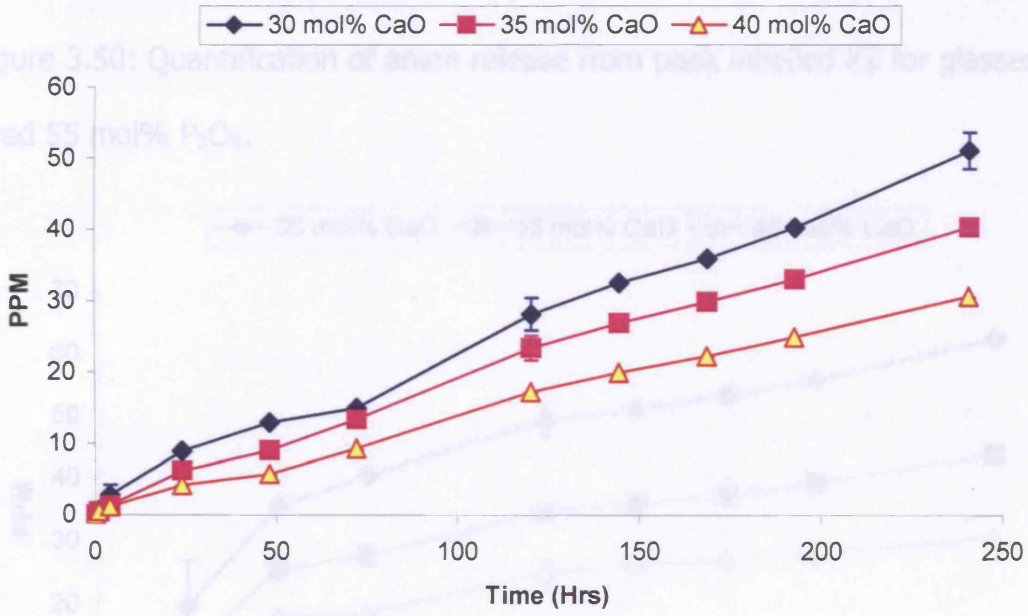

Figure 3.49: Quantification of anion release from peak labelled X1 for glasses with fixed 55 mol% P_2O_5.

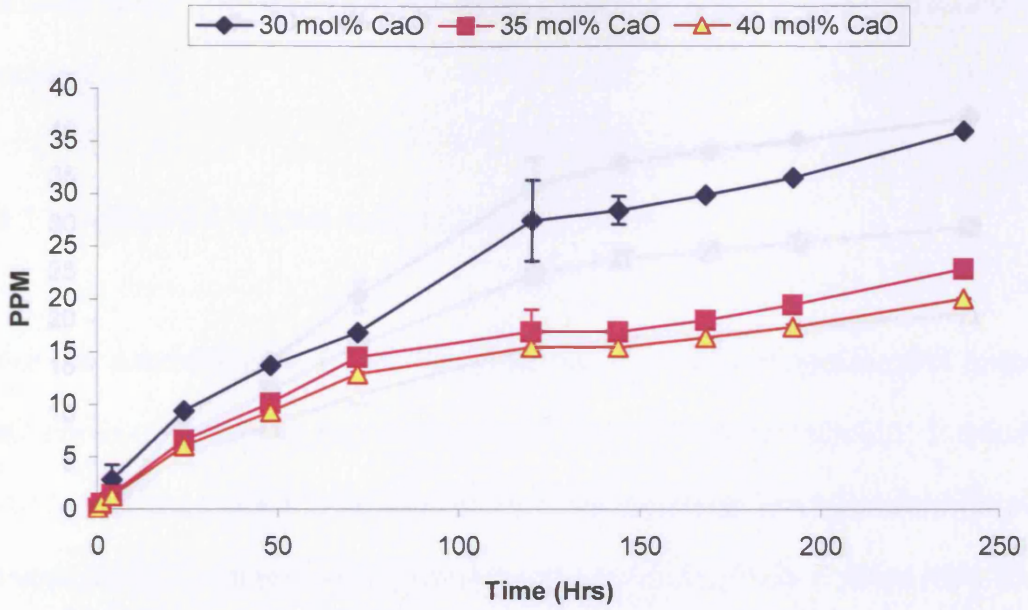

Figure 3.50: Quantification of anion release from peak labelled X2 for glasses with fixed 55 mol% P_2O_5.

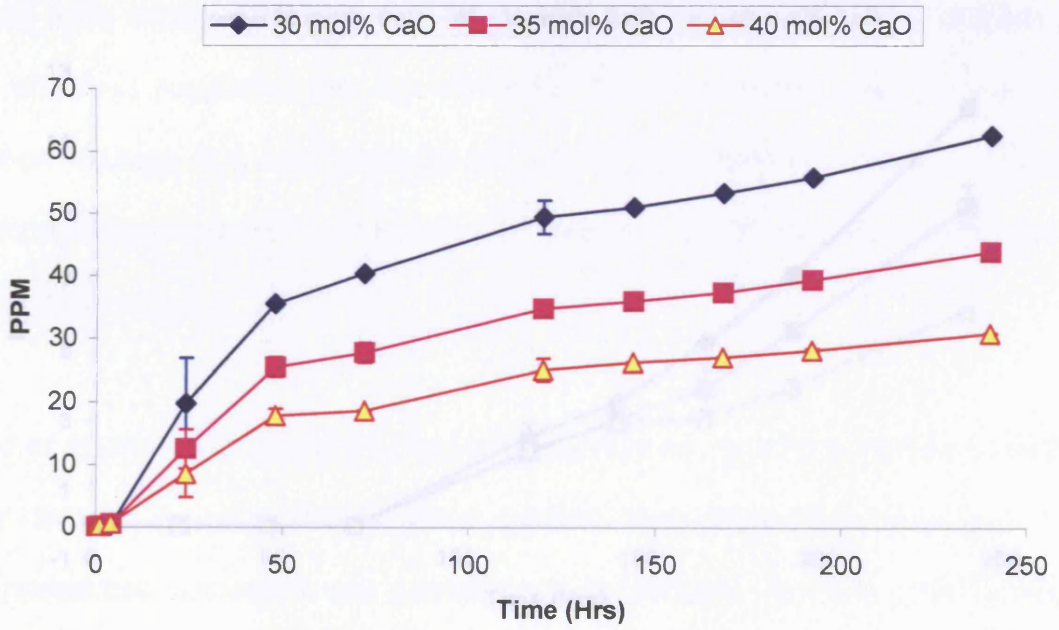

Figure 3.51: Quantification of anion release from peak labelled X3 for glasses with fixed 55 mol% P_2O_5.

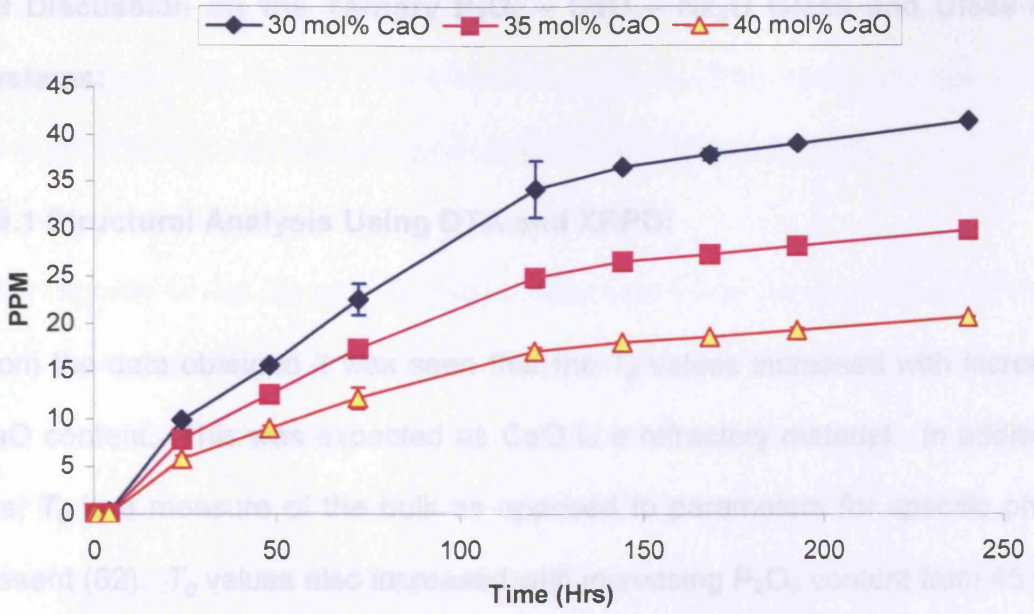

Figure 3.52: Quantification of anion release from peak labelled X4 for glasses with fixed 55 mol% P_2O_5.

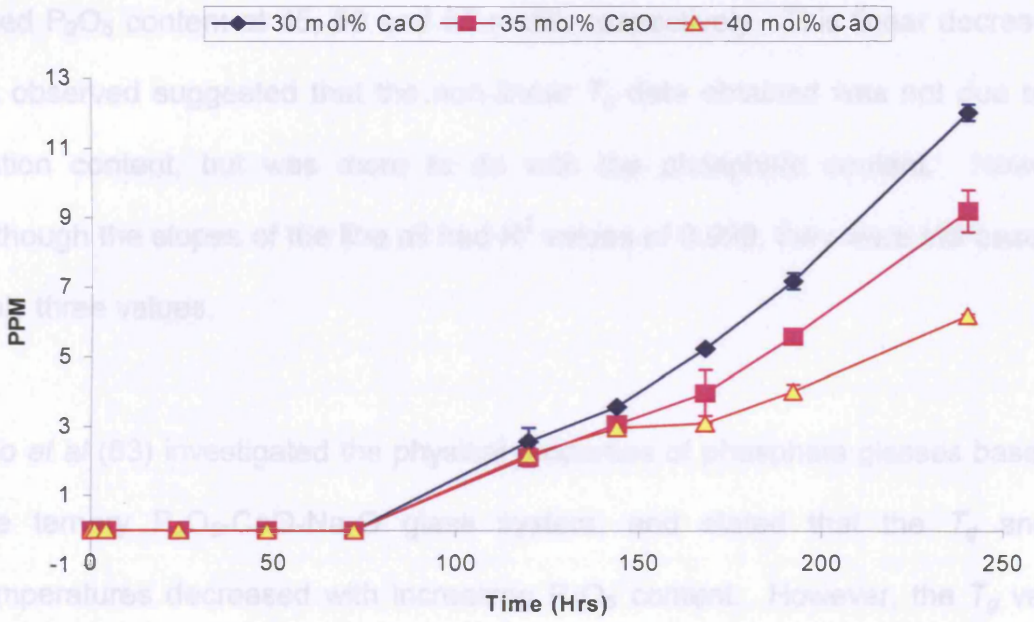

Figure 3.53: Quantification of anion release from peak labelled X5 for glasses with fixed 55 mol% P_2O_5.

3.9 Discussion on the Ternary P_2O_5 – CaO – Na_2O Glass and Glass-Fibre Systems:

3.9.1 Structural Analysis Using DTA and XRPD:

From the data obtained it was seen that the T_g values increased with increasing CaO content. This was expected as CaO is a refractory material. In addition to this, T_g is a measure of the bulk as opposed to parameters for specific phases present (82). T_g values also increased with increasing P_2O_5 content from 45 to 50 mol%, however the values then dropped with a further increase of P_2O_5 to 55 mol%. By extrapolating the T_g values to 100 mol% Na_2O content, it was seen that the values obtained from the slope of the lines were 502.67, 492.33 and 461°C for fixed P_2O_5 content at 45, 50 and 55 mol%, respectively. This linear decrease in T_g observed suggested that the non-linear T_g data obtained was not due to the cation content, but was more to do with the phosphate content. However, although the slopes of the line all had R^2 values of 0.999, they were still based on only three values.

Uo *et al* (83) investigated the physical properties of phosphate glasses based on the ternary P_2O_5-CaO-Na_2O glass system, and stated that the T_g and T_c temperatures decreased with increasing P_2O_5 content. However, the T_g values presented in their paper contained some anomalies and for some of the compositions (i.e. the 50 mol% P_2O_5 compositions) no T_g values were given.

Andersson (84) proposed a simpler view of T_g against composition. He stated that the higher the Na_2O content, the lower the T_g. This statement was found to be in accordance with the values obtained from this investigation.

With regards to the T_c and T_m peaks observed it was apparent that there was more than a single event occurring, as no correlation was seen between the T_c and T_m peaks observed, with the exception of glass code $P_{55}Ca_{40}Na_5$. Furthermore no correlation was seen between the numbers of T_c or T_m peaks from the DTA traces with the number of crystalline phases identified from the XRPD analysis (see Table 3.6 below).

Table 3.6: Number of T_c and T_m peaks observed from the DTA traces obtained, along with number of phases identified from XRPD analysis.

Glass Code	Number of Peaks observed		No. of Phases Identifed (XRPD)
	Tc	Tm	
$P_{45}Ca_{30}Na_{25}$	2	1	1
$P_{45}Ca_{35}Na_{20}$	2	1	1
$P_{45}Ca_{40}Na_{15}$	1	2	2
$P_{50}Ca_{30}Na_{20}$	1	2	1
$P_{50}Ca_{35}Na_{15}$	2	1	1
$P_{50}Ca_{40}Na_{10}$	1	2	2
$P_{55}Ca_{30}Na_{15}$	1	2	1
$P_{55}Ca_{35}Na_{10}$	1	2	2
$P_{55}Ca_{40}Na_5$	1	1	1

As can be seen from the above table, for compositions containing two T_c peaks it was suggestive of the fact that two crystalline phases were present within that composition. However, for all the glasses investigated (with the exception of glass code $P_{55}Ca_{40}Na_5$),where two T_c peaks were observed, only one T_m peak was seen; vice versa, where only a single T_c peak was observed, two T_m peaks were seen.

There was also no correlation seen between the number of T_c peaks observed and the number of phases identified from XRPD analysis. For both glass codes $P_{45}Ca_{30}Na_{25}$ and $P_{45}Ca_{35}Na_{20}$, two T_c peaks were observed but the only phase identified was the $Na_4Ca(PO_3)_6$ phase. For glass code $P_{45}Ca_{40}Na_{15}$ a sharp single T_c peak was observed, whilst XRPD analysis revealed the presence of two crystalline phases. These were the $NaCa(PO_3)_3$ and $Ca_2P_2O_7$ phases. The $NaCa(PO_3)_3$ phase was also identified as the main phase for the compositions with fixed 50 mol% P_2O_5 content, with the exception of glass code $P_{50}Ca_{40}Na_{10}$ in which a second phase (CaP_2O_6) was also identified. For the composition with glass code $P_{55}Ca_{30}Na_{15}$ a single $NaCa(PO_3)_3$ phase was identified, and for glass code $P_{55}Ca_{35}Na_{10}$ two phases were identified, these were the $NaCa(PO_3)_3$ and CaP_2O_6 phases. For glass code $P_{55}Ca_{40}Na_5$, only a single CaP_2O_6 phase was identified.

However, some correlation was seen between the T_m peaks and the phases identified from XRPD analysis. Of all nine compositions investigated, only glass codes $P_{50}Ca_{30}Na_{20}$ and $P_{55}Ca_{30}Na_{15}$ did not show any correlation.

In all cases where two T_c peaks were observed, these were seen as a shoulder protruding from the main T_c peak. It may be that a second phase (if present) was present in small quantities and could not to be detected via XRPD analysis. In addition the presence of a single T_m peak could have been indicative of both the main and small second phase exhibiting very similar T_m temperatures. In the case for the compositions with fixed 55 mol% P_2O_5, the T_c peaks seen were so broad that they could have easily concealed a second peak within them. An example of this was the glass code $P_{55}Ca_{35}Na_{10}$, where only a single (broad) T_c peak was seen with two T_m peaks, and XRPD analysis revealed the presence of two crystalline phases within that composition. For some of the glasses investigated, there were a few odd peaks in the XRPD traces obtained that could not be matched to anything in the database. This further suggested the presence of a small amount of some other phase(s) present within these compositions.

Another suggestion put forward was related to the different thermal histories of the glasses investigated. In order to run XRPD the ground up glasses were crystallised for two hours at their respective crystallisation temperatures, and re-ground in order to run the XRPD analysis. In effect, introducing further thermal prehistories into the glass which could have also attributed to the non correlation seen between the number of T_c peaks observed with the number of phases identified from XRPD analysis

One other point to add would be that the phases identified from the XRPD analysis were not pure stoichiometric compounds. This could also have attributed

to the spurious peaks for which no match was found. Also for the main phase [i.e. the $NaCa(PO_3)_3$ phase] identified from the compositions investigated, a pattern of up to 36° 2θ only was obtained from the Crystallographica Search-Match database.

With regards to the thermal analysis conducted on the ternary glass-fibre system, it was seen that the T_g values decreased as compared to the bulk glasses, with the exception of glass codes $P_{55}Ca_{35}Na_{10}$ and $P_{55}Ca_{40}Na_5$, where a slight increase in T_g was observed. A change in the thermal parameters of the glass-fibres obtained was expected, as they had undergone additional thermal treatment, in order to produce the fibres. As such the decrease in T_g observed could have possibly been attributed to loss of P_2O_5 during the re-melting process of the bulk glasses.

3.9.2 NMR Results:

NMR analysis revealed that both Q^1 and Q^2 species were present in the compositions containing 45 mol% P_2O_5. As stated the crystalline phases identified from XRPD were the $Na_4Ca(PO_3)_6$ (a calcium bridged trimetaphosphate, Q^2), $NaCa(PO_3)_3$ (a sodium calcium metaphosphate, Q^2) and $Ca_2P_2O_7$ (a calcium pyrophosphate, Q^1) phases.

On the other hand, for compositions with fixed 50 and 55 mol% P_2O_5, only Q^2 species were identified. Again, the phases identified from these compositions

were the $NaCa(PO_3)_3$ (Q^2), and the CaP_2O_6 (a beta calcium metaphosphate, Q^2) phases.

Q^2 species are mainly long chains and/or rings of P-O-P bonds found in the backbone of the chain. However, Q^1 species can be found in two locations, either as chain terminators or isolated phosphate dimers. From the Q^1 to Q^2 ratios obtained for the species identified (section 3.4, Table 3.4,), along with the pyrophosphate identified from XRPD analysis, it was evident that most if not all of the Q^1 species identified for the 45 mol% P_2O_5 compositions were phosphate dimers. Therefore, the packing density for these compositions would have been greater than the fixed 50 and 55 mol% P_2O_5 compositions investigated. Also, the suggested structure for the calcium bridged trimetaphosphate (85) consisted of two triphosphate rings bridged by a single calcium, again suggesting that the packing density of the 45 mol% P_2O_5 compositions would be greater than the other two systems investigated. This would have therefore somewhat accounted for the non-linear data obtained from the thermal analyses conducted with regards to the T_g values obtained, along with the dissolution rates. The very low amount of Q^1 ratios calculated for the 50 and 55 mol% phosphate compositions suggested that these Q^1 species were probably chain terminators.

Furthermore, if the fixed 45 mol% P_2O_5 compositions contained a mixture of Q^1's and Q^2's, it was possible that some phase separation would have been expected within the glass network. For glass codes $P_{45}Ca_{30}Na_{25}$ and $P_{45}Ca_{35}Na_{20}$ two T_c peaks were observed in their respective DTA traces.

3.9.3 Structural Properties of the Ternary P_2O_5–CaO–Na_2O Glass and Glass-Fibre Systems:

As stated previously glass-fibres were only obtained from the fixed 50 and 55 mol% P_2O_5 compositions. Hence, it was further evidence for the structural differences between the fixed 45 mol% P_2O_5 compositions, and the fixed 50 and 55 mol% compositions.

During the melting process of the glasses with fixed 45 mol% P_2O_5, the viscosity was too low to allow fibres to be pulled. Upon dropping the temperature in order to achieve a suitable viscosity for this glass, the glass melt would crystallise in the bushing.

Goldstein and Davies (86) stated that in the language of network theory every glass forming atom (silicon, phosphorous etc.) was bound to three or four oxygens, and every oxygen was bound either to two glass formers, or to one glass former and one metal ion, i.e. sodium or calcium. Goldstein and Davies went on to state that a bond between oxygen and a metal ion was not regarded as contributing to the degree of polymerisation of the network (i.e. the network connectivity). In other words, the oxygen atoms per network former were directly bonded to other network formers. In illustration, vitreous silica has an average number of four oxygen atoms, and as every oxygen contributes to the network, this results in a three dimensional polymer. Therefore it could be deduced that vitreous silica has a network connectivity of 4.

Extensive studies have shown that phosphate glasses also contained a polymeric structure which was controlled by the glass composition. These were in rough agreement with the predictions of Zachariasen and Van Wazer (87;88). In illustration, the basic structural unit of these glasses was the PO_4^{3-} group, which could be attached to a maximum of three neighbouring groups. Therefore, it could be deduced that pure phosphate glass would have a network connectivity of 3. This simple observation could be taken further to include the addition of cations into the network.

The following formula was used to incorporate the addition of cations into the network: $NC = \frac{3 \times (2 \times MF\ P_2O_5) - (2 \times [MF\ Na_2O + MF\ CaO])}{2 \times MF\ P_2O_5}$

Where NC = Network connectivity, and MF = mole fraction.

Bunker *et al* (89) stated that the number of cross-links in the polymer, defined as the cross-link density (CLD), could also be calculated taking into account the addition of modifiers to the glass such as Na_2O and CaO. The addition of these network modifiers resulted in the cleavage of P-O-P linkages and the creation of non-bridging oxygens.

The CLD (89) was calculated using the formula: x = 2y – 1 / y, where x was the cross link density, and y the mole fraction of P_2O_5. Using these formulae the NC and CLD calculated for the compositions used are presented in Table 3.7. It was also worth noting that the above formulae did not take into account any residual OH groups that could be left in the composition from the melt process. The cross-link density predicted for glasses containing 50 mol% P_2O_5 was 0.

For phosphate glasses containing 50 mol% P_2O_5 or less, the average chain length was obtained using the following equation:

$$n = \frac{2}{[M + M']/P - 1}$$

Where *n* is the average chain length, *M* the mole fraction of monovalent cations, *M'* the mole fraction of divalent cations and *P* the mole fraction of phosphorous in the glass. The average chain lengths of the glasses are also presented in Table 3.7.

Table 3.7: Calculated NC, CLD and average chain length of the compositions investigated.

Glass Code	Cross-Link Density (CLD)	Network Connectivity (NC)	Average no. Chain length.
$P_{45}Ca_{30}Na_{25}$	-0.22	1.78	2.25
$P_{45}Ca_{35}Na_{20}$	-0.22	1.78	2.00
$P_{45}Ca_{40}Na_{15}$	-0.22	1.78	1.80
$P_{50}Ca_{30}Na_{20}$	0	2.00	3.33
$P_{50}Ca_{35}Na_{15}$	0	2.00	2.86
$P_{50}Ca_{40}Na_{10}$	0	2.00	2.50
$P_{55}Ca_{30}Na_{15}$	0.182	2.18	5.49
$P_{55}Ca_{35}Na_{10}$	0.182	2.18	4.39
$P_{55}Ca_{40}Na_5$	0.182	2.18	3.63

Bunker *et al* (89) studied glasses of similar compositions used in this study, and they found that phosphate glasses were predominantly made up of long chain polymeric phosphate anions which were connected to one another via ionic bonds to the modifier cations. For such structures it was evident that the divalent cations could serve as ionic cross-links between the non-bridging oxygen atoms of two different chains. Van Wazer and Campanella (90) suggested that such a cross-linking system would take the form of a metal chelate structure. Bunker *et al* stated that the formation of such cross-links explained the increase in chemical durability as the mol% of CaO in the glass was increased.

It was seen in Table 3.7 that with increasing CaO content there was a decrease in the average chain length number, indicating increasing formation of cross-links between the phosphate chains. Sodium ions disrupted the network and formed non-bridging oxygens and the bond between the P-O-P was completely broken. When calcium ions were added, the bond again would be broken creating non-bridging oxygens. However, one Ca^{2+} ion would still be in contact with two oxygen atoms, therefore creating a link which had a much stronger effect on the network connectivity than the Na^{+} ions.

The calculated NC for the fixed 50 and 55 mol% P_2O_5 compositions was above 0, and the CLD was also 0 or above, and fibres were obtained from these compositions. However, the CLD values calculated for the 45 mol% P_2O_5 compositions fell into negative values (i.e. below 0) and the NC was below 2, and it was not possible to obtain fibres from these compositions. Therefore, it could be assumed that glasses with a NC below 2 or a CLD below 0 would not form fibres. No data was available or found on ternary phosphate-based glass-fibres with less than 50 mol% P_2O_5 in its composition.

It was suggested from a private communication with Dr. Robert Hill (Imperial College, London) that a CLD of above 0 would correspond to a 3D network. In contrast, a CLD of 0 would give a polymer of infinite molar mass. Changes dramatically occur at the point when a glass moves from being a continuous cross-linked network into a linear system. This transition from a 3D network to a linear system occurs at a CLD of 0 (i.e. at a NC of 2 for the compositions

investigated). Therefore, in a glass with a CLD of less than 0, it was expected that the melt would be a lot more fluid and a lot more viscous. Furthermore, these properties would be expected from a glass with very short chain lengths.

For the 45 mol% P_2O_5 glasses, it was observed that when the bulk glass was re-melted in order to pull fibres, it was either at too low a viscosity from which fibres could be obtained, or that upon lowering the temperature in an attempt to achieve a suitable viscosity, the glass crystallized in the bushing of the crucible. In other words, upon the melting of a short chain glass (see Table 3.7 above), its viscosity would be too low from which to pull fibres, and the molten glass would drip straight through the bushing as was the case for the compositions with fixed 45 mol% P_2O_5.

Murgatroyd (91) wrote that in order to draw fibres, it was necessary first to heat glass to a high temperature so that it was in a liquid state, and while the glass was hot and molten it was extended with great rapidity. The drawing of a continuous thread from a molten bead was only possible because, even at the high temperatures employed, a number of bonds exist which were strong enough to withstand the stresses used in pulling the thread from the melt. The continuity of the fibre depended on the ability of the strongest bonds to hold together as they were pulled out of the melt. The act of drawing the fibre therefore caused the strongest bonds to be selected from the melt and to be aligned parallel to the axis of the fibre, i.e. in the direction of the pull. Murgatroyd also stated that any regions of weak bonds adjacent to the lines of strong bonds were also extended

along the axis of the fibre between the strong bonds. However, none of these bonds existed in the axial direction, due to the bonds not being able to withstand the drawing tension at the high temperatures from which fibres were drawn.

Otto and Preston (92) wrote that on the basis of tests they had conducted, they were compelled to believe that the high strengths of fibres were not due to an oriented molecular structure or to an oriented flaw structure. Brannan (93) later also stated that glass fibres approximately 50 microns in diameter showed normal values of Poisson's ratio very similar to that of the bulk glass before and after heat treatment. Thus, the properties investigated lent no support to the view that strong bonds were preferentially oriented in the glass fibres.

Milberg and Daly (94) then postulated that the assumption of an excessively broad chain-axis distribution could easily lead to completely incorrect conclusions concerning the details of the chain structure. If it was to be assumed that the metaphosphate chains were built up of identical PO_4^{3-} tetrahedra, and that alternate tetrahedra were tilted in opposite directions, the translational repeat unit in the chain would consist of two tetrahedra. However, in order to have the shortest P – P vector, and still maintain reasonably good agreement between the P – O vectors, it was necessary to assume that the metaphosphate chain was a helical version of the extended chain (see Figure 3.54).

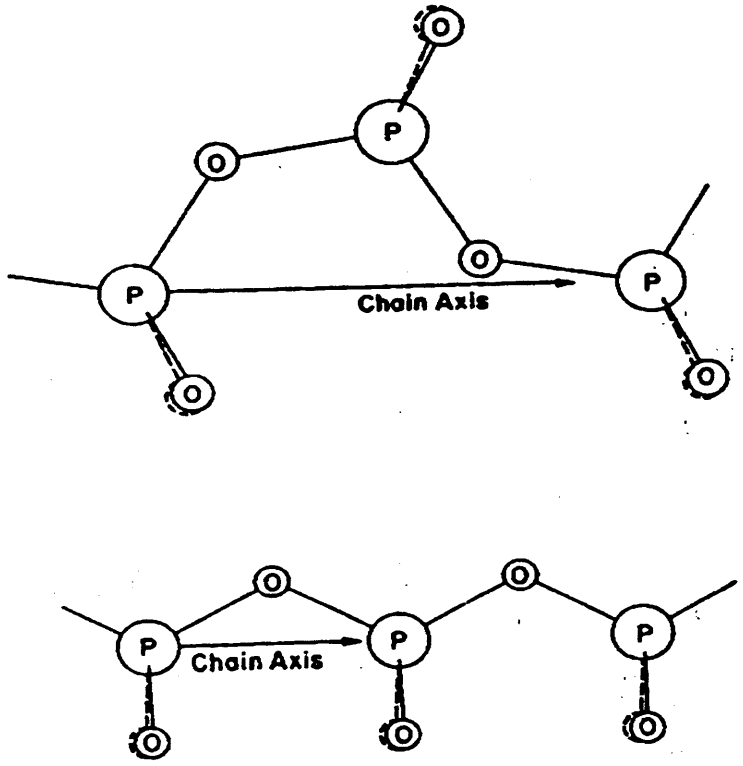

Figure 3.54: Preferred orientation of the phosphate chains suggested by Milberg and Daly (94).

Milberg and Daly also stated that the patterns obtained from the sodium metaphosphate glass fibres strongly indicated that the fibres were composed of long chains of PO_4^{3-} tetrahedra and that the axes of these chains had a strong preference for lying along the fibre axis direction.

3.9.4 Degradation Rates, pH and Ion Release Profiles of the 45 mol% P_2O_5 Compositions:

3.9.4.1 Degradation Rates:

The dissolution rates of the ternary compositions investigated mirrored those conducted in a previous study (95). However, in the previous study measurements were taken from glass discs in a static environment, whereas in the present study the solution was changed at 1 hour, 4 hours and then every 24 hours. From the two different methods investigated, the cumulative release study was found to be a more accurate form of analysis due to no precipitation build-up, which was experienced in the static study.

In the previous study a decrease in weight loss was seen with increasing CaO content for the compositions with a fixed 45 mol% P_2O_5 content, and in the present study a decrease was seen with an initial increase in CaO content from 30 to 35 mol%, after which the weight loss increased again with a further addition of CaO to 40 mol%. The rates obtained were 7.5×10^{-4}, 4.3×10^{-4} and 8.9×10^{-4} $mg.mm^{-2}.hr^{-1}$ for compositions containing 30, 35 and 40 mol% CaO, respectively.

One proposed possibility for the patterns observed from the dissolution rates was derived from the XRPD analyses conducted. It was seen that a single phase was identified for the fixed 30 and 35 mol% compositions, which was the $Na_4Ca(PO_3)_6$ phase. However, for the composition with fixed 40 mol% CaO, two phases were

identified. These were $NaCa(PO_3)_3$, and $Ca_2P_2O_7$. This suggested that a structural change had taken place along with possible phase separation. However, the phase diagrams (96-98) showed that this particular composition lay very close to a eutectic point.

3.9.4.2 pH and Ion Release Profiles:

It was seen from the cation release profiles obtained that the calcium ion release profiles exactly mirrored the profiles seen from the dissolution rates obtained. The composition with fixed 40 mol% CaO content released the highest amount of calcium ions into solution, followed by the fixed 30, and then 35 mol% CaO compositions.

The sodium ion release patterns mirrored those obtained from the cyclic metaphosphate $P_3O_9^{3-}$ release. The 30 mol% CaO composition released the highest amount of sodium ions, followed by the 40 then 35 mol% CaO compositions.

As seen from the anion release curves, all three compositions investigated showed a decrease in the rates of release for the PO_4^{3-} orthophosphate and the linear anionic phosphate species ($P_2O_7^{4-}$ and $P_3O_{10}^{5-}$) with increasing CaO content. The data collated suggested that the PO_4^{3-} orthophosphate and linear anionic species ($P_2O_7^{4-}$ and $P_3O_{10}^{5-}$) were branched and cross-linked with the Ca^{2+} ions, hence a decrease in their rates of release were seen with increasing

CaO content. Van Wazer and Campanella (90) stated that Ca^{2+} ions can form chelates that have strong complexing abilities with linear polyphosphates. This was observed in this study from the correlation seen between the weight loss patterns observed and the calcium ion release data

The highest rate of release was seen for the $P_3O_9^{3-}$ anionic species. Van Wazer and Holst (87) conducted titration studies on more than a hundred different compositions. In titrating the acids they found that the same amount of base was needed to reach the first neutralisation point before and after hydrolysis. This showed that for every phosphorous atom there was one strongly ionised hydrogen, and therefore only straight chain or unbranched ring phosphate anions could be found in aqueous solutions of phosphoric acids.

Feike *et al* (99) conducted Double Quantum NMR studies on two binary sodium phosphate glasses. They observed that a 2-2 peak occurred at -23ppm. They stated that this motif contained pairs of Q^2 groups which were only connected to other Q^2 groups. Thus they concluded that the simplest structural unit which met these criteria was the $P_3O_9^{3-}$ anion, i.e. a ring of three Q^2 groups.

This also correlated with this study conducted where the peaks for the Q^2 species were seen at -22.1, -22.4 and -23.7 ppm respectively for the compositions investigated (see section 3.4, Table 3.4). This seemed to advocate that the $P_3O_9^{3-}$ anionic species dominated the dissolution processes. Also due to the detection of large amounts of the $P_3O_9^{3-}$ anion, this suggested that there was a

significant proportion of this fragment present in the original glass structure. With regards to the amounts released, it was proposed that most if not all of this anion was unbranched, with the remaining negative charge on the $P_3O_9^{3-}$ anion ionically linked with the Na^+ ion. The correlation seen with the rate of release for the Na^+ cation and the $P_3O_9^{3-}$ anion release seemed to corroborate this suggestion.

Bunker *et al* (89) stated that three types of reactions can occur in the dissolution mechanisms of phosphate-based glasses. These are acid / base reactions, hydrolysis reactions, and hydration reactions. Hydrolysis reactions are the cleaving of P-O-P bonds and this mechanism exhibits clear pH dependence.

Watanabe *et al* (100) stated that the hydrolysis of the small-ring (cyclic trimeta- and tetrameta-) phosphates decreased in acidic solutions and increased in basic solutions. Therefore, the hydrolysis of these small-ring metaphosphates was an acid / base catalysed reaction in all solvents.

Wen and Jijian (101) stated that if the pH value of the solution was ≥5, the dissolution of the phosphate glasses was controlled by the hydrolysis process of the phosphate chain. As was seen from Figure 3.16 (section 3.6), the pH for the compositions with fixed 30 and 35 mol% CaO remained neutral for the duration of the study, whereas the composition with fixed 40 mol% CaO dropped to about 5.5.

Therefore, the proposed mode of dissolution for the compositions with fixed 45 mol% P_2O_5 was the hydrolysis reaction, with the $P_3O_9^{3-}$ cyclic metaphosphate undergoing acid / base catalysis.

3.9.5 Degradation Rates, pH and Ion Release Profiles of the 50 and 55 mol% P_2O_5 Compositions:

3.9.5.1 Degradation Rates:

The dissolution rates obtained revealed a decrease with an increase in CaO content. The rates obtained for the compositions with fixed 50 mol% P_2O_5 were 1.89 x 10^{-3}, 5.8 x 10^{-4} and 5.6 x 10^{-4} $mg.mm^{-2}.hr^{-1}$ respectively. The rates obtained for glasses with fixed 55 mol% P_2O_5, were 3.9 x 10^{-4}, 3.6 x 10^{-4} and 2.9 x 10^{-4} $mg.mm^{-2}.hr^{-1}$ respectively.

This decrease in the dissolution rates was again attributed to the cross linking ability of the Ca^{2+} ion. However, this did not account for the difference observed from glass code $P_{50}Ca_{30}Na_{20}$, as compared to the rest of the compositions investigated. The difference seen was an order of magnitude. One possible explanation for the vast difference seen for the dissolution rate for this glass was again attributed to structural differences. Previous studies had shown that when the CaO content of a ternary phosphate glass composition was 30 mol% or below, the dissolution rates were significantly enhanced, as compared to compositions with CaO content being above 30 mol% (102;103).

3.9.5.2 pH and Ion Release Profiles:

The sodium ion release rates obtained from the fixed 50 mol% P_2O_5 compositions mirrored the profiles seen from the dissolution rates obtained from the same compositions. By contrast, the calcium ion release profiles seen were the highest in glass code $P_{50}Ca_{30}Na_{20}$, followed by glass codes $P_{50}Ca_{40}Na_{10}$ then $P_{50}Ca_{35}Na_{15}$. The sodium ion release profiles observed from the fixed 55 mol% compositions showed a decrease in release with increasing CaO content, whereas the calcium ion release profiles exhibited the reverse pattern. The highest calcium ions were released from the composition with fixed 40 mol% CaO, then 35 mol% CaO, followed by the 30 mol% CaO composition.

The anion release profiles exhibited very little release as compared to the cations released from the same compositions. The release profiles showed that the PO_4^{3-} and $P_2O_7^{4-}$ anion showed no correlation with their respective compositions, and very little of both these anions was released. Again the cyclic $P_3O_9^{3-}$ metaphosphate anion was the highest released phosphate species, followed by the $P_3O_{10}^{5-}$ linear anionic species. Compositions with fixed 55 mol% P_2O_5 all released relatively small amounts of anions as compared to the fixed 50 mol% compositions.

As stated by Bunker *et al* (89) hydrolysis reactions result in the cleavage of P-O-P bonds, and have the potential to totally disrupt the polymeric phosphate network, to produce orthophosphates. Hydration reactions however, involve the dissolution of intact entire chains. Bunker *et al* went on to say that the data they collated was more consistent with a dissolution mechanism involving simple hydration of the phosphate chains, for compositions based on the $(50\text{-}X)M_2O - XCaO - 50P_2O_5$ formula, where M stands for metal ion. Totally hydrated chains disentangle from partially hydrated chains still attached to the surface of the glass and float off into solution, resulting in uniform glass dissolution and linear kinetics. Using the hydration model, it was possible to explain why glass dissolution was accelerated in acidic solutions. In acids, phosphate chains are protonated which disrupt ionic cross-links between chains. Water is then able to penetrate the glass faster, resulting in rapid chain hydration and uniform dissolution.

The highest dissolution rate observed in the study conducted was seen for the composition with glass code $P_{50}Ca_{30}Na_{20}$, along with the highest release of sodium and calcium ions into solution. Bunker *et al* stated that hydrogen depth profiles revealed that consumption of protons by glass degrading below pH 6 did not involve selective leaching of cations from the glass via an ion exchange process. Titrations at pH 4 and pH 5 indicated that enough protons had been consumed to have removed all alkali from the glass to a depth of over 10 microns. Therefore, they concluded that H^+ and OH^- were consumed in reactions involving the phosphate network, and that these reactions accompanied network

dissolution since none of the reaction products appeared to be left on the surface of the glass (89).

Therefore, the above hydration model proposed by Bunker *et al* accounted for the dissolution patterns observed for both the fixed 50 and 55 mol% P_2O_5 compositions. Furthermore the hydration model was also observed when the higher ($P_3O_9^{3-}$ and $P_3O_{10}^{5-}$) phosphate species were taken into account, which all showed a decrease in their rate of release with an increase in CaO content. This suggested that they were cross-linked (branched) via the Ca^{2+} ions acting as a chelate (90), and were thus being released as chains.

Delahaye *et al* (104) also conducted studies on phosphate glasses with the (50-X)M_2O – XCaO – 50P_2O_5 formula. They stated that their initial dissolution rates were also similar to those reported by Bunker *et al*. However, Delahaye *et al* stated that surface reactions limited the phosphate glass dissolution at pH 3, and that the increasing ionic strength of the solution decreased the dissolution rate. This was said to be due to an increase in the electrostatic interactions between the polyphosphate chains in the hydrated layer, which resulted in an increase in the hydrated chain cohesion, which in turn reduced the dissolution rate. These observations were consistent with the profiles and dissolution rates obtained for the fixed 55 mol% P_2O_5 compositions.

Wen and Jijian stated that when the pH value of the solution was <5, the dissolution of the phosphate glass was controlled by the hydration process, in which the long linear chains in the glass were disentangled and dissolved (101). However, according to a commonly used hypothesis (89), glass dissolution should be inhibited when the solution becomes saturated with the least soluble species which can leach from the glass.

3.10 Discussion on the Use of Response Factors:

3.10.1 Response factors Used for the 45 mol% P_2O_5 compositions:

By using a Response Factor (RF) given by the peak area (A) versus concentration (C) gradient obtained from the $P_3O_{10}^{5-}$ calibration (as shown in section 3.7.3, Figure 3.26), it was possible to quantify the additional eluting polyphosphate species.

For the fixed 45 mol% P_2O_5 compositions, it was reasonable to assume that the X1 peak was a tetraphosphate (P_4) anionic linear chain species (P_4O_{13}), due to the correlation seen with the anionic rates of release quantified earlier. A decrease with increasing CaO content was observed with the linear phosphate species for the 45 mol% P_2O_5 compositions (See Figures 3.19, 3.22 and 3.24). The X2 peak appeared to be a cyclic species, as it exhibited rates of release profiles similar to the $P_3O_9^{3-}$ species (See Figure 3.23). However, it cannot be unequivocally stated whether this peak was a cyclic tetrametaphosphate (P_4O_{12})

species, or a P_5 anionic species without the appropriate standards. The X4 labelled peak also exhibited similar release patterns to the $P_3O_9^{3-}$ anion, suggesting that this could be a cyclic P_6O_{18} species. XRPD data conducted (105) showed that the main phase identified from the compositions with fixed 30 and 35 mol% CaO content, was a $Na_4Ca(PO_3)_6$. This phase was not identified for the 40mol% CaO glass, hence the difference seen in the rates of release. The suggestion put forward for the X5 peak, was a P_7O_{22} linear anion, due to correlation seen with increasing CaO content. It was also interesting to note that this anion did not appear in solution until 144 hours for the fixed 30 and 35 mol% CaO compositions, and appeared earlier (at the 72 hour time point) for the fixed 40 mol% composition. This observation further supported the structural difference within these compositions as suggested earlier.

It must also be stated that the suggestions proposed above can only be verified via obtaining the appropriate standards for these higher phosphate species.

3.10.2 Response Factors Used for the 50 and 55 mol% P_2O_5 Compositions:

Using the hypothesis proposed by Stover *et al* (81) it was possible to quantitate the extra polyphosphate peaks observed in the (IC) chromatograms obtained. It was due to the presence of these higher phosphate peaks that the weight loss values obtained did not match with the cation and anion release profile data collated in terms of amounts dissolved. Initial analysis revealed that relatively large amounts of these polyphosphate species were released, and all followed patterns similar to those obtained from the weight loss data, where a decrease in

the rates of release was seen with an increase in CaO content. Also it was noticeable that the highest amounts of these polyphosphate anions were released from glass code $P_{50}Ca_{30}Na_{20}$ (which would also account for the order of magnitude difference observed from the dissolution rates obtained for this composition). It was also seen for compositions with fixed 50 mol% P_2O_5 that peaks labelled X1, X2 and X4 (Figures 3.44, 3.45 and 3.47) showed correlation with the profiles seen in Figure 3.38 (i.e. the cyclic $P_3O_9^{3-}$ species), thus suggesting that these anions were also cyclic species.

However, the identity of the anions observed (X1 – X5) could not be stated as this could only be confirmed via obtaining known reagents or standards for the higher linear and cyclic polyphosphates, which were unavailable at the time of this study. Also due to the fact that all the higher phosphates (X1 – X5) quantified for the fixed 55 mol% P_2O_5 compositions exhibited similar patterns (i.e. a decrease in release with increasing CaO content), suggestions as to their identity could not be put forward.

All peaks observed showed a decrease in their rate of release with an increase in CaO content. This corroborated the hydration model proposed above, due to the presence of chains present in these compositions. It also showed that the solution was indeed saturated with higher phosphate species, which further supported the suggestion of glass dissolution inhibition due to saturation with the least soluble species.

A parallel study was also conducted with collaborators from the Muscle Cell Biology Group, Hammersmith Hospital, London. It was found that these compositions were too soluble for muscle cell attachment. Therefore, a quaternary component is to be added in order to try and reduce the dissolution rates.

Summary:

To summarise, in this chapter, ternary phosphate-based glasses and glass-fibres were investigated, where the phosphate content was varied. It was ascertained that a minimum of 50 mol% P_2O_5 content was required in order to produce fibres. This was related to the network connectivity (NC), cross-link density CLD and average chain length (ACL). Therefore, in order to produce glass and glass-fibres at compositions which gave the greatest amount of flexibility in terms of ion incorporation, 50 mol% P_2O_5 content was fixed for all remaining compositions to be investigated.

Ion release profiles exhibited similar patterns as observed for the dissolution studies. Higher phosphate species were observed and quantified, however, identification of these higher phosphates was not possible due to lack of available standards.

CHAPTER 4

The Quaternary P_2O_5 – CaO – Na_2O – B_2O_3 Glass System

4.0 The Quaternary P_2O_5 – CaO – Na_2O – B_2O_3 Glass System:

4.1 Quaternary Compositions Investigated:

In the previous chapter, ternary phosphate-based glasses and glass-fibres were investigated, where the phosphate content was varied. It was ascertained that a minimum of 50 mol% P_2O_5 content was required in order to produce fibres. Therefore, in order to produce glass and glass-fibres at compositions which gave the greatest amount of flexibility in terms of ion incorporation, 50 mol% P_2O_5 content was fixed for all remaining compositions investigated. The CaO content was varied as before at 30, 35 and 40 mol%. The amount of boric oxide (B_2O_3) incorporated was substituted for sodium oxide (Na_2O).

The reason for incorporating a quaternary component was to decrease the dissolution rates obtained from the previous glass systems investigated. This was conducted in order to obtain glass compositions upon which biocompatibility assessments could be carried out, as the initial biocompatibility assessments conducted on the ternary (P_2O_5-CaO-Na_2O) compositions proved to be unsatisfactory. It was seen from these compositions that the glass-fibres degraded too quickly in order to achieve satisfactory cell attachment. Therefore, B_2O_3 was added due to two reasons: firstly, due to it being a well known glass network former it was hypothesised that B_2O_3 would go into the backbone of the phosphate network, thus strengthening it. Secondly, it was also known to be relevant to some biological species. The glass codes and compositions

investigated are presented in Table 4.1. Glass fibres were obtained from all the glasses investigated within this system.

Table 4.1: Compositions investigated with glass codes.

Glass Codes	P_2O_5 (mol%)	CaO (mol%)	Na_2O (mol%)	B_2O_3 (mol%)
$P_{50}Ca_{30}Na_{19}B_1$	50	30	19	1
$P_{50}C_{35}Na_{14}B_1$	50	35	14	1
$P_{50}Ca_{40}Na_9B_1$	50	40	9	1
$P_{50}Ca_{30}Na_{18}B_2$	50	30	18	2
$P_{50}Ca_{35}Na_{13}B_2$	50	35	13	2
$P_{50}Ca_{40}Na_8B_2$	50	40	8	2
$P_{50}Ca_{30}Na_{17}B_3$	50	30	17	3
$P_{50}Ca_{35}Na_{12}B_3$	50	35	12	3
$P_{50}Ca_{40}Na_7B_3$	50	40	7	3
$P_{50}Ca_{30}Na_{16}B_4$	50	30	16	4
$P_{50}Ca_{35}Na_{11}B_4$	50	35	11	4
$P_{50}Ca_{40}Na_6B_4$	50	40	6	4
$P_{50}Ca_{30}Na_{15}B_5$	50	30	15	5
$P_{50}Ca_{35}Na_{10}B_5$	50	35	10	5
$P_{50}Ca_{40}Na_5B_5$	50	40	5	5

The duration of melt temperatures used, along with casting temperatures for the above compositions are presented in Table 2.2 (Chapter 2).

4.2 Differential Thermal Analysis:

All DTA traces obtained exhibited clear traces from which T_g, T_c and T_m values were obtained. Examples of the bulk glass DTA traces obtained, overlaid with their subsequent glass– fibre DTA traces, are shown in Figures 4.1 and 4.2.

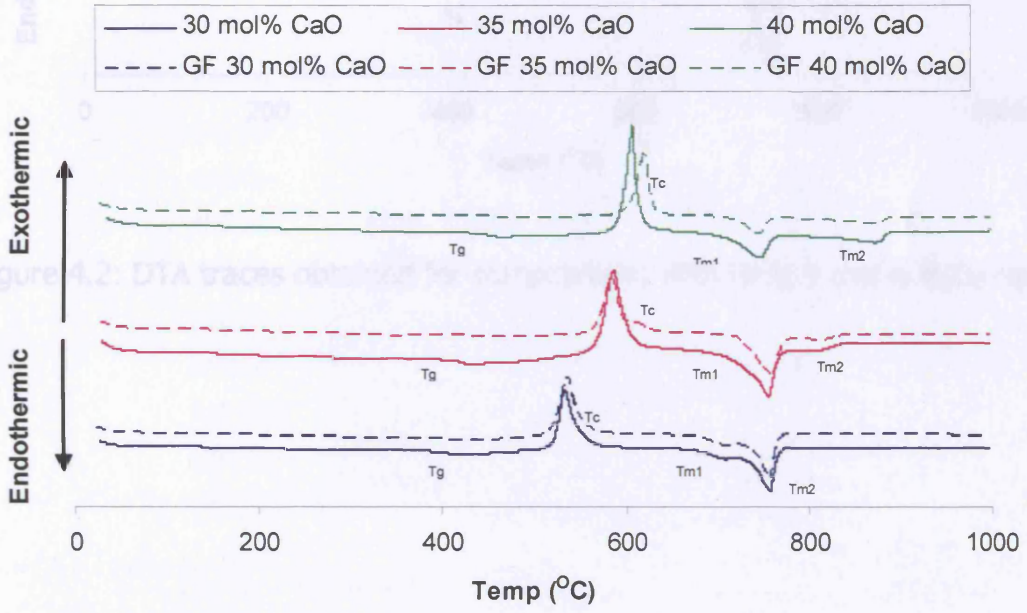

Figure 4.1: DTA traces obtained for compositions with fixed 1 mol% B_2O_3 content.

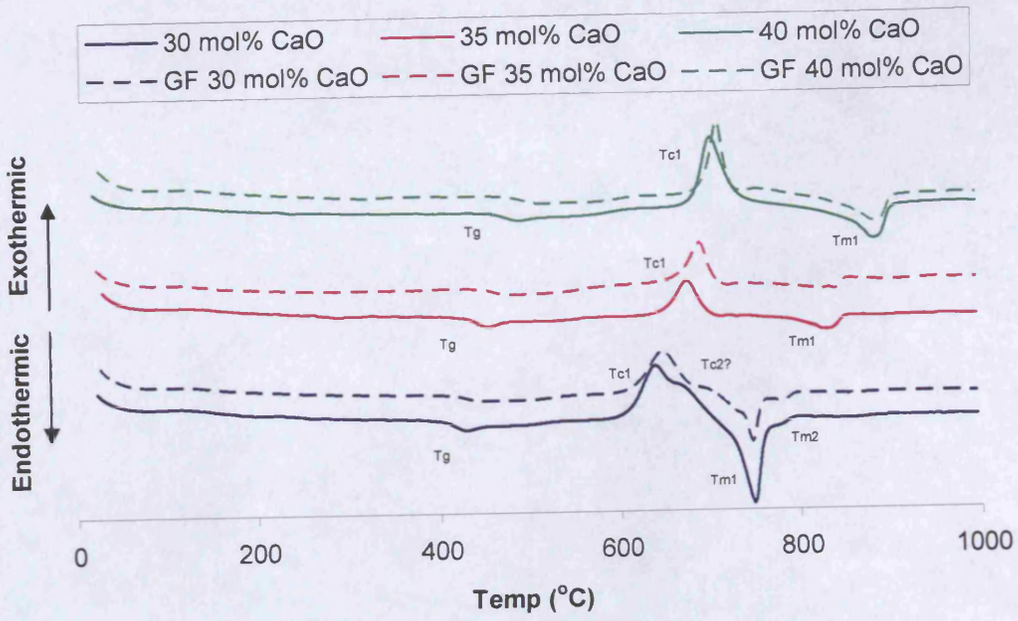

Figure 4.2: DTA traces obtained for compositions with fixed 5 mol% B_2O_3 content.

All T_g values obtained exhibited an increase with increasing CaO content, along with increasing B_2O_3 mol%. Similar patterns were also obtained for the glass–fibre T_g values obtained, however, these values were slightly higher than the bulk glass T_g values. Figure 4.3 and 4.4 present the T_g values obtained from the bulk glasses and the glass-fibre compositions investigated, respectively.

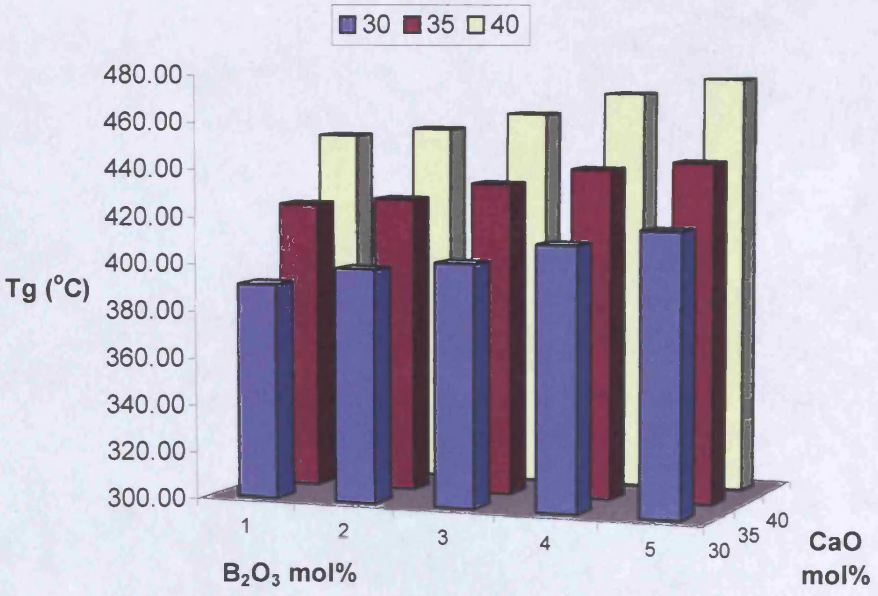

Figure 4.3: T_g values obtained for the bulk glass compositions investigated.

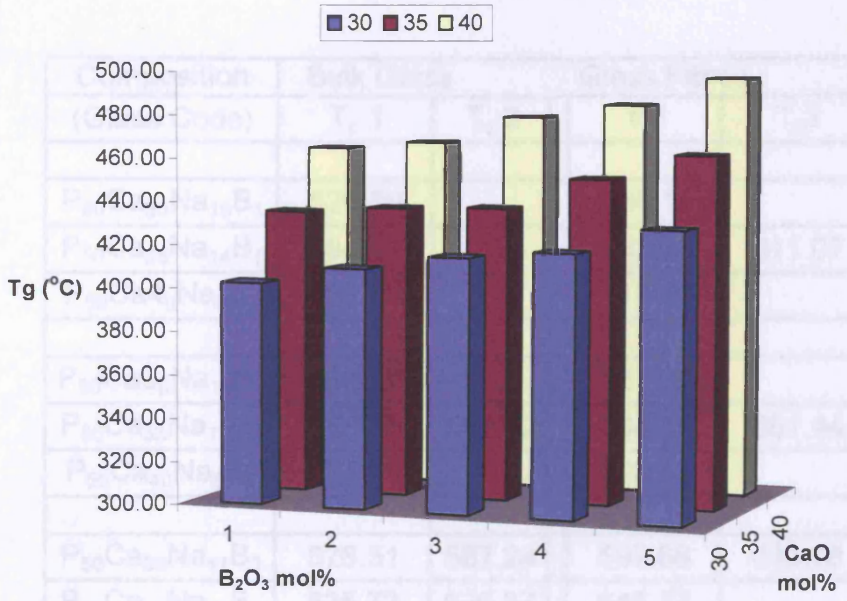

Figure 4.4: T_g values obtained for the glass-fibre compositions investigated.

The T_c values obtained exhibited exactly the same patterns as seen with the T_g values. However the T_m values obtained showed no patterns or correlation with the compositions investigated.

In addition, some compositions investigated exhibited either two T_c or two T_m peaks. The T_c and T_m values obtained have been tabulated in Table 4.2 and 4.3, respectively.

Table 4.2: T_c values for bulk glass and glass-fibre compositions investigated.

Composition	Bulk Glass		Glass Fibres.	
(Glass Code)	T_c 1	T_c 2	T_c1	T_c2
$P_{50}Ca_{30}Na_{19}B_1$	520.59		535.13	
$P_{50}Ca_{35}Na_{14}B_1$	584.01		582.62	611.07
$P_{50}Ca4_0Na_9B_1$	603.72		617.46	
$P_{50}Ca3_0Na_{18}B_2$	568.57		567.60	
$P_{50}Ca_{35}Na_{13}B_2$	586.15	597.82	604.16	651.44
$P_{50}Ca_{40}Na_8B_2$	624.98		628.11	
$P_{50}Ca_{30}Na_{17}B_3$	578.51	587.24	597.66	648.78
$P_{50}Ca_{35}Na_{12}B_3$	635.72	636.37	645.73	
$P_{50}Ca_{40}Na_7B_3$	661.55		659.40	
$P_{50}Ca_{30}Na_{16}B_4$	599.06	616.42	610.53	634.37
$P_{50}Ca_{35}Na_{11}B_4$	666.74		656.82	
$P_{50}Ca_{40}Na_6B_4$	682.15		680.69	
$P_{50}Ca_{30}Na_{15}B_5$	637.38	666.19	645.59	694.30
$P_{50}Ca_{35}Na_{10}B_5$	672.73		686.76	686.98
$P_{50}Ca_{40}Na_5B_5$	700.16		704.07	

An increase in T_c values was seen with an increase in CaO, along with an increase in B_2O_3 mol% content.

Table 4.3: T_m values for bulk glass and glass–fibre compositions investigated.

Composition	Bulk Glass		Glass Fibres.		
(Glass Code)	T_m 1	T_m 2	T_m 1	T_m 2	T_m3
$P_{50}Ca_{30}Na_{19}B_1$	713.28	756.55	707.74	756.33	
$P_{50}Ca_{35}Na_{14}B_1$	753.59	803.55	757.37	813.24	
$P_{50}Ca4_0Na_9B_1$	742.65	870.05	742.43	869.58	
$P_{50}Ca3_0Na_{18}B_2$	694.31	751.37	705.66	756.15	
$P_{50}Ca_{35}Na_{13}B_2$	743.21	813.96	745.81	816.29	
$P_{50}Ca_{40}Na_8B_2$	735.22	871.18	732.51	870.27	
$P_{50}Ca_{30}Na_{17}B_3$	749.41		753.11		
$P_{50}Ca_{35}Na_{12}B_3$	740.44	803.79	740.03	813.07	
$P_{50}Ca_{40}Na_7B_3$	848.71	872.38	711.70	875.84	
$P_{50}Ca_{30}Na_{16}B_4$	749.95		748.31		
$P_{50}Ca_{35}Na_{11}B_4$	818.36	820.69	736.28	822.33	
$P_{50}Ca_{40}Na_6B_4$	873.96		871.92		
$P_{50}Ca_{30}Na_{15}B_5$	748.64	778.21	746.42	777.63	
$P_{50}Ca_{35}Na_{10}B_5$	827.62	829.24	822.48	838.07	899.00
$P_{50}Ca_{40}Na_5B_5$	882.28	882.74	884.82		

As can be seen from the above table, no correlation was observed between the T_m values obtained and the compositions investigated. However, a general increase in T_m values could be seen with increasing B_2O_3 content. It was also noted that the T_m values obtained for the glass-fibres from glass code $P_{50}Ca_{30}Na_{10}B_5$ exhibited 3 T_m peaks.

4.3 XRD Analysis:

The XRPD traces obtained were all matched against the ICDD database using the Crystallographica Search-Match software. Again, each composition was crystallised at its respective crystallisation temperature (T_c), obtained via DTA analysis. An example of the XRPD traces obtained is shown in Figure 4.5. The phases identified from the traces have been tabulated in Table 4.4.

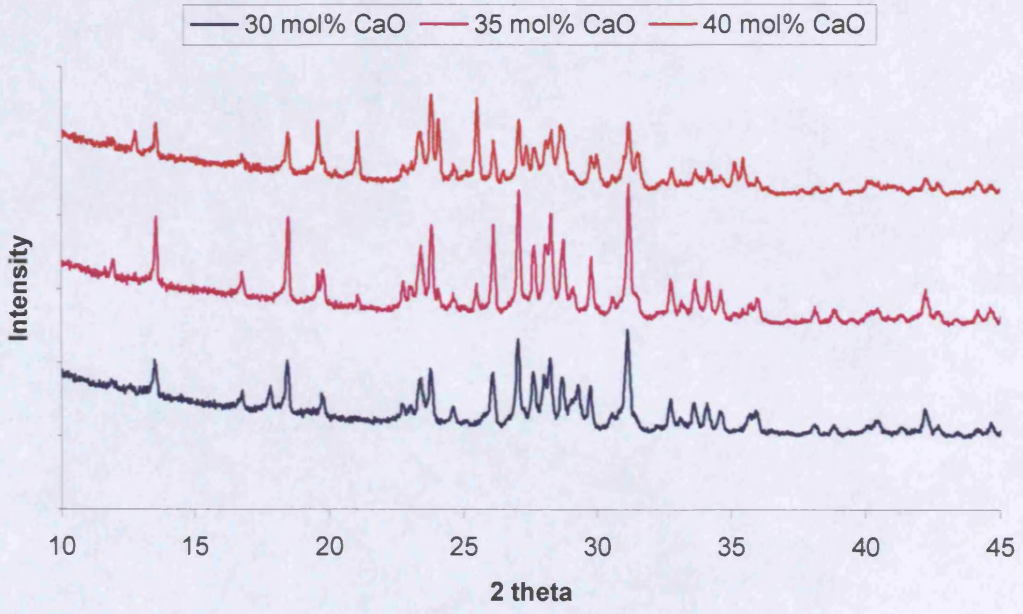

Figure 4.5: XRPD traces obtained for compositions with 1 mol% B_2O_3 content.

Table 4.4: XRPD phases identified from compositions investigated.

Glass Codes.	Phase 1 / ICDD card no.	Phase 2 / ICDD card no.	Phase 3 / ICDD card no.
$P_{50}Ca_{30}Na_{19}B_1$	$NaCa(PO_3)_3$ / 23-669	BPO_4 / 34-132	
$P_{50}Ca_{35}Na_{14}B_1$	$NaCa(PO_3)_3$ / 23-669	CaP_2O_6 / 11-39	BPO_4 / 34-132
$P_{50}Ca_{40}Na_9B_1$	$NaCa(PO_3)_3$ / 23-669	CaP_2O_6 / 11-39	BPO_4 / 34-132
$P_{50}Ca_{30}Na_{18}B_2$	$NaCa(PO_3)_3$ / 23-669	BPO_4 / 34-132	
$P_{50}Ca_{35}Na_{13}B_2$	$NaCa(PO_3)_3$ / 23-669	CaP_2O_6 / 11-39	BPO_4 / 34-132
$P_{50}Ca_{40}Na_8B_2$	CaP_2O_6 / 11-39	$NaCa(PO_3)_3$ / 23-669	BPO_4 / 34-132
$P_{50}Ca_{30}Na_{17}B_3$	$NaCa(PO_3)_3$ / 23-669	BPO_4 / 34-132	
$P_{50}Ca_{35}Na_{12}B_3$	$NaCa(PO_3)_3$ / 23-669	CaP_2O_6 / 11-39	BPO_4 / 34-132
$P_{50}Ca_{40}Na_7B_3$	CaP_2O_6 / 11-39	$NaCa(PO_3)_3$ / 23-669	BPO_4 / 34-132
$P_{50}Ca_{30}Na_{16}B_4$	$NaCa(PO_3)_3$ / 23-669	BPO_4 / 34-132	
$P_{50}Ca_{35}Na_{11}B_4$	$NaCa(PO_3)_3$ / 23-669	CaP_2O_6 / 11-39	BPO_4 / 34-132
$P_{50}Ca_{40}Na_6B_4$	CaP_2O_6 / 11-39	$NaCa(PO_3)_3$ / 23-669	BPO_4 / 34-132
$P_{50}Ca_{30}Na_{15}B_5$	$NaCa(PO_3)_3$ / 23-669	BPO_4 / 34-132	
$P_{50}Ca_{35}Na_{10}B_5$	$NaCa(PO_3)_3$ / 23-669	CaP_2O_6 / 11-39	BPO_4 / 34-132
$P_{50}Ca_{40}Na_5B_5$	CaP_2O_6 / 11-39	$NaCa(PO_3)_3$ / 23-669	BPO_4 / 34-132

It was interesting to note that a boron phosphate phase was identified from compositions containing as little as 1 mol% B_2O_3.

4.4 Degradation Analysis:

4.4.1 Bulk Glass Degradation Studies:

The dissolution studies were conducted using the cumulative method, and showed an almost linear decrease in the dissolution rates obtained with increasing CaO content, along with increasing B_2O_3 content from 1 – 5 mol% B_2O_3. Figures 4.6 – 4.10 show the plots obtained from the dissolution studies conducted.

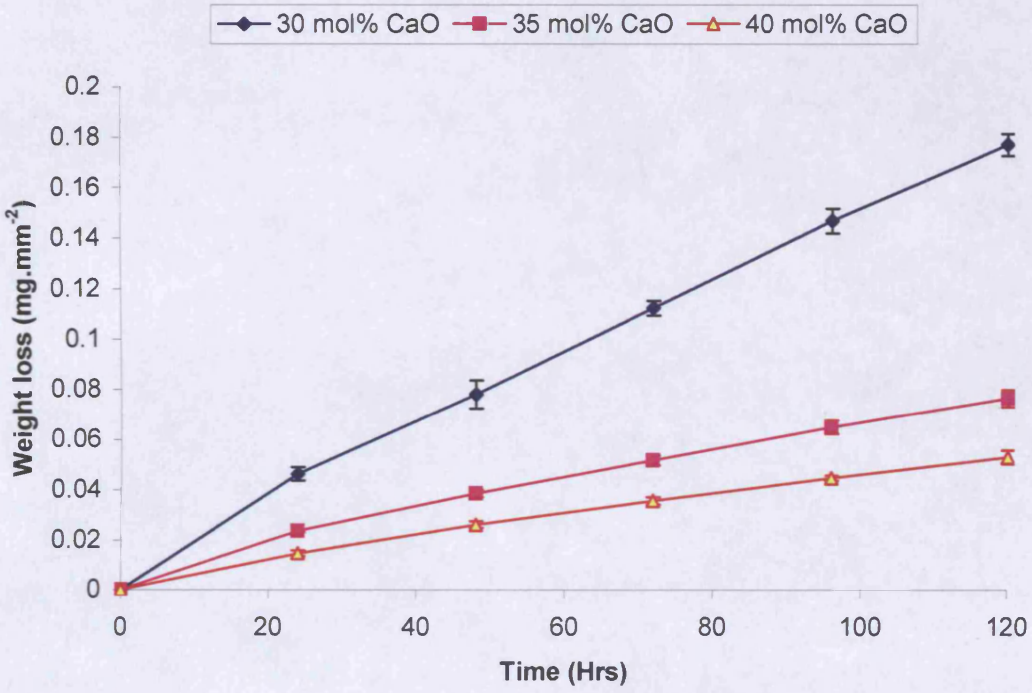

Figure 4.6: Weight loss plots obtained from compositions containing 1 mol% B_2O_3.

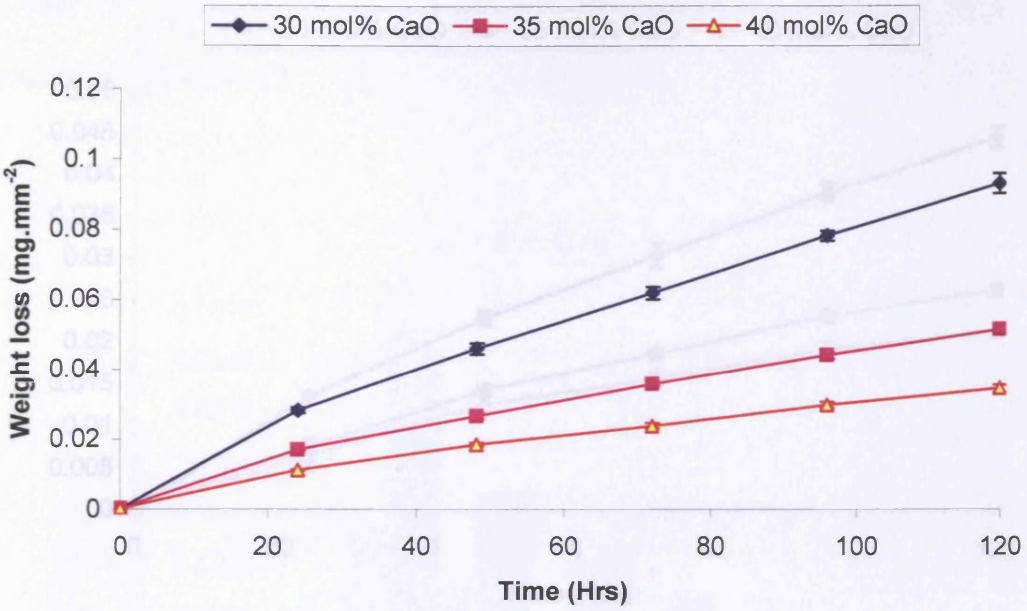

Figure 4.7: Weight loss plots obtained from compositions containing 2 mol% B_2O_3.

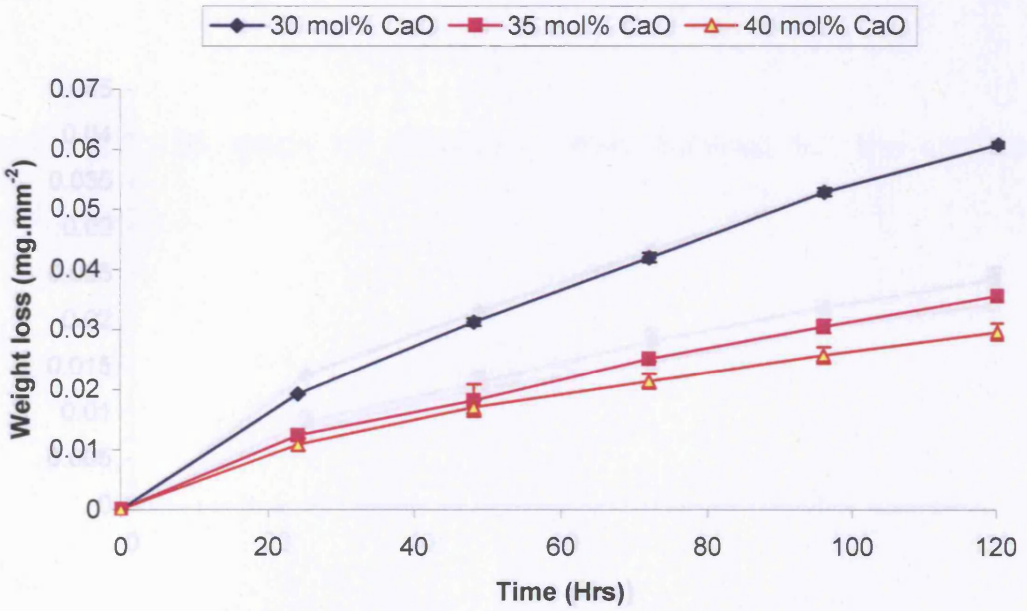

Figure 4.8: Weight loss plots obtained from compositions containing 3 mol% B_2O_3.

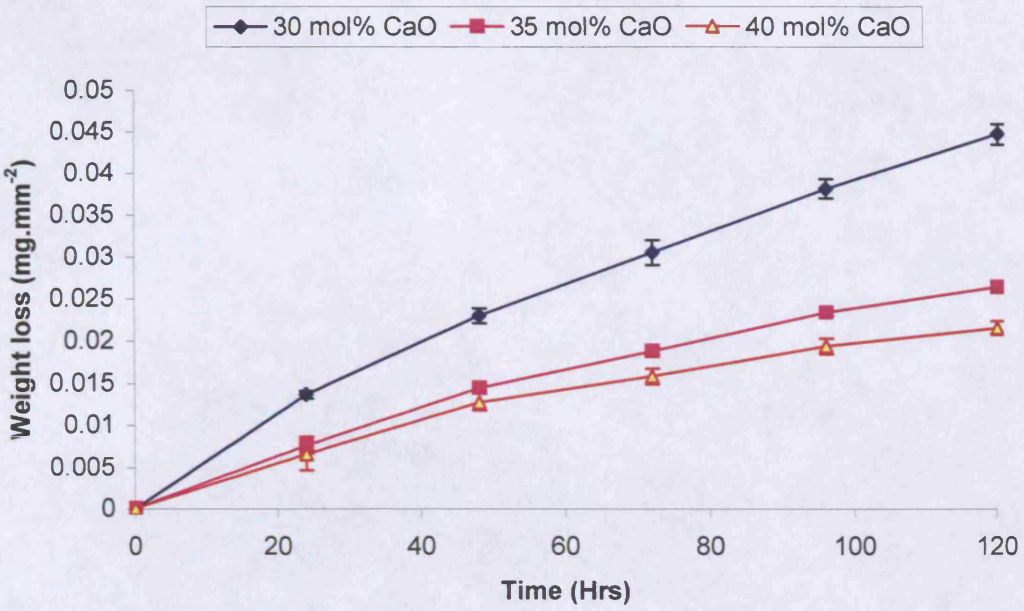

Figure 4.9: Weight loss plots obtained from compositions containing 4 mol% B_2O_3.

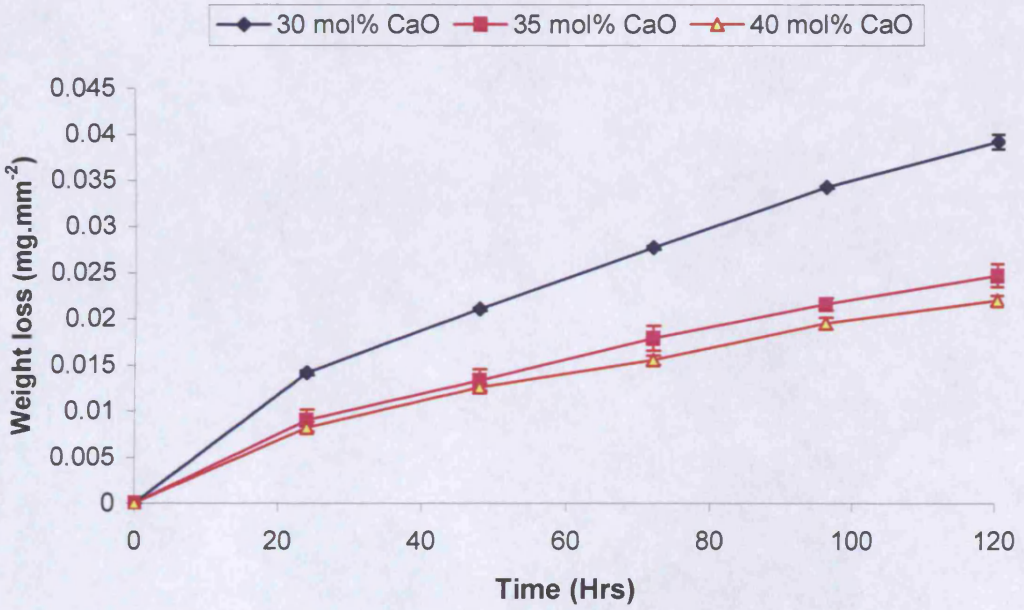

Figure 4.10: Weight loss plots obtained from compositions containing 5 mol% B_2O_3.

By fitting a line of best fit through the plots obtained, dissolution rates in terms of $mg.mm^{-2}.hr^{-1}$ were obtained and are plotted against the CaO and B_2O_3 mol% contents in Figure 4.11.

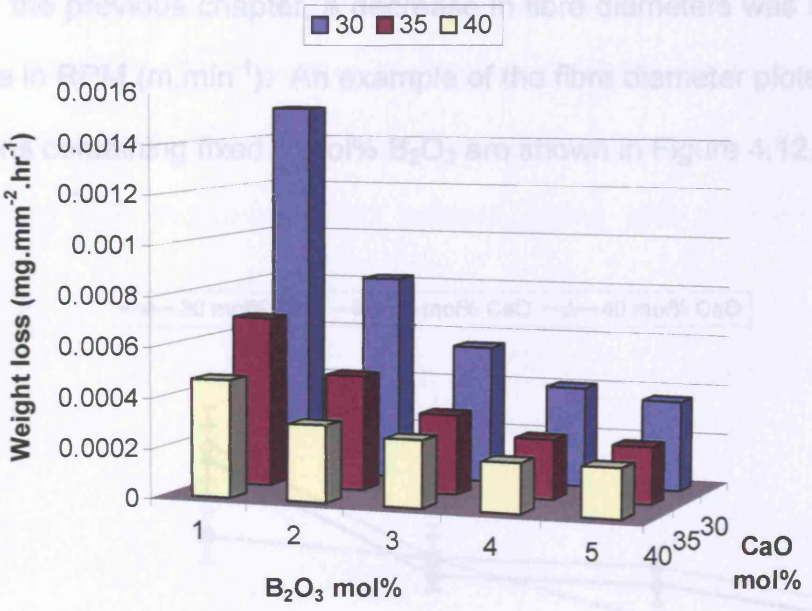

Figure 4.11: 3D graph of dissolution rates obtained for the compositions investigated.

4.4.2 Glass – Fibre Degradation Analysis:

4.4.2.1 Glass–Fibre Diameter Measurements:

As seen in the previous chapter, a decrease in fibre diameters was obtained with an increase in RPM ($m.min^{-1}$). An example of the fibre diameter plots obtained for compositions containing fixed 1 mol% B_2O_3 are shown in Figure 4.12.

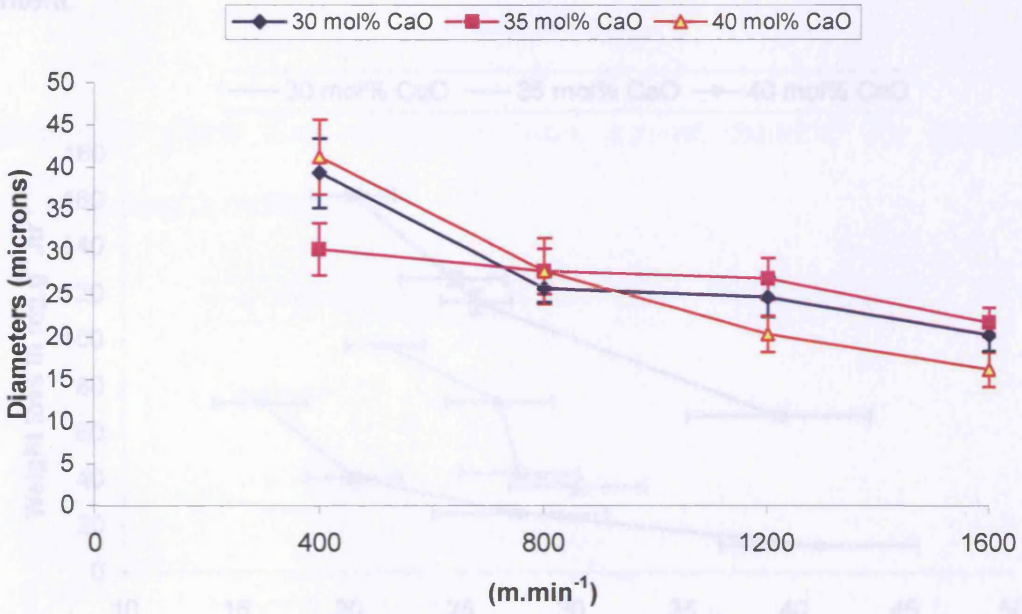

Figure 4.12: Fibre diameters obtained for compositions with fixed 1 mol% B_2O_3.

4.4.2.2 Glass – Fibre Degradation Studies:

The glass-fibre dissolution studies were conducted the same way as described in Chapter 3 section 3.5.2. The glass fibre dissolution rates obtained were plotted as weight loss per gram per hour against diameter measurements obtained (Figures 4.13 – 4.17). As seen from the thermal analyses conducted and the bulk glass dissolution rates obtained, a decrease in the glass-fibre dissolution rates were obtained with increasing CaO content, along with an increase in B_2O_3 content.

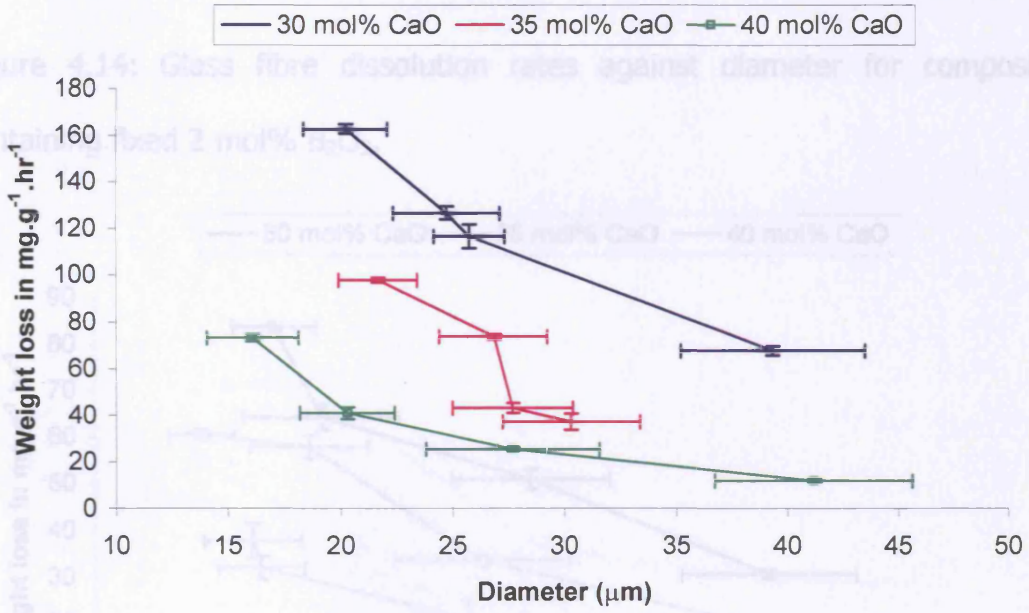

Figure 4.13: Glass fibre dissolution rates against diameter for compositions containing fixed 1 mol% B_2O_3.

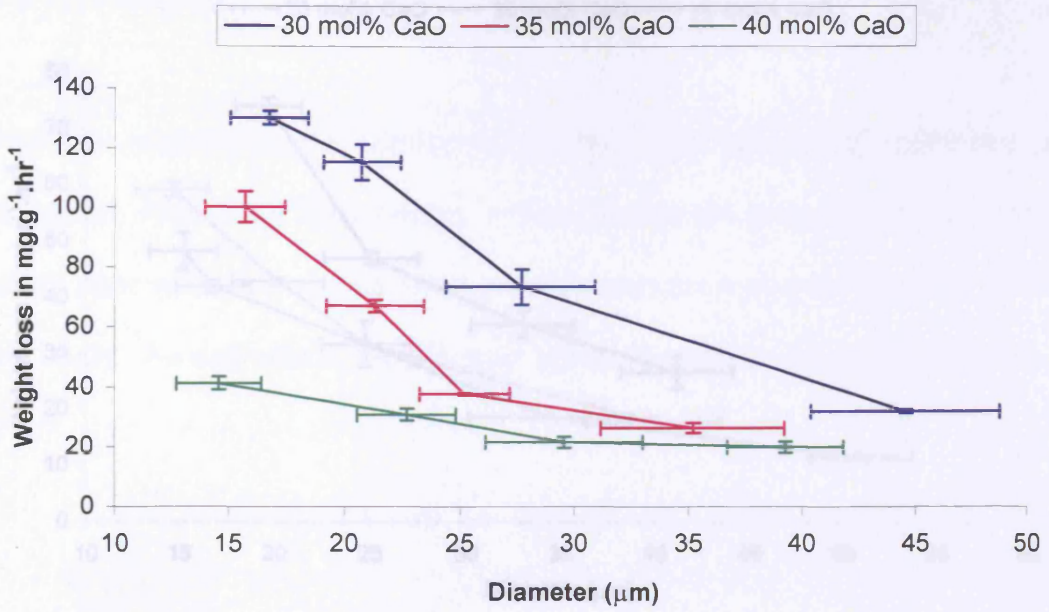

Figure 4.14: Glass fibre dissolution rates against diameter for compositions containing fixed 2 mol% B_2O_3.

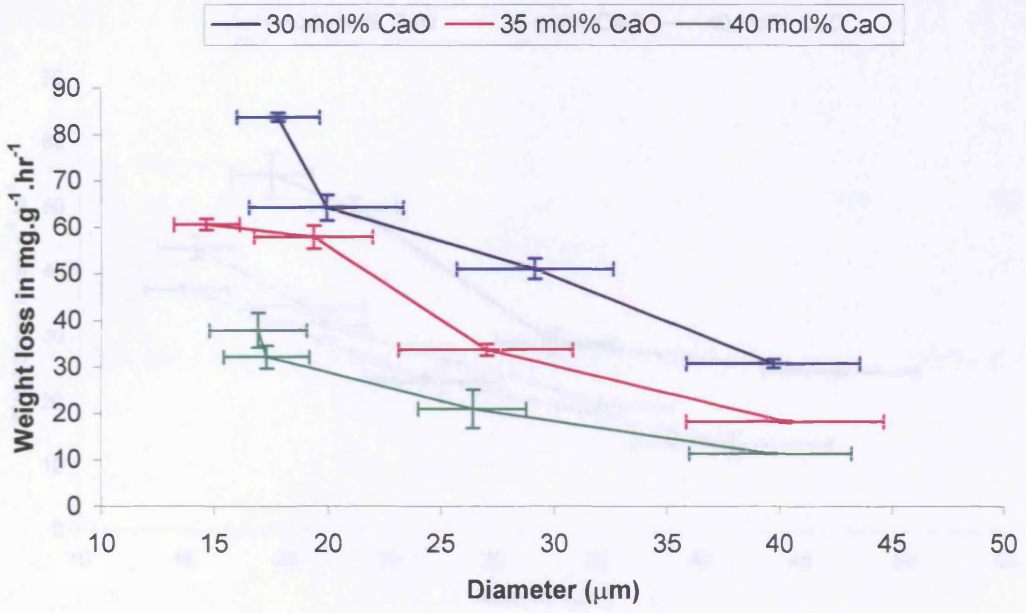

Figure 4.15: Glass fibre dissolution rates against diameter for compositions containing fixed 3 mol% B_2O_3.

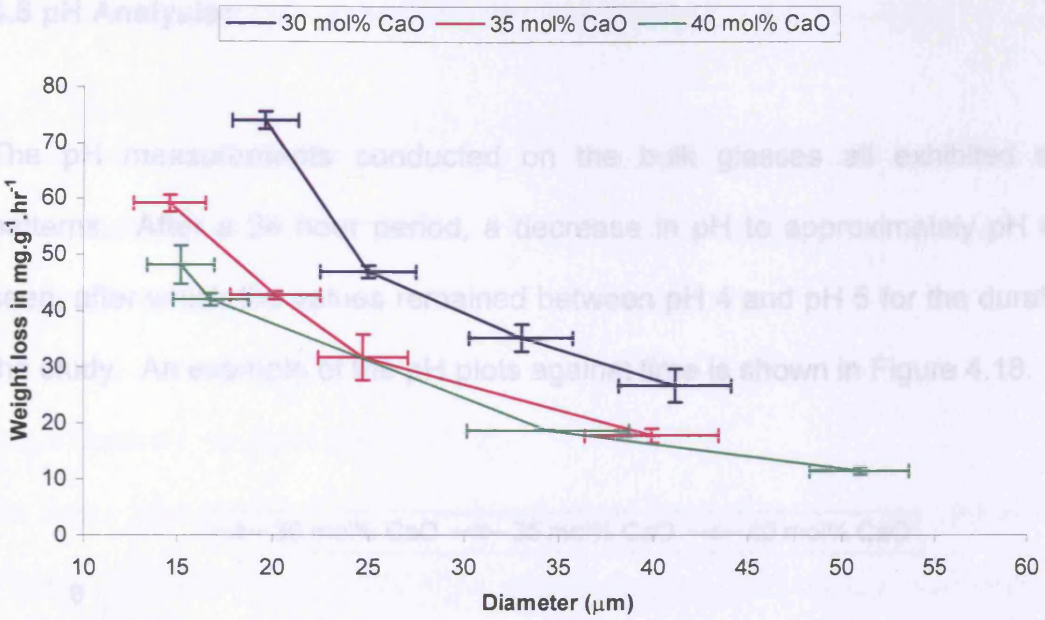

Figure 4.16: Glass fibre dissolution rates against diameter for compositions containing fixed 4 mol% B_2O_3.

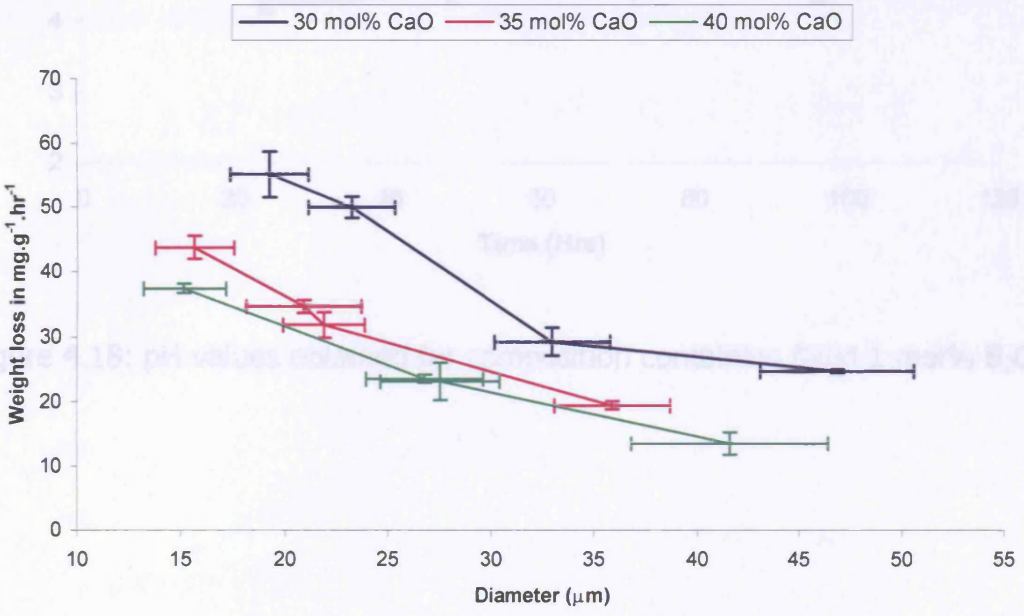

Figure 4.17: Glass fibre dissolution rates against diameter for compositions containing fixed 5 mol% B_2O_3.

4.5 pH Analysis:

The pH measurements conducted on the bulk glasses all exhibited similar patterns. After a 24 hour period, a decrease in pH to approximately pH 4 was seen, after which the values remained between pH 4 and pH 5 for the duration of the study. An example of the pH plots against time is shown in Figure 4.18.

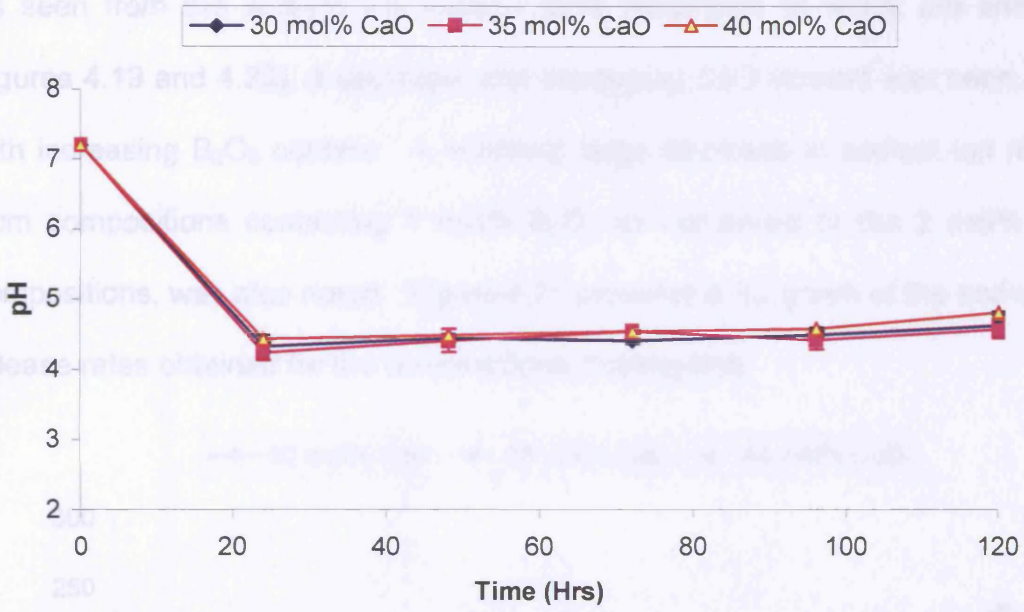

Figure 4.18: pH values obtained for composition containing fixed 1 mol% B_2O_3.

4.6 Ion Release Profiles for Glasses Containing 1 – 5 mol% B_2O_3:

Ion release profiles were measured from each of the triplicate solutions as they were changed on a daily basis. The values obtained (in ppm) were plotted against time.

4.6.1 Sodium Ion Release Profiles:

As seen from the sodium ion release plots (examples of which are shown in Figures 4.19 and 4.20), a decrease with increasing CaO content was seen, along with increasing B_2O_3 content. A relatively large decrease in sodium ion release from compositions containing 1 mol% B_2O_3 as compared to the 2 mol% B_2O_3 compositions, was also noted. Figure 4.21 presents a 3D graph of the sodium ion release rates obtained for the compositions investigated.

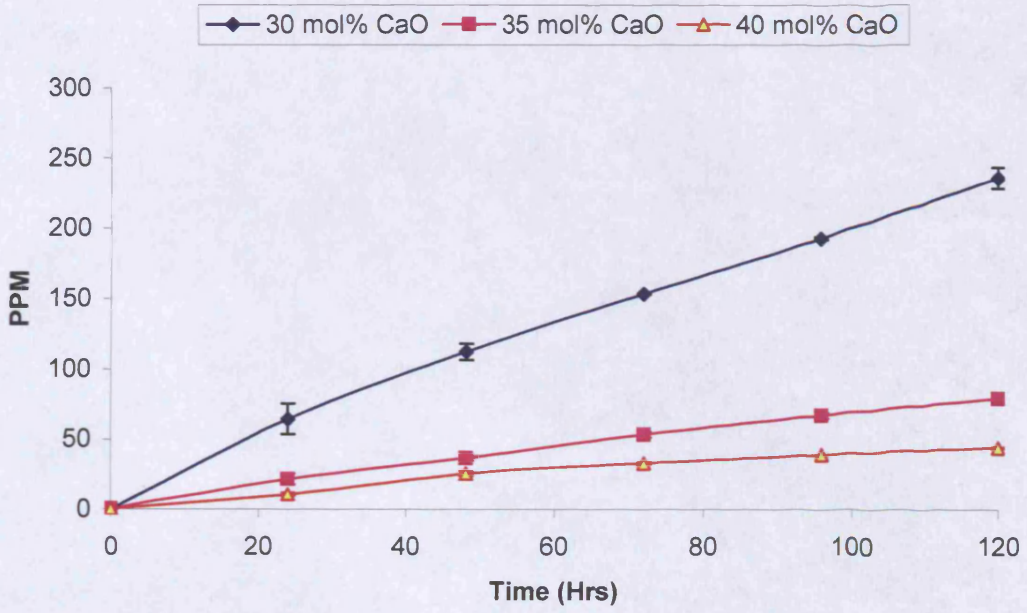

Figure 4.19: Sodium ion release from compositions with fixed 1 mol% B_2O_3.

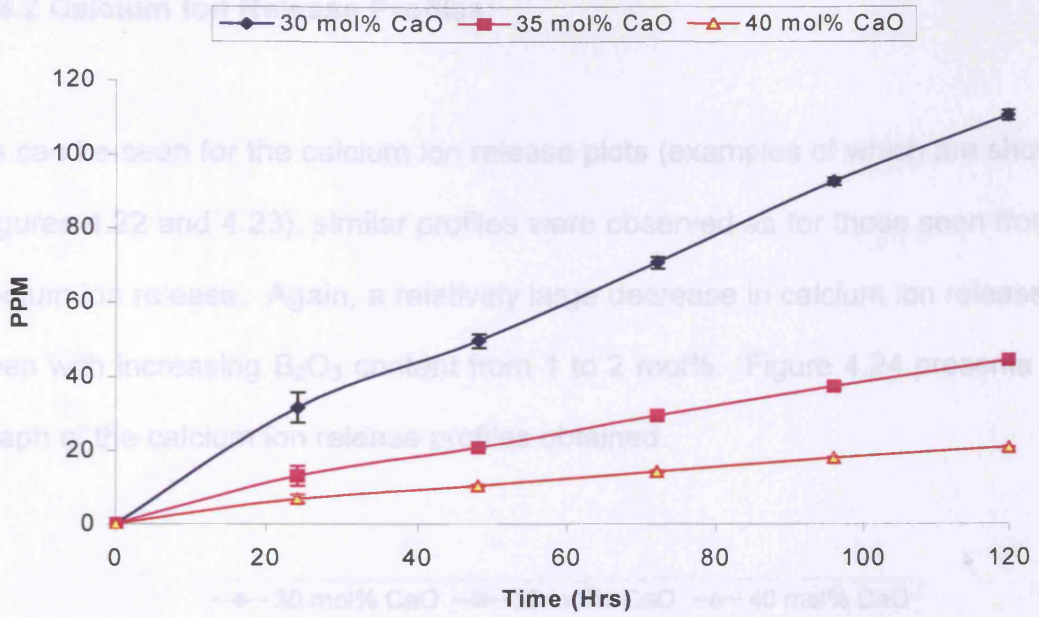

Figure 4.20: Sodium ion release from compositions with fixed 2 mol% B_2O_3.

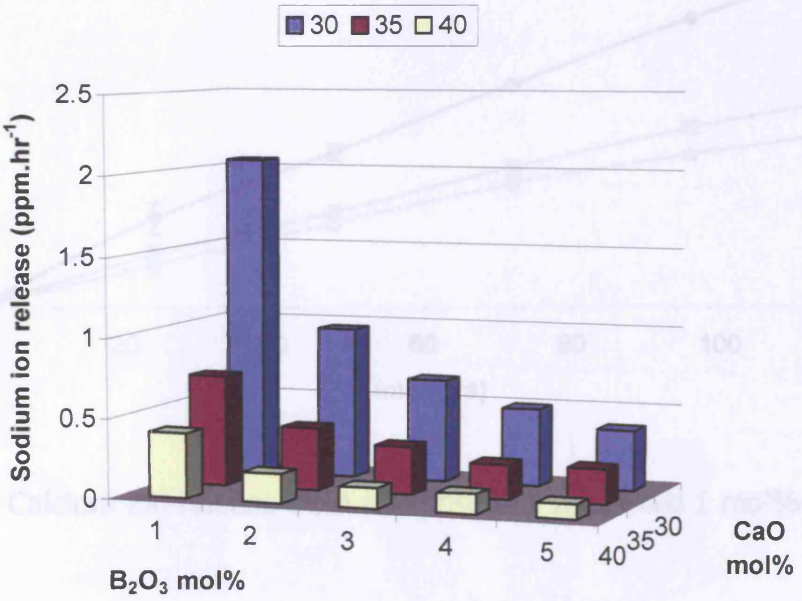

Figure 4.21: 3D graph of the sodium ion release rates obtained from compositions with fixed 1 – 5 mol% B_2O_3 content.

4.6.2 Calcium Ion Release Profiles:

As can be seen for the calcium ion release plots (examples of which are shown in Figures 4.22 and 4.23), similar profiles were observed as for those seen from the sodium ion release. Again, a relatively large decrease in calcium ion release was seen with increasing B_2O_3 content from 1 to 2 mol%. Figure 4.24 presents a 3D graph of the calcium ion release profiles obtained.

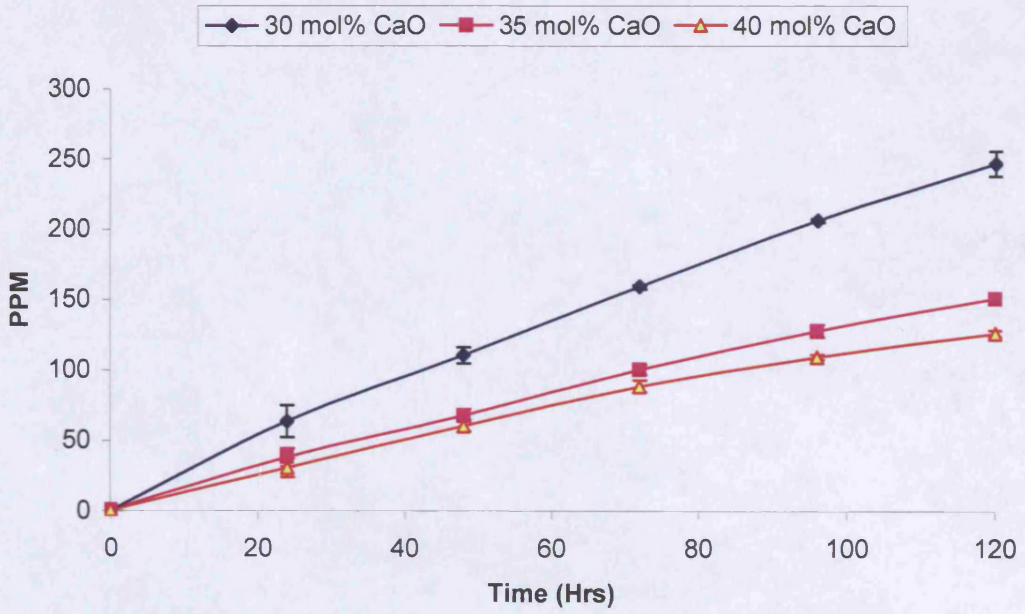

Figure 4.22: Calcium ion release from compositions with fixed 1 mol% B_2O_3.

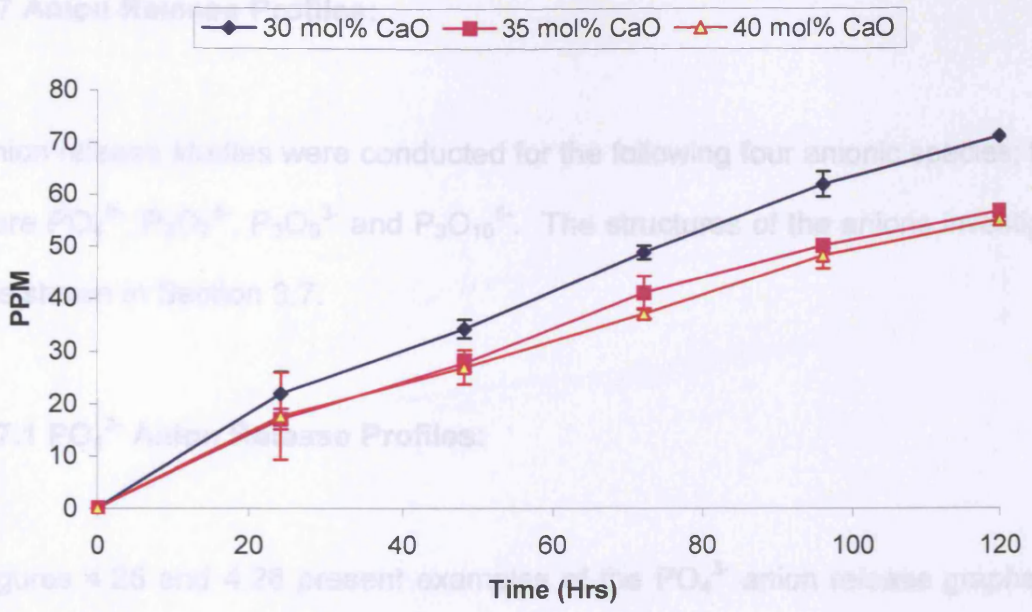

Figure 4.23: Calcium ion release from compositions with fixed 5 mol% B_2O_3.

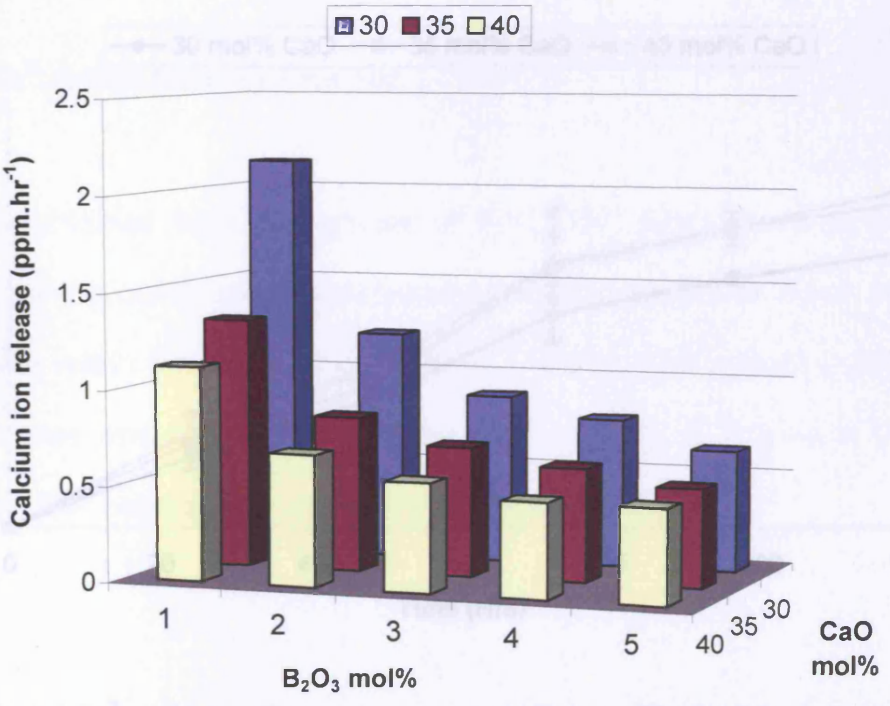

Figure 4.24: 3D graph of the calcium ion release profiles obtained for compositions with varying CaO and fixed 1 – 5 mol% B_2O_3 content`.

4.7 Anion Release Profiles:

Anion release studies were conducted for the following four anionic species; these were PO_4^{3-}, $P_2O_7^{4-}$, $P_3O_9^{3-}$ and $P_3O_{10}^{5-}$. The structures of the anions investigated are shown in Section 3.7.

4.7.1 PO_4^{3-} Anion Release Profiles:

Figures 4.25 and 4.26 present examples of the PO_4^{3-} anion release graphs. As can be seen, the PO_4^{3-} anion exhibited no pattern or correlation with the compositions investigated.

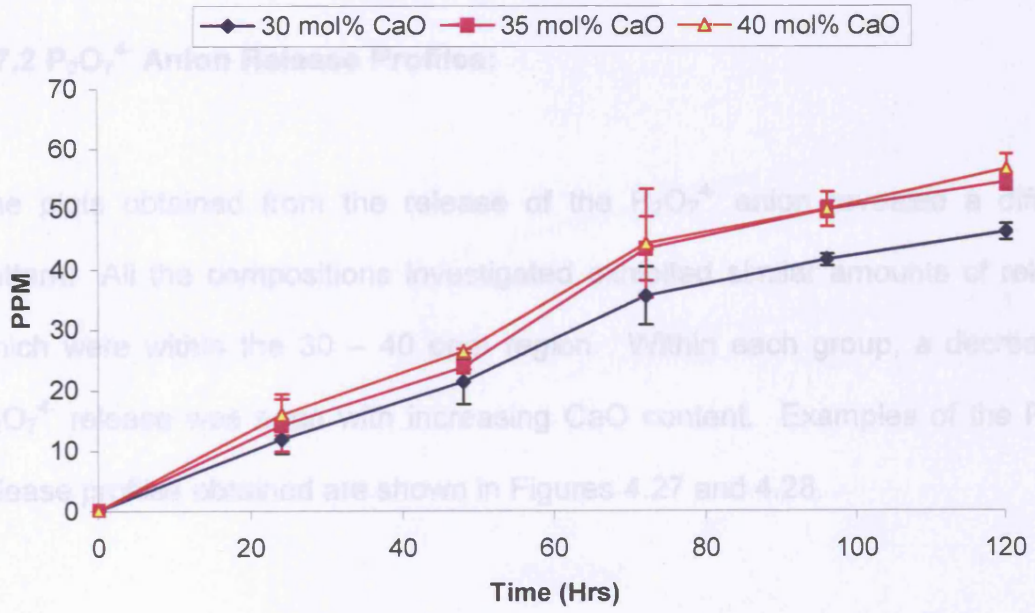

Figure 4.25: PO_4^{3-} anionic release from compositions with fixed 1 mol% B_2O_3.

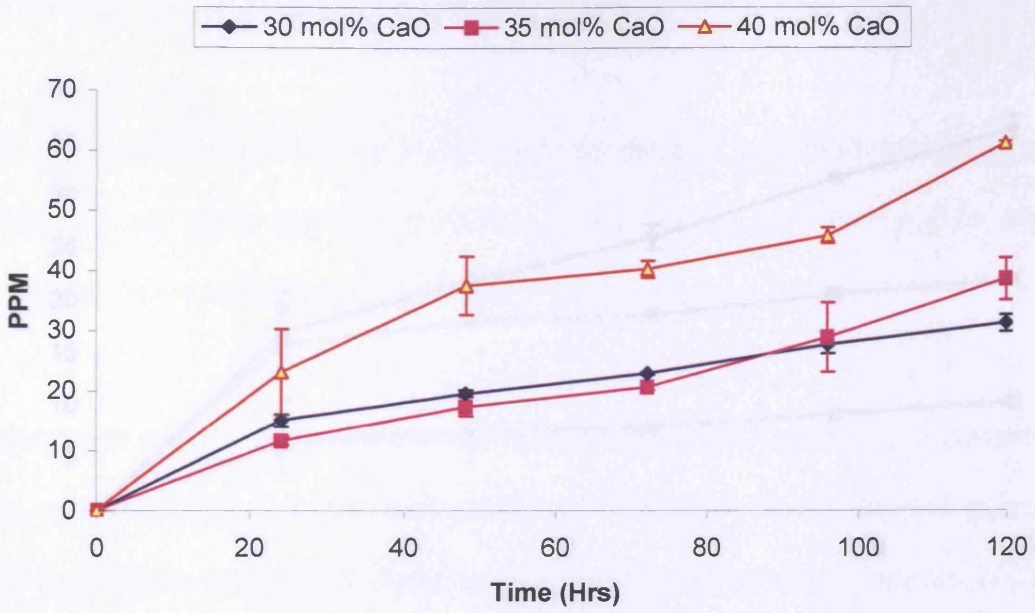

Figure 4.26: PO_4^{3-} anionic release from compositions with fixed 3 mol% B_2O_3.

4.7.2 $P_2O_7^{4-}$ Anion Release Profiles:

The plots obtained from the release of the $P_2O_7^{4-}$ anion revealed a different pattern. All the compositions investigated exhibited similar amounts of release, which were within the 30 – 40 ppm region. Within each group, a decrease in $P_2O_7^{4-}$ release was seen with increasing CaO content. Examples of the $P_2O_7^{4-}$ release profiles obtained are shown in Figures 4.27 and 4.28.

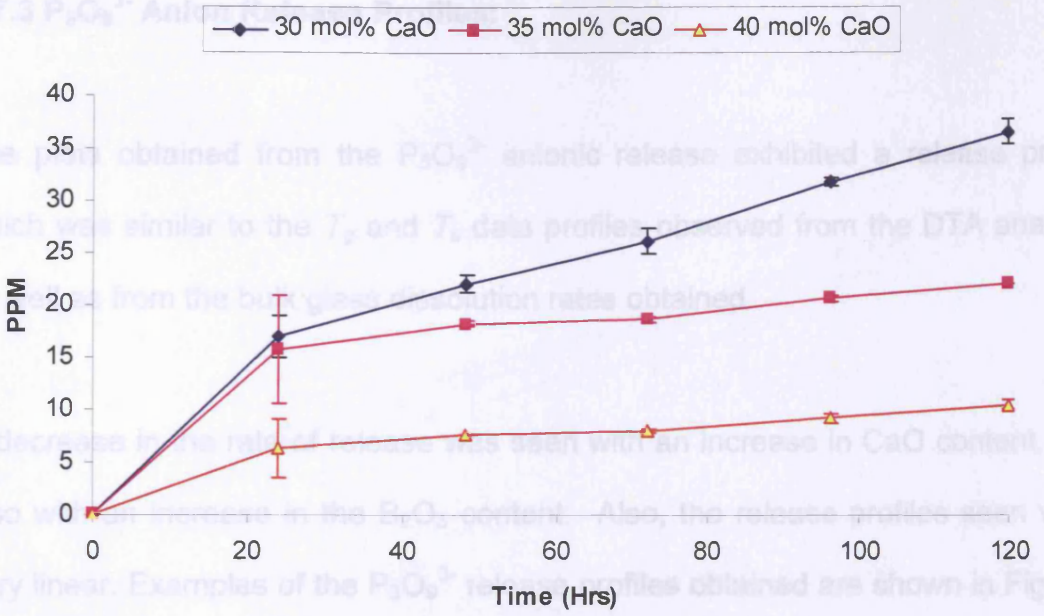

Figure 4.27: $P_2O_7^{4-}$ anionic release from compositions with fixed 1 mol% B_2O_3.

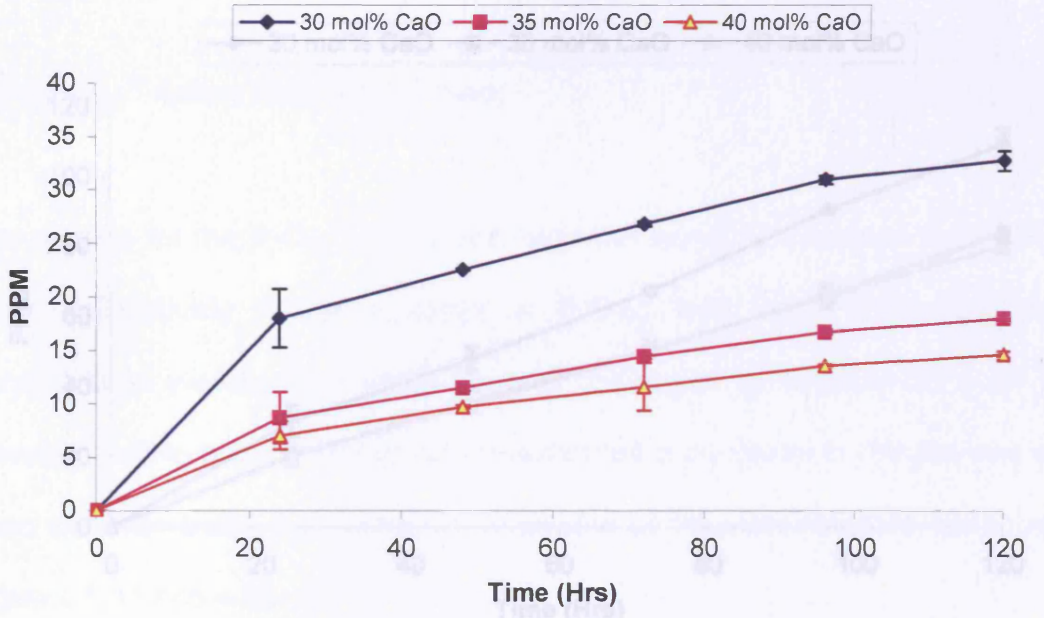

Figure 4.28: $P_2O_7^{4-}$ anionic release from compositions with fixed 5 mol% B_2O_3.

4.7.3 $P_3O_9^{3-}$ Anion Release Profiles:

The plots obtained from the $P_3O_9^{3-}$ anionic release exhibited a release profile which was similar to the T_g and T_c data profiles observed from the DTA analysis as well as from the bulk glass dissolution rates obtained.

A decrease in the rate of release was seen with an increase in CaO content, and also with an increase in the B_2O_3 content. Also, the release profiles seen were very linear. Examples of the $P_3O_9^{3-}$ release profiles obtained are shown in Figures 4.29 and 4.30.

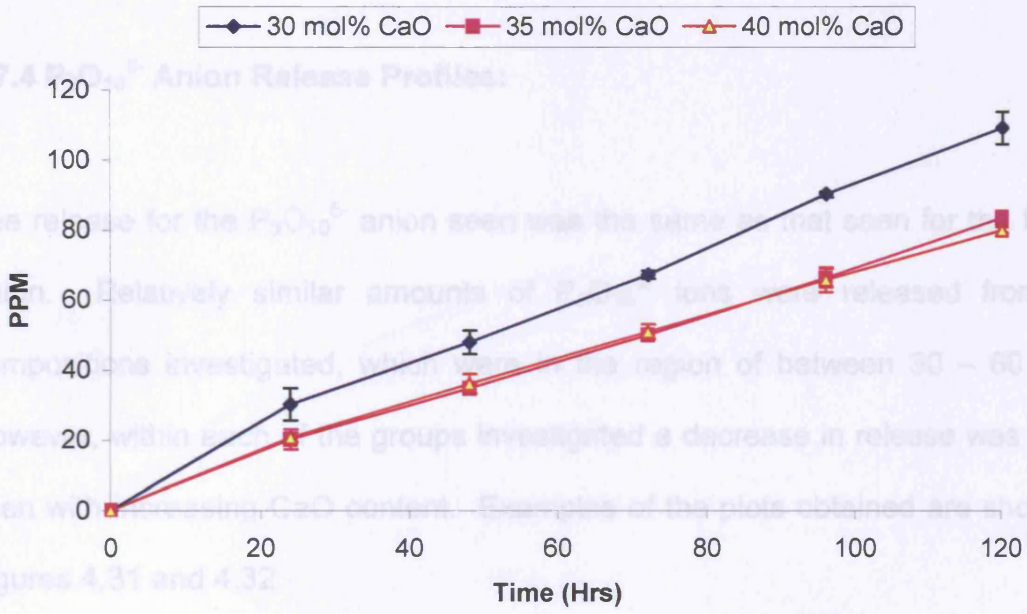

Figure 4.29: $P_3O_9^{3-}$ anionic release from compositions with fixed 1 mol% B_2O_3.

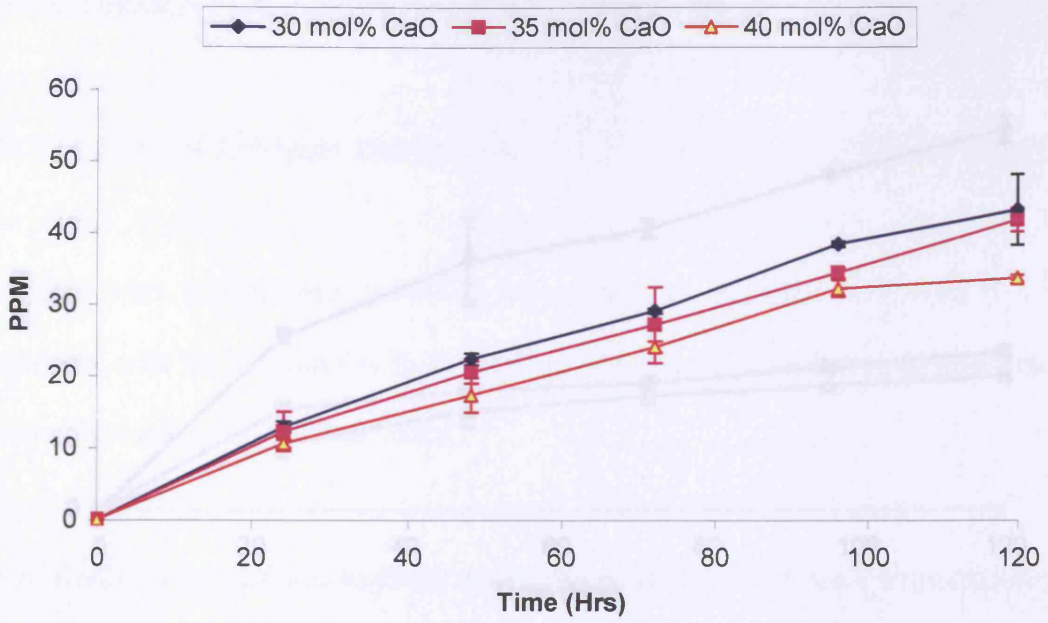

Figure 4.30: $P_3O_9^{3-}$ anionic release from compositions with fixed 3 mol% B_2O_3.

4.7.4 $P_3O_{10}^{5-}$ Anion Release Profiles:

The release for the $P_3O_{10}^{5-}$ anion seen was the same as that seen for the $P_2O_7^{4-}$ anion. Relatively similar amounts of $P_3O_{10}^{5-}$ ions were released from the compositions investigated, which were in the region of between 30 – 60 ppm. However, within each of the groups investigated a decrease in release was again seen with increasing CaO content. Examples of the plots obtained are shown in Figures 4.31 and 4.32.

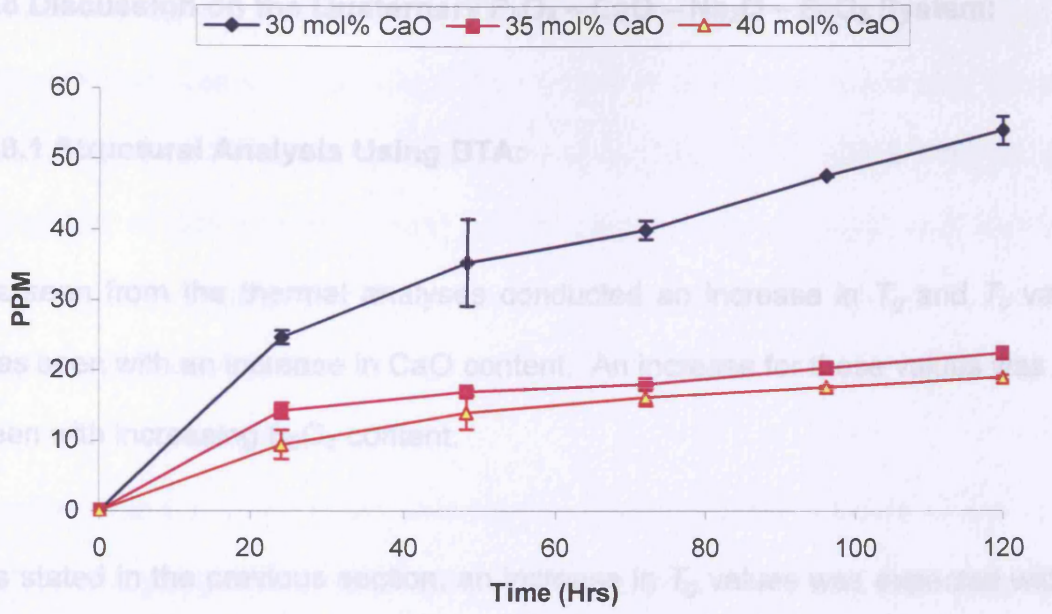

Figure 4.31: $P_3O_{10}^{5-}$ anionic release from compositions with fixed 1 mol% B_2O_3.

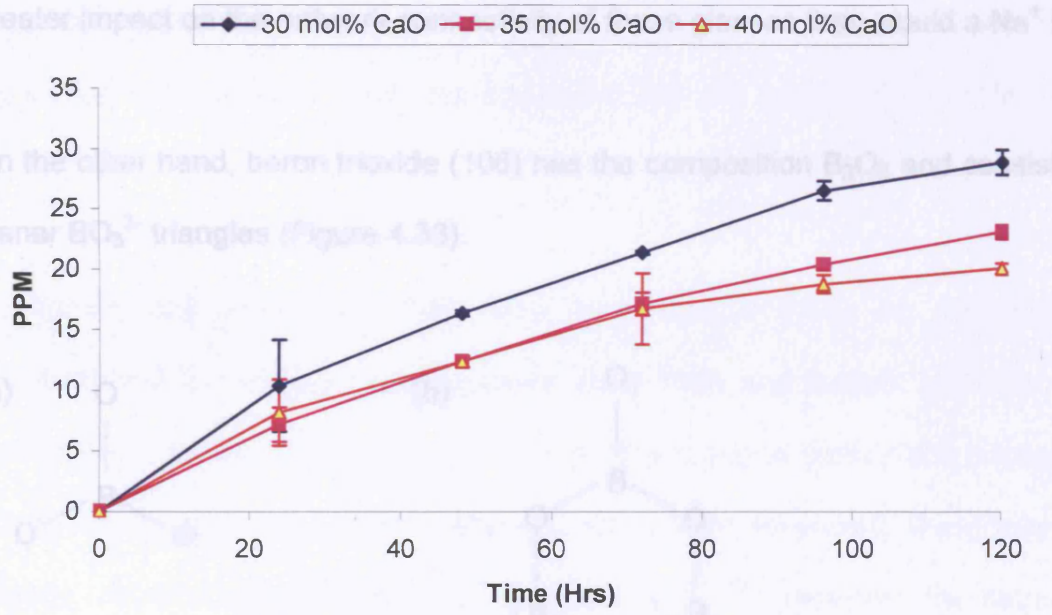

Figure 4.32: $P_3O_{10}^{5-}$ anionic release from compositions with fixed 5 mol% B_2O_3.

4.8 Discussion on the Quaternary P_2O_5 – CaO – Na_2O – B_2O_3 System:

4.8.1 Structural Analysis Using DTA:

As seen from the thermal analyses conducted an increase in T_g and T_c values was seen with an increase in CaO content. An increase for these values was also seen with increasing B_2O_3 content.

As stated in the previous section, an increase in T_g values was expected with an increase in CaO content, as CaO is a refractory material. Also, Ca^{2+} ions are known to act as chelates between two phosphate chains, thereby having a greater impact on the network connectivity of these glasses than would a Na^+ ion.

On the other hand, boron trioxide (106) has the composition B_2O_3 and consists of planar BO_3^{3-} triangles (Figure 4.33).

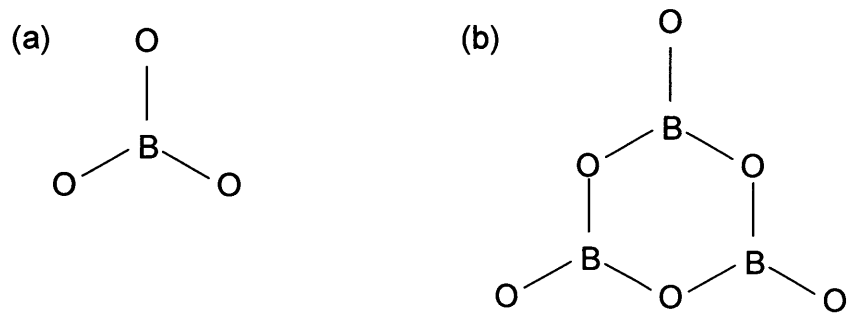

Figure 4.33: (a) Planar BO_3^{3-} triangle, (b) Planar boroxol ring.

In a boron trioxide glass, the BO_3^{3-} polyhedra share oxygen atoms resulting in a three-dimensional network, where six membered boroxol rings are also found. In another study conducted by Youngman *et al* (107) it was stated that this glass consisted of domains that were rich or poor in boroxol rings, and that these domains were proposed to be the structural basis of the intermediate–range order in glassy boron trioxide.

Koudelka and Mosner (108) investigated borophosphate glasses of the ZnO – B_2O_3 – P_2O_5 system. A large glass-forming region was found at the phosphate side of the ternary system with homogeneous glasses containing up to 20 – 40 mol% B_2O_3. Their results showed that the thermal expansion coefficient decreased with an increase in B_2O_3 content whereas the T_g values increased with increasing B_2O_3 content. This was consistent with the values obtained from this investigation.

Youngman and Zwanziger (109) also conducted a study on the network modification in potassium borate glasses using NMR and Raman spectroscopy. Ten different variations on the structural groups found in glassy and crystalline potassium borates were given. Amongst the groups presented, there was the already mentioned boroxol ring, and the non-ring BO_3^{3-}. However, the structural group of interest presented was the non-ring BO_4^{5-} (See Figure 4.34 below).

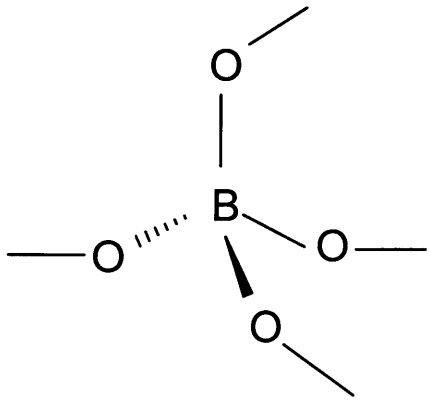

Figure 4.34: The non-ring BO_4^{5-} group.

The remainder of the groups presented were variations on the formation of the three groups shown above. They went on to state that the addition of alkali oxide modifiers M_2O (where M = Li, Na, K, Rb, Cs) to B_2O_3 resulted in significant changes in the boron coordination and hence the glass structure. The added modifier could act in one of two ways by forming non-bridging oxygens;

$$2\,(BO_3^{3-}) \xrightarrow{M_2O} 2\,(BO_3^{3-}) + 2M^{+} \qquad (1)$$

and by forming four coordinate boron (BO_4^{-});

$$2\,(BO_3^{3-}) \xrightarrow{M_2O} 2\,(BO_4^{5-}) + 2M^{+} \qquad (2)$$

They also went on to state that the existence of a four coordinate boron was clear from their NMR studies, where its nearly tetrahedral symmetry gave rise to a relatively narrow resonance, and that the rate of the four coordinate boron formation decreased as the size of the alkali cation increased.

As stated above, boron atoms in borate glasses can form structural units of BO_3^{3-} and BO_4^{5-}. Their mutual participation in the structure of borophosphate glasses has showed that in phosphate-rich glasses, tetrahedral BO_4^{5-} units were preferred (108). Therefore the incorporation of BO_4^{5-} units into the chain-like phosphate glass structure resulted in an enhancement of dimensionality of the structural network from 1D to 3D. Such a cross-linking effect on the network resulted in glasses having increased T_g.

4.8.2 XRD Analysis:

XRPD analyses revealed that there was no correlation between the DTA traces obtained and the phases identified from XRPD analysis. For example, the bulk glass samples revealed either single or double T_c and T_m peaks, whereas from XRPD a minimum of two and a maximum of three phases were identified from the compositions investigated (See Table 4.4 for phases identified).

As can be seen from the phases identified, the $NaCa(PO_3)_3$ phase was identified for all the compositions investigated, which was expected as the compositions all had a fixed P_2O_5 content of 50 mol%. As also seen from the previous section on ternary phosphate glasses, this was the main phase identified for the composition with glass code $P_{50}Ca_{30}Na_{20}$. Compositions containing higher amounts of CaO content exhibited a calcium rich phase, which was the CaP_2O_6 phase. The third phase identified for the compositions investigated was the BPO_4 phase.

For all compositions containing 30 mol% CaO content, only two phases were identified, the second of which was the BPO_4. One other point to note was that the boron (BPO_4) phase was identified from compositions containing as little as 1 mol% B_2O_3.

Brow (110) investigated the structure of zinc phosphate and zinc borophosphate glasses. He conducted a study of oxygen bonding in these glasses using XPS. He concluded that the oxygen site distributions in the ternary Zn borophosphate glasses supported the model developed from previous analyses of cation-sensitive structural probes. Namely, that tetrahedral borophosphate units were incorporated into the glass structure when B_2O_3 was added to the Zn metaphosphate glass, leading to an increasing concentration of B – O – P bonds at the expense of both the P – O – P and P – O – Zn sites.

As mentioned previously Koudelka and Mosner (108) also investigated zinc borophosphate glasses. They conducted studies of the thermal properties of the glass systems investigated using DTA analysis. The thermal behaviour of the $ZnO - B_2O_3 - P_2O_5$ system revealed that most of the glasses they studied crystallised in the temperature range between 600 – 800 °C, and that XRPD analyses showed that one of the crystallisation products was the boron phosphate BPO_4 and the second was a zinc phosphate. The appearance of BPO_4 in the crystallisation products showed the importance of PO_4 and BO_4 structural units in the network of borophosphate glasses. They went on to state that the structure of crystalline BPO_4 was composed of PO_4 and BO_4 tetrahedra, interconnected into a network similar to that of SiO_2, and it was proposed that the borophosphate glasses studied contained B – O – P linkages within their structural network.

Therefore, it could be concluded that the increase seen in the T_g and T_c values obtained via DTA analysis with increasing B_2O_3 content was due to the formation of B – O – P bonds, that replaced some of the existing P – O – P bonds within the network of the glasses investigated.

4.8.3 Degradation Rates and pH Profiles:

As stated in the beginning of this chapter a quaternary component was added in an attempt to decrease the dissolution rates for both the bulk glasses and glass-fibres obtained.

The dissolution rate profiles obtained exhibited similar patterns to the thermal analyses profiles seen. A decrease in the rates was seen with increasing CaO content, and also with an increase in B_2O_3 content. The glasses with fixed 1 mol% B_2O_3 exhibited the same pattern as seen for the glasses with fixed 50 mol% P_2O_5 seen in the previous section. There was a large decrease in the dissolution rates from glass code $P_{50}Ca_{30}Na_{19}B_1$ to glass code $P_{50}Ca_{35}Na_{14}B_1$, as seen with the glasses with fixed 50 mol% P_2O_5, where a 10^{-3} figure was obtained for the composition with fixed 30 mol% CaO content, and a 10^{-4} figure was obtained for the compositions with fixed 35 and 40 mol% CaO content.

In general a decrease in weight loss was seen with the introduction of boron, even with as little as a 1 mol% addition. This difference was even more apparent with the weight loss values obtained from the glass fibre analyses.

With regards to the bulk glass dissolution rate values, a reduction was seen when comparing the ternary 50 mol% P_2O_5 glass system to the fixed 1 mol% B_2O_3 glass system. Nevertheless, such reduction seen was not that significant. For glass code $P_{50}Ca_{30}Na_{20}$ the dissolution rate obtained was 1.89 x 10^{-3} mg.mm^{-2}.hr^{-1}, and the rate obtained for glass code $P_{50}Ca_{30}Na_{19}B_1$ was 1.52 x10^{-3} mg.mm^{-2}.hr^{-1}.

A small decrease in the dissolution rates was also expected with the glass-fibres. However, comparing the values obtained from the fixed 50 mol% P_2O_5 glass-fibres to the fibres obtained from the 1 mol% B_2O_3 compositions, the decrease seen was almost half of those values obtained from the ternary fixed 50 mol% P_2O_5 glass-fibres. Further incorporation of B_2O_3 up to 5 mol% revealed that the weight loss values obtained had halved again as compared to the 1 mol% B_2O_3 values obtained.

The pH of the solutions investigated all revealed similar patterns. After an initial 24 hour period, the pH values dropped to around 4. After this point the pH values fluctuated from pH 4 to pH 5 and towards the end of the study, the values raised slightly again to pH 5. These pH values obtained were slightly higher than those obtained from the ternary fixed 50 and 55 mol% P_2O_5 compositions.

4.8.4 Ion Release Profiles:

The cation release profiles obtained also followed the profiles seen above from the thermal and degradation analyses conducted. The sodium and calcium ion release all decreased with increasing CaO content, and increasing B_2O_3 content. The sodium ion release seen for compositions with fixed 50 mol% P_2O_5, and the compositions with fixed 1 mol% B_2O_3 were almost identical. However, higher calcium ion release was seen from the 1 mol% B_2O_3 compositions. Overall more calcium ions were released into solution than sodium ions.

With regards to the anion release, no correlation was seen for the PO_4^{3-} anion. This was expected since the PO_4^{3-} anion is usually present as a result of the breakdown of the higher phosphate chain or ring species.

The linear $P_2O_7^{4-}$ and $P_3O_{10}^{5-}$ species exhibited exactly the same pattern as was expected, due to correlations observed from these anions in the previous section. There was little difference seen in the amounts of the $P_2O_7^{4-}$ and $P_3O_{10}^{5-}$ released from compositions containing 1 – 5 mol% B_2O_3. However, within each group a decrease in release was seen with increasing CaO content. This suggested that these anionic species were cross-linked with the Ca^{2+} ion acting as a chelate between the phosphate chains.

The cyclic $P_3O_9^{3-}$ metaphosphate species was the highest released anionic species from the compositions investigated. This again was expected, firstly due

to the correlations observed from the last chapter concerning the ternary compositions; and secondly, due to the $NaCa(PO_3)_3$ phase being identified from all the boron compositions investigated.

Summary:

The decrease in the dissolution rates observed with increasing B_2O_3 content was related to the incorporation of B_2O_3 into the backbone of the phosphate network and creating BPO_4 groups. This accounted for the increase seen in T_g and T_c values obtained, along with the decreasing dissolution rates obtained for both the bulk glass and glass-fibres.

B_2O_3 was expected to go into the network as it is a well known glass network former. However, the decrease in dissolution rates was expected to be more prominent than what was obtained. The pH values obtained were only slightly higher than those obtained from the ternary fixed 50 and 55 mol% P_2O_5 compositions from the previous chapter. The relatively slight decrease in degradation accounted for the pH values obtained still being significantly below neutral.

Again, biocompatibility studies conducted with collaborators revealed that these compositions were still too soluble for successful cell attachment and proliferation. Therefore, a further quaternary component was investigated.

CHAPTER 5

The Quaternary P_2O_5 – CaO – Na_2O – Fe_2O_3 Glass System

5.0 The Quaternary P_2O_5 – CaO – Na_2O – Fe_2O_3 Glass System:

5.1 General Introduction:

In the previous section, the quaternary component B_2O_3 was added in an attempt to reduce the dissolution rates obtained from the original ternary compositions. It was seen that via the addition of B_2O_3 the dissolution rates decreased, however, the decrease seen was very small. In other words, the compositions investigated in chapter 4 were still not satisfactory materials to be used as cell delivery vehicles, due to their high dissolution rates and low pH values. To achieve satisfactory cell attachment the biomaterial must initially exhibit a certain amount of durability.

In this section iron oxide (Fe_2O_3) was added in order to try and further reduce the dissolution rates. Fe_2O_3 was chosen due to the component iron being naturally found in the body. Thus it was added to the original ternary composition in order that it should not elicit an inflammatory response upon dissolution of the material within the host tissue. Fe_2O_3 is known to significantly improve the durability of phosphate-based glasses (111), and was added from 1 – 5 mol%, again in place of Na_2O. See Table 5.1 for glass codes and compositions investigated.

Table 5.1: Glass codes and compositions investigated in the P_2O_5 – CaO – Na_2O – Fe_2O_3 system.

Glass Codes	P_2O_5 (mol%)	CaO (mol%)	Na_2O (mol%)	Fe_2O_3 (mol%)
$P_{50}Ca_{30}Na_{19}Fe_1$	50	30	19	1
$P_{50}Ca_{35}Na_{14}Fe_1$	50	35	14	1
$P_{50}Ca_{40}Na_9Fe_1$	50	40	9	1
$P_{50}Ca_{30}Na_{18}Fe_2$	50	30	18	2
$P_{50}Ca_{35}Na_{13}Fe_2$	50	35	13	2
$P_{50}Ca_{40}Na_8Fe_2$	50	40	8	2
$P_{50}Ca_{30}Na_{17}Fe_3$	50	30	17	3
$P_{50}Ca_{35}Na_{12}Fe_3$	50	35	12	3
$P_{50}Ca_{40}Na_7Fe_3$	50	40	7	3
$P_{50}Ca_{30}Na_{16}Fe_4$	50	30	16	4
$P_{50}Ca_{35}Na_{11}Fe_4$	50	35	11	4
$P_{50}Ca_{40}Na_6Fe_4$	50	40	6	4
$P_{50}Ca_{30}Na_{15}Fe_5$	50	30	15	5
$P_{50}Ca_{35}Na_{10}Fe_5$	50	35	10	5
$P_{50}Ca_{40}Na_5Fe_5$	50	40	5	5

For the melting and annealing temperatures used, see Chapter 2, section 2.1, Table 2.3.

5.2 Thermal Analysis:

As seen all DTA traces obtained exhibited clear T_g, T_c and T_m peaks. The traces shown below have their respective glass fibre (GF) traces overlaid on top of the bulk glass traces obtained. An example of the traces obtained can be seen in Figure 5.1.

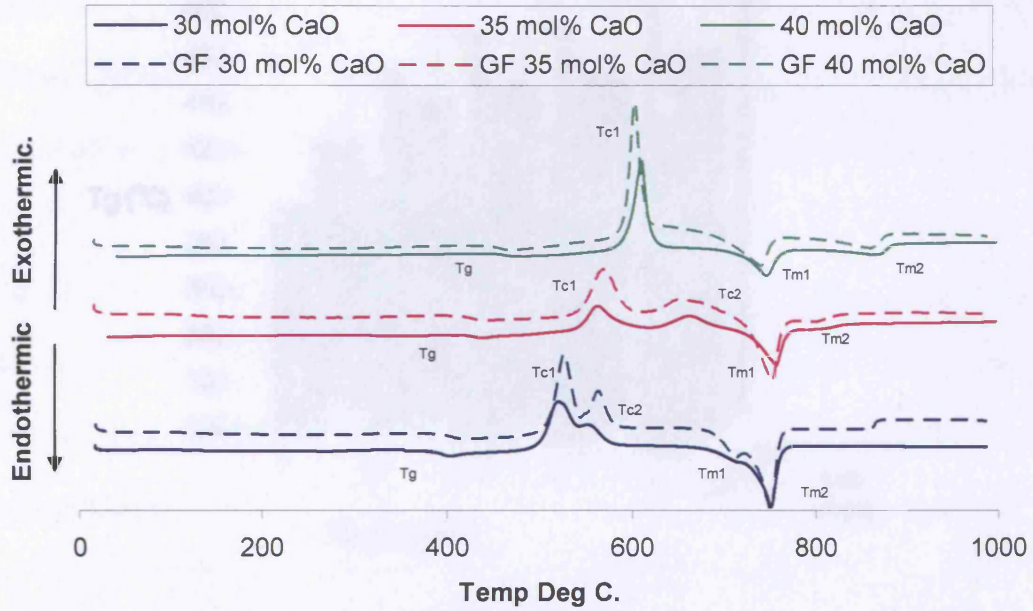

Figure 5.1: DTA traces from bulk glass and glass-fibres for compositions with 1 mol% Fe_2O_3.

All the compositions investigated showed an increase in T_g with an increase in CaO content, along with an increase in Fe_2O_3 mol% content as expected. Similar patterns were also seen from the T_g values obtained for the glass-fibres. Figure 5.2 shows a 3D representation of the T_g values obtained from the bulk glasses investigated.

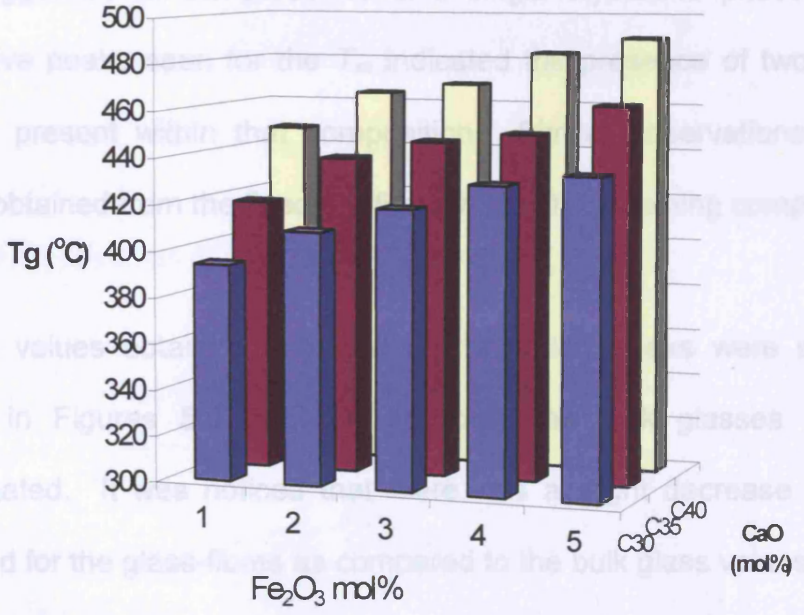

Figure 5.2: 3D representation of bulk glass T_g values.

As seen in Figure 5.1, clear T_c and T_m peaks were also observed for the compositions investigated. Some of the traces obtained exhibited single sharp peaks for the T_c whilst others exhibited either two T_c peaks or a single broad peak. As stated in chapter 3, the presence of a single T_c peak was an indication of a single crystallisation event occurring within that composition, whereas the presence of two T_c peaks was indicative of two crystallisation events occurring,

and so on. Figure 5.1 shows the DTA traces obtained for compositions containing fixed 1 mol% Fe_2O_3. As can be seen for the trace with glass code $P_{50}Ca_{30}Na_{19}Fe_1$ two T_c and two T_m peaks were seen. The peak for T_{c1} is clearer upon magnification. For glass code $P_{50}Ca_{35}Na_{14}Fe_1$ a broad T_c peak was observed along with two T_m peaks. The third trace for glass code $P_{50}Ca_{40}Na_9Fe_1$ showed a distinct single T_c peak and two separate T_m peaks. The single T_c peak was suggestive of the presence of a single crystalline phase. However, the distinctive peaks seen for the T_m indicated the presence of two clearly different phases present within that composition. Similar observations were made for traces obtained from the fixed 2 – 5 mol% Fe_2O_3 containing compositions.

The T_c values obtained from the crystallisation peaks were collated and are shown in Figures 5.3 and 5.4, for both the bulk glasses and glass-fibres investigated. It was noticed that there was a slight decrease in the T_c values obtained for the glass-fibres as compared to the bulk glass values obtained.

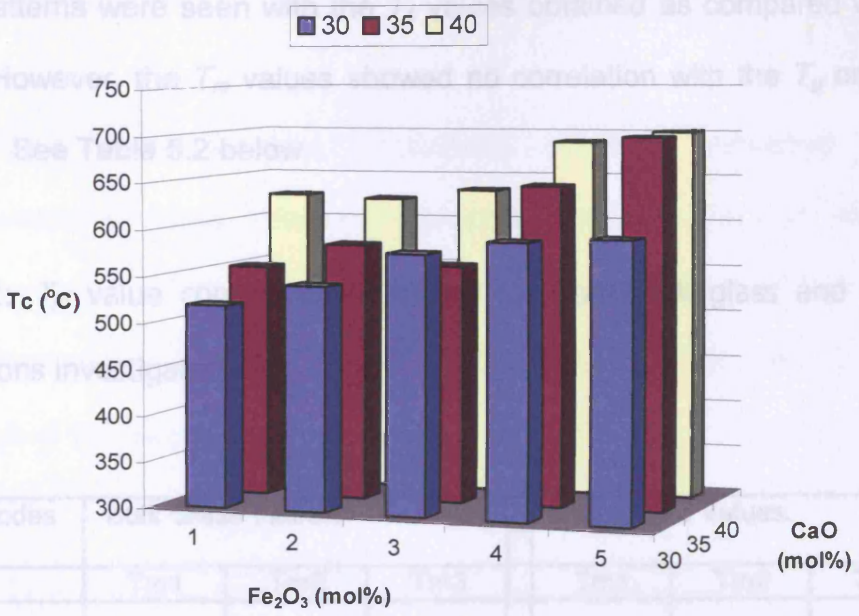

Figure 5.3: T_c values for the iron bulk glass compositions.

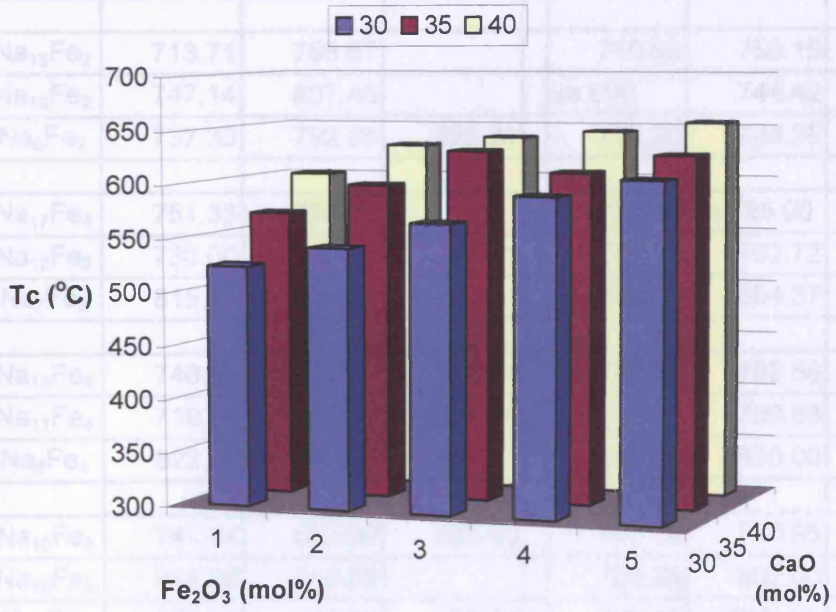

Figure 5.4: T_c values for the iron glass-fibre compositions.

Similar patterns were seen with the T_c values obtained as compared with the T_g values. However, the T_m values showed no correlation with the T_g or T_c values obtained. See Table 5.2 below.

Table 5.2: T_m value comparison obtained for both bulk glass and glass-fibre compositions investigated.

Glass Codes	Bulk Glass Values.			Glass-Fibre Values.		
	Tm1	Tm2	Tm3	Tm1	Tm2	Tm3
$P_{50}Ca_{30}Na_{19}Fe_1$	712.64	750.51		710.68	750.24	
$P_{50}Ca_{35}Na_{14}Fe_1$	749.46	799.56		750.43	796.10	
$P_{50}Ca_{40}Na_9Fe_1$	736.14	856.35	905.00	737.38	857.30	
$P_{50}Ca_{30}Na_{18}Fe_2$	713.71	756.57		710.82	753.15	
$P_{50}Ca_{35}Na_{13}Fe_2$	747.14	807.46		vs 690	744.42	820.83
$P_{50}Ca_{40}Na_8Fe_2$	737.30	792.35	856.81	729.30	794.36	871.23
$P_{50}Ca_{30}Na_{17}Fe_3$	751.33	789.61		753.23	vs 795.00	
$P_{50}Ca_{35}Na_{12}Fe_3$	730.00	797.61	838.61	736.70	792.72	831.83
$P_{50}Ca_{40}Na_7Fe_3$	815.11	864.29		730.00	804.37	855.36
$P_{50}Ca_{30}Na_{16}Fe_4$	746.28	799.53	830.00	742.61	792.56	820.00
$P_{50}Ca_{35}Na_{11}Fe_4$	719.33	807.20	vs 830.00	731.65	789.68	820.00
$P_{50}Ca_{40}Na_6Fe_4$	822.78	855.00	887.71	815.33	850.00	879.34
$P_{50}Ca_{30}Na_{15}Fe_5$	741.04	801.00	835.00	741.19	790.95	815.00
$P_{50}Ca_{35}Na_{10}Fe_5$	816.08	838.89		724.28	802.00	835.00
$P_{50}Ca_{40}Na_5Fe_5$	824.27	855.00	887.47	820.12	vs 852.00	885.59

vs = very small peak.

5.3 XRD Analysis:

The samples obtained were crystallised at their respective crystalline temperatures which were obtained via thermal analysis. The crystalline phases identified were matched using the Crystallographica Search-Match software (Oxford Cryosystems, UK) and ICDD Database, (Vols 1 – 45). See Figure 5.5 for an example of the traces obtained.

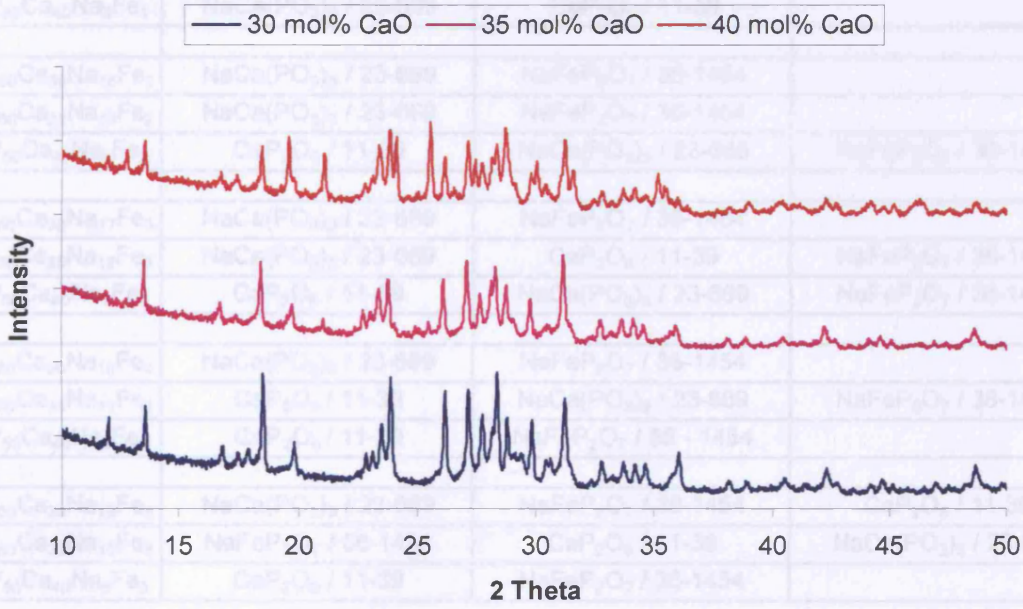

Figure 5.5: XRPD traces for compositions with fixed 1 mol% Fe_2O_3 content.

The phases identified from the compositions investigated have been tabulated (see Table 5.3).

Table 5.3: Phases identified from the quaternary P_2O_5 – CaO – Na_2O – Fe_2O_3 glass system

Glass Codes	Phase 1 / ICDD card no.	Phase 2 / ICDD card no.	Phase 3 / ICDD card no.
$P_{50}Ca_{30}Na_{19}Fe_1$	$NaCa(PO_3)_3$ / 23-669	$NaPO_3$ / 11-648	
$P_{50}Ca_{35}Na_{14}Fe_1$	$NaCa(PO_3)_3$ / 23-669	CaP_2O_6 / 11-39	
$P_{50}Ca_{40}Na_9Fe_1$	$NaCa(PO_3)_3$ / 23-669	CaP_2O_6 / 11-39	
$P_{50}Ca_{30}Na_{18}Fe_2$	$NaCa(PO_3)_3$ / 23-669	$NaFeP_2O_7$ / 36-1454	
$P_{50}Ca_{35}Na_{13}Fe_2$	$NaCa(PO_3)_3$ / 23-669	$NaFeP_2O_7$ / 36-1454	
$P_{50}Ca_{40}Na_8Fe_2$	CaP_2O_6 / 11-39	$NaCa(PO_3)_3$ / 23-669	$NaFeP_2O_7$ / 36-1454
$P_{50}Ca_{30}Na_{17}Fe_3$	$NaCa(PO_3)_3$ / 23-669	$NaFeP_2O_7$ / 36-1454	
$P_{50}Ca_{35}Na_{12}Fe_3$	$NaCa(PO_3)_3$ / 23-669	CaP_2O_6 / 11-39	$NaFeP_2O_7$ / 36-1454
$P_{50}Ca_{40}Na_7Fe_3$	CaP_2O_6 / 11-39	$NaCa(PO_3)_3$ / 23-669	$NaFeP_2O_7$ / 36-1454
$P_{50}Ca_{30}Na_{16}Fe_4$	$NaCa(PO_3)_3$ / 23-669	$NaFeP_2O_7$ / 36-1454	
$P_{50}Ca_{35}Na_{11}Fe_4$	CaP_2O_6 / 11-39	$NaCa(PO_3)_3$ / 23-669	$NaFeP_2O_7$ / 36-1454
$P_{50}Ca_{40}Na_6Fe_4$	CaP_2O_6 / 11-39	$NaFeP_2O_7$ / 36 - 1454	
$P_{50}Ca_{30}Na_{15}Fe_5$	$NaCa(PO_3)_3$ / 23-669	$NaFeP_2O_7$ / 36-1454	CaP_2O_6 / 11-39
$P_{50}Ca_{35}Na_{10}Fe_5$	$NaFeP_2O_7$ / 36-1454	CaP_2O_6 / 11-39	$NaCa(PO_3)_3$ / 23-669
$P_{50}Ca_{40}Na_5Fe_5$	CaP_2O_6 / 11-39	$NaFeP_2O_7$ / 36-1454	

Note that an iron containing phase was not identified from compositions containing fixed 1 mol% Fe_2O_3 content.

5.4 Degradation Analysis:

5.4.1 Bulk Glass Degradation Studies:

The dissolution studies were again conducted using the cumulative method. The plots obtained all exhibited relatively linear dissolution profiles for the duration of the study. A decrease in the dissolution rates was seen with an increase in CaO mol% in addition to an increase in Fe_2O_3 content from 1 – 5 mol%. Figures 5.6 – 5.10 represent the bulk glass dissolution profiles observed.

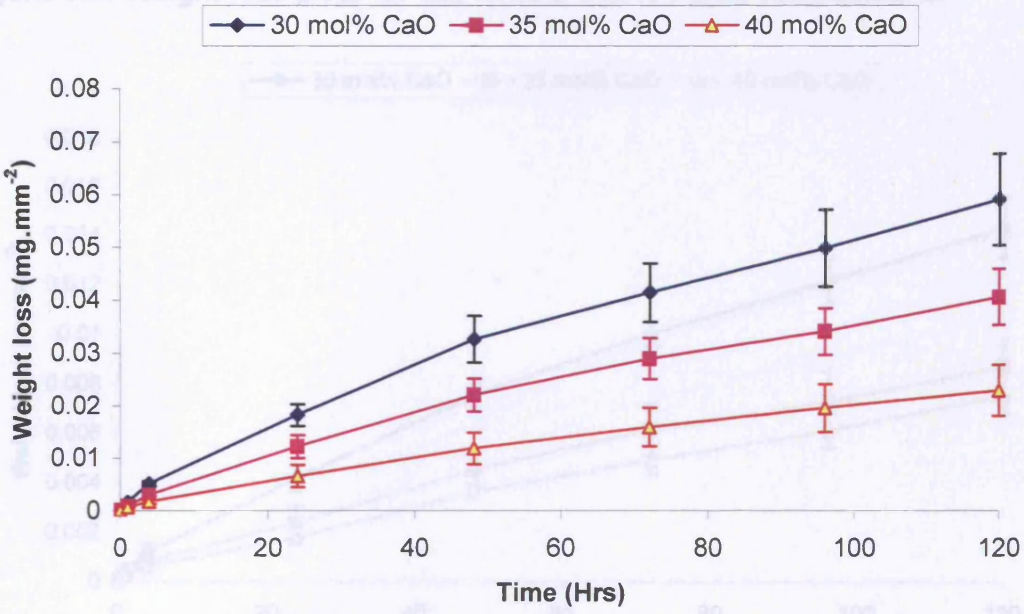

Figure 5.6: Weight loss plots for the fixed 1 mol% Fe_2O_3 compositions.

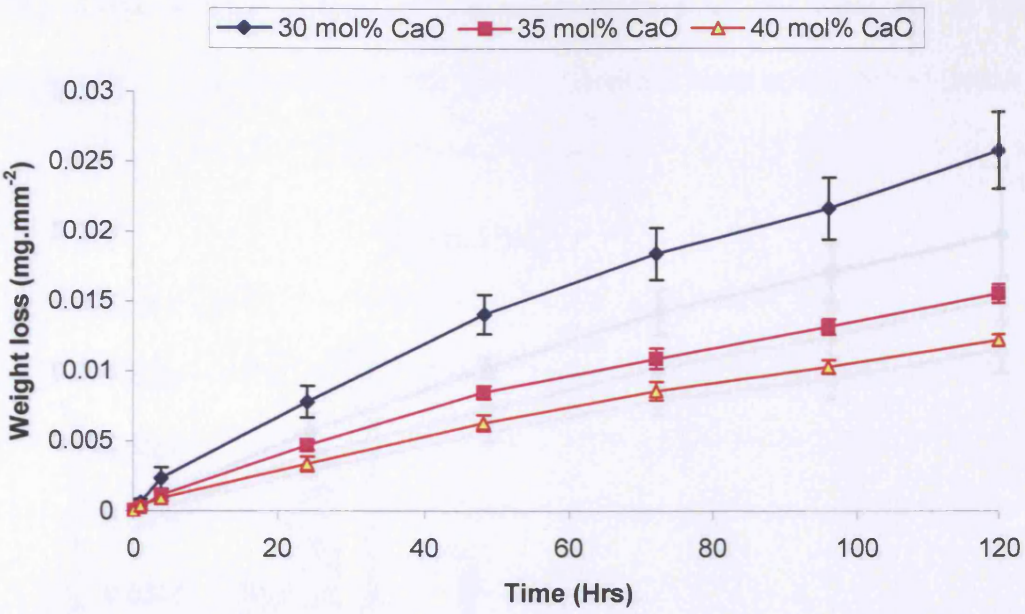

Figure 5.7: Weight loss plots for the fixed 2 mol% Fe_2O_3 compositions.

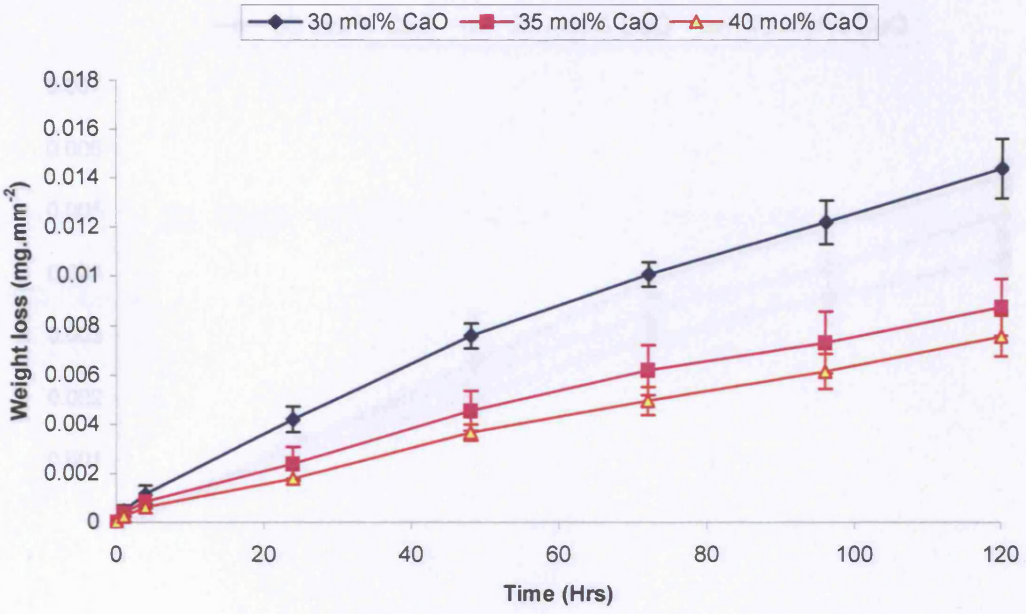

Figure 5.8: Weight loss plots for the fixed 3 mol% Fe_2O_3 compositions.

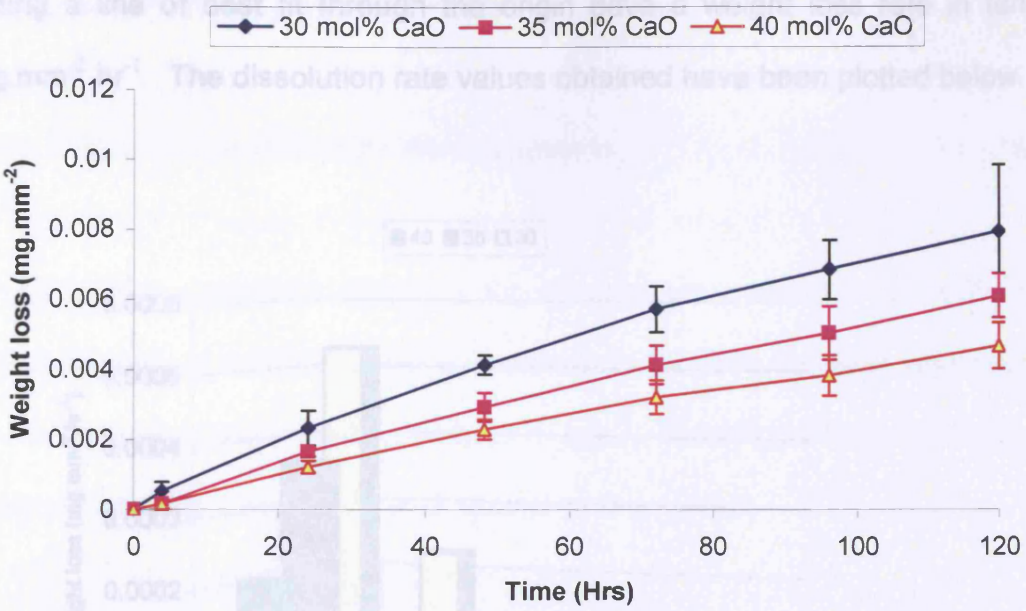

Figure 5.9: Weight loss plots for the fixed 4 mol% Fe_2O_3 compositions.

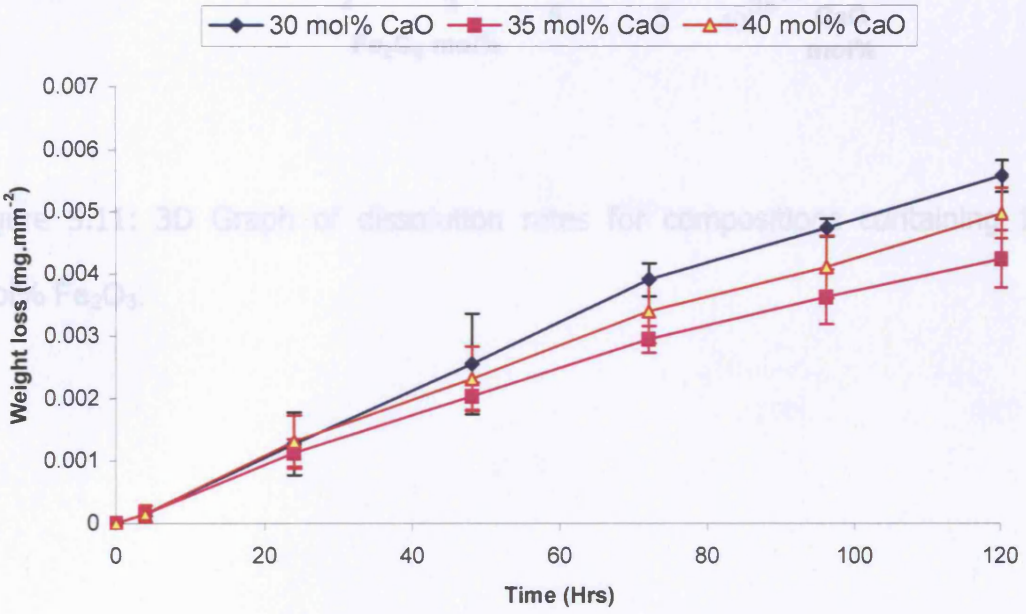

Figure 5.10: Weight loss plots for the fixed 5 mol% Fe_2O_3 compositions.

Fitting a line of best fit through the origin gave a weight loss rate in terms of $mg.mm^{-2}.hr^{-1}$. The dissolution rate values obtained have been plotted below.

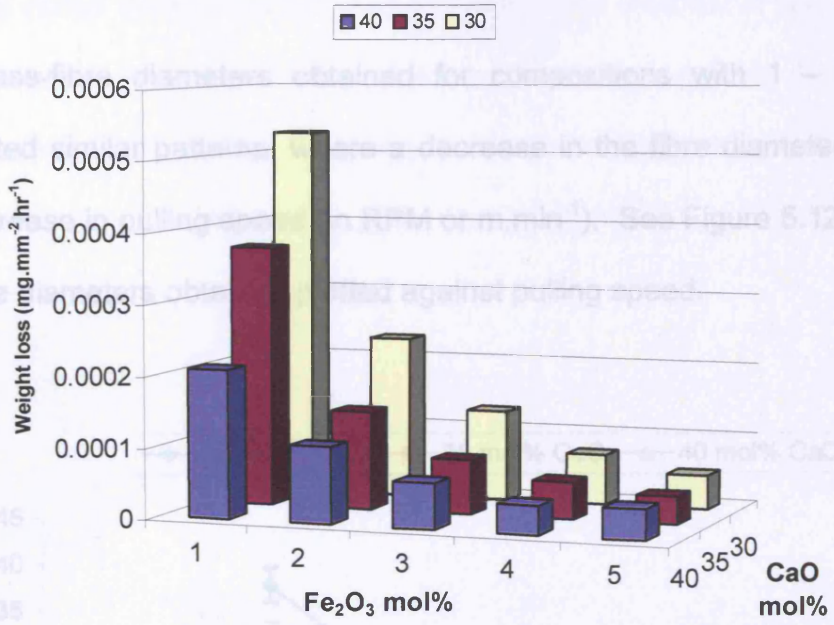

Figure 5.11: 3D Graph of dissolution rates for compositions containing 1 – 5 mol% Fe_2O_3.

5.4.2 Glass-Fibre Degradation Analysis:

5.4.2.1 Glass-Fibre Diameter Measurements:

All glass-fibre diameters obtained for compositions with 1 – 5 mol% Fe_2O_3 exhibited similar patterns, where a decrease in the fibre diameter was seen with an increase in pulling speed (in RPM or $m.min^{-1}$). See Figure 5.12 for an example of fibre diameters obtained plotted against pulling speed.

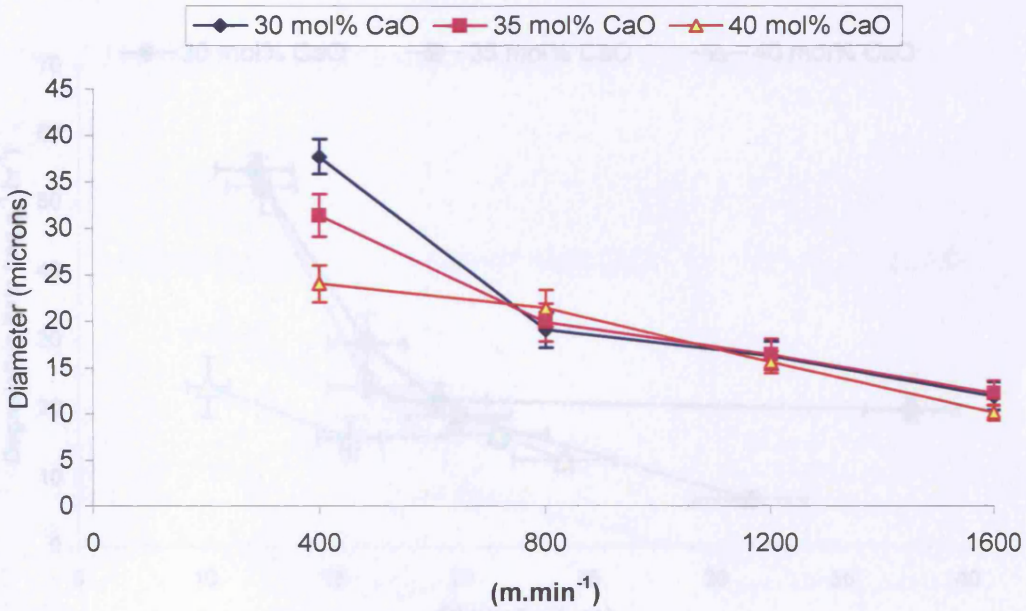

Figure 5.12: Glass-fibre diameters from compositions containing 1 mol% Fe_2O_3.

5.4.2.2 Glass-Fibre Degradation Analysis:

The glass-fibre dissolution analysis was conducted as in section 3. This method proved useful in ranking the fibres in order of the dissolution rates obtained. The graphs were plotted as weight loss per unit time against fibre diameter. A decrease in the fibre dissolution rates was seen with an increase in CaO content, along with an increase in Fe_2O_3 content (See Figures 5.13 – 5.17 for the plots obtained). .

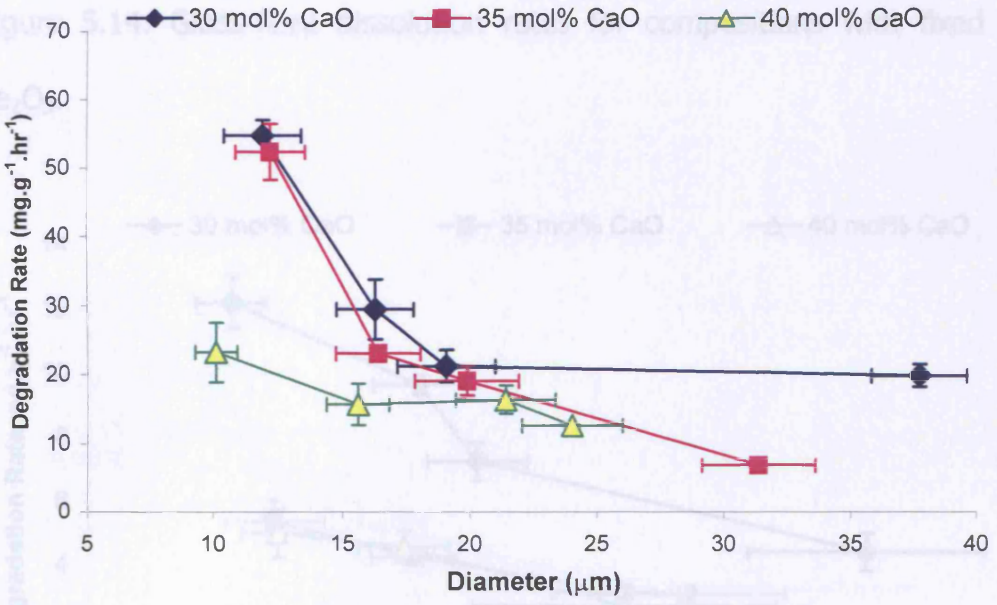

Figure 5.13: Glass-fibre dissolution rates for compositions with fixed 1 mol% Fe_2O_3.

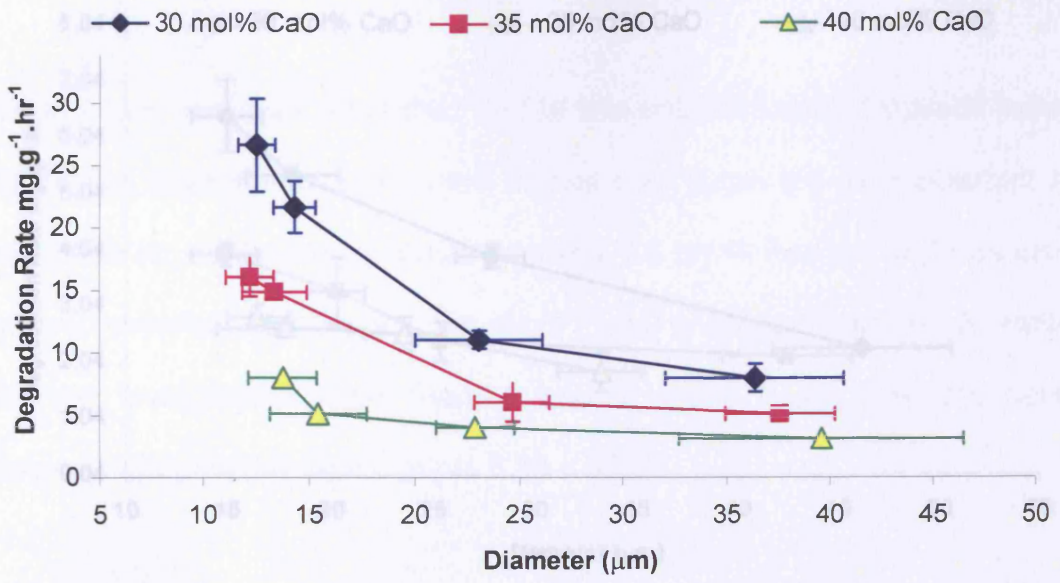

Figure 5.14: Glass-fibre dissolution rates for compositions with fixed 2 mol% Fe_2O_3.

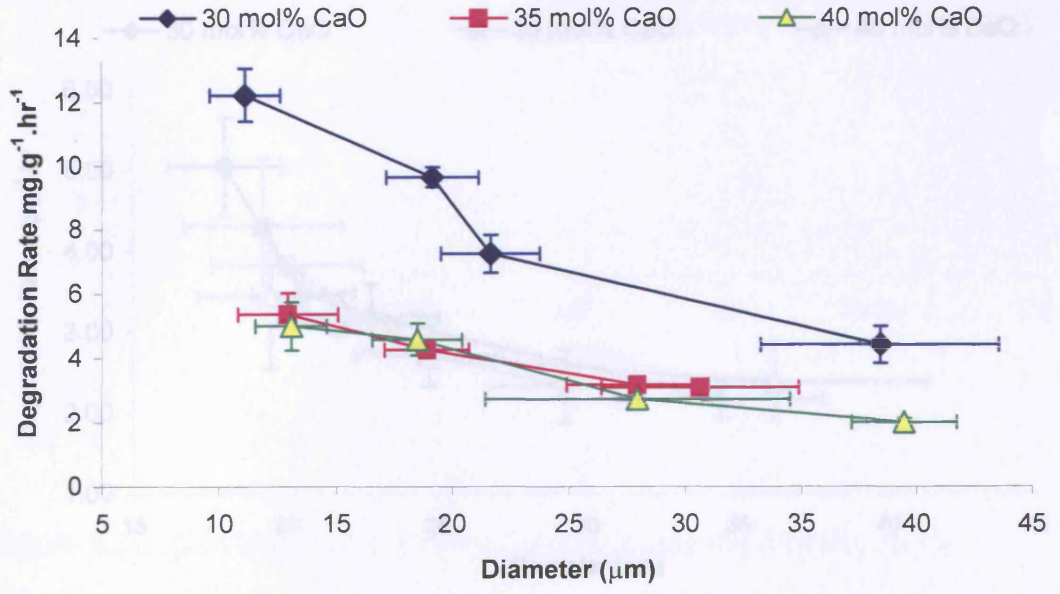

Figure 5.15: Glass-fibre dissolution rates for compositions with fixed 3 mol% Fe_2O_3.

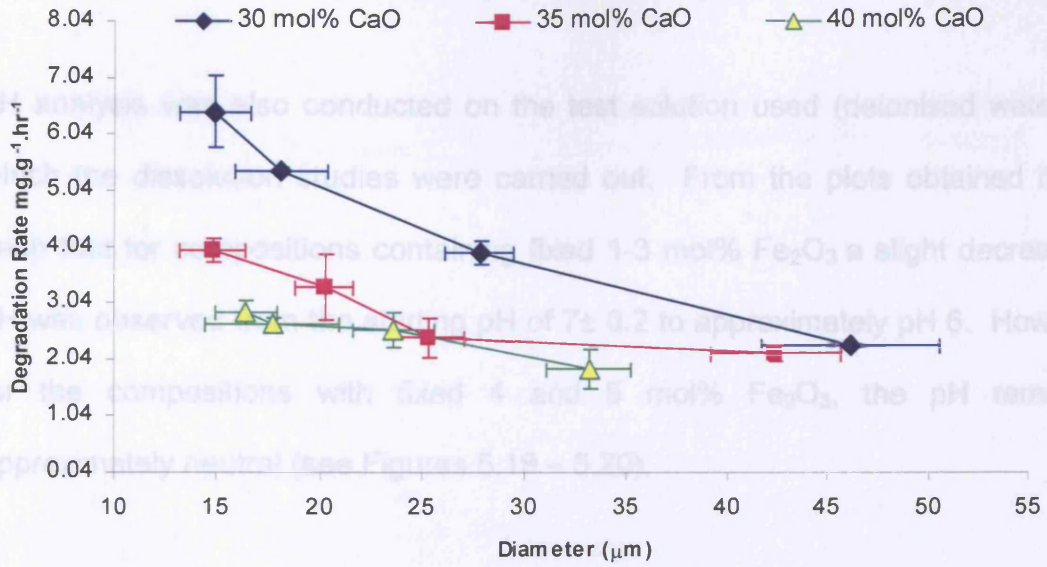

Figure 5.16: Glass-fibre dissolution rates for compositions with fixed 4 mol% Fe_2O_3.

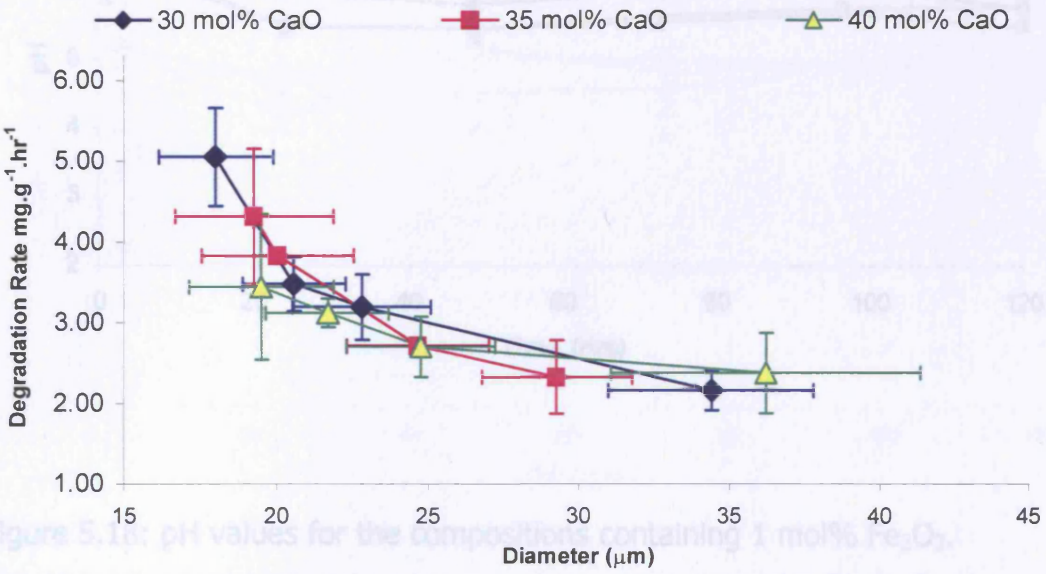

Figure 5.17: Glass-fibre dissolution rates for compositions with fixed 5 mol% Fe_2O_3.

5.5 pH Analysis:

pH analysis was also conducted on the test solution used (deionised water) on which the dissolution studies were carried out. From the plots obtained it was seen that for compositions containing fixed 1-3 mol% Fe_2O_3 a slight decrease in pH was observed from the starting pH of 7± 0.2 to approximately pH 6. However, for the compositions with fixed 4 and 5 mol% Fe_2O_3, the pH remained approximately neutral (see Figures 5.18 – 5.20).

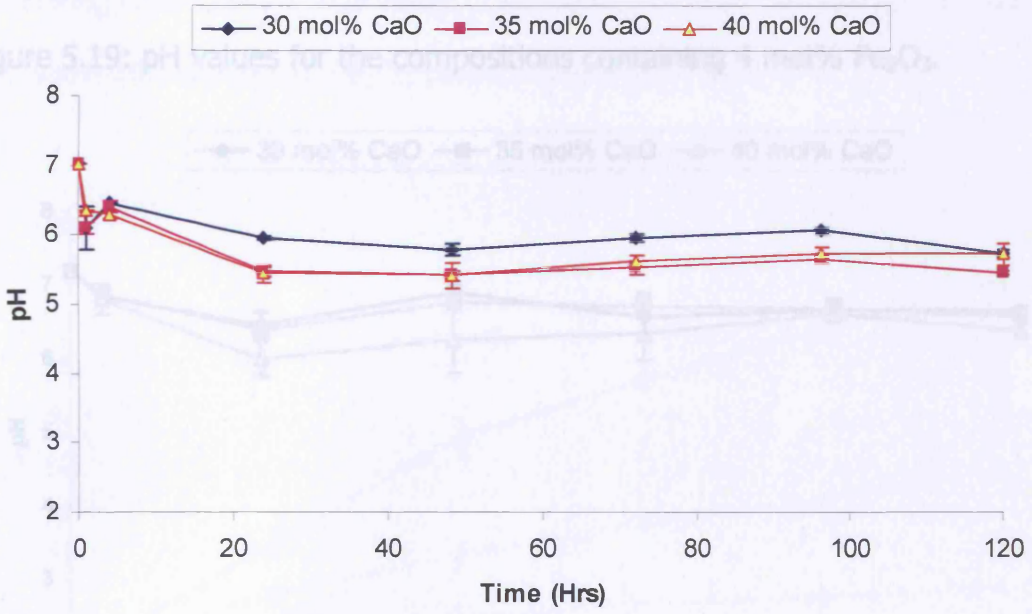

Figure 5.18: pH values for the compositions containing 1 mol% Fe_2O_3.

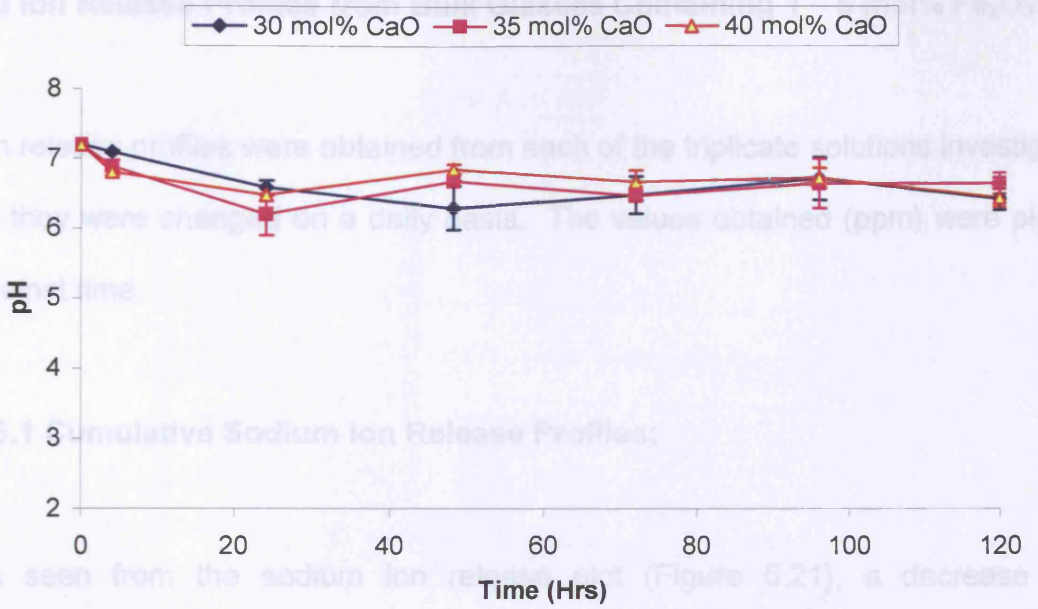

Figure 5.19: pH values for the compositions containing 4 mol% Fe_2O_3.

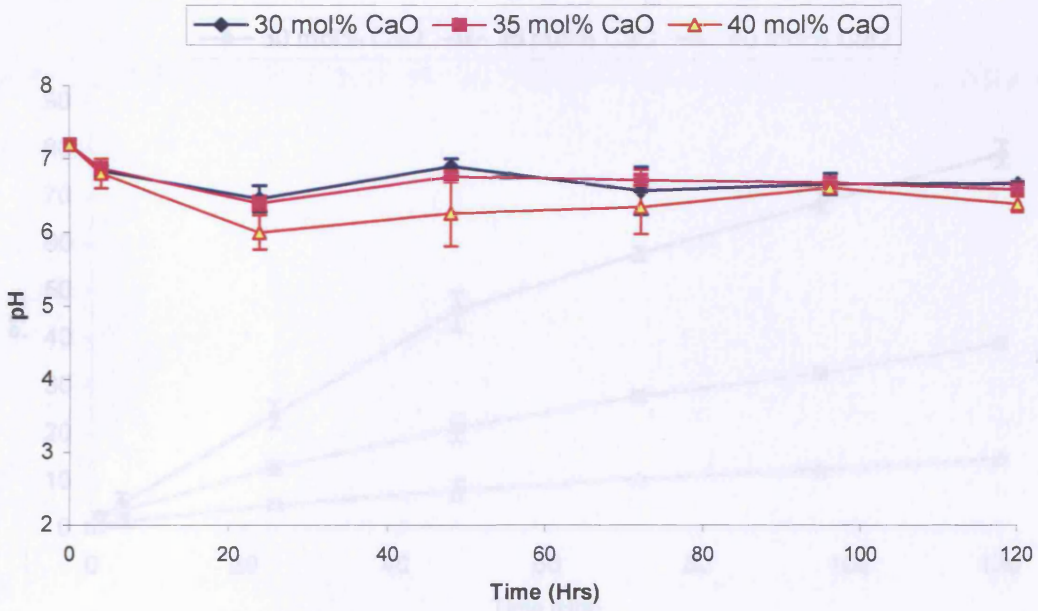

Figure 5.20: pH values for the compositions containing 5 mol% Fe_2O_3.

5.6 Ion Release Profiles from Bulk Glasses Containing 1 – 5 mol% Fe_2O_3:

Ion release profiles were obtained from each of the triplicate solutions investigated as they were changed on a daily basis. The values obtained (ppm) were plotted against time.

5.6.1 Cumulative Sodium Ion Release Profiles:

As seen from the sodium ion release plot (Figure 5.21), a decrease with increasing CaO content was seen. Decreasing sodium ion release profiles were also seen with increasing Fe_2O_3 content (see Figure 5.22).

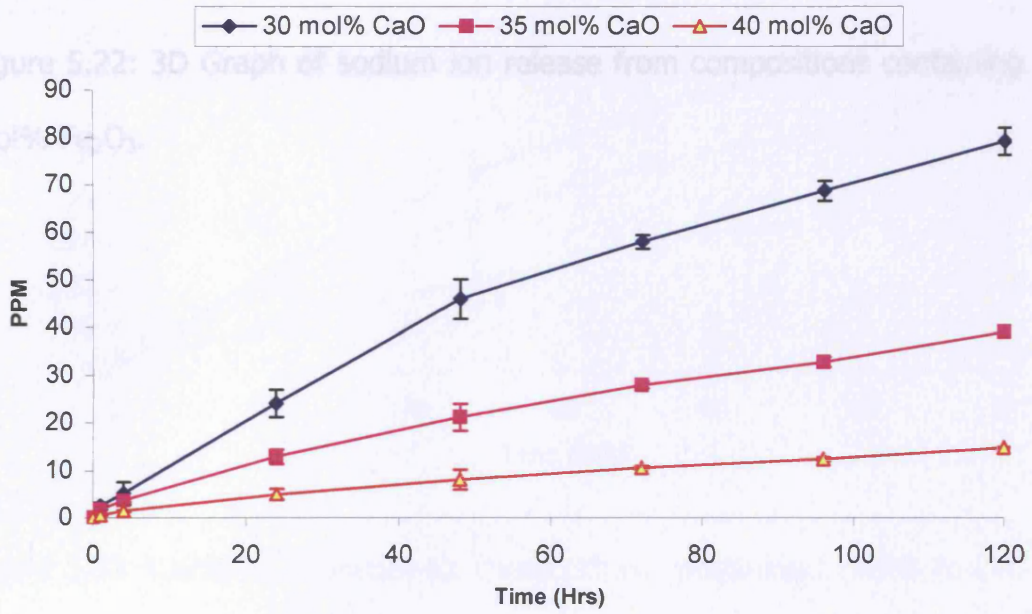

Figure 5.21: Sodium ion release for compositions containing 1 mol% Fe_2O_3.

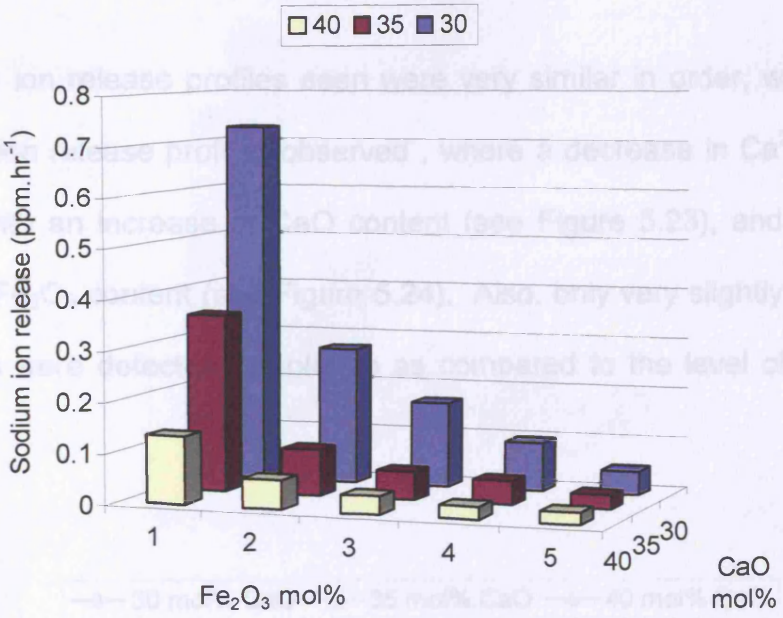

Figure 5.22: 3D Graph of sodium ion release from compositions containing 1 – 5 mol% Fe_2O_3.

5.6.2 Calcium Ion Release Profiles:

The calcium ion release profiles seen were very similar in order, with respect to the sodium ion release profiles observed , where a decrease in Ca^{2+} ion release was seen with an increase in CaO content (see Figure 5.23), and also with an increase in Fe_2O_3 content (see Figure 5.24). Also, only very slightly higher levels of Ca^{2+} ions were detected in solution as compared to the level of sodium ions detected.

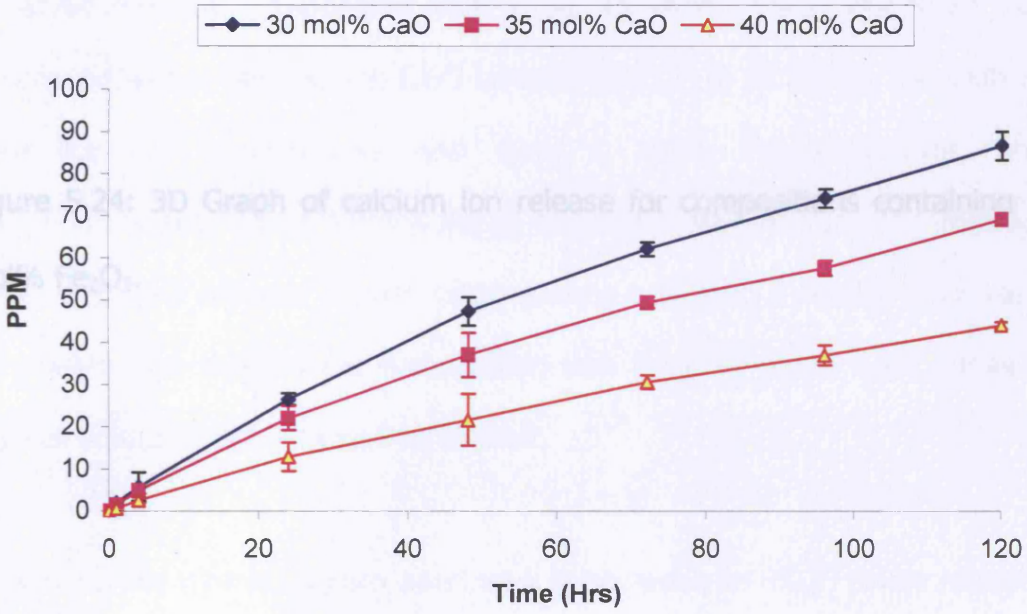

Figure 5.23: Calcium ion release for compositions containing 1 mol% Fe_2O_3.

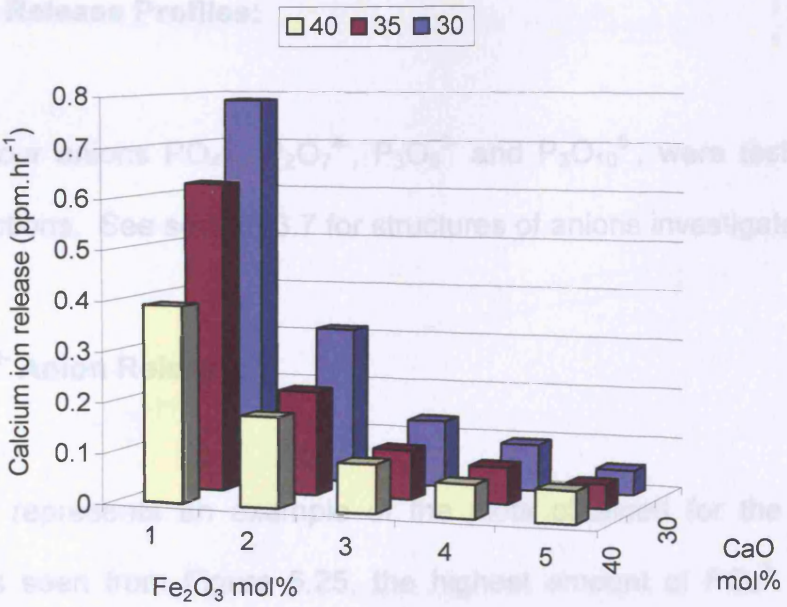

Figure 5.24: 3D Graph of calcium ion release for compositions containing 1 – 5 mol% Fe_2O_3.

5.6.3 Anion Release Profiles:

The same four anions PO_4^{3-}, $P_2O_7^{4-}$, $P_3O_9^{3-}$ and $P_3O_{10}^{5-}$, were tested as in the previous sections. See section 3.7 for structures of anions investigated.

5.6.3.1 PO_4^{3-} Anion Release:

Figure 5.25 represents an example of the plots obtained for the PO_4^{3-} anion release. As seen from Figure 5.25, the highest amount of PO_4^{3-} release was observed for the composition with fixed 40 mol% CaO, the PO_4^{3-} release decreased with a decrease in CaO content from 35 to 30 mol%. No pattern was seen for the compositions with fixed 2 mol% Fe_2O_3 content, whereas compositions with 3 and 4 mol% Fe_2O_3 showed a decrease in PO_4^{3-} release with increasing CaO content. Again, compositions with fixed 5 mol% Fe_2O_3 exhibited no pattern and showed the composition with fixed 40 mol% CaO released the highest amount of PO_4^{3-} ions into solution.

In general the overall pattern seen was a decrease in PO_4^{3-} anion release with increasing Fe_2O_3 content.

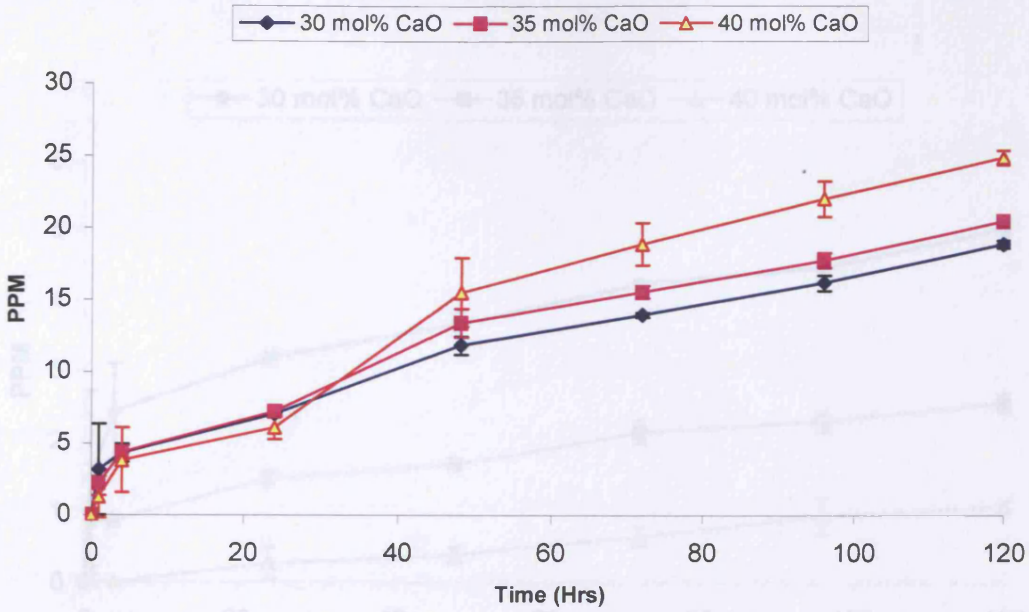

Figure 5.25: PO_4^{3-} anionic release for glasses containing 1 mol% Fe_2O_3.

5.6.3.2 $P_2O_7^{4-}$ Anion Release:

The plots obtained for the $P_2O_7^{4-}$ anion release showed that very little of this anionic species (of the order of 4ppm over 120 hours) was released into solution. Compositions containing 1 – 3 mol% Fe_2O_3 all showed a decrease in $P_2O_7^{4-}$ release with increasing CaO content, along with increasing Fe_2O_3 content. Compositions containing 4 and 5 mol% Fe_2O_3 showed no correlation; however, a further decrease with increasing Fe_2O_3 content was seen. See Figure 5.26 for an example of the plots obtained.

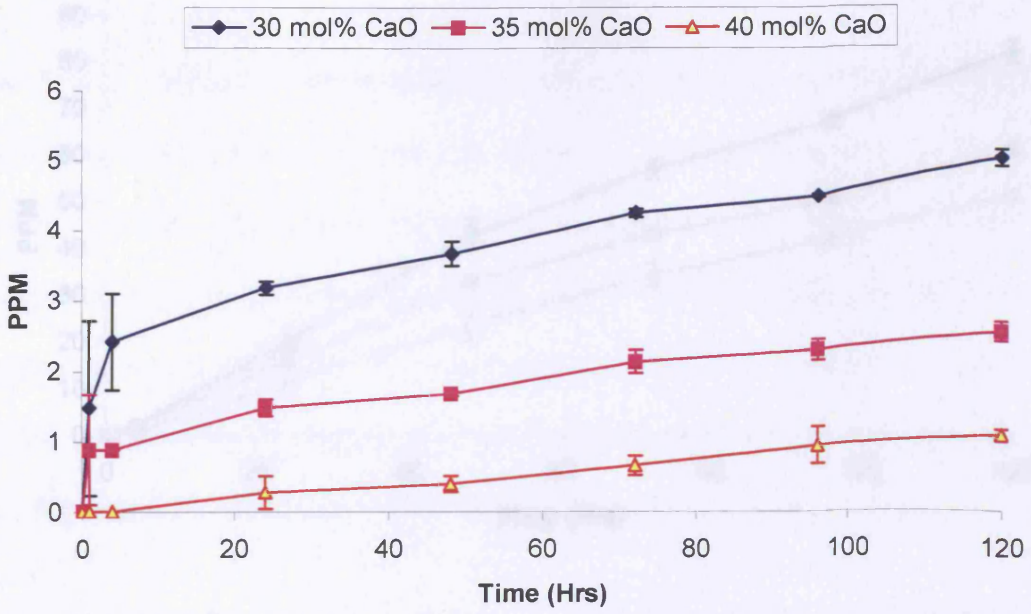

Figure 5.26: $P_2O_7^{4-}$ anionic release for compositions containing 1 mol% Fe_2O_3.

5.6.3.3 $P_3O_9^{3-}$ Anion Release:

The $P_3O_9^{3-}$ anionic release was the highest releasing anion out of the four anions investigated. The compositions containing 1 – 4 mol% Fe_2O_3 content all exhibited similar patterns, where a decrease with increasing CaO content along with increasing Fe_2O_3 content was seen. For the compositions with fixed 5 mol% Fe_2O_3 no discernible pattern was seen, however, a decrease in $P_3O_9^{3-}$ release was observed. Also, the majority of the plots obtained for this anionic species revealed a relatively linear mode of release with time (See Figures 5.27 and 5.28).

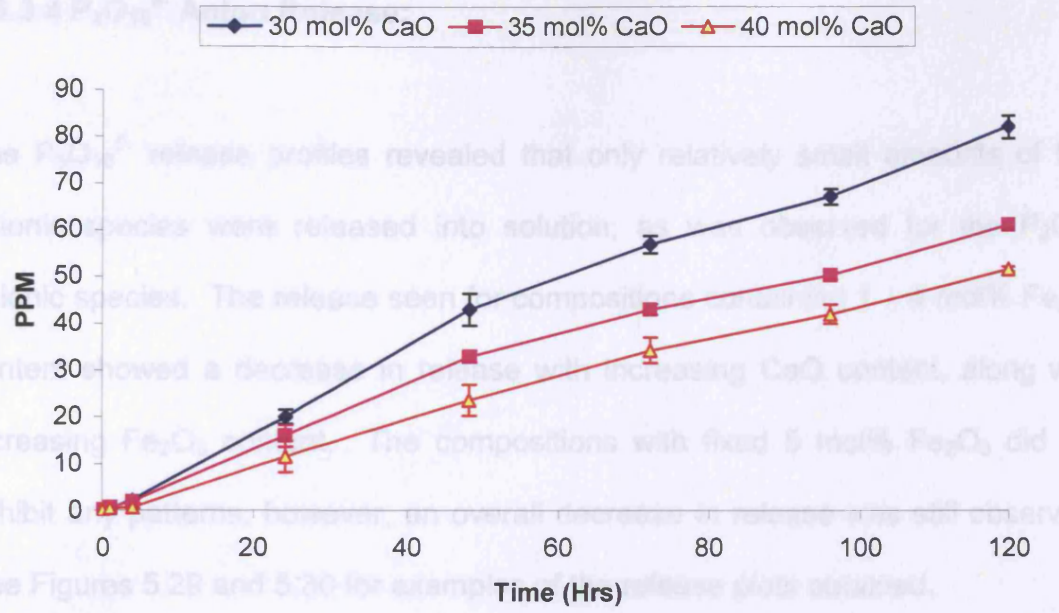

Figure 5.27: $P_3O_9^{3-}$ anionic release for compositions containing 1 mol% Fe_2O_3.

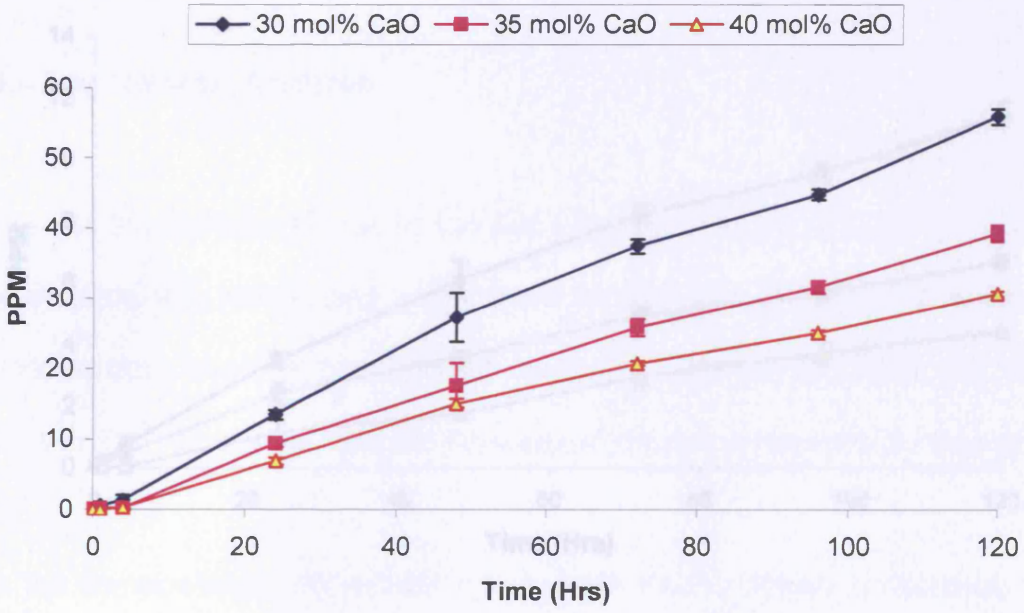

Figure 5.28: $P_3O_9^{3-}$ anionic release for compositions containing 2 mol% Fe_2O_3.

5.6.3.4 $P_3O_{10}^{5-}$ Anion Release:

The $P_3O_{10}^{5-}$ release profiles revealed that only relatively small amounts of this anionic species were released into solution, as was observed for the $P_2O_7^{4-}$ anionic species. The release seen for compositions containing 1 – 4 mol% Fe_2O_3 content showed a decrease in release with increasing CaO content, along with increasing Fe_2O_3 content. The compositions with fixed 5 mol% Fe_2O_3 did not exhibit any patterns, however, an overall decrease in release was still observed. See Figures 5.29 and 5.30 for examples of the release plots obtained.

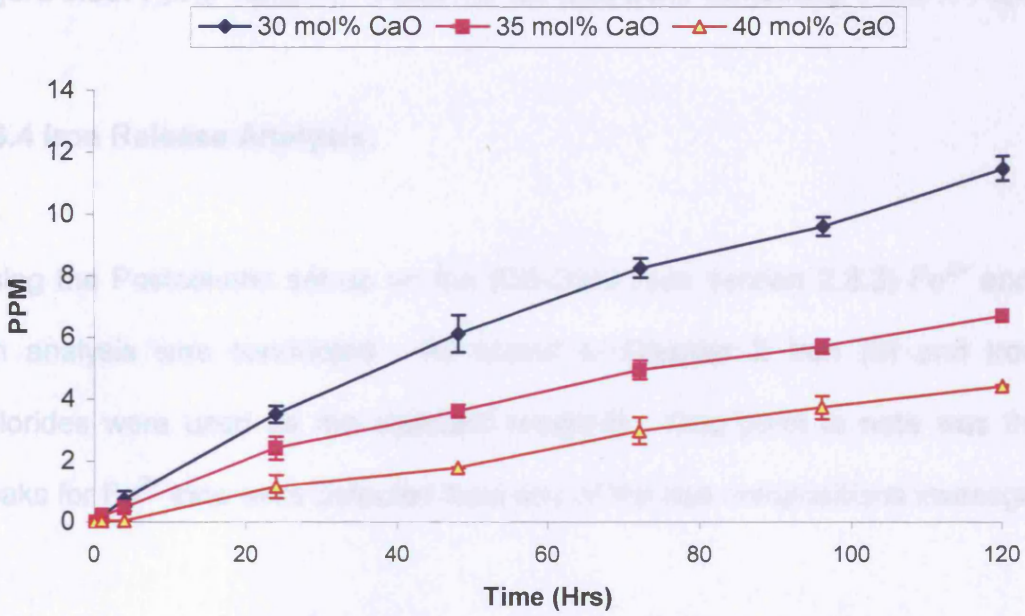

Figure 5.29: $P_3O_{10}^{5-}$ anionic release for compositions containing 1 mol% Fe_2O_3.

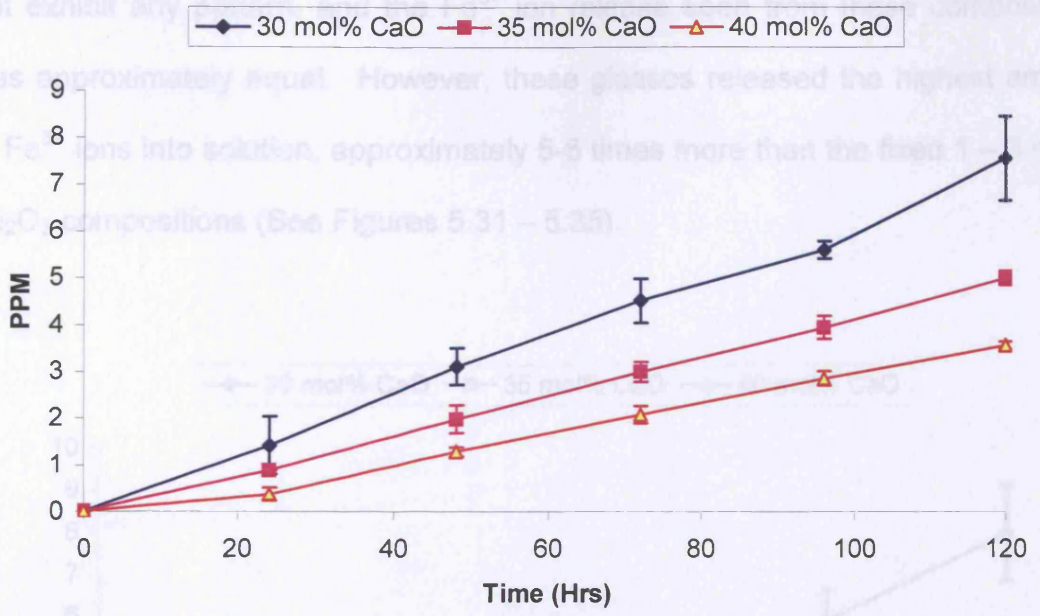

Figure 5.30: $P_3O_{10}^{5-}$ anionic release for compositions containing 4 mol% Fe_2O_3.

5.6.4 Iron Release Analysis:

Using the Postcolumn set-up on the ICS-2500 (see section 2.8.3) Fe^{2+} and Fe^{3+} ion analysis was conducted. As stated in Chapter 2 Iron (II) and Iron (III) chlorides were used as the standard reagents. One point to note was that no peaks for Fe^{2+} ions were detected from any of the iron compositions investigated.

For the compositions with a fixed 1 – 3 mol% Fe_2O_3 content a decrease in the Fe^{3+} ion release was seen with an increase in CaO content. A slight decrease in the overall Fe^{3+} ion release was also observed for these compositions. For compositions with fixed 1 – 2 mol% Fe_2O_3, Fe^{3+} ion release was only detected after the 24 hour time point. The compositions with fixed 4 – 5 mol% Fe_2O_3 did

not exhibit any pattern, and the Fe^{3+} ion release seen from these compositions was approximately equal. However, these glasses released the highest amount of Fe^{3+} ions into solution, approximately 5-6 times more than the fixed 1 – 3 mol% Fe_2O_3 compositions (See Figures 5.31 – 5.35).

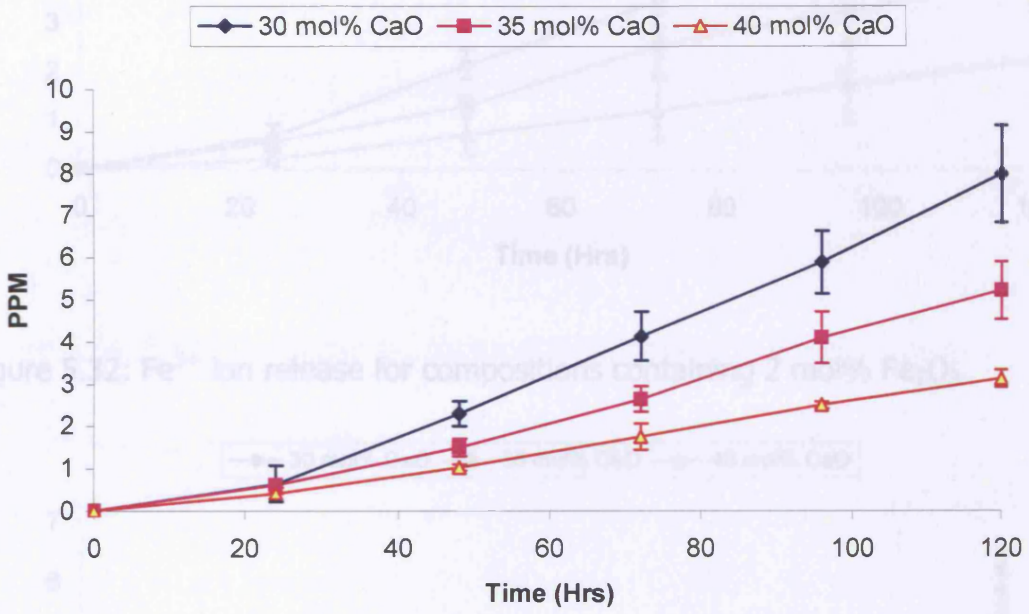

Figure 5.31: Fe^{3+} ion release for compositions containing 1 mol% Fe_2O_3.

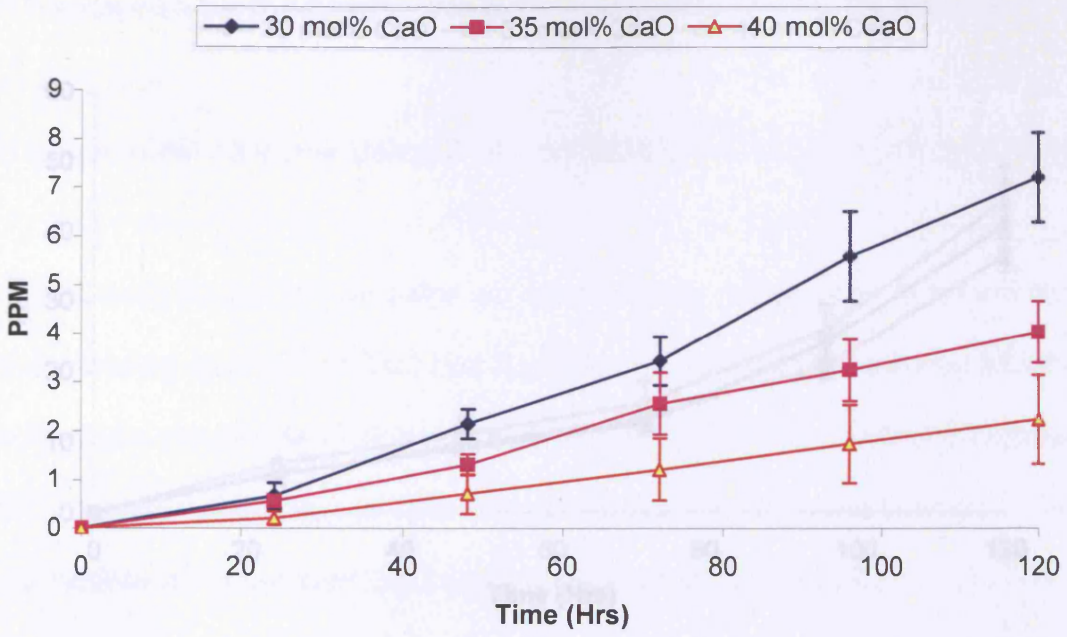

Figure 5.32: Fe^{3+} ion release for compositions containing 2 mol% Fe_2O_3.

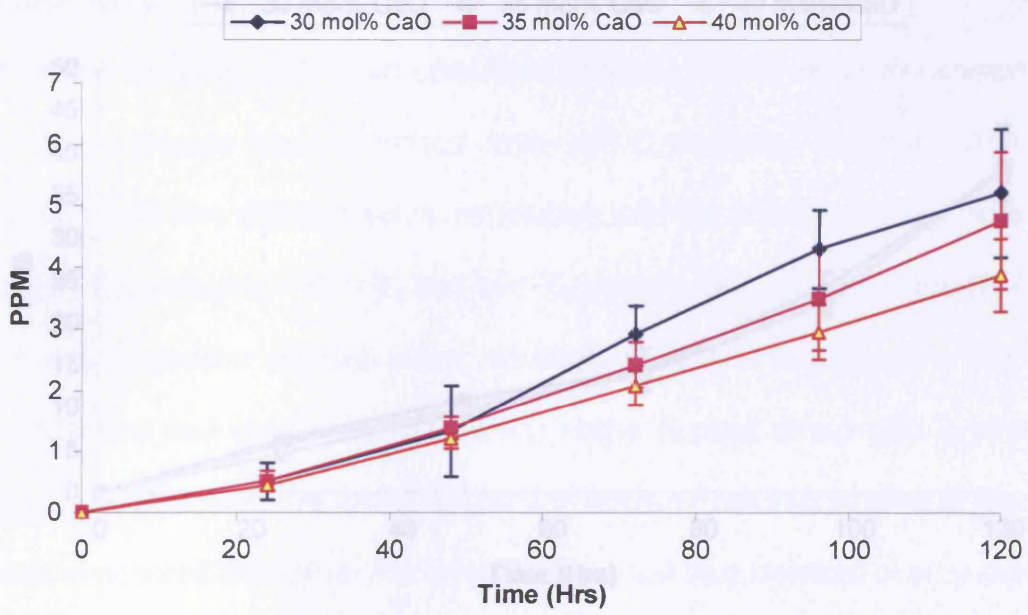

Figure 5.33: Fe^{3+} ion release for compositions containing 3 mol% Fe_2O_3.

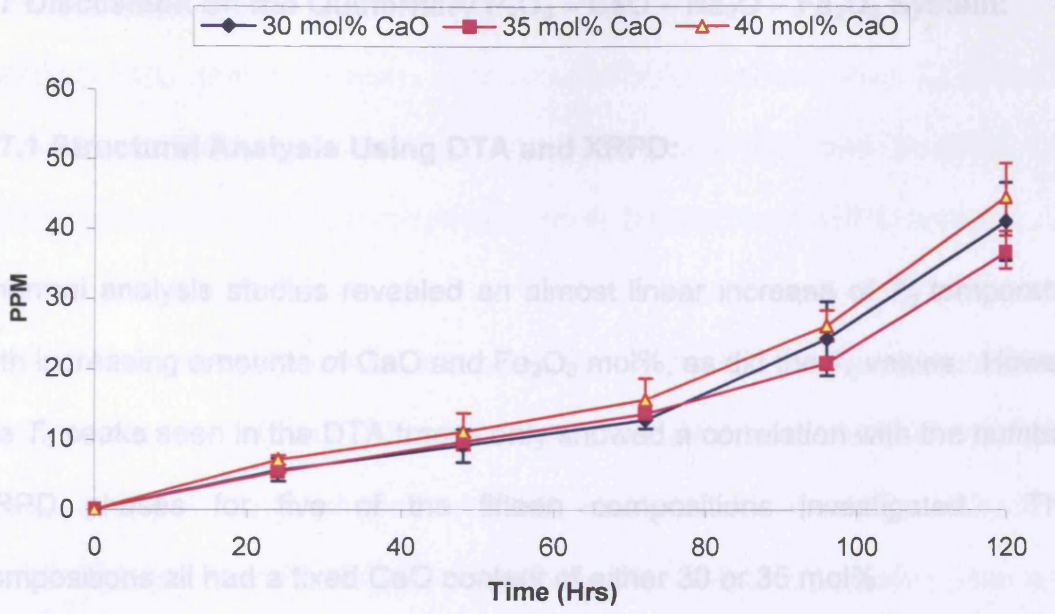

Figure 5.34: Fe^{3+} ion release for compositions containing 4 mol% Fe_2O_3.

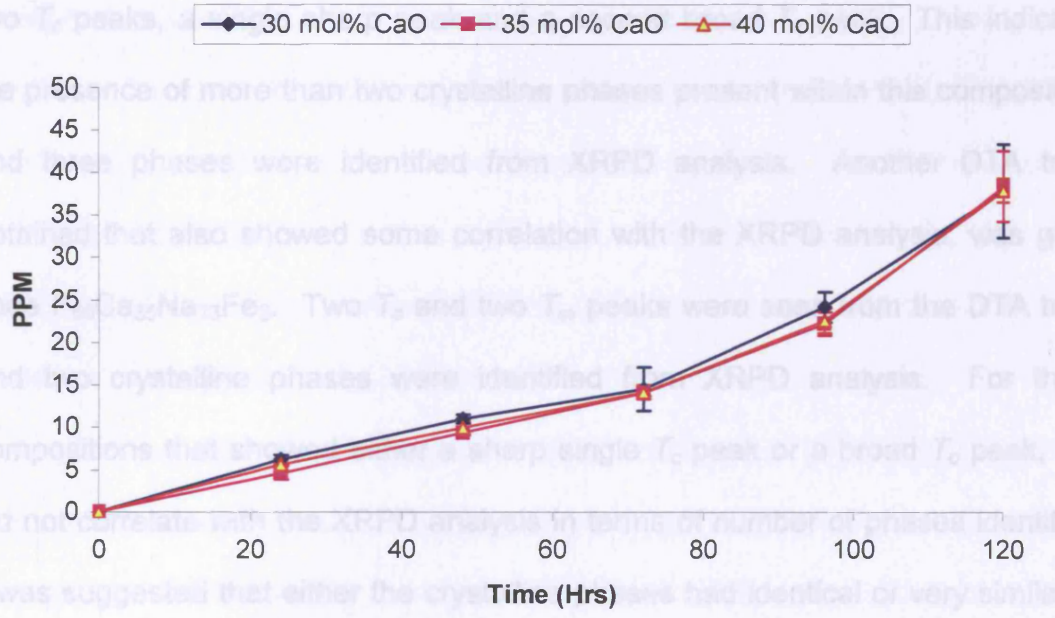

Figure 5.35: Fe^{3+} ion release for compositions containing 5 mol% Fe_2O_3.

5.7 Discussion on the Quaternary P_2O_5 – CaO – Na_2O – Fe_2O_3 System:

5.7.1 Structural Analysis Using DTA and XRPD:

Thermal analysis studies revealed an almost linear increase of T_g temperatures with increasing amounts of CaO and Fe_2O_3 mol%, as did the T_c values. However, the T_c peaks seen in the DTA traces only showed a correlation with the number of XRPD phases for five of the fifteen compositions investigated. These compositions all had a fixed CaO content of either 30 or 35 mol%.

It was also seen that the composition with glass code $P_{50}Ca_{30}Na_{17}Fe_3$ exhibited two T_c peaks, a single sharp peak and a second broad T_c peak. This indicated the presence of more than two crystalline phases present within this composition, and three phases were identified from XRPD analysis. Another DTA trace obtained that also showed some correlation with the XRPD analysis, was glass code $P_{50}Ca_{35}Na_{13}Fe_3$. Two T_c and two T_m peaks were seen from the DTA trace and two crystalline phases were identified from XRPD analysis. For those compositions that showed either a sharp single T_c peak or a broad T_c peak, and did not correlate with the XRPD analysis in terms of number of phases identified, it was suggested that either the crystalline phases had identical or very similar T_c temperatures, or that the other phase(s) were present in very small quantities.

The T_m peaks however, showed good correlation with the number of phases identified from XRPD analysis. For compositions exhibiting two T_m peaks, two crystalline phases were identified from XRPD analysis, and for DTA traces exhibiting three T_m peaks, three phases were detected from XRPD analysis.

The XRPD analyses revealed the presence of three recurring phases from the compositions investigated. These were the $NaCa(PO_3)_3$, $NaFeP_2O_7$ and CaP_2O_6 phases. The CaP_2O_6 phase was seen as the main phase for compositions containing higher levels of CaO. Equally, the $NaFeP_2O_7$ phase was seen as the dominant phase for compositions containing elevated amounts of Fe_2O_3. It was also noted that for 14 of the 15 compositions investigated, there were some minor peaks within the XRPD traces that were not associated with any of the phases identified. The majority of these peaks were located at 2 theta positions of, 28.15, 35.83, 42.10, and five of the compositions had additional unidentified peaks at 44.50 and 48.50 (2 theta). The peaks that were not matched may have been reflections of one of the phases identified, as they systematically occurred in the presence of the $[NaCa(PO_3)_3]$ phase, which incidentally only generated an XRPD trace pattern of up to 36 (2 theta) in the ICDD database. The $NaCa(PO_3)_3$ phase is a tri-clinic phase, and due to its low symmetry and highly complex structure, is very poorly defined within the database. Even after communication with the author who defined the phase (112), atomic positions to generate a complete pattern were not available. The other possibility for the few peaks not matching within the traces obtained could have been due to the non – stoichiometry of the phases present within each of the compositions investigated.

5.7.2 Structural Properties Investigated:

Fe_2O_3 is not a glass former, and was predicted to go into the glass structure as a glass modifier, in a similar manner to the cations. It is well known that iron can exist in one of two oxidation states, Fe^{2+} and Fe^{3+}. If iron was present within the compositions in the Fe^{2+} oxidation state, it was expected to act as a very strong chelate, such as the Ca^{2+} ions between two oxygen atoms. However, if the iron was present in an oxidation state of Fe^{3+}, it was suggested that it could go into the backbone of the phosphate network, as was seen with the boron atoms.

Studies conducted previously (section 3.8.2) revealed that it was possible to predict Q^n species present within the glass compositions investigated using the concept of Network Connectivity (NC).

Using the equation below and assuming Fe was in the structure as Fe^{3+} (i.e. Fe_2O_3):

$$NC = \frac{3 \times \{2 \times [P_2O_5 - Fe_2O_3] + 2 \times 4 \times [2 \times Fe_2O_3]\} - (2 \times [RO + R_2O])}{(2 \times P_2O_5) + (2 \times Fe_2O_3)}$$

Where P_2O_5 = (mole fraction of P_2O_5), and Fe_2O_3 = (mole fraction of Fe_2O_3), RO = mole fraction of alkali metal (monovalent cation), and R_2O = mole fraction of alkali earth metal (divalent cation), an assessment of the Q^n species that were likely to be present within the compositions investigated was made. The above equation

was based on the assumption that the charge on the phosphorous atom (P^{5+}) was locally charge balanced by the iron atom (if it was in oxidation state Fe^{3+}). The ($P_2O_5 - Fe_2O_3$) was representative of the P_2O_5 not charge balanced by the Fe_2O_3 (i.e. the PO_4^{3-} tetrahedra still had one double bonded oxygen), and the ($2 \times Fe_2O_3$) represented the PO_4 with no double-bonded oxygen, hence x4. Also, the above equation only applied when the Fe_2O_3 content was below that of the P_2O_5.

The calculations revealed that due to the presence of 50 mol% of the P_2O_5 network former, Q^2 species were predicted. Q^2 species are metaphosphates, i.e. chains or rings of P – O – P bonds, with Na^+ and Ca^{2+} acting as network modifiers. XRPD analyses revealed that the predictions correlated with the predicted Q^n species, via the detection of the phases $NaCa(PO_3)_3$ (sodium calcium metaphosphate), and CaP_2O_6 (β- Calcium metaphosphate). See Table 5.4 for calculated NC and Q^n species predicted for the compositions investigated.

Table 5.4: NC calculations and predicted Q^n species.

Glass Codes	Calculated NC	Predicted Q^n Species.
$P_{50}Ca_{30}Na_{19}Fe_1$	2.08	Q^2
$P_{50}Ca_{35}Na_{14}Fe_1$	2.08	Q^2
$P_{50}Ca_{40}Na_9Fe_1$	2.08	Q^2
$P_{50}Ca_{30}Na_{18}Fe_2$	2.15	Q^2
$P_{50}Ca_{35}Na_{13}Fe_2$	2.15	Q^2
$P_{50}Ca_{40}Na_8Fe_2$	2.15	Q^2
$P_{50}Ca_{30}Na_{17}Fe_3$	2.23	Q^2
$P_{50}Ca_{35}Na_{12}Fe_3$	2.23	Q^2
$P_{50}Ca_{40}Na_7Fe_3$	2.23	Q^2
$P_{50}Ca_{30}Na_{16}Fe_4$	2.30	Q^2
$P_{50}Ca_{35}Na_{11}Fe_4$	2.30	Q^2
$P_{50}Ca_{40}Na_6Fe_4$	2.30	Q^2
$P_{50}Ca_{30}Na_{15}Fe_5$	2.36	Q^2
$P_{50}Ca_{35}Na_{10}Fe_5$	2.36	Q^2
$P_{50}Ca_{40}Na_5Fe_5$	2.36	Q^2

The above formula could also be applied to the boron compositions investigated in the previous section; however, boron is a well known glass former. Therefore, it was predicted to go into the structural backbone of the network.

5.7.3 Degradation rates, pH and Ion Release Profiles:

The dissolution rates seen also exhibited similar patterns to the T_g and T_c values obtained, where a decrease in rates was observed with an increase in CaO content and increasing Fe_2O_3 content. Correlation was also seen with the glass-fibre dissolution rates. Again, a decrease in dissolution was seen with increasing CaO mol% and increasing the Fe_2O_3 content from 1 to 5 mol%. The reduction seen in the dissolution rates from 1 - 5 mol% Fe_2O_3 content, for both the bulk glass, and glass-fibres was an order of magnitude lower. An increase in the dissolution rates was also seen for fibres pulled at higher RPMs. This correlated with a decrease in fibre diameter, which in turn increased the dissolution rate of the glass-fibres. This increased dissolution rate was attributed to a large increase in surface area of the glass-fibres obtained.

The pH profiles obtained showed that these compositions, especially those containing 4 - 5 mol% Fe_2O_3 content, remained relatively neutral. This was attributed to the low dissolution rates obtained, due to the enhanced chemical durability of the compositions investigated. This also suggested that these compositions would be most suitable to be used as biodegradable cell delivery implant materials, due to the relatively neutral pH obtained.

The ion release profiles showed that the sodium and calcium ions were released into solution in relatively large amounts, suggesting these ions were the first products to be released upon dissolution.

The anion release profiles showed that the $P_3O_9^{3-}$ anion was again the highest released anion, and this was expected due to the $P_3O_9^{3-}$ anionic species detected via XRPD analysis in the $NaCa(PO_3)_3$ phase. The PO_4^{3-} anion is usually the remnant of the other phosphate species being degraded in solution, and anion release studies showed that this species was present in relatively high concentrations.

The $P_2O_7^{4-}$ species was detected at very low levels in the ion release profiles obtained, with calculations suggesting that only a tiny amount of this species was present in the original glass composition, probably as chain terminators. However, XRPD detected a $NaFeP_2O_7$ (a pyrophosphate) phase in all the compositions investigated, with the exception of those containing a fixed 1 mol% Fe_2O_3 content. One possible explanation put forward for this was attributed to the structure of the compositions investigated.

Yu *et al.* (113) conducted studies on the properties and structure of sodium – iron phosphate glasses. They investigated compositions that had varying amounts of phosphate, sodium and iron. Using Mossbauer spectroscopy they were able to investigate the presence of iron in both the 2+ and 3+ oxidation states. They stated that a strengthening of the cross-bonding between phosphate chains via Fe^{3+} had been suggested (114), for the improved chemical durability seen whilst adding Fe_2O_3 to lead phosphate glasses. However, they proposed that the improvement in chemical durability observed in their studies was attributed to the replacement of P – O – P bonds in the glass by more hydration resistant Fe – O – P bonds, and to the strong cross-linking of the phosphate chains by the iron ions. The general structure of these sodium-iron-phosphate glasses was suggested to be consisting of PO_4^{3-} tetrahedra joined in various ways by the oxygen polyhedra which contained Fe^{2+}, Fe^{3+} or Na^+ ions. The coordination number of the Fe^{2+} and Fe^{3+} ions was especially important in developing a more detailed structural model for these glasses. It was stated that other phosphate glass studies had reported that Fe^{2+} had been widely concluded to be in the octahedral coordination. They also stated that although there was not total agreement, other studies had also reported Fe^{3+} to be in octahedral or distorted octahedral coordination. Figure 5.36 depicts the suggested structure for these sodium - iron phosphate glasses.

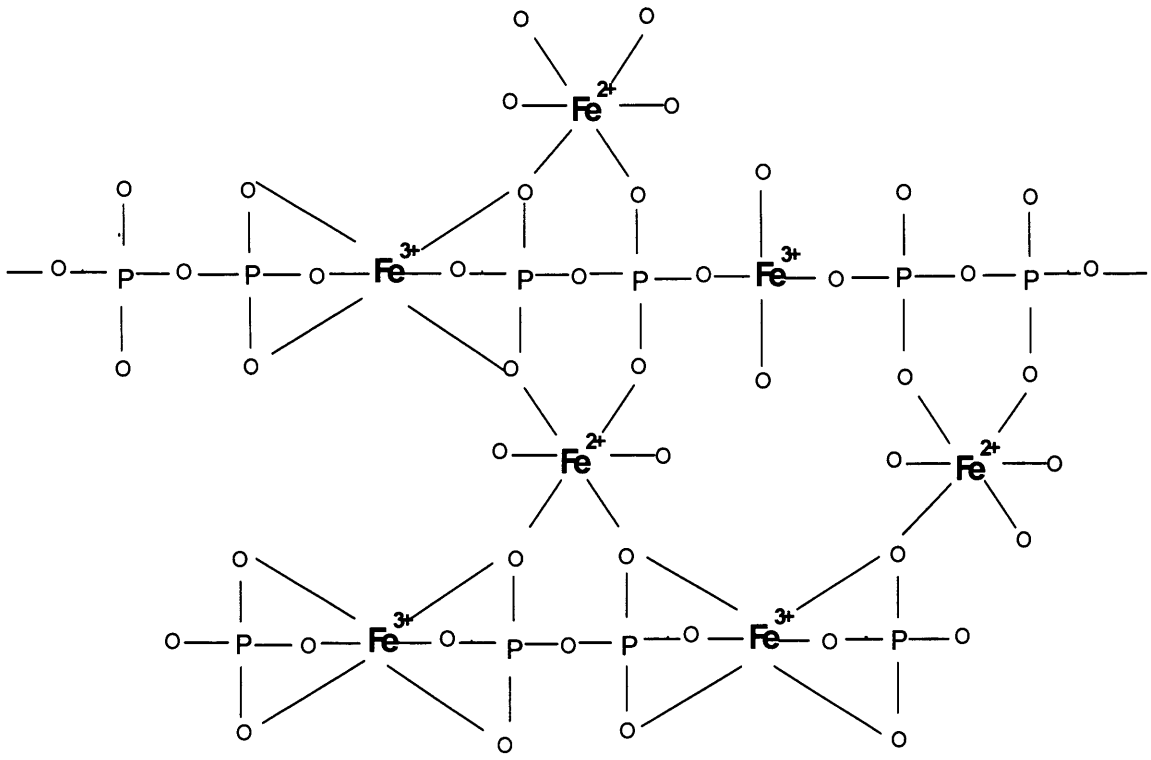

Figure 5.36: Idealised structure for iron pyrophosphate glass where iron(II) ions are in octahedral sites and P_2O_7 groups are joined by iron(III) ions in tetrahedral or octahedral coordination (113).

Yu *et al* concluded by stating that with increasing Fe_2O_3 content, all of the bridging P – O – P bonds which joined adjacent PO_4^{3-} tetrahedra in the higher phosphate glasses were replaced by Fe^{3+} ions to form P – O – Fe^{3+} bonds, with the exception of the one P – O – P bond in the pyrophosphate ($P_2O_7^{4-}$) group. The Fe^{3+} ions were in either tetrahedral or octahedral coordination, which were probably so highly distorted as to resemble tetrahedral coordination. In either case, the Fe^{3+} ions were said to act as a network former. The larger Fe^{2+} ions

were also said to be in octahedral sites, and could bond with any single bonded oxygens that were present. Thus it was said, that the Fe^{2+} ions could be viewed as network modifiers, along with any alkali or alkaline earth cations.

Mogus-Milankovic *et al.* (115) conducted structural studies of iron phosphate glasses, which were binary iron phosphate compositions. They concluded via Raman and Mossbauer spectroscopy studies, that Fe^{3+} was present and acted as a network former, which occupied tetrahedral sites in the phosphate network, which decreased the number of P – O – P bonds, and were replaced by Fe – O – P bonds. They also stated that in the 50/50 iron phosphate composition, the structure consisted of isolated PO_4^{3-} groups with the Fe^{3+} ions present as FeO_4 groups. Mogus-Milankovic *et al.* (116;117) also conducted studies on sodium phosphate glasses containing either Al_2O_3 or Fe_2O_3. It was concluded that the effect of Al_2O_3 addition to the sodium phosphate glasses was very different than the addition of Fe_2O_3.

The above conclusions would definitely account for the increase in T_g values obtained. Fang *et al.* (118) investigated the glass transition of iron phosphate glasses, and concluded that the addition of alkali oxides increased the T_g. This increase in T_g was observed with increasing CaO content within the compositions investigated in this section. Furthermore, with regards to the structural model proposed by Yu *et al.* above, this would have also accounted for the pyrophosphate phase identified from XRPD analyses. Studies conducted by

Fang *et al.* (119;120) also observed the presence of an iron pyrophosphate phase within their iron phosphate glass compositions investigated.

Decreasing dissolution rates were obtained for both the bulk glass and glass-fibres investigated. An order of magnitude difference was seen from compositions with fixed 1 – 5 mol% Fe_2O_3. This decrease could also be attributed to the above structural studies conducted. The order of magnitude difference observed in the dissolution rates obtained could also be explained in terms of an increase in the chemical durability of the bonds formed.

Ray *et al.* (121) also investigated a binary iron phosphate glass, with the composition 40 Fe_2O_3 – 60 P_2O_5. They stated that in their glass, chemical durability in deionised water was very high. They suggested that this chemical durability was independent of the relative Fe^{2+} and Fe^{3+} concentrations, but improved with increasing Fe_2O_3 content, observed in the studies conducted.

Marasinghe *et al.* (111) also conducted studies on binary iron phosphate compositions. They also concluded by stating that the relatively poor chemical durability of phosphate glasses was attributed to the abundance of easily hydrated P – O – P bonds in these glasses. Hydration of the bridging oxygen of the P – O – P bonds resulted in terminal P – OH bonds, thus destroying the cross linkage between the chains, in what was viewed as a depolymerisation effect. However, if the oxygen ions in iron phosphate glasses took part in more hydration resistant Fe^{2+} – O – P or Fe^{3+} – O – P bonds, this would impose greater chemical

durability on these glasses. Marasinghe *et al.* (122) in another study concluded that the general coordination of the majority of iron ions in their compositions investigated appeared to be in a distorted octahedral coordination. However, a study by Karabulut *et al.* (123) concluded that both Fe^{2+} and Fe^{3+} ions had mixed tetrahedral and octahedral coordination.

Choueka *et al.* (124) investigated calcium phosphate glass-fibres with the composition 54% PO_4, 27% Ca, 12% ZnO, 2.5% $NaPO_3$, and 4.5% Fe_2O_3. They stated that by annealing the fibres at different temperatures they underwent a mode of dissolution that allowed them to maintain their structural integrity for longer time periods. Lin *et al.* (125) also investigated the development of bioabsorbable glass-fibres. The calcium iron phosphate glasses contained an iron oxide content ranging from 5 wt% to 22 wt%. It was found that the dissolution rate, fibre strength and the T_g temperature were strongly affected by the increasing iron oxide content. The glass dissolution rate exhibited a 50 fold reduction for the 22 wt% Fe_2O_3 composition, whilst the highest tensile strength (over 1000MPa) was measured for fibres from this composition. This also contributed to the decrease seen in the glass-fibre dissolution rates obtained.

As seen above no Fe^{2+} ions were detected during ion chromatography analysis. Even though iron was added as Fe_2O_3 (i.e. in Fe^{3+} coordination), the effect of the glass melting temperatures employed was not certain. If there were some Fe^{2+} ions present in the original glass structure, then the reason for the non-detection of these ions was probably due to the Fe^{2+} ions being oxidised in solution. This oxidation of Fe^{2+} ions was said to be moderately rapid in neutral solutions, but somewhat slower in acidic solutions (126). As can be seen from the pH analyses conducted, the solutions all remained relatively neutral.

Summary:

Studies conducted with collaborators from Hammersmith Hospital, revealed that compositions containing 4 and 5 mol% Fe_2O_3 content, were sufficient for successful cell attachment and proliferation. Muscle cells not only attached to these compositions but also fused along the axis of the fibres to produce myotubes (72). The successful biocompatibility of these compositions was attributed to the neutrality of the solution during the dissolution studies, and also the enhanced chemical durability of the fibres.

CHAPTER 6

The Quaternary P_2O_5 – CaO – Na_2O – SiO_2 Glass System

6.0 The Quaternary P_2O_5 – CaO – Na_2O – SiO_2 Glass System:

6.1 Quaternary Compositions Investigated:

In the previous section, the quaternary component Fe_2O_3 was introduced to reduce the dissolution rates obtained from the original ternary and boron compositions investigated. It was seen that via the addition of B_2O_3 the dissolution rates did decrease, however, the decrease seen was very small. In contrast, the dissolution rates seen from the iron compositions exhibited a decrease which was an order of magnitude lower, and biocompatibility studies revealed (127) successful attachment and proliferation of muscle precursor cells to these iron compositions.

In this section, SiO_2 was added as a quaternary component in order to determine the effect of silica upon the original ternary compositions investigated. There is a significant amount of literature available on silicate glasses, and Larry Hench's Bioglass® has also received much attention for its biocompatibility with hard tissue. However, there is very little if any literature available on the effect of SiO_2 on a predominantly phosphate based glass. Therefore the following investigation was conducted in order to elucidate the effect of SiO_2 (via 1 – 5 mol% incorporation) upon a phosphate based glass composition. Table 6.1 presents the glass codes and compositions investigated.

Table 6.1: Glass codes and compositions investigated in the P_2O_5 – CaO – Na_2O – SiO_2 system.

Glass Codes	P_2O_5 (mol%)	CaO (mol%)	Na_2O (mol%)	SiO_2 (mol%)
$P_{50}Ca_{30}Na_{19}Si_1$	50	30	19	1
$P_{50}Ca_{35}Na_{14}Si_1$	50	35	14	1
$P_{50}Ca_{40}Na_9Si_1$	50	40	9	1
$P_{50}Ca_{30}Na_{18}Si_2$	50	30	18	2
$P_{50}Ca_{35}Na_{13}Si_2$	50	35	13	2
$P_{50}Ca_{40}Na_8Si_2$	50	40	8	2
$P_{50}Ca_{30}Na_{17}Si_3$	50	30	17	3
$P_{50}Ca_{35}Na_{12}Si_3$	50	35	12	3
$P_{50}Ca_{40}Na_7Si_3$	50	40	7	3
$P_{50}Ca_{30}Na_{16}Si_4$	50	30	16	4
$P_{50}Ca_{35}Na_{11}Si_4$	50	35	11	4
$P_{50}Ca_{40}Na_6Si_4$	50	40	6	4
$P_{50}Ca_{30}Na_{15}Si_5$	50	30	15	5
$P_{50}Ca_{35}Na_{10}Si_5$	50	35	10	5
$P_{50}Ca_{40}Na_5Si_5$	50	40	5	5

The melting and annealing temperatures and times used are listed in Table 2.4, section 2.1.

6.2 Thermal Analysis:

All DTA traces obtained exhibited clear T_g, T_c and T_m peaks. The traces shown below have their respective glass fibre (GF) traces overlaid on top of the bulk glass (BG) traces obtained (see Figures 6.1 and 6.2).

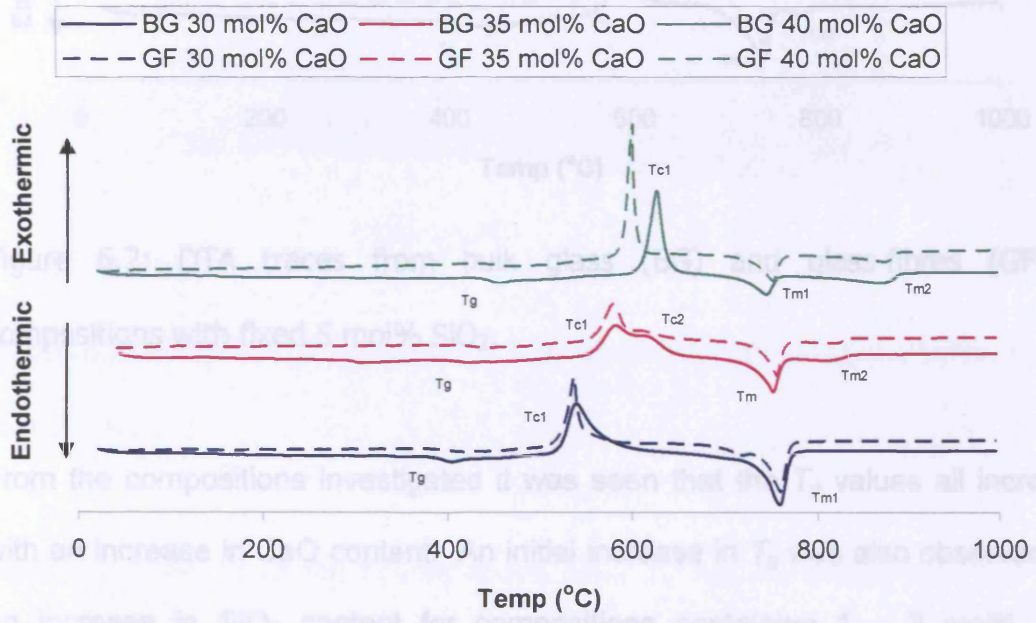

Figure 6.1: DTA traces from bulk glass (BG) and glass-fibres (GF) for compositions with fixed 1 mol% SiO_2.

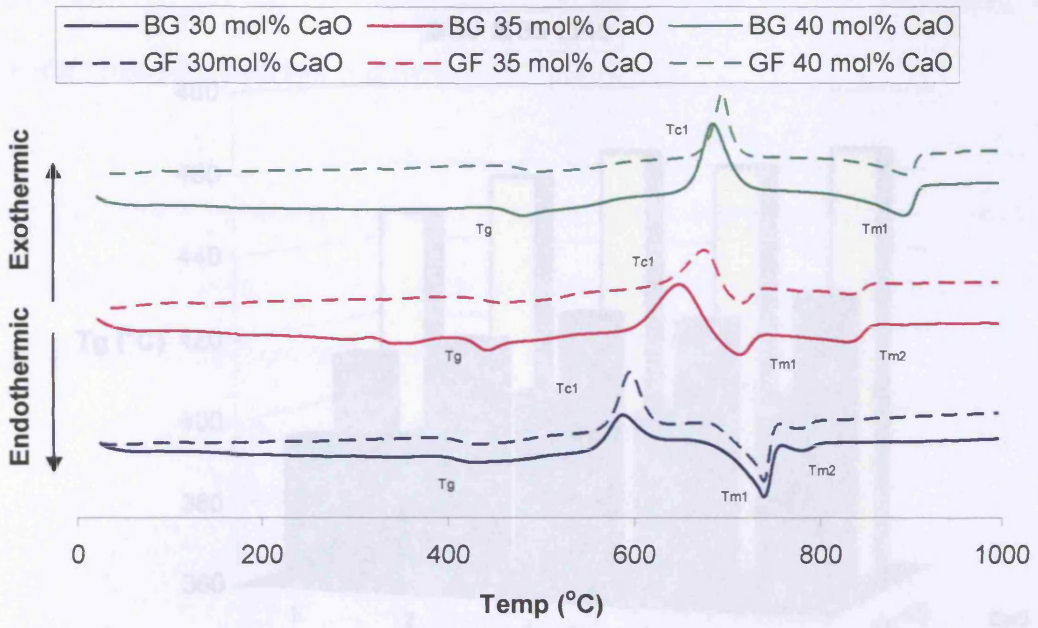

Figure 6.2: DTA traces from bulk glass (BG) and glass-fibres (GF) for compositions with fixed 5 mol% SiO_2.

From the compositions investigated it was seen that the T_g values all increased with an increase in CaO content. An initial increase in T_g was also observed with an increase in SiO_2 content for compositions containing 1 – 3 mol% SiO_2. However, the T_g value then dropped for the composition containing 4 mol% SiO_2, and increased again for the composition containing 5 mol% SiO_2 to a value equal to that of the fixed 3 mol% SiO_2 composition (see Figure 6.3 below).

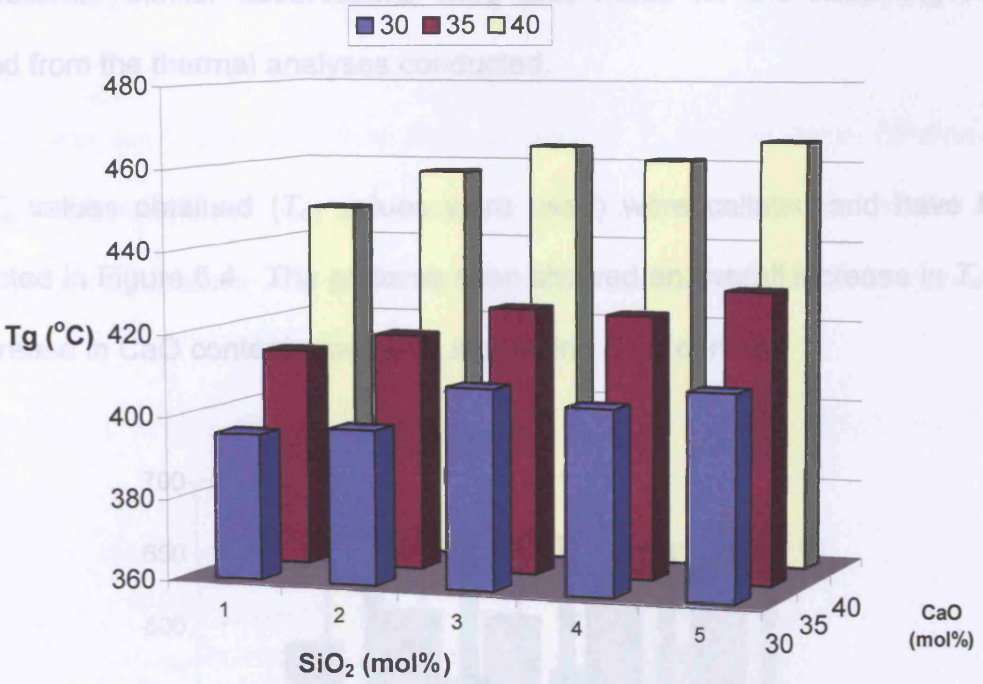

Figure 6.3: 3D graph of T_g values for bulk glass (BG) compositions containing 1 – 5 mol% SiO_2.

As can be seen from the figures above clear T_c, and T_m peaks were observed from the traces obtained. Single T_c peaks were indicative of a single crystalline phase present within that composition and two T_c peaks were indicative of two crystalline phases present. For glass code $P_{50}Ca_{30}Na_{19}Si_1$, a single T_c peak was seen along with a single T_m peak. This was suggestive of a single crystalline phase present within that composition. For glass code $P_{50}Ca_{35}Na_{14}Si_1$ two T_c peaks were seen along with two T_m peaks, and this suggested that two crystalline phases were present within that composition. Glass code $P_{50}Ca_{40}Na_9Si_1$ exhibited a single sharp T_c peak; however, two T_m peaks were seen for this

composition. Similar observations were also made for the remaining traces collated from the thermal analyses conducted.

The T_c values obtained (T_{c1} values were used) were collated and have been presented in Figure 6.4. The patterns seen showed an overall increase in T_c with an increase in CaO content along with increasing SiO_2 content.

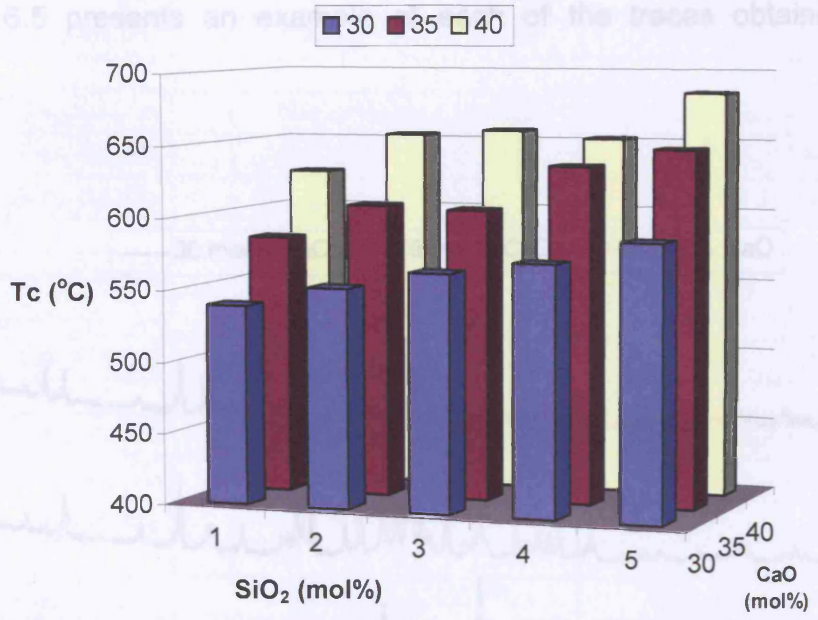

Figure 6.4: 3D graph of T_{c1} values for compositions containing 1 – 5 mol% SiO_2.

The T_m values obtained showed no correlation or pattern with compositions investigated.

6.3 XRD Analysis:

The samples were crystallised at their respective T_c temperatures obtained via thermal analysis. The crystalline phases identified for each of the compositions investigated were matched against the Crystallographica Search-Match software.

Figures 6.5 presents an example of each of the traces obtained via XRPD analysis.

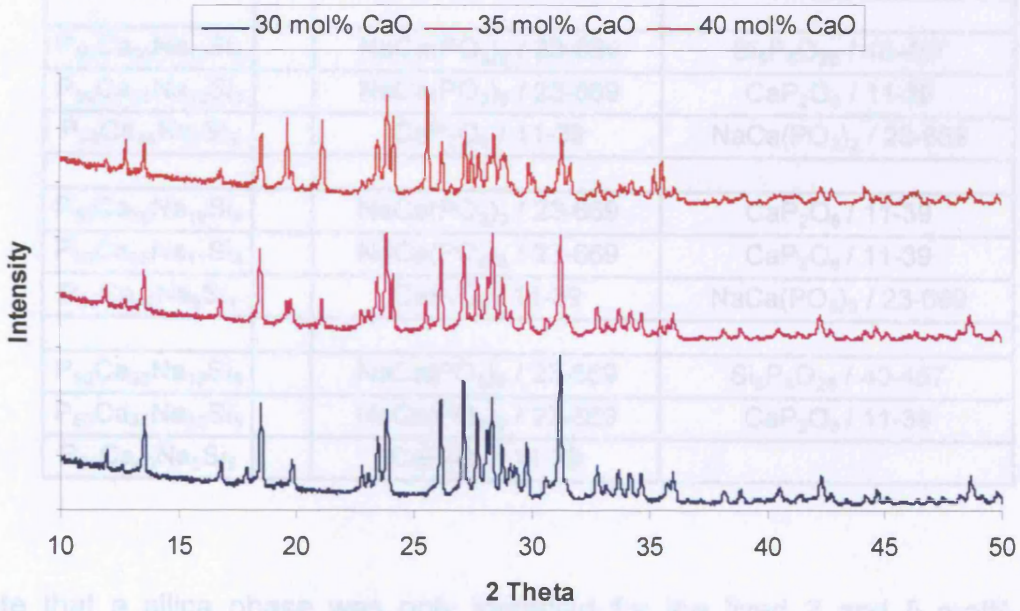

Figure 6.5: XRPD traces for compositions containing 1 mol% SiO_2.

The phases identified for the compositions investigated have been tabulated in Table 6.2.

Table 6.2: XRPD Phases identified for compositions investigated.

Glass Codes		Phase 1 / ICDD card no.	Phase 2 / ICDD card no.
$P_{50}Ca_{30}Na_{19}Si_1$		$NaCa(PO_3)_3$ / 23-669	
$P_{50}Ca_{35}Na_{14}Si_1$		$NaCa(PO_3)_3$ / 23-669	CaP_2O_6 / 11-39
$P_{50}Ca_{40}Na_9Si_1$		$NaCa(PO_3)_3$ / 23-669	CaP_2O_6 / 11-39
$P_{50}Ca_{30}Na_{18}Si_2$		$NaCa(PO_3)_3$ / 23-669	CaP_2O_6 / 11-39
$P_{50}Ca_{35}Na_{13}Si_2$		$NaCa(PO_3)_3$ / 23-669	CaP_2O_6 / 11-39
$P_{50}Ca_{40}Na_8Si_2$		CaP_2O_6 / 11-39	$NaCa(PO_3)_3$ / 23-669
$P_{50}Ca_{30}Na_{17}Si_3$		$NaCa(PO_3)_3$ / 23-669	$Si_5P_6O_{25}$ / 40-457
$P_{50}Ca_{35}Na_{12}Si_3$		$NaCa(PO_3)_3$ / 23-669	CaP_2O_6 / 11-39
$P_{50}Ca_{40}Na_7Si_3$		CaP_2O_6 / 11-39	$NaCa(PO_3)_3$ / 23-669
$P_{50}Ca_{30}Na_{16}Si_4$		$NaCa(PO_3)_3$ / 23-669	CaP_2O_6 / 11-39
$P_{50}Ca_{35}Na_{11}Si_4$		$NaCa(PO_3)_3$ / 23-669	CaP_2O_6 / 11-39
$P_{50}Ca_{40}Na_6Si_4$		CaP_2O_6 / 11-39	$NaCa(PO_3)_3$ / 23-669
$P_{50}Ca_{30}Na_{15}Si_5$		$NaCa(PO_3)_3$ / 23-669	$Si_5P_6O_{25}$ / 40-457
$P_{50}Ca_{35}Na_{10}Si_5$		$NaCa(PO_3)_3$ / 23-669	CaP_2O_6 / 11-39
$P_{50}Ca_{40}Na_5Si_5$		CaP_2O_6 / 11-39	

Note that a silica phase was only identified for the fixed 3 and 5 mol% SiO_2 compositions.

6.4 Degradation Analysis:

6.4.1 Bulk Glass Degradation Studies:

The dissolution studies were conducted using the cumulative method. The plots obtained all exhibited linear dissolution profiles for the compositions investigated for the duration of the study (see Figures 6.6 – 6.10).

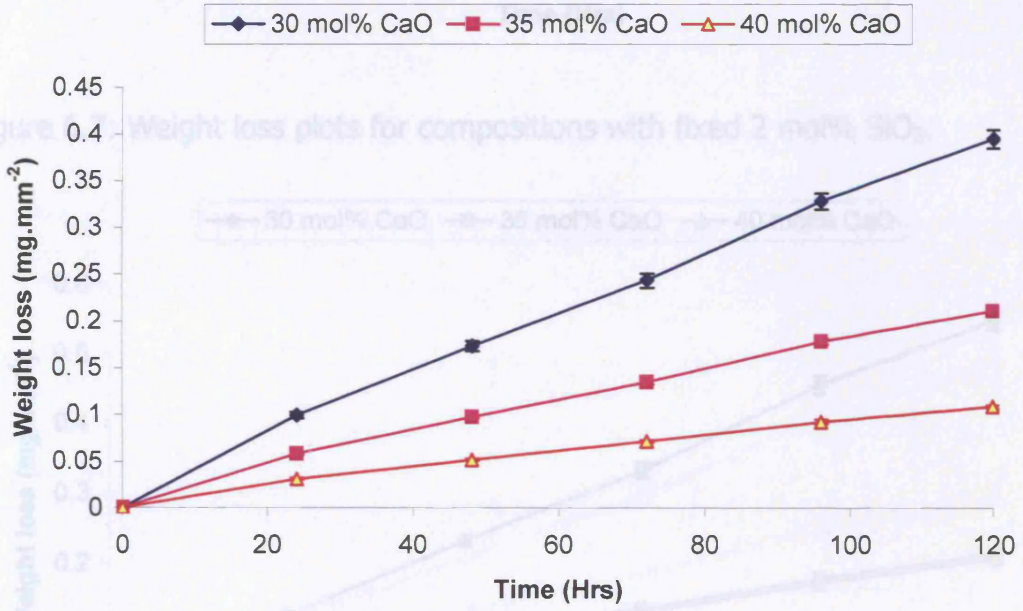

Figure 6.6: Weight loss plots for compositions with fixed 1 mol% SiO_2.

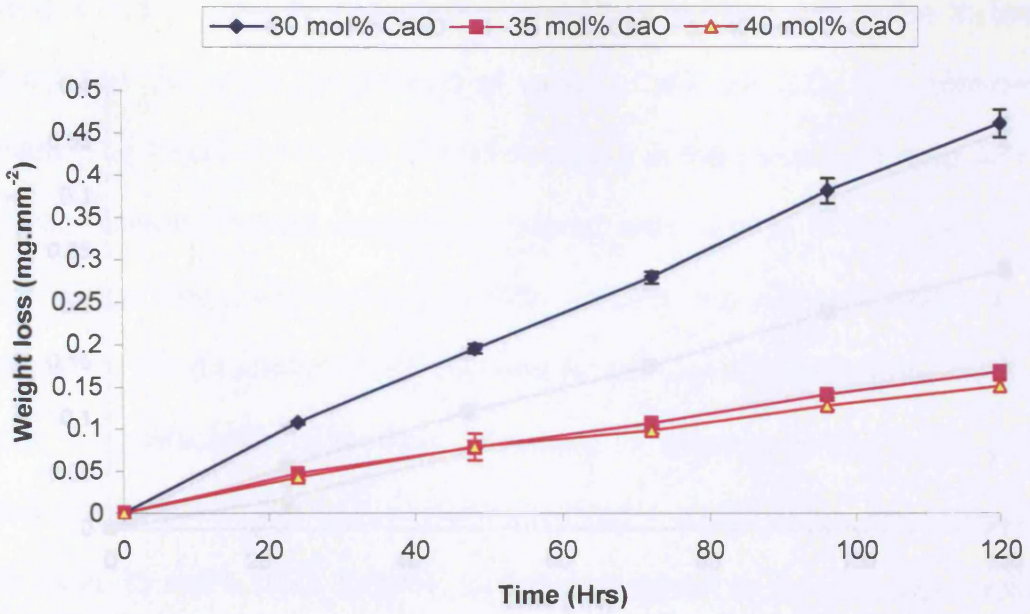

Figure 6.7: Weight loss plots for compositions with fixed 2 mol% SiO_2.

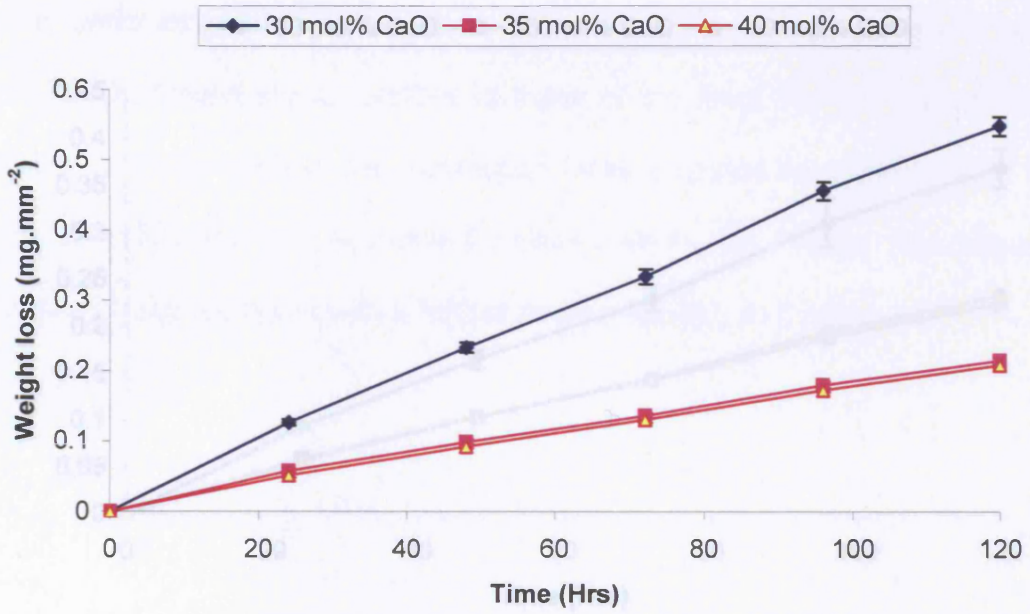

Figure 6.8: Weight loss plots for compositions with fixed 3 mol% SiO_2.

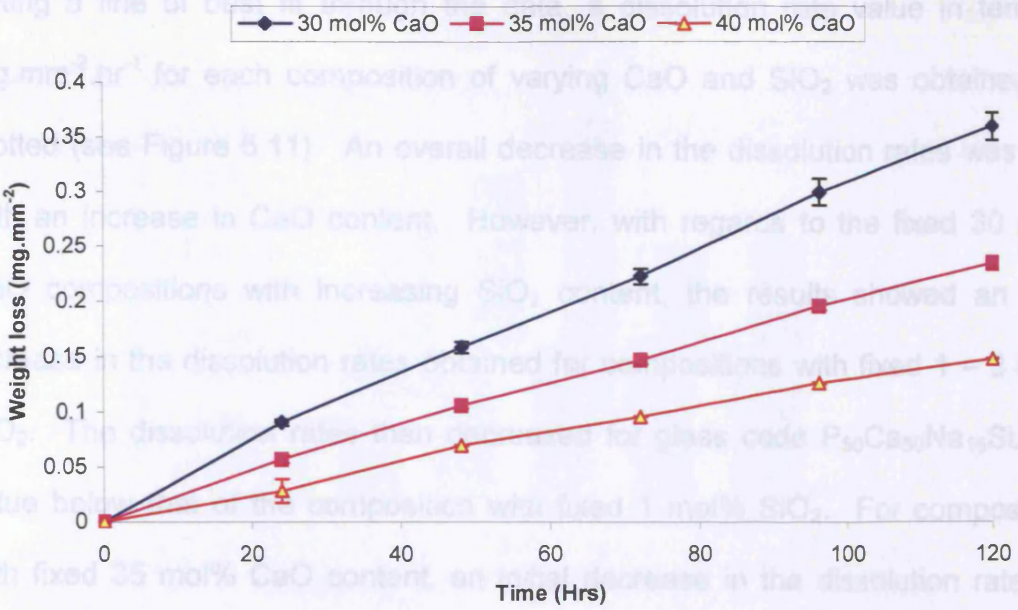

Figure 6.9: Weight loss plots for compositions with fixed 4 mol% SiO_2.

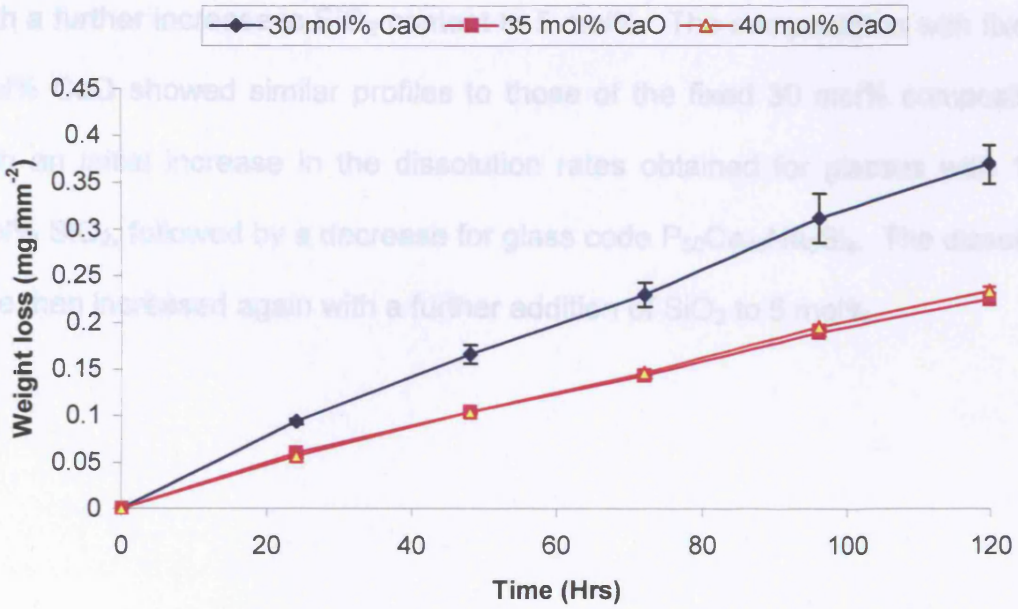

Figure 6.10: Weight loss plots for compositions with fixed 5 mol% SiO_2.

Fitting a line of best fit through the data, a dissolution rate value in terms of $mg.mm^{-2}.hr^{-1}$ for each composition of varying CaO and SiO_2 was obtained and plotted (see Figure 6.11). An overall decrease in the dissolution rates was seen with an increase in CaO content. However, with regards to the fixed 30 mol% CaO compositions with increasing SiO_2 content, the results showed an initial increase in the dissolution rates obtained for compositions with fixed 1 – 3 mol% SiO_2. The dissolution rates then decreased for glass code $P_{50}Ca_{30}Na_{16}Si_4$ to a value below that of the composition with fixed 1 mol% SiO_2. For compositions with fixed 35 mol% CaO content, an initial decrease in the dissolution rate was seen for compositions containing 1 – 2 mol% SiO_2. The dissolution rate then increased for compositions with 3 and 4 mol% SiO_2, and subsequently levelled off with a further increase in SiO_2 content to 5 mol%. The compositions with fixed 40 mol% CaO showed similar profiles to those of the fixed 30 mol% compositions, with an initial increase in the dissolution rates obtained for glasses with 1 – 3 mol% SiO_2, followed by a decrease for glass code $P_{50}Ca_{40}Na_6Si_4$. The dissolution rate then increased again with a further addition of SiO_2 to 5 mol%.

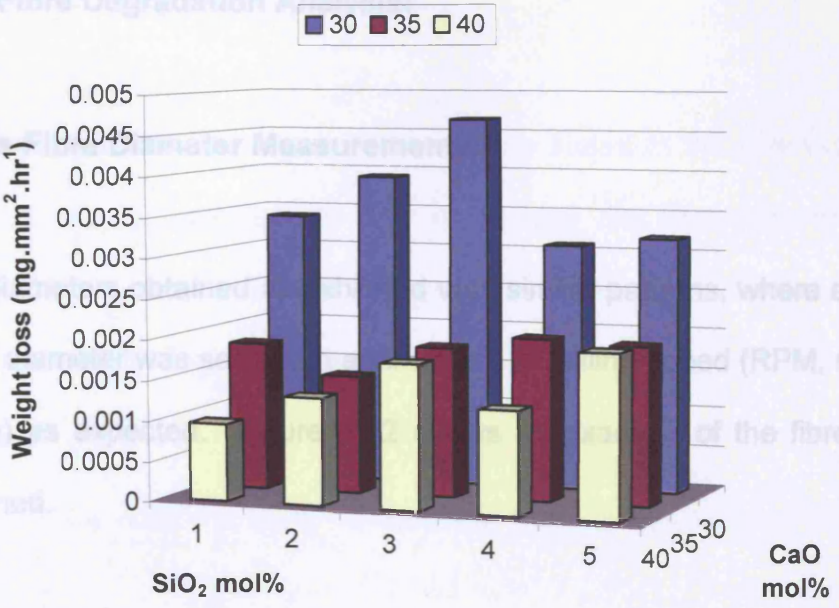

Figure 6.11: 3D graph of the dissolution rates for the compositions investigated.

6.5 Glass-Fibre Degradation Analysis:

6.5.1 Glass-Fibre Diameter Measurements:

The fibre diameters obtained all exhibited very similar patterns, where a decrease in the fibre diameter was seen with an increase in pulling speed (RPM, revolutions per minute) as expected. Figure 6.12 shows an example of the fibre diameter plots obtained.

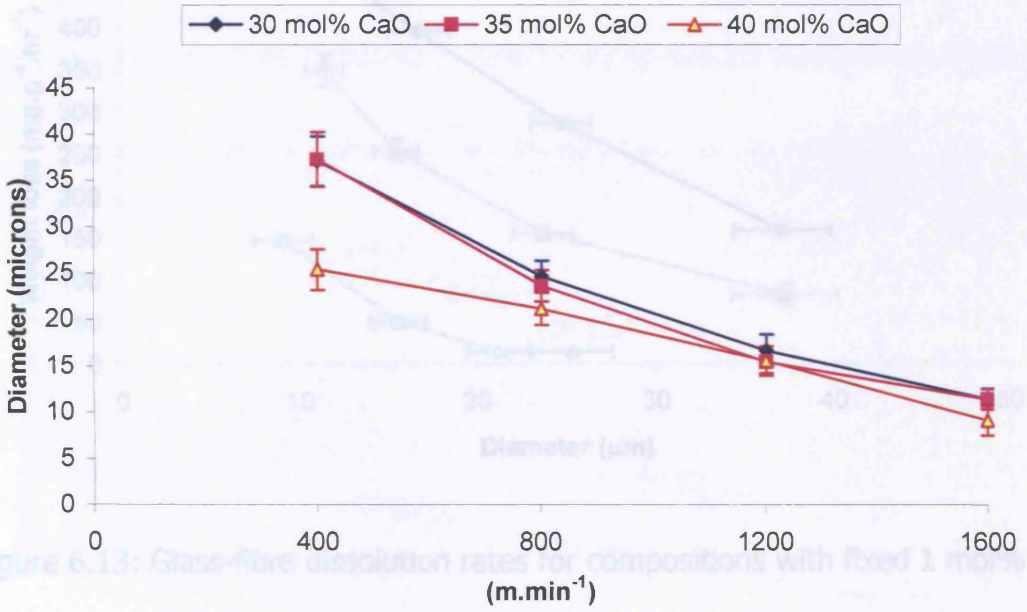

Figure 6.12: Glass-fibre diameters for compositions with fixed 1 mol% SiO_2.

6.5.2 Glass-Fibre Degradation Studies:

The fibre dissolution studies were conducted as stated in the previous sections. This method was an appropriate way of ranking the fibres in order of their dissolution rates obtained. The graphs were plotted as weight loss per unit hour against diameter (see Figures 6.13 – 6.17).

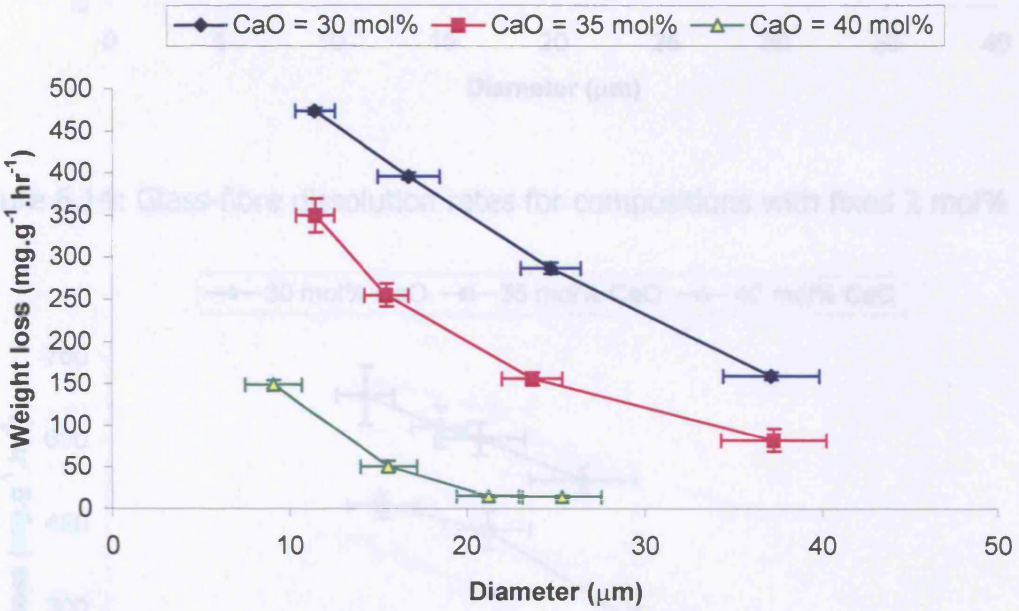

Figure 6.13: Glass-fibre dissolution rates for compositions with fixed 1 mol% SiO_2.

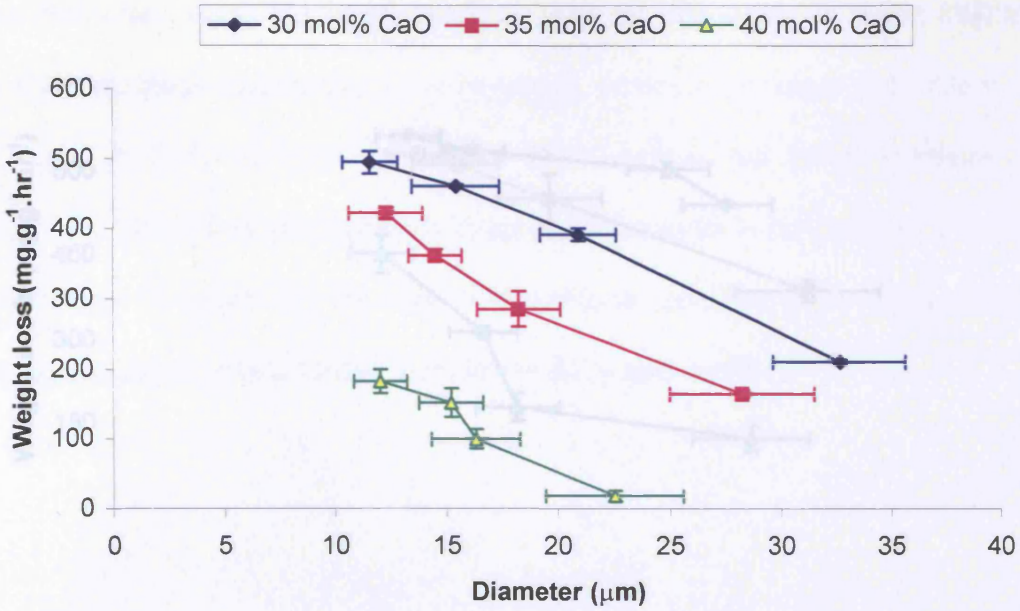

Figure 6.14: Glass-fibre dissolution rates for compositions with fixed 2 mol% SiO_2.

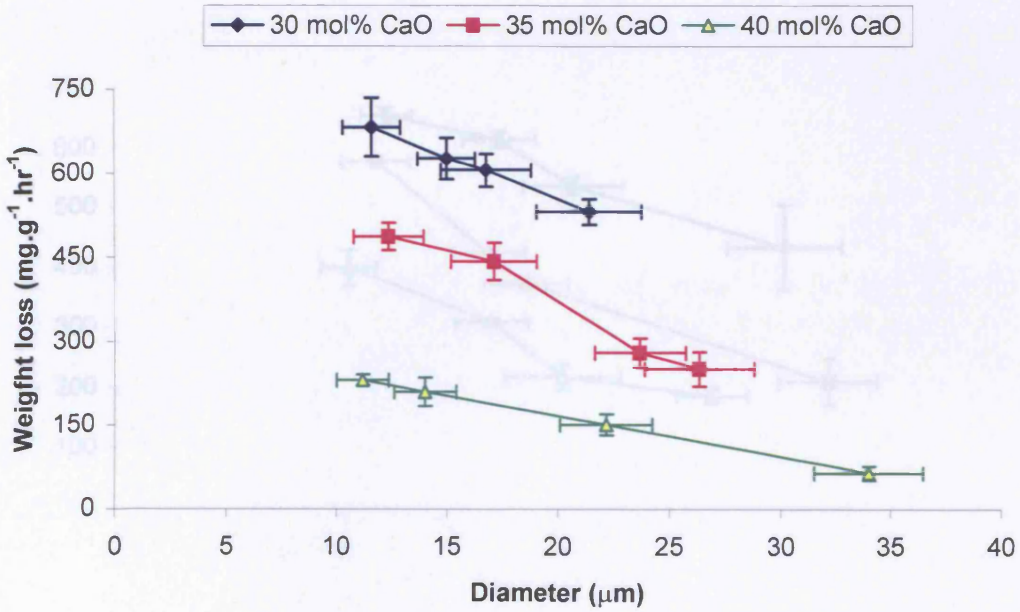

Figure 6.15: Glass-fibre dissolution rates for compositions with fixed 3 mol% SiO_2.

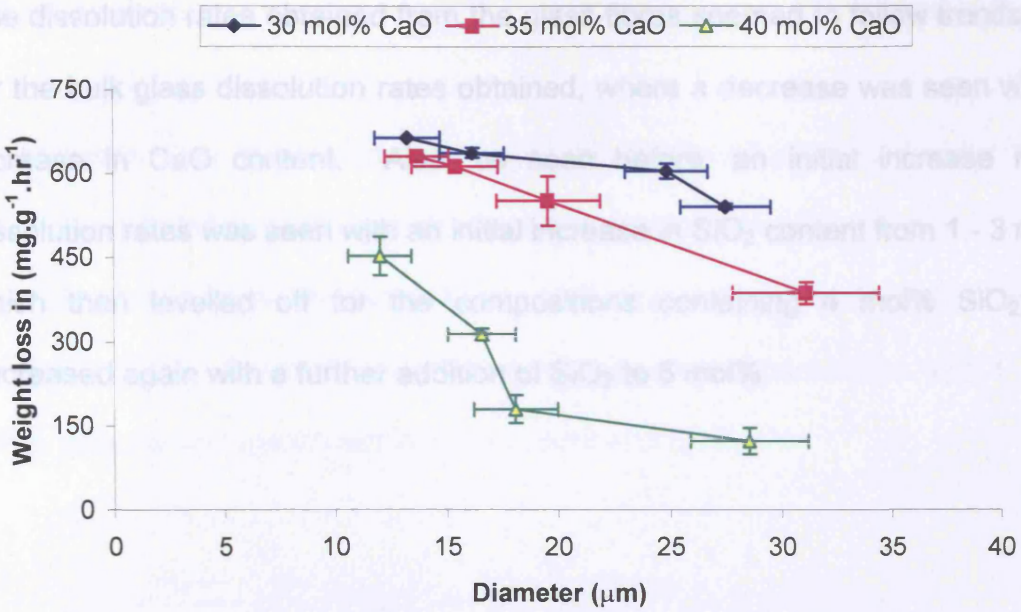

Figure 6.16: Glass-fibre dissolution rates for compositions with fixed 4 mol% SiO_2.

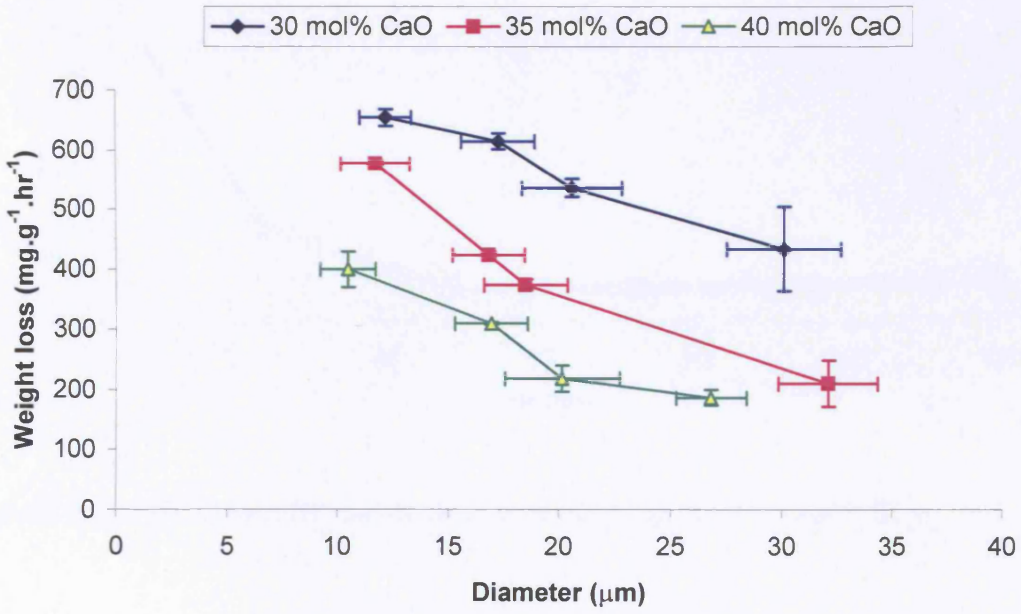

Figure 6.17: Glass-fibre dissolution rates for compositions with fixed 5 mol% SiO_2.

The dissolution rates obtained from the glass-fibres seemed to follow trends seen for the bulk glass dissolution rates obtained, where a decrease was seen with an increase in CaO content. Also, as seen before, an initial increase in the dissolution rates was seen with an initial increase in SiO_2 content from 1 - 3 mol%, which then levelled off for the compositions containing 4 mol% SiO_2, and decreased again with a further addition of SiO_2 to 5 mol%.

6.6 pH Analysis:

pH analyses were conducted on the test solution used (deionised water) within which the bulk glass dissolution studies were conducted. From the plots obtained it was seen that for all the compositions investigated the pH dropped to between pH 2 and pH 3. Examples of pH plots obtained for compositions with 1 and 5 mol% SiO_2 content are shown in Figures 6.18 and 6.19.

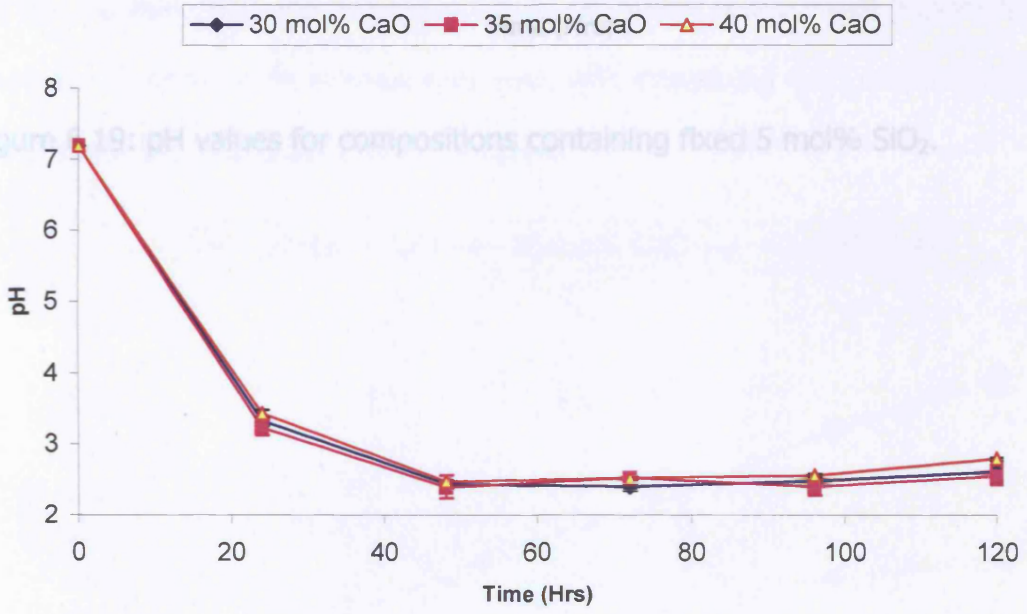

Figure 6.18: pH values for compositions containing fixed 1 mol% SiO_2.

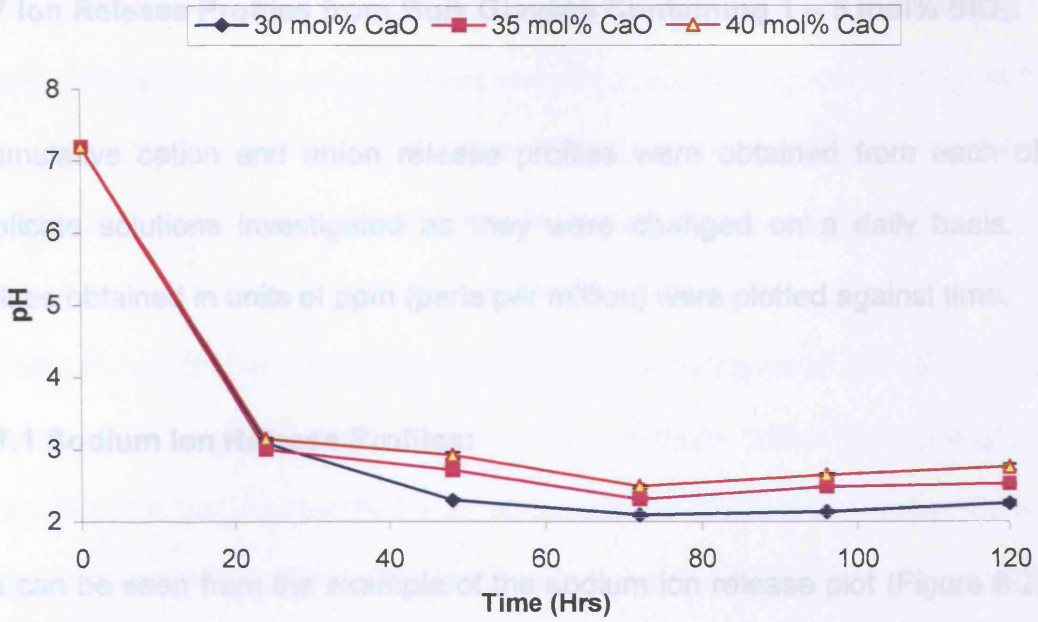

Figure 6.19: pH values for compositions containing fixed 5 mol% SiO_2.

6.7 Ion Release Profiles from Bulk Glasses Containing 1 – 5 mol% SiO_2:

Cumulative cation and anion release profiles were obtained from each of the triplicate solutions investigated as they were changed on a daily basis. The values obtained in units of ppm (parts per million) were plotted against time.

6.7.1 Sodium Ion Release Profiles:

As can be seen from the example of the sodium ion release plot (Figure 6.20), a decrease in sodium ion release was seen with increasing CaO content within the 1 – 5 mol% SiO_2 compositions investigated.

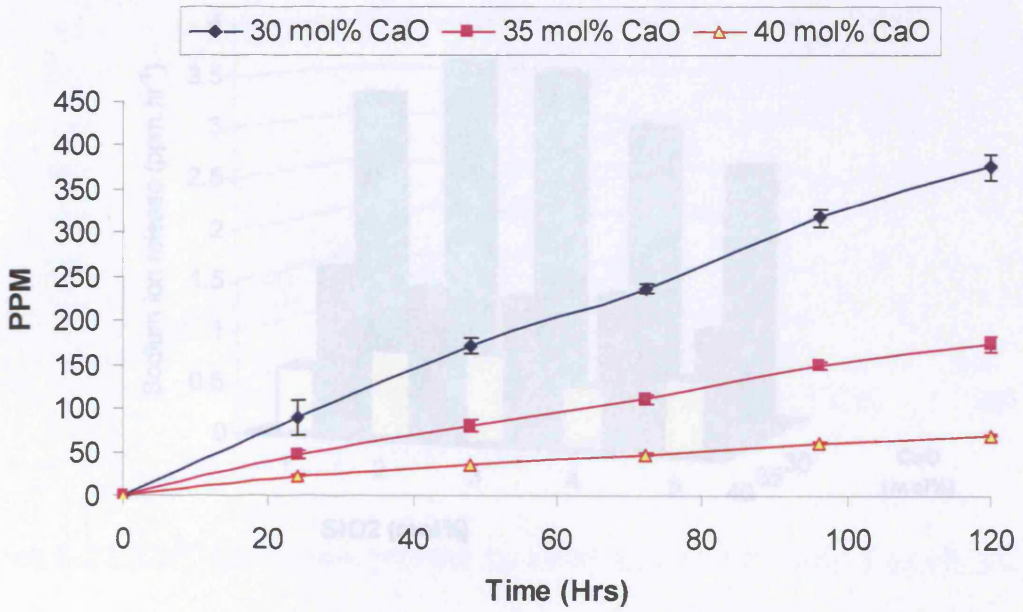

Figure 6.20: Na^+ ion release for compositions with fixed 1 mol% SiO_2.

Although a decrease was seen with increasing CaO content, the patterns seen when viewed relative to silica content showed obvious relationships (Figure 6.21). For compositions containing fixed 30 mol% CaO content, an initial increase in the sodium ion release rate was seen with increasing SiO_2 content. However, these rates then decreased with further additions of SiO_2 from 2 – 5 mol%. For compositions with fixed 35 mol% CaO, an overall decrease in the rate of release was seen for compositions ranging from 1 – 5 mol% SiO_2. Compositions with fixed 40 mol% CaO content revealed an increase in the rate of release for glasses with 1 – 3 mol% SiO_2. The rate then decreased with a further addition of SiO_2 to 4 mol%, and increased again when 5 mol% SiO_2 was added.

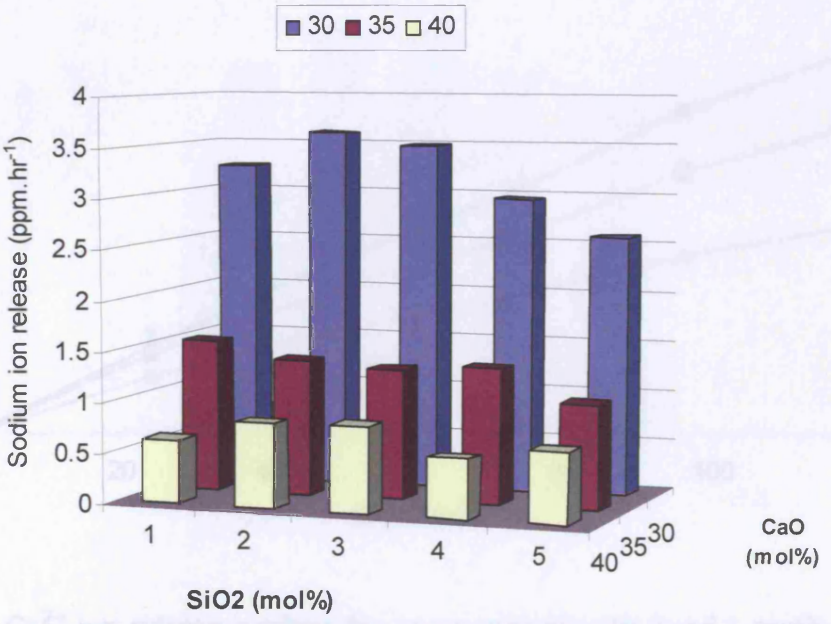

Figure 6.21: 3D Graph of Na^+ ion release profiles for glasses with fixed SiO_2 mol%.

6.7.2. Calcium Ion Release Profiles:

The calcium ion release profiles seen were very similar to the sodium ion release profiles, with a decrease in Ca^{2+} ion release observed with an increase in CaO content within the compositions (for examples of Ca^{2+} plots obtained, see Figure 6.22). The profiles seen with increasing SiO_2 content were the same as those observed for the sodium ion release. Furthermore, only slightly higher levels of Ca^{2+} ions were detected in solution as compared to the level of sodium ions detected.

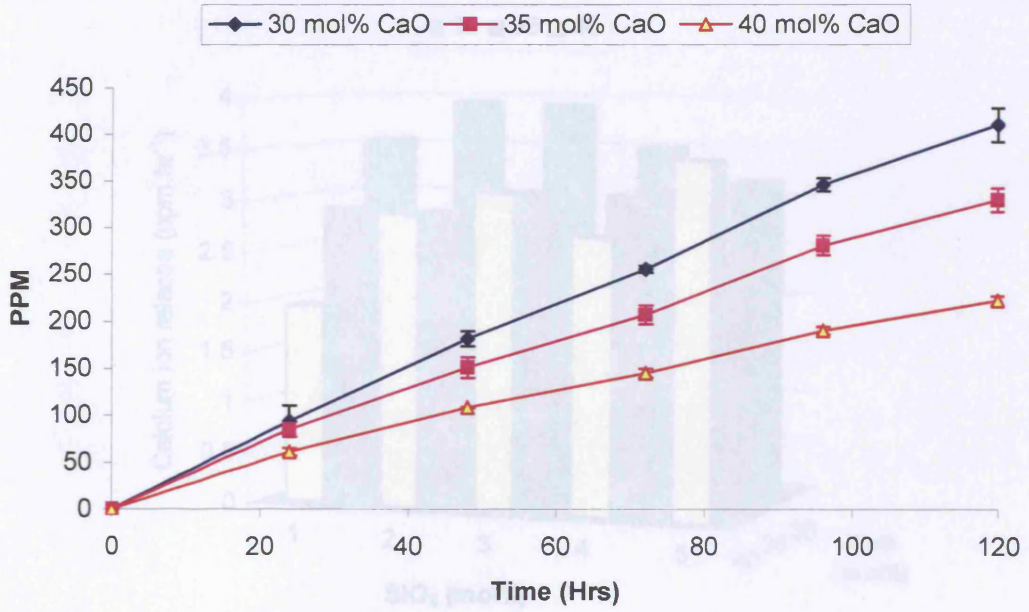

Figure 6.22: Ca^{2+} ion release profiles for compositions with fixed 1 mol% SiO_2.

Figure 6.23 shows the cumulative Ca^{2+} ion release versus compositions of varying CaO and SiO_2 contents. Compositions with fixed 30 mol% CaO content showed an initial increase in the rate of Ca^{2+} ion release. Further additions of SiO_2 from 2 – 5 mol% showed an overall decrease in the rates of Ca^{2+} ion release for these compositions. Glasses with fixed 35 mol% CaO content revealed similar profiles. For glasses with fixed 40 mol% CaO, an increase in the Ca^{2+} ion rate of release was seen for compositions containing 1 – 3 mol% SiO_2. These rates then decreased for glass code $P_{50}Ca_{40}Na_6Si_4$, and then increased again for glass code $P_{50}Ca_{40}Na_5Si_5$.

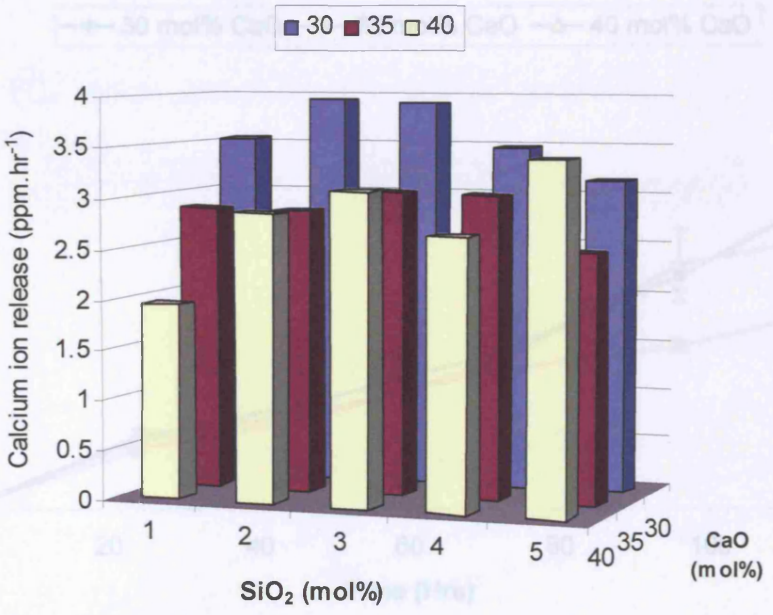

Figure 6.23: Graph of Ca^{2+} ion release rates for glasses with fixed 1 -5 mol % SiO_2.

6.7.3 Anion Release Profiles:

6.7.3.1 PO_4^{3-} Anion Release:

Anion analyses were conducted as in the previous sections, where the PO_4^{3-}, $P_2O_7^{4-}$, $P_3O_9^{3-}$ and $P_3O_{10}^{5-}$ anions were measured (see section 3.7 for structures of anions investigated). The following figures (Figures 6.24 – 6.28) represent the plots obtained for the PO_4^{3-} anion release.

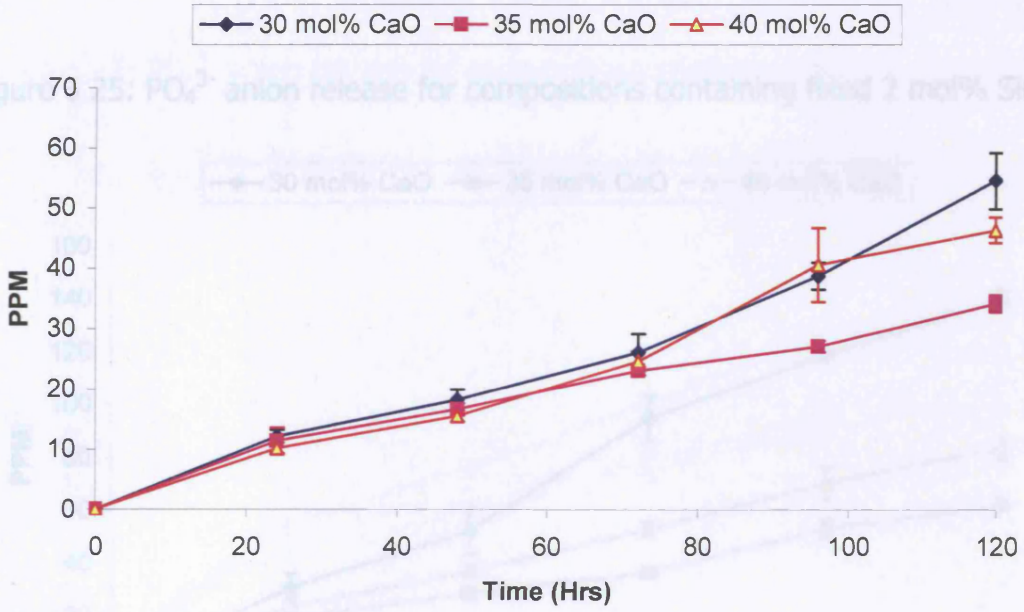

Figure 6.24: PO_4^{3-} anion release for compositions containing fixed 1 mol% SiO_2.

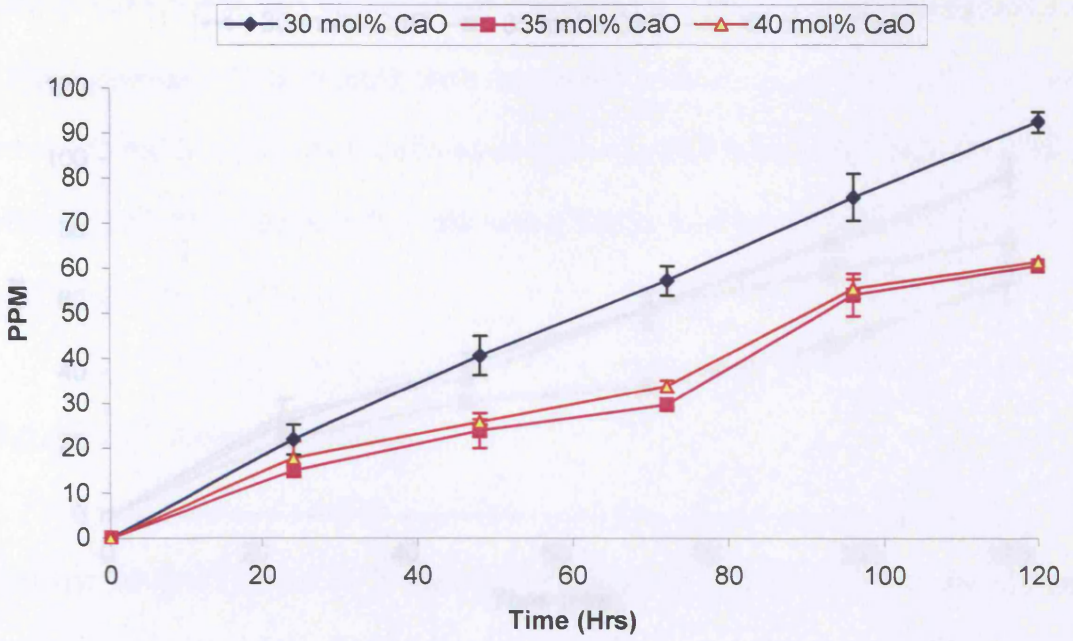

Figure 6.25: PO_4^{3-} anion release for compositions containing fixed 2 mol% SiO_2.

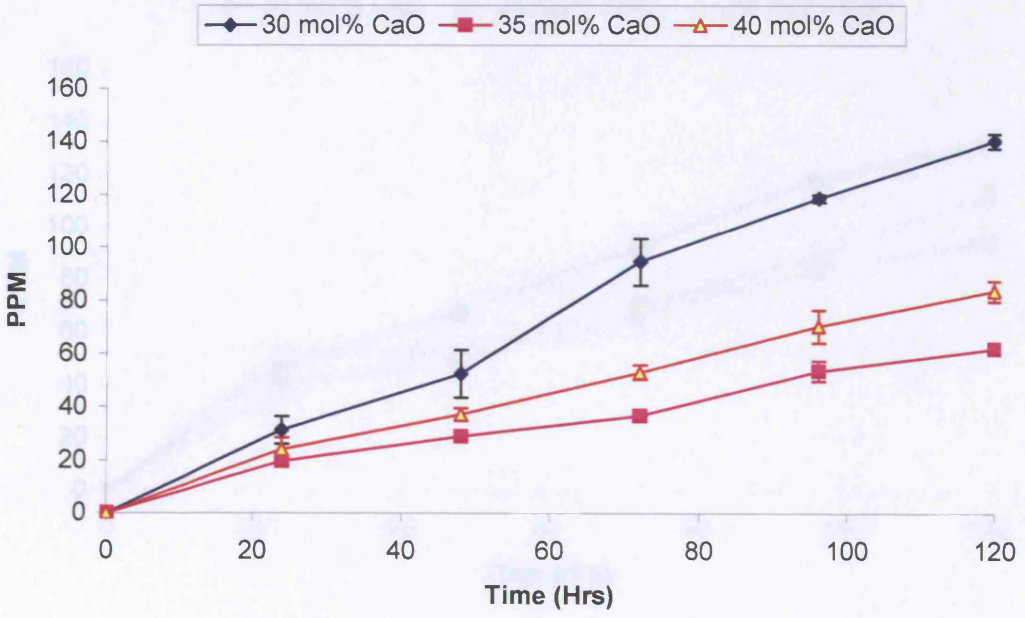

Figure 6.26: PO_4^{3-} anion release for compositions containing fixed 3 mol% SiO_2.

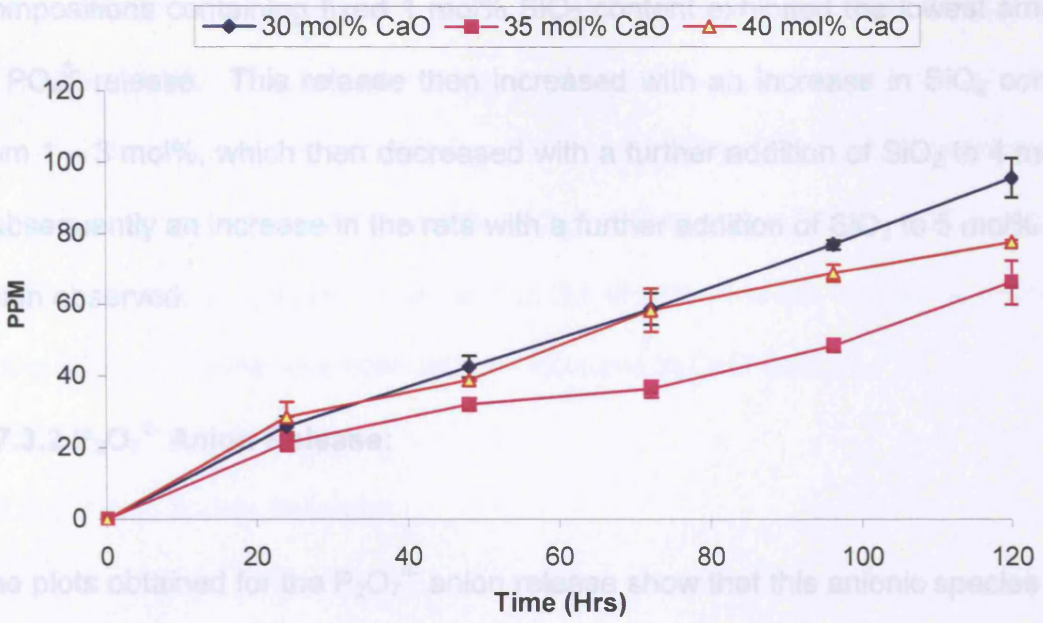

Figure 6.27: PO_4^{3-} anion release for compositions containing fixed 4 mol% SiO_2.

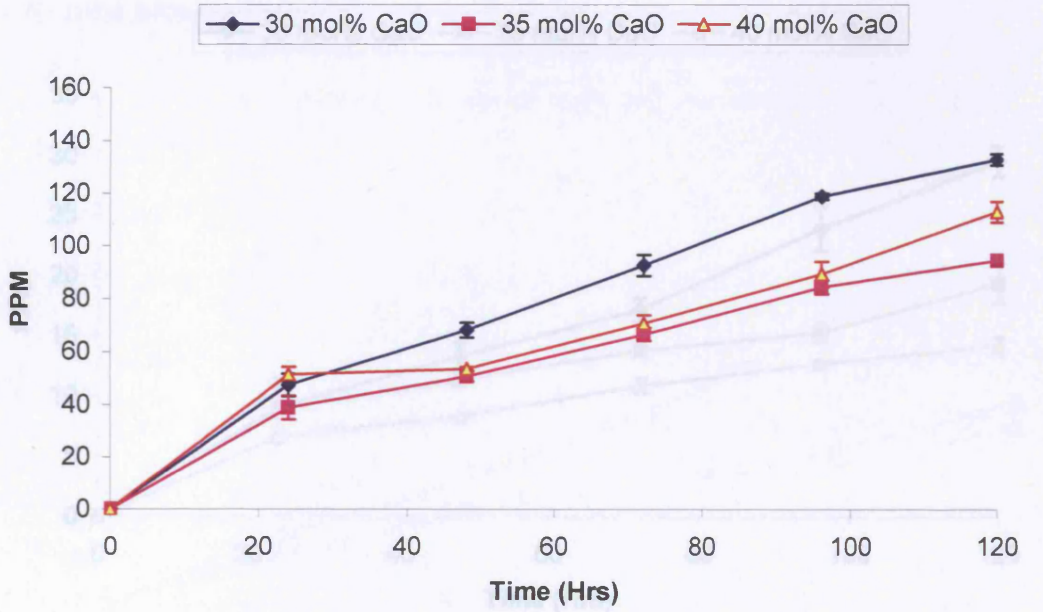

Figure 6.28: PO_4^{3-} anion release for compositions containing fixed 5 mol% SiO_2.

Compositions containing fixed 1 mol% SiO_2 content exhibited the lowest amount of PO_4^{3-} release. This release then increased with an increase in SiO_2 content from 1 – 3 mol%, which then decreased with a further addition of SiO_2 to 4 mol%. Subsequently an increase in the rate with a further addition of SiO_2 to 5 mol% was again observed.

6.7.3.2 $P_2O_7^{4-}$ Anion Release:

The plots obtained for the $P_2O_7^{4-}$ anion release show that this anionic species was released at the lowest level of all the anionic species investigated. Figure 2.29 represents an example of the $P_2O_7^{4-}$ release profiles obtained.

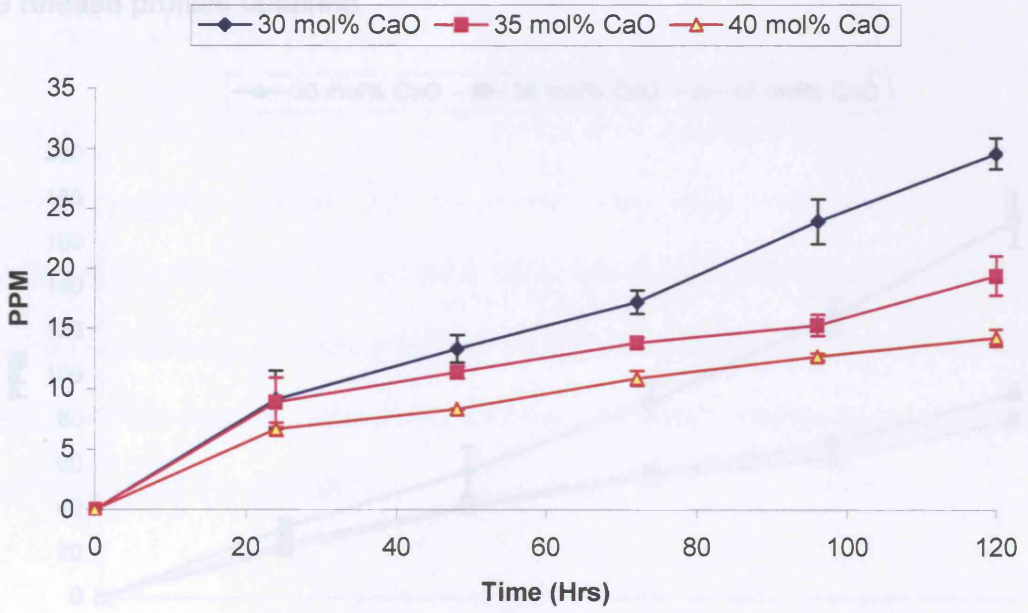

Figure 6.29: $P_2O_7^{4-}$ anion release profile for compositions containing fixed 1 mol% SiO_2.

The release profile trends seen for the $P_2O_7^{4-}$ anion release were the same as those seen for the PO_4^{3-} anionic release. A linear increase in the rates of release was seen for compositions containing 1 – 3 mol% SiO_2. This rate then decreased for compositions with fixed 4 mol% SiO_2, and increased again with a further increase in SiO_2 to 5 mol%. However, unlike the PO_4^{3-} anion release, a decrease in the rates of release was seen with an increase in CaO content.

6.7.3.3 $P_3O_9^{3-}$ Anion Release:

The $P_3O_9^{3-}$ anion was the highest released anionic species, as seen for all the glass compositions investigated. Figures 6.30 and 6.31 represent examples of the release profiles obtained.

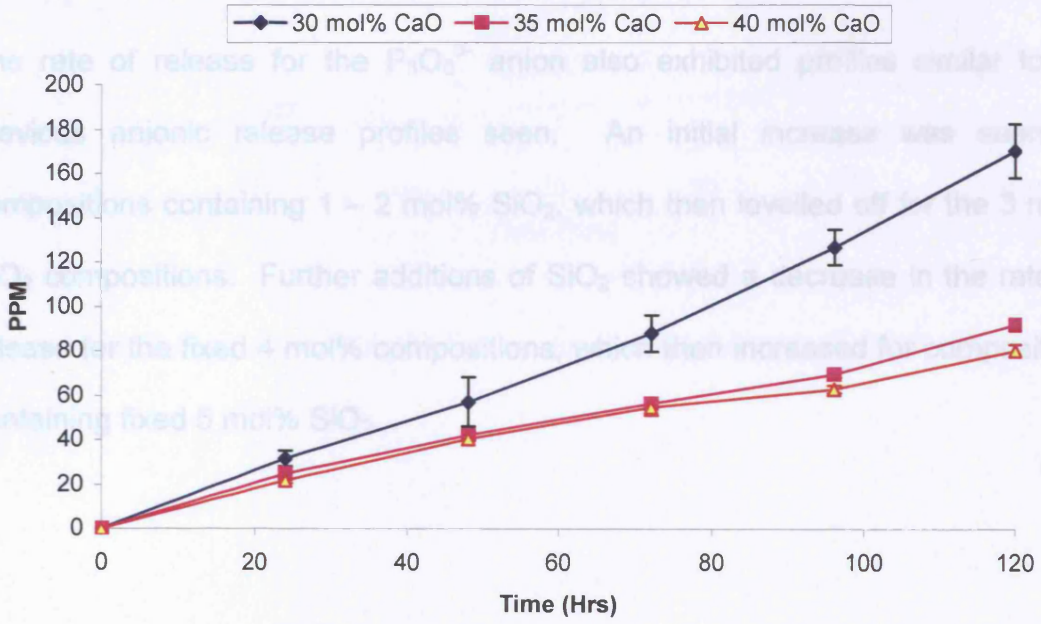

Figure 6.30: $P_3O_9^{3-}$ anion release for compositions containing fixed 1 mol% SiO_2.

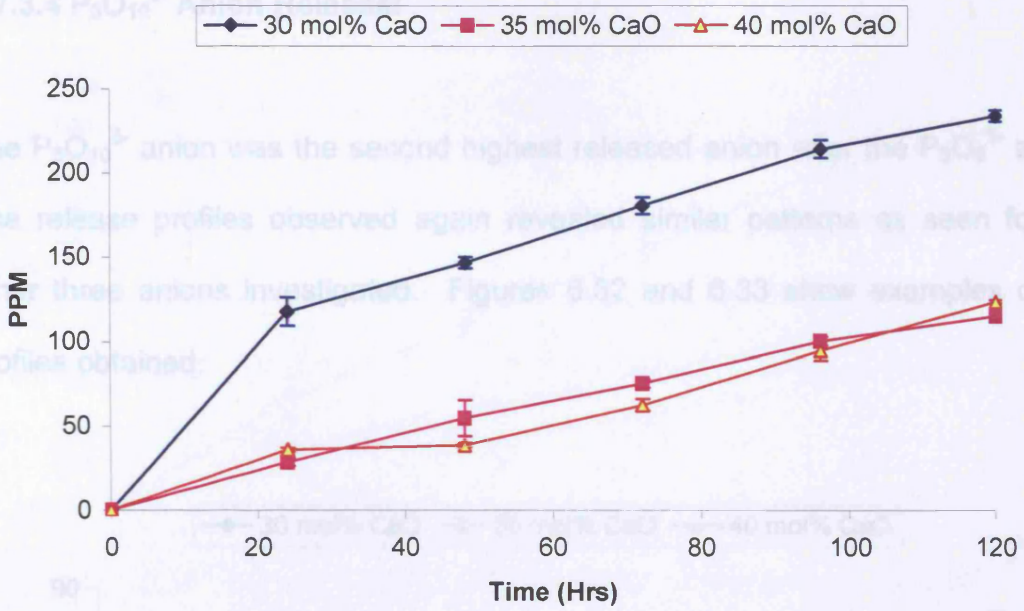

Figure 6.31: $P_3O_9^{3-}$ anion release for compositions containing fixed 5 mol% SiO_2.

The rate of release for the $P_3O_9^{3-}$ anion also exhibited profiles similar to the previous anionic release profiles seen. An initial increase was seen for compositions containing 1 – 2 mol% SiO_2, which then levelled off for the 3 mol% SiO_2 compositions. Further additions of SiO_2 showed a decrease in the rates of release for the fixed 4 mol% compositions, which then increased for compositions containing fixed 5 mol% SiO_2.

6.7.3.4 $P_3O_{10}^{5-}$ Anion Release:

The $P_3O_{10}^{5-}$ anion was the second highest released anion after the $P_3O_9^{3-}$ anion. The release profiles observed again revealed similar patterns as seen for the other three anions investigated. Figures 6.32 and 6.33 show examples of the profiles obtained.

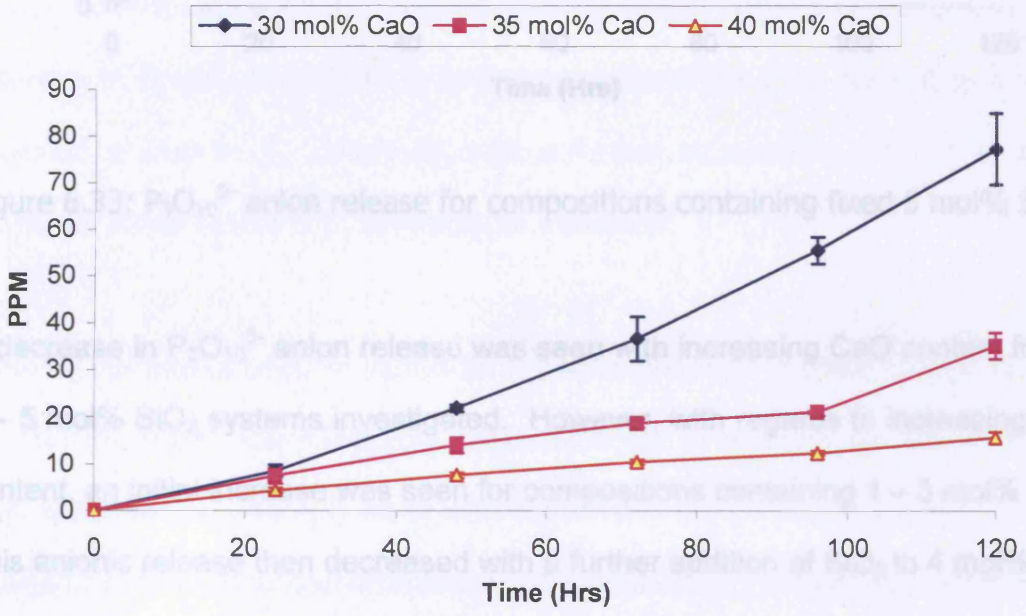

Figure 6.32: $P_3O_{10}^{5-}$ anion release for compositions containing fixed 1 mol% SiO_2.

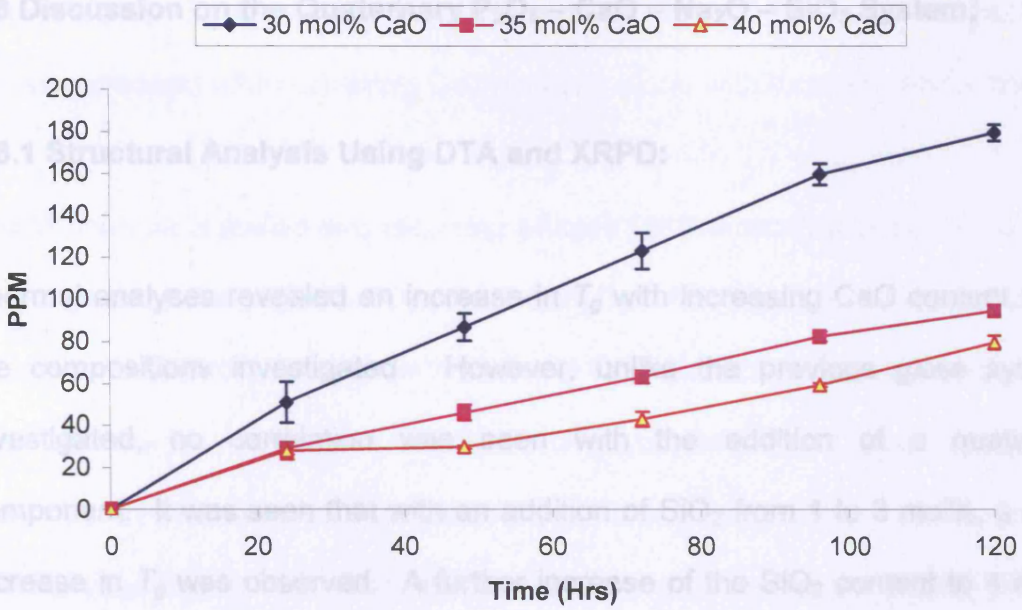

Figure 6.33: $P_3O_{10}^{5-}$ anion release for compositions containing fixed 5 mol% SiO_2.

A decrease in $P_3O_{10}^{5-}$ anion release was seen with increasing CaO content for the 1 – 5 mol% SiO_2 systems investigated. However, with regards to increasing SiO_2 content, an initial increase was seen for compositions containing 1 – 3 mol% SiO_2. This anionic release then decreased with a further addition of SiO_2 to 4 mol%, and increased again with an addition of SiO_2 to 5 mol%.

6.8 Discussion on the Quaternary P_2O_5 – CaO – Na_2O – SiO_2 System:

6.8.1 Structural Analysis Using DTA and XRPD:

Thermal analyses revealed an increase in T_g with increasing CaO content for all the compositions investigated. However, unlike the previous glass systems investigated, no correlation was seen with the addition of a quaternary component. It was seen that with an addition of SiO_2 from 1 to 3 mol%, a linear increase in T_g was observed. A further increase of the SiO_2 content to 4 mol%, revealed a drop in T_g. However, with a further increase in SiO_2 content to 5 mol%, an increase in the T_g temperature was seen.

Most of the peaks seen from the DTA traces obtained correlated well with the number of phases identified from XRPD analysis. For example, for glass code $P_{50}Ca_{30}Na_{19}Si_1$, a single T_c peak was seen along with a single T_m peak. XRPD analysis for this composition revealed the presence of a single crystalline phase. Two T_c and T_m peaks were seen for glass code $P_{50}Ca_{35}Na_{14}Si_1$, and two phases were identified from XRPD analysis. However, for glass code $P_{50}Ca_{40}Na_9Si_1$, a single T_c peak was seen from the trace obtained, along with two T_m peaks. XRPD analysis for this composition revealed the presence of two crystalline phases. For the remainder of the compositions investigated within this system, single and double T_c and T_m peaks were observed. Although two phases were identified for these compositions from XRPD analysis, only a single phase was identified for glass code $P_{50}Ca_{40}Na_5Si_5$.

Regarding the T_c values obtained it was seen that unlike the T_g values, these values increased with increasing CaO content, along with increasing SiO_2 content.

XRPD analysis revealed two recurring phases for the compositions investigated. These phases were $NaCa(PO_3)_3$ and CaP_2O_6. The CaP_2O_6 phase was seen mainly for those compositions with elevated CaO content. However, it was noted that this was the only phase identified for glass code $P_{50}Ca_{40}Na_5Si_5$. Another phase which was identified in two out of the fifteen compositions investigated was the $Si_5P_6O_{25}$ phase. This was only identified for glass codes $P_{50}Ca_{30}Na_{17}Si_3$ and $P_{50}Ca_{30}Na_{15}Si_5$. This or any other silica containing phase was not detected for any of the other compositions investigated.

In addition, unlike the other glass systems investigated, the Network Connectivity could not be calculated for these compositions as no appropriate hypothesis was formulated. The lack of a hypothesis was due to insufficient information regarding the reaction between a P^{5+} ion and a Si^{4+} ion, and also due to the non-linear data obtained.

6.8.2 Degradation rates, pH and Ion Release Profiles:

The dissolution rates obtained exhibited similar trends to the T_g values observed, in that a decrease was seen with increasing CaO content. However, with regards to the addition of silica, an initial increase in the dissolution rates was seen with increasing SiO_2 content. The rates then decreased when the SiO_2 content reached 4 mol%. With a further addition of SiO_2 to 5 mol% it was seen that the rates increased again to the same level as the 1 mol% SiO_2 compositions.

The dissolution rates seen for the glass-fibres also exhibited similar patterns as those mentioned above. The dissolution rates of the glass-fibres (as well as the bulk glasses) were very much higher than the boron and iron quaternary systems investigated. The highest dissolution rate (i.e. highly soluble) obtained for the bulk glasses from all the glass systems investigated was from the ternary $P_{50}C_{30}N_{20}$ composition. The dissolution rate obtained for this composition was 0.0019 $mg.mm^{-2}.hr^{-1}$. However, the highest dissolution rate obtained from the silica compositions was for glass code $P_{50}Ca_{30}Na_{17}Si_3$. The dissolution rate for this glass was 0.0046 $mg.mm^{-2}.hr^{-1}$, i.e. more than twice as soluble as the ternary composition mentioned above. The silica based glass fibre compositions were also more than twice as soluble as the ternary compositions investigated.

The pH profiles of the silica compositions investigated in deionised water showed that the pH dropped to very low values of around pH 2 for all the compositions investigated. The low values obtained suggested that the glasses were undergoing rapid dissolution, and this was verified from the high dissolution rates obtained.

The ion release profiles showed that the sodium and calcium ions were released into solution in relatively large amounts, suggesting that these ions were the first products of dissolution. Calcium ions were released in slightly higher quantities than were the sodium ions.

The anion release profiles revealed that the $P_3O_9^{3-}$ anion was again the highest released anion out of the four anions investigated. The release profiles for this anion were almost identical to the profiles seen for the cations. The high release profiles seen for this anion were expected as the $NaCa(PO_3)_3$ phase was detected via XRPD for all the compositions investigated, with the exception of glass code $P_{50}Ca_{40}Na_5Si_5$.

The PO_4^{3-} anion was also detected in relatively large amounts. This anion is usually the remnant of breakdown from the other phosphate ions that are released into solution upon degradation. However, from the amounts released it appears that this anion was either present in the glass structure of the compositions investigated, or that the higher phosphate species in solution were undergoing rapid hydrolysis.

The $P_2O_7^{4-}$ anion was released at the lowest levels, followed by the $P_3O_{10}^{5-}$ anion. These anions are linear in structure, and the rate of release profiles for these anions mirrored those observed from the PO_4^{3-} anion release, along with the bulk glass weight loss profiles seen.

From the observations seen above, it was clear that the addition of 1 – 5 mol% of SiO_2 into the ternary P_2O_5 – CaO – Na_2O glass structure caused significant disruption of the glass network.

Nagase *et al* (128) examined the intraperitoneal toxicity of calcium phosphate glass containing various concentrations of silica in mice. Calcium phosphate glasses containing large amounts of silica were said to be toxic. Nagase *et al* went on to state that the release of Si^{4+}, Ca^{2+} and P^{5+} ions in water from the calcium phosphate glass depended on the amount of silica in the glasses. The dissolved silica (Si^{4+}) was said to be monomeric, and/or not highly polymerised. They went on to suggest that the concentration of this monomeric or low molecular silica ion determined the toxicity of the materials, but the total content of non-dissolved silica had no relation to its toxicity.

Larsen *et al* (129) investigated phosphate based glasses based on the 2MgO – Al_2O_3 – 3.3 P_2O_5 glass system, with increasing SiO_2 content from 0, 5, 12, 18, 24 and 30 mol%. Their studies on the structural effect of the addition of SiO_2 to the binary sodium phosphate system revealed that no change was found in the phosphate structures after SiO_2 addition to compositions having a constant

$Na_2O:P_2O_5$ ratio. For these compositions it was concluded that the silicate structures scavenged the non-bridging Na^+ ions, thus implying the presence of discrete silicate structures. It was also interesting to note from their study conducted that, even for the compositions with the highest amount of SiO_2 content (up to 30 mol%) no silica containing phase was identified from the XRPD analyses.

As seen from the XRPD results obtained for the SiO_2 glass system investigated, only 2 out of the 15 compositions investigated revealed the presence of a silicon phase. These were compositions with glass codes $P_{50}Ca_{30}Na_{17}Si_3$ and $P_{50}Ca_{30}Na_{15}Si_5$. These compositions consequently exhibited the highest dissolution rates. If the silicate was indeed scavenging the Na^+ ions, and discrete silicate structures were being formed, this would have accounted for some of the lack of silica phases identified via XRPD analysis. However, another possible explanation was that some if not most of the silica remained in an amorphous phase/state. Sayer *et al* (130) investigated the structure and composition of silicon-stabilised tricalcium phosphate. It was stated that the resulting calcium phosphate was modified by the incorporation of silica into its structure with the excess silica contributing to an amorphous component. If the silica did remain in an amorphous phase, this would also have accounted for the lack of silicon phases identified from XRPD analysis.

Furthermore, as stated earlier, the silica based phase identified from XRPD analysis was the SiP_6O_{25} phase. The structural characterisation of this phase was

conducted by Poojary *et al* (131). They stated that there were three crystallographically distinct silicon atoms in the structure, all positioned along the *c* axis of the crystal. Silicon 1 (Si1) lay on a three-fold axis and was octahedrally coordinated by symmetry related oxygen atoms. Silicon 2 (Si2) also lay on a three fold axis and its six coordination sites were also occupied by symmetry related oxygen atoms. Si1 and Si2 were said to be bridged to each other via three phosphate groups. Silicon 3 (Si3) also lay on a three fold axis; however, Si3 was said to have a tetrahedral coordination. These tetrahedrally bonded silicons were centred and were indirectly connected through octahedrally bonded silicon groups, and this arrangement led to small voids between Si2 and Si3 groups. All the phosphate oxygens were bonded to silicon as well, so that there were no Si-OH or P-OH groups in the structure. It was also suggested that these groups existed at the surface due to unfulfilled bridging.

The SiP_6O_{25} phase, being present at or near the surface of the glass, would therefore account for the high dissolution rates obtained for the two compositions mentioned above, from which the SiP_6O_{25} phase was identified via XRPD analysis. Also, the development of voids would account for the increase in the dissolution rates observed with increasing SiO_2 content, as water could easily penetrate the structure and hence disrupt the phosphate chains and/or rings present. It was probably more likely that the silica additions had produced two effects: (i) a more open glass structure and (ii) bonds that were more sensitive to moisture.

Shan and Jijian (132) investigated the dissolution products of a phosphate glass scale inhibitor and its scale inhibition mechanism. The composition they investigated was 50 mol% P_2O_5, 30 mol% Na_2O, 18 mol% CaO and 2 mol% SiO_2. They stated that the weight loss of the glass was proportional to the dissolution time. They went on to state that the dissolution of the glass in water was controlled by the hydrolysis and hydration reaction, with the hydration reaction dominating the dissolution process. However, no further information was given as to the effect of silica on or in the glass composition investigated.

As has been discussed in the previous chapters, the hydration reaction readily occurs at the surface of the glass, when water diffuses into the glass and a hydrated layer forms on the surface. The long linear PO_4^{3-} chains in the hydrated layer then become entirely surrounded by water, which disrupt the ionic bonds between the phosphate chains. These totally hydrated chains then disentangle from the hydrated layer and float off into solution.

Summary:

In brief, the addition of SiO_2 from between 1-5 mol% into the structure totally disrupted the phosphate glass network, and it has been suggested that this was due to the development of voids within the structure. Thus it was suggested that additions of SiO_2 had produced two effects: (i) a more open glass structure and (ii) bonds that were more sensitive to moisture.

CHAPTER 7

Summary of Thesis

7.0 Summary of Thesis:

The original bulk glass compositions used were based on the ternary P_2O_5 – CaO- Na_2O glass system. This system was composed of ionic components already present within the body and therefore minimal inflammatory responses were expected. In addition this system had already been investigated within the department, where the P_2O_5 content of the glasses was fixed at 45 mol%, with the CaO and Na_2O mol% making up the remainder. Initial studies revealed that glass-fibres could not be produced from these compositions, and this was attributed to the structure of the glasses. It was ascertained that the network connectivity and cross-link density of these compositions led to the formation of short chain lengths within the glass structure, which in turn contributed to a high viscosity from which fibres could not be obtained. It was also found that the network connectivity calculated for these compositions correlated well with the NMR data obtained, with regards to the Q^n species identified.

The composition of the ternary glasses was altered starting with the phosphate content, which was increased to 50 and 55 mol% P_2O_5 (again with the CaO and Na_2O making up the remainder). Glass-fibres were successfully produced from these compositions, and thus it was ascertained that a minimum of 50 mol% P_2O_5 was required for fibre production. Again, using the Network Connectivity calculations, good correlation with NMR was also obtained.

No literature was found on phosphate anion release studies using ion chromatography analysis; therefore, this also became a novel aspect of the project. Using ion chromatography analysis the rates of release of the individual anionic species, within the different compositions investigated were ascertained. Also, hypotheses were proposed for using a Response Factor to calculate the amounts of the additional (higher) phosphate species seen in the chromatograms obtained. However, biocompatibility studies revealed that these ternary compositions were too soluble for cell attachment and proliferation to occur.

A quaternary component was therefore added in order to reduce the degradation rates obtained. The first quaternary component added was B_2O_3 (boric oxide). This was added firstly due to the fact that B_2O_3 was a well known glass former, and secondly it was also potentially relevant biologically. The degradation analyses conducted revealed that B_2O_3 did indeed reduce the degradation rates obtained, as compared to the rates obtained from the ternary compositions investigated. From XRPD studies conducted it was seen that the detection of a BPO_4 phase, showed that boron was present within the backbone (P-O-P) structure of the glasses investigated. This therefore accounted for the reduction in degradation rates obtained. However, these compositions also proved to be too soluble for cell attachment and proliferation.

A further quaternary component investigated was iron oxide (Fe_2O_3), due to iron being a naturally occurring ion within the body. Thus no inflammatory responses were expected. Fe_2O_3 was incorporated at 1 – 5 mol% substituted for Na_2O. An

order of magnitude difference was seen with the degradation rates from 1 – 5 mol% Fe_2O_3. Furthermore, studies conducted with collaborators showed that 4 – 5 mol% Fe_2O_3 was sufficient for successful cell attachment and proliferation of muscle precursor cells on the fibres produced (72). The biocompatibility was attributed to the chemical durability of the fibres obtained, which in turn was due to the presence of Fe^{3+} within the compositions. Fe^{3+} was suggested to be present in distorted tetrahedral and octahedral coordination within the backbone of the phosphate network.

The final series of glasses investigated looked at the incorporation of silicon (SiO_2) as a quaternary component. SiO_2 was incorporated at 1 - 5 mol%, again in place of the Na_2O. It was found that SiO_2 totally disrupted the glass network, and it was suggested that this was due to the development of voids within the structure. These voids may account for the increase in the dissolution rates observed with increasing SiO_2 content, as water could easily penetrate the structure and hence disrupt the phosphate chains and/or rings present. It was thus suggested that additions of SiO_2 had produced two effects: (i) a more open glass structure and (ii) bonds that were more sensitive to moisture.

In parallel studies the produced phosphate glass fibres were evaluated for their biocompatibility properties. These studies were mainly conducted in collaboration with the Hammersmith Hospital, London (72). The initial objective of the project was to attach muscle cells to the fibres, in order to formulate alternative therapies for diseases such as muscular dystrophy. However, as the project progressed

other cell types such as fibroblasts, collagen, nerve cells and even spinal cord cells were being evaluated for the biocompatibility of the glass-fibres produced.

7.1 Future Work:

In future studies, one of the initial aspects that could be investigated would be to look at incorporating other ions into the original ternary composition. For example, ions that could possibly have further biological properties. The formation of composites, such as polymer composites using the fibres produced within these studies, could also be investigated in order to reduce or even increase the degradation properties of some commercial polymers already used in the field of Biomaterials. In addition, tailoring of the fibres (topography) to have specific surface roughness could also contribute to a more biocompatible phosphate fibre.

There are also a number of other improvements that could be conducted that would lead to technical products, example being textile products from the fibres produced.

One of the future aspects of the study would be to investigate methods of fibre spacing onto the drum. Some literature reports had suggested that fibre spacing was important in order to achieve satisfactory cell attachment onto fibre scaffolds. Mastering this technology could possibly lead to 3D fibrous bodies, which could find application as Tissue Engineering substrates.

Other avenues that could also be explored would be to coat the fibres with various substances as they were being pulled onto the drum. This would involve the creation of a new mechanical device which could be utilised for this purpose. The substances used to coat the fibres could be as vast and varied as a liquid polymer, Hydroxyapatite (HA), or even biological products such as fibronectin, and even collagen.

CHAPTER 8

References

8.0 References:

(1) Kurkjian CR, Prindle WR. Perspectives on the History of Glass Composition. Journal of the American Ceramics Society 1998; 81(4):795-813.

(2) Goldschmidt VM. Investigation Concerning Structure and Properties of Crystals. Skr Nor Vidensk-Akad Kl 1: Mat Naturvidensk Kl 1926; 8:130.

(3) Zachariasen WH. The Atomic Arrangement in Glass. American Chemical Society 1932; 54(3):3841-3851.

(4) Hagg G. The Vitreous State. Journal of Chem Phys 1935; 3:42-49.

(5) Cooper AR. W.H. Zachariasen - The Melody Lingers On. Journal of Non-Crystalline Solids 1982; 49:1-17.

(6) Warren BE, Krutter H, Morningstar O. Fourier Analysis of X-Ray Patterns of Vitreous SiO_2 and B_2O_3. Journal of the American Ceramics Society 1936; 19:202-206.

(7) Franks K. The Structure and Properties of Soluble Phosphate Based Glasses. 2000.

(8) Stokes GG. Notice of the Researches of the late Rev. William Vernon Harcourt, on the Conditions of Transparency in Glass, and the Connexion Between the Chemical Constitution and Optical Properties of Different

Glasses. Report of the British Association for the Advancement of Science 1871.

(9) Kriedl NJ, Weyl WA. Phosphates in Ceramic Ware: IV, Phosphate Glasses. Journal of the American Ceramics Society 1941; 24:372-378.

(10) Weber MJ. Science and Technoloy of Laser Glass. Journal of Non-Crystalline Solids 1990; 123:208-222.

(11) Tick PA. Water Durable Glasses with Ultra Low Melting Temperatures. Physics and Chemistry of Glasses 1984; 25(6):149-154.

(12) Brow RK, Phifer CC, Xu XJ, Day DE. An X-Ray Photoelectron Spectroscopy Study of Anion Bonding in Tin (II) Fluorophosphate Glass. Physics and Chemistry of Glasses 1992; 33(2):33-39.

(13) Wazer JRV, Holst KA. Structures and Properties of the Condensed Phosphates. I. Some General Considerations About Phosphoric Acids. Journal of the American Ceramics Society 1950; 72(2):639-643.

(14) Wazer JRV. Structure and Properties of the Condensed Phosphates. II. A Theory of the Molecular Structure of Sodium Phosphate Glasses. Journal of the American Ceramics Society 1950; 72(2):644-647.

(15) Wazer JRV. Structure and Properties of the Condensed Phosphates III. Solubility Fractionation and Other Solubility Studies. Journal of the American Ceramics Society 1950; 72(2):647-655.

(16) Wazer JRV, Campanella DA. Structure and Properties of the Condensed Phosphates IV. Complex Ion Formation in Polyphosphate Solutions. Journal of the American Ceramics Society 1950; 72(2):655-662.

(17) Griffith EJ. New Sodium Phosphates. Journal of the American Chemical Society 1956; 78(16):3867-3871.

(18) Ondik HM, Block S, MacGillavry CH. The Structure of the Monoclinic Form of Sodium Tetrametaphosphate Tetrahydrate. Acta Crystallogr 1961; 14:555-561.

(19) Ondik HM. The Structure of the Triclinic Form of Sodium Tetrametaphosphate Tetrahydrate. Acta Crystallogr 1964; 17:1139-1142.

(20) Grenier JC, Martin C, Durif A. Nouvelle Etude Du Diagramme D'Equilibre $Ca(PO_3)_2$-$NaPO_3$. Donnees Cristallographiques Sur $CaNa_4(PO_3)_6$ et $CaNa(PO_3)_3$. Bull Soc Fr Mineral Cristallogr 1970; 93:52-55.

(21) Duriff A. Chimie Minerale: Donnees Cristallograhiques sur le Trimetaphosphate de Calcium-Sodium Trihydrate: $CaNaP_3O_9.3H_2O$. C R Acad Sc Paris 1972; 275(Serie C.):1379-1382.

(22) Averbouch-Pouchot MT, Durif A. Structure of Tetrapotassium Tetrametaphosphate Tetrahydrate. Acta Crystallographica Section C 1985; 41(9 - 12):1564-1566.

(23) Durif A. Crystal Chemistry of Condensed Phosphates. Kluwer Academic / Plenum Publishers., 1995.

(24) Averbouch-Pouchot MT, Durif A. Topics in Phosphate Chemistry. World Scientific Publishing., 1996.

(25) Schulke U, Averbouch-Pouchot MT, Durif A. Crystal Structure of Sodium Cyclo-octaphosphate Hexahydrate, $Na_8P_8O_{24}.6H_20$. Journal of Solid State Chemistry 1992; 98:213-218.

(26) Averbouch-Pouchot MT. $CaNa_2P_4O_{12}$, A New Compound in the $Ca(PO_3)_3$ - $NaPO_3$ System. European Journal Solid State Inorganic Chemistry 1996; 33:15-18.

(27) McAdam A, Jost K, Beagley B. Refinement of the Structure of Sodium Hexametaphosphate Hexahydrate, $Na_6(P_6O_{18}).6H_2O$. Acta Crystallogr 1972; B 28:2740-2743.

(28) Jost H, Von K. Die Struktur des Natrium-Hexametaphosphates $Na_6(P_6O_{18}).6H_2O$. Acta Crystallogr 1965; 19:555-560.

(29) Ben-Chaabane T, Smiri-Dogguy L, Laligant Y, Le-Bail A. LiP_6O_{18}: X-Ray Powder Structure Determination of Lithium Cyclohexaphosphate. European Journal Solid State Inorganic Chemistry 1998; 35:255-264.

(30) Ben Amara M, Vlasse M, Le Flem G, Hagenmuller P. Structure of the Low-Temperature Variety of Calcium Sodium Orthophosphate, $NaCaPO_4$. Acta Crystallogr 1983; C39:1483-1485.

(31) Webb NC. The Crystal Structure of B-CaP_2O_7. Acta Crystallogr 1966; 21:942-948.

(32) Hudgens JJ, Martin SW. Glass Transition and Infra-Red Spectra of Low-Alkali, Anhydrous Lithium Phosphate Glasses. Journal of the American Ceramics Society 1993; 76(7):1691-1696.

(33) Suzuya K, Price DL, Loong CK, Martin SW. Sructure of Vitreous P_2O_5 and Alkali Phosphate Glasses. Journal of Non-Crystalline Solids 1998; 232-234:650-657.

(34) Uo M, Mizuno M, Kuboki Y, Makishima A, Watari F. Properties and Cytotoxicity of Water Soluble Na_2O-CaO-P_2O_5 Glasses. Biomaterials 1998; 19:2277-2284.

(35) Shih PY, Yung SW, Chin T-S. Thermal and Corrosion Behaviour of P_2O_5 - Na_2O - CuO Glasses. Journal of Non-Crystalline Solids 1998; 224:143-152.

(36) Bell RN, Audrieth LF, Hill OF. Preparation of Sodium Tetrametaphosphate. Industrial and Engineering Chemistry 1952; 44(1):568-572.

(37) Strauss UP, Treitler TL. Chain Branching in Glassy Phosphates: Dependance on the Na/P Ratio and Rate of Degradation at 25°C. Journal 1955; 77:1473-1476.

(38) Crowther J, Westman AER. The Hydrolysis of the Condensed Phosphates.III. Sodium Tetrametaphosphate and Sodium Tetraphosphate. Canadian Journal of Chemistry 1956; 34(2):969-981.

(39) Bunker BC, Arnold GW, Wilder JA. Phosphate Glass Dissolution in Aqueous Solutions. Journal of Non-Crystalline Solids 1984; 64:291-316.

(40) Martin SW. Review of the Structures of Phosphate Glasses. European Journal Solid State Inorganic Chemistry 1992; 28:163-205.

(41) Brow RK, Kirkpatrick RJ, Turner GL. The Short Range Structure of Sodium Phosphate Glasses I. Mas NMR Studies. Journal of Non-Crystalline Solids 1990; 116:39-45.

(42) Hartmann P, Vogel J, Schnabel B. NMR Study of Phosphate Glasses and Glass Ceramic Structures. Journal of Non-Crystalline Solids 1994; 176:157-163.

(43) Kirkpatrick RJ, Brow RK. Nuclear Magnetic Resonance Investigation of the Structures of Phosphate and Phosphate-Containing Glasses: A Review. Solid State Nuclear Magnetic Resonance 1995; 5:9-21.

(44) Abrahams I, Hawkes GE, Knowles JC. Phosphorous Speciation in Sodium - Calcium - Phosphate Ceramics. J Chem Soc Dalton Trans 1997;1483-1484.

(45) Abrahams I, Franks K, Hawkes GE, Philippou G, Knowles JC, Bodart P et al. ^{23}Na, ^{27}Al, ^{31}P NMR and X-Ray Powder Diffraction Study of Na/Ca/Al Phosphate Glasses and Ceramics. Journal Materials Chemistry 1997; 7(8):1573-1580.

(46) Hoppe U. A Structural Model for Phosphate Glasses. Journal of Non-Crystalline Solids 1996; 195:138-147.

(47) Hoppe U, Walter G, Kranold R, Stachel D, Barz A. X-Ray Diffraction Study on the Mixed Alkali-Alkaline Earth Effect in Ba, Na Metaphosphate Glasses. Journal of Non-Crystalline Solids 1998; 224:153-162.

(48) Kranold R, Walter G, Lembke U, Rieker Th, Stachel D. The Intermediate Range Order of Metaphosphate Glasses by X-Ray Diffraction. Journal of Non-Crystalline Solids 1998; 232-234:502-508.

(49) Brow RK. Review: The Structure of Simple Phosphate Glasses. Journal of Non-Crystalline Solids 2000; 263&264:1-28.

(50) Pemberton JE, Latifzadeh L. Raman Spectroscopy of Calcium Phosphate Glasses with Varying CaO Modifier Concentrations. Chem Mater 1991; 3(1):195-200.

(51) Meyer K. Characterisation of the Structure of Binary Calcium Ultraphosphate Glasses by Infra-Red and Raman Spectroscopy. Physics and Chemistry of Glasses 1998; 39(2):108-117.

(52) Hudgens JJ, Brow RK, Tallant DR, Martin SW. Raman Spectroscopy Study of the Structure of Lithium and Sodium Ultraphosphate Glasses. Journal of Non-Crystalline Solids 1998; 223:21-31.

(53) Shih PY, Yung SW, Chin T-S. FTIR ad XPS Studies of P_2O_5 - Na_2O - CuO Glasses. Journal of Non-Crystalline Solids 1999; 244:211-222.

(54) Peitl O, Zanotto ED, L.L.Hench. Highly Bioactive P_2O_5-Na_2O-CaO-SiO_2 Glass Ceramics. Journal of Non-Crystalline Solids 2001; 292:115-126.

(55) Hoppe U, Walter G, Kranold R, Stachel D. Structural Specifics of Phosphate Glasses Probed by Diffraction Methods: A Review. Journal of Non-Crystalline Solids 2000; 263 & 264:29-47.

(56) Hoppe U, Kranold R, Stachel D, Barz A, Hannon AC. Variation in P - O Bonding in Phosphate Glasses - A Neutron Diffraction Study. Z Naturforsch 2000; 55 a:369-380.

(57) Walter G, Vogel J, Hoppe U, Hartmann P. The Structure of $CaO\text{-}Na_2O\text{-}MgO\text{-}P_2O_5$ Invert Glass. Journal of Non-Crystalline Solids 2001; 296:212-223.

(58) Sales BC, Otaigbe JU, Bealll GH, Boatner LA, Ramey JO. Structure of Zinc Polyphosphate Glasses. Journal of Non-Crystalline Solids 1998; 226:287-293.

(59) Sales BC, Boatner LA, Ramey JO. Chromatographic Studies of the Structures of Amorphous Phosphates: A Review. Journal of Non-Crystalline Solids 2000; 263+264:155-166.

(60) Drake CF, Allen WM. The Use of Controlled-Release Glass for the Controlled Delivery of Bioactive Materials. Biochemical Society transactions 1985; 13:516-520.

(61) Franks K, Abrahams I, Knowles JC. Development of Soluble Glasses for Biomedical Use. Part 1:*In Vitro* Solubility Measurements. Journal of Materials Science: Materials in Medicine 2000; 11:609-614.

(62) Salih V, Franks K, James M, Abrahams I, Hastings GW, Knowles JC et al. Development of Soluble Glasses for Biomedical Use. Part 2: The biological response of human osteoblast cell lines to phosphate-based soluble glasses. Journal of Materials Science: Materials in Medicine 2000; 11:615-620.

(63) Franks K, Abrahams I, Georgiou G, Knowles JC. Investigation of Thermal Parameters and Crystallisation in a Ternary $CaO-Na_2O-P_2O_5$ Based Glass System. Biomaterials 2001; 22:497-501.

(64) Franks K, Salih V, Knowles JC, Olsen.I. The Effect of MgO on the Solubility Behaviour and Cell Proliferation in a Quaternary Soluble Phosphate Based Glass System. Journal of Materials Science: Materials in Medicine 2002; 13:549-556.

(65) Knowles JC, Franks K, Abrahams I. Investigation of the Solubility and Ion Release in the Glass System K_2O - Na_2O - CaO - P_2O_5. Biomaterials 2001; 22(December):3091-3096.

(66) J.C.Knowles. Phosphate-Based Glasses for Biomedical Applications. Journal of Materials Chemistry 2003; 13(10):2395-2401.

(67) Kesisoglou A, Knowles JC, Olsen.I. Effects of Phosphate-Based Glasses on T Lymphocytes *in Vitro*. Journal of Materials Science: Materials in Medicine 2002; 13:1189-1192.

(68) Gough JE, Christian P, Scotchford CA, Rudd CD, Jones IA. Synthesis, Degradation, and *In Vitro* Cell Responses of Sodium Phosphate Glasses

for Craniofacial Bone Repair. Journal of Biomedical Materials Research 2002; 59:481-489.

(69) Gough JE, Christian P, Scotchford CA, Jones IA. Long Term Craniofacial Osteoblast Culture on a Sodium Phosphate and Calcium/Sodium Phosphate Glass. Journal of Biomedical Materials Research 2003; 66A:233-240.

(70) Ahmed I, Lewis MP, Olsen.I, Knowles JC. Phosphate Glasses for Tissue Engineering: Part 2. Processing and Characterisation of a Ternary Based P_2O_5-CaO-Na_2O Glass-Fibre System. Biomaterials 2004; 25(3):501-507.

(71) Ahmed I, Lewis MP, Olsen.I, Knowles JC. Phosphate Glasses for Tissue Engineering: Part 1. Processing and Characterisation of a Ternary Based P_2O_5-CaO-Na_2O Glass System. Biomaterials 2004; 25(3):491-499.

(72) Ahmed I, Collins CA, Lewis MP, Olsen I, Knowles JC. Processing, Characterisation and Biocompatibility of Iron-Phosphate Glass-Fibres for Tissue Engineering. Biomaterials 2004; 25(16):3223-3232.

(73) Bitar M, Salih V, Mudera V, Knowles JC, Lewis MP. Soluble Phosphate Glasses: *In Vitro* Studies Using Human Cells of Hard and Soft Tissue Origin. Biomaterials 2004; 25(12):2283-2292.

(74) Franks K. The Structure and Properties of Soluble Phosphate Based Glasses. 2000.

(75) Franks K, Abrahams I, Knowles JC. Development of Soluble Glasses for Biomedical Use. Part 1:In Vitro Solubility Measurements. Journal of Materials Science: Materials in Medicine 2000; 11:609-614.

(76) Franks K, Abrahams I, Georgiou G, Knowles JC. Investigation of Thermal Parameters and Crystallisation in a Ternary $CaO-Na_2O-P_2O_5$ Based Glass System. Biomaterials 2001; 22:497-501.

(77) Franks K, Salih V, Knowles JC, Olsen.I. The Effect of MgO on the Solubility Behaviour and Cell Proliferation in a Quaternary Soluble Phosphate Based Glass System. Journal of Materials Science: Materials in Medicine 2002; 13:549-556.

(78) Knowles JC, Franks K, Abrahams I. Investigation of the Solubility and Ion Release in the Glass System K_2O - Na_2O - CaO - P_2O_5. Biomaterials 2001; 22(December):3091-3096.

(79) Williams DF. The Williams Dictionary of Biomaterials. Liverpool University Press, 1999.

(80) Atkins P, Jones L. Chemistry. Molecules, Matter and Change. 3rd ed. W.H. Freeman and Company., 1997.

(81) Stover FS, Bulmahn JA, Gard JK. Polyphosphate Separations and Chain Length Characterisation Using Minibore Ion Chromatography with Conductivity Detection. Journal of Chromatography A 1994; 688:89-95.

(82) Franks K, Abrahams I, Georgiou G, Knowles JC. Investigation of Thermal Parameters and Crystallisation in a Ternary $CaO-Na_2O-P_2O_5$ Based Glass System. Biomaterials 2001; 22:497-501.

(83) Uo M, Mizuno M, Kuboki Y, Makishima A, Watari F. Properties and Cytotoxicity of Water Soluble $Na_2O-CaO-P_2O_5$ Glasses. Biomaterials 1998; 19:2277-2284.

(84) Andersson OH. Glass Transition Temperature of Glasses in the $SiO_2-Na_2O-CaO-P_2O_5-Al_2O_3-B_2O_3$ System. Journal of Materials Science: Materials in Medicine 1992; 3:326-328.

(85) Abrahams I, Franks K, Hawkes GE, Philippou G, Knowles JC, Bodart P et al. ^{23}Na, ^{27}Al, ^{31}P NMR and X-Ray Powder Diffraction Study of Na/Ca/Al Phosphate Glasses and Ceramics. Journal Materials Chemistry 1997; 7(8):1573-1580.

(86) Goldstein M, Davies TH. Glass Fibres with Oriented Chain Molecules. Journal of the American Ceramics Society 1955; 38(7):223-226.

(87) Wazer JRV, Holst KA. Structures and Properties of the Condensed Phosphates. I. Some General Considerations about Phosphoric Acids. Journal of the American Ceramics Society 1950; 72(2):639-643.

(88) Zachariasen WH. The Atomic Arrangement in Glass. American Chemical Society 1932; 54(3):3841-3851.

(89) Bunker BC, Arnold GW, Wilder JA. Phosphate Glass Dissolution in Aqueous Solutions. Journal of Non-Crystalline Solids 1984; 64:291-316.

(90) Wazer JRV, Campanella DA. Structure and Properties of the Condensed Phosphates IV. Complex Ion Formation in Polyphosphate Solutions. Journal of the American Ceramics Society 1950; 72(2):655-662.

(91) Murgatroyd JB. The Delayed Elastic Effect in Glass Fibres and the Constitution of Glass in Fibre Form. Journal of the Society of Glass Technology 1948; 32:291-300.

(92) Otto WH, Preston FW. Evidence Against Oriented Structure in Glass Fibres. Journal of the Society of Glass Technology 1950; 34:63-68.

(93) Brannan RT. Further Evidence Against the Orientation of Structure in Glass Fibres. Journal of the American Ceramics Society 1953; 36:230-231.

(94) Milberg ME, Daly MC. Structure of Oriented Sodium Metaphosphate Glass Fibres. Journal of Chemical Physics 1963; 39(11):2966-2973.

(95) Ahmed I, Lewis MP, Olsen.I, Knowles JC. Phosphate Glasses for Tissue Engineering: Part 1. Processing and Characterisation of a Ternary Based P_2O_5-CaO-Na_2O Glass System. Biomaterials 2003; 25:491-499.

(96) Roth RS. Phase Equilibria Diagrams. USA: The American Ceramic Society. 2001.

(97) Roth RS, Negas T, Cook LP. Phase Diagrams for Ceramists. USA: The American Ceramic Society, INC., 1981.

(98) Levin EM, McMurdie HF. Phase Diagrams for Ceramists. 1975 Supplement ed. USA: The American Ceramic Society, INC., 1975.

(99) Feike M, Jager C, Spiess HW. Connectivity's of Coordination Polyhedra in Phosphate Glasses from 31P Double-Quantum NMR Spectroscopy. Journal of Non-Crystalline Solids 1998; 223:200-206.

(100) Watanabe M, Sato S, Saito H. The Mechanism of the Hydrolysis of Condensed Phosphates. IV. The Hydrolysis of Pyro-, Tripoly-, Trimeta-, and Tetrametaphosphates in Aqueous Organic Solvents. Bulletin of the Chemical Society of Japan 1976; 49(9):2474-2478.

(101) Wen L, Jijian C. New Phosphate Glass for Precision Moulding. American Ceramic Society Bulletin 2001; 80(3):62-64.

(102) Franks K, Salih V, Knowles JC, Olsen.I. The Effect of MgO on the Solubility Behaviour and Cell Proliferation in a Quaternary Soluble Phosphate Based Glass System. Journal of Materials Science: Materials in Medicine 2002; 13:549-556.

(103) Knowles JC, Franks K, Abrahams I. Investigation of the Solubility and Ion Release in the Glass System K_20 - Na_20 - CaO - P_2O_5. Biomaterials 2001; 22(December):3091-3096.

(104) Delahaye F, Montagne L, Palavit G, Touray JC, Baillif P. Acid Dissolution of Sodium-Calcium Metaphosphate Glasses. Journal of Non-Crystalline Solids 1998; 242:25-32.

(105) Ahmed I, Lewis MP, Olsen.I, Knowles JC. Phosphate Glasses for Tissue Engineering: Part 1. Processing and Characterisation of a Ternary Based P_2O_5-CaO-Na_2O Glass System. Biomaterials 2004; 25(3):491-499.

(106) Joo C, Werner-Zwangier U, Zwanziger JW. The Ring Structure of Boron Trioxide Glass. Journal of Non-Crystalline Solids 2000; 261:282-286.

(107) Youngman RE, Haubrich ST, Zwanziger JW, Janicke MT, Chmelka BF. Short and Intermediate Range Structural Ordering in Glassy Boron Oxide. Science 1995; 269(5229):1416-1420.

(108) Koudelka L, Mosner P. Borophosphate Glasses of the ZnO-B_2O_3-P_2O_5 System. Materials Letters 2000; 42:194-199.

(109) Youngman RE, Zwanziger JW. Network Modification in Potassium Borate Glasses: Structural Studies with NMR and Raman Spectroscopies. Journal of Physical Chemistry 1996; 100:16720-16728.

(110) Brow RK. An XPS Study of Oxygen Bonding in Zinc Phosphate and Zinc Borophosphate Glasses. Journal of Non-Crystalline Solids 1996; 194:267-273.

(111) Marasinghe GK, Karabulut M, Ray CS, Day DE, Shumsky MG, Yelon WB. Structural Features of Iron Based Phosphate Glasses. Journal of Non-Crystalline Solids 1997; 222:144-152.

(112) Grenier JC, Martin C, Durif A. Nouvelle Etude Du Diagramme D'Equilibre $Ca(PO_3)_2$-$NaPO_3$. Donnees Cristallographiques Sur $CaNa_4(PO_3)_6$ et $CaNa(PO_3)_3$. Bull Soc Fr Mineral Cristallogr 1970; 93:52-55.

(113) Yu X, Day DE, Long GJ, Brow RK. Properties and Structure of Sodium-Iron Phosphate Glasses. Journal of Non-Crystalline Solids 1997; 215:21-31.

(114) Sales BC, Ramsey RS, Bates JB, Boatner LA. Investigation of the Structural Properties of Lead-Iron Phosphate Glasses Using Liquid Chromatography and Raman Scattering Spectroscopy. Journal of Non-Crystalline Solids 1986; 87:137-158.

(115) Mogus-Milankovic A, Pivac B, Furic K. Structural Study of Iron Phosphate Glasses. Physics and Chemistry of Glasses 1997; 38(2):74-78.

(116) Mogus-Milankovic A, Gajovic A, Santic A, Day DE. Structure of Sodium Phosphate Glasses Containing Al_2O_3 and/or Fe_2O_3. Part I. Journal of Non-Crystalline Solids 2001; 289:204-213.

(117) Mogus-Milankovic A, Santic A, Gajovic A, Day DE. Electrical Properties of Sodium Phosphate Glasses Containing Al_2O_3 and /or Fe_2O_3. Part II. Journal of Non-Crystalline Solids 2001; 296:57-64.

(118) Fang X, Ray CS, Day DE. Glass Transition and Fragility of Iron Phosphate Glasses. II. Effect of Mixed-Alkali. Journal of Non-Crystalline Solids 2003; 319:314-321.

(119) Fang X, Ray CS, Marasinghe GK, Day DE. Properties of Mixed Na_2O and K_2O Iron Phosphate Glasses. Journal of Non-Crystalline Solids 2000; 263&264:293-298.

(120) Fang X, Ray CS, Mogus-Milankovic A, Day DE. Iron Redox Equilibrium, Structure and Properties of Iron Phosphate Glasses. Journal of Non-Crystalline Solids 2001; 283:162-172.

(121) Ray CS, Fang X, Karabulut M, Marasinghe GK, Day DE. Effect of Melting Temperature and Time on Iron Valence and Crystallisation of Iron Phosphate Glasses. Journal of Non-Crystalline Solids 1999; 249:1-16.

(122) Marasinghe GK, Karabulut M, Day DE, Booth CH, Allen PG, Butcher JJ et al. EXAFS / XANES Studies of Iron Phosphate Glasses. SSRL Activity Report 1997;(7):284-287.

(123) Karabulut M, Marasinghe GK, Ray CS, Day DE, Wadill GD, Booth CH. An Investigation of the Local Iron Environment in Iron Phosphate Glasses Having Different Fe(II) Concentrations. Journal of Non-Crystalline Solids 2002; 306:182-192.

(124) Choueka J, Charvet JL, Alexander H, Oh YH, Joseph G, Blumenthal NC et al. Effect of Annealing Temperature on the Degradation of Reinforcing

Fibres for Absorbable Implants. Journal of Biomedical Materials Research 1995; 29:1309-1315.

(125) Lin ST, Krebs SL, Kadiyala S, Leong KW, LaCourse WC, Kumar B. Development of Bioabsorbable Glass Fibres. Biomaterials 1994; 15(13):1057-1061.

(126) Greenwood NN, Earnshaw A. Chemistry of the Elements. 1st ed. Pergamon Press Plc. 1984.

(127) Ahmed I, Collins CA, Lewis MP, Olsen I, Knowles JC. Processing, Characterisation and Biocompatibility of Iron-Phosphate Glass-Fibres for Tissue Engineering. Biomaterials 2004; 25(16):3223-3232.

(128) Nagase M, Abe Y, Chigira M, Udagawa E. Toxicity of Silica-Containing Calcium Phosphate Glasses Demonstrated in Mice. Biomaterials 1992; 13(3):173-175.

(129) Larsen PH, Poulsen FW, Berg.R.W. The Influence of SiO_2 Addition to $2MgO\text{-}Al_2O_3\text{-}3.3P_2O_5$ Glass. Journal of Non-Crystalline Solids 1999; 244:16-24.

(130) Sayer M, Stratilatov AD, Reid J, Calderin L, Stott MJ, Yin X et al. Structure and Composition of Silicon-Stabilised Tricalcium Phosphate. Biomaterials 2003; 24:369-382.

(131) Poojary DM, Borade RB, Clearfield A. Structural Characterisation of Silicon Orthophosphate. Inorganica Chimica Acta 1993; 208:23-29.

(132) Shan W, Jijian C. Dissolution Products of a Phosphate Glass Scale Inhibitor and Its Scale Inhibition Mechanism. Glass Technology 2001; 42(415):122-125.

(133) Monzyk, B. 1986. Phosphate Fibre: A Unique Reinforcement. Plastic Compounding. Sept/Oct. pp 42 – 46.

(134) Bruckner, R and Stockhurst, H. 1985. Influence of Mechanical and Thermal Prehistory on the Structure of Glass Fibres. Journal De Physique. Vol C8. Supplement no.12, ppC8-527.

(135) Kurkjian, C.R. 2000. Mechanical Properties of Phosphate Glasses. Journal of Non-Crystalline Solids. Vol 263&264 pp 207 – 212.

(136) Karabulut, M et al. 2001. Mechanical and Structural Properties of Phosphate Glasses. Journal of Non-Crystalline Solids. Vol 288 pp 8 – 17.

(137) Lin, S.T. et al. 1994. Development of Bioabsorbable Glass Fibres. Biomaterials. Vol 15, no 13. pp 1057 – 1061.

(138) Moffat, W.G., Pearseall, G.W., Wulff, J. eds. 1964. The Structure and Properties of Materials. Vol 1 Structure. John Wiley and Sons Inc. USA.

(139) Varshneya, A.K. Fundamentals of Inorganic Glasses. 1994. Academic Press. London. U.K. ISBN no. 0-12-714970-8.

CHAPTER 9

Appendices

9.0 Appendix:

9.1 List of Conference Proceedings and Abstracts:

1. M. Bitar, I. Ahmed, J.C. Knowles, V. Salih, and M. P. Lewis. 'Development of Novel Soluble Glasses for Tissue Engineering of Hard Tissue'. Proceedings of the Tissue and Cell Engineering Society, University of Glasgow. 2002.

2. I.Ahmed, M.P. Lewis, I. Olsen, and J.C. Knowles. 'Processing, Characterisation and Biocompatibility of Iron-Phosphate Glass-Fibres for Tissue Engineering'. Proceedings of the 1st Annual Biomaterials Workshop, Cranfield University. Shrivenham, March 2003.

3. E.A. Abouneel, I. Ahmed, S.N. Nazhat and J.C. Knowles. 'DSC as a Rapid Test Method for Determining T_g of Phosphate Based Glass-Fibres'. Proceedings of the 1st Annual Biomaterials Workshop, Cranfield University. Shrivenham, March 2003.

4. I. Ahmed, C. Collins, I. Olsen, M. P. Lewis and J. C. Knowles. Iron-Phosphate Glass Fibres for Tissue Engineering. Proceedings of the 7th World Biomaterials Congress, Sydney, Australia. May 2004.

5. I. Ahmed, C. Collins, I. Olsen, M. P. Lewis and J. C. Knowles. Phosphate-Based Glass Fibres for Tissue Engineering Applications. Proceedings of the 3rd Annual Conference, University of Brighton. July 2004.

6. E.A. Abouneel, I. Ahmed, J. Pratten, S.N. Nazhat, J.C. Knowles. Characterization of a Novel Antimicrobial Releasing Glass-Fibre. Proceedings of the 3rd Annual Conference, University of Brighton. July 2004.

9.2 List of Publications:

1. I.Ahmed, M.P. Lewis, I. Olsen and J.C. Knowles. Phosphate Glasses for Tissue Engineering: Part 1: Processing and Characterisation of a Ternary Based P_2O_5-CaO-Na_2O Glass System. Biomaterials. 2004. 25(3) pp 491 – 499.

2. I.Ahmed, M.P. Lewis, I. Olsen and J.C. Knowles. Phosphate Glasses for Tissue Engineering: Part 2: Processing and Characterisation of a Ternary Based P_2O_5-CaO-Na_2O Glass-Fibre System. Biomaterials. 2004. 25(3) pp 501 – 507.

3. I.Ahmed, C. Collins, M.P. Lewis, I. Olsen, J.C. Knowles. Processing, Characterisation and Biocompatibility of Iron-Phosphate Glass-Fibres for Tissue Engineering. Biomaterials. 2004. (25)16 pp 3223 – 3232.

4. I. Ahmed, M.P. Lewis, S.N. Nazhat and J.C. Knowles. Quantification of Anion and Cation Release from a Range of Ternary Phosphate-Based Glasses with Fixed 45mol% P_2O_5. Journal of Biomaterials Applications. 2005. DOI: 10.1177/0885328202049396

5. E. A. Abouneel, I. Ahmed, J. Pratten, S. N. Nazhat and J.C. Knowles. Antibacterial Copper Releasing Soluble Phosphate-Based Glass Fibres. Biomaterials. 2005. (26) pp 2247 – 2254.